


# REPORT DOCUMENTATION PAGE

Form Approved  
OMB No. 0704-0188

Public reporting burden for this collection of information is estimated to average 1 hour per response, including the time for reviewing instructions, searching existing data sources, gathering and maintaining the data needed, and completing and reviewing the collection of information. Send comments regarding this burden estimate or any other aspect of this collection of information, including suggestions for reducing this burden, to Washington Headquarters Services, Directorate for Information Operations and Reports, 1215 Jefferson Davis Highway, Suite 1204, Arlington, VA 22202-4302, and to the Office of Management and Budget, Paperwork Reduction Project (0704-0188), Washington, DC 20503.

1. AGENCY USE ONLY (Leave blank)		2. REPORT DATE 1995		3. REPORT TYPE AND DATES COVERED	
4. TITLE AND SUBTITLE Heterogenous-Phase Reactions of Nitrogen Dioxide with Vermicule-Supported Magnesium Oxide As Applied to the Control of Jet Engine Test Cell Emissions				5. FUNDING NUMBERS	
6. AUTHOR(S) MAJ Larry Thomas Kinn				8. PERFORMING ORGANIZATION REPORT NUMBER AFIT/CI/CIA 95-006 D	
7. PERFORMING ORGANIZATION NAME(S) AND ADDRESS(ES) AFIT Students Attending: University of Florida				10. SPONSORING/MONITORING AGENCY REPORT NUMBER	
9. SPONSORING/MONITORING AGENCY NAME(S) AND ADDRESS(ES) DEPARTNENT OF THE AIR FORCE AFIT/CI 2950 P STREET, BDLG 125 WRIGHT-PATTERSON AFB OH 45433-7765				10. SPONSORING/MONITORING AGENCY REPORT NUMBER	
11. SUPPLEMENTARY NOTES					
12a. DISTRIBUTION/AVAILABILITY STATEMENT Approved for Public Release IAW AFR 190-1 Distribution Unlimited BRIAN D. GAUTHIER, MSgt, USAF Chief Administration				12b. DISTRIBUTION CODE	
13. ABSTRACT (Maximum 200 words)					
 <p>DTIC QUALITY INSPECTED 3</p>					
14. SUBJECT TERMS 19950606 052				15. NUMBER OF PAGES	
				16. PRICE CODE	
17. SECURITY CLASSIFICATION OF REPORT		18. SECURITY CLASSIFICATION OF THIS PAGE		19. SECURITY CLASSIFICATION OF ABSTRACT	
				20. LIMITATION OF ABSTRACT	

HETEROGENEOUS-PHASE REACTIONS OF NITROGEN DIOXIDE WITH  
VERMICULITE-SUPPORTED MAGNESIUM OXIDE

By

LARRY THOMAS KIMM

Accession For	
NTIS CRA&I	<input checked="checked" type="checkbox"/>
DTIC TAB	<input type="checkbox"/>
Unannounced	<input type="checkbox"/>
Justification .....	
By .....	
Distribution /	
Availability Codes	
Dist	Avail and/or Special
A-1	

A DISSERTATION PRESENTED TO THE GRADUATE SCHOOL  
OF THE UNIVERSITY OF FLORIDA IN PARTIAL FULFILLMENT  
OF THE REQUIREMENTS FOR THE DEGREE OF  
DOCTOR OF PHILOSOPHY

UNIVERSITY OF FLORIDA

1995

This work is dedicated to my family, especially my wife, Lisa, whose patience, love and support during this effort made it all possible, and to my children, Meredyth and Wilson, who always give me the best welcome home after a long day.

## ACKNOWLEDGMENTS

I am extremely grateful for the support of my doctoral committee chairman, Dr. Eric R. Allen, for his wealth of knowledge in academic research, for sharing in the excitement of discovery, as well as for providing encouragement when problems arose. I will always fondly remember our enlightening discussions about my research, as well as life in general, as high points in my research. I also appreciate the sage advice of Dr. Dale A. Lundgren, whose practical and applied approach to engineering goes a long way beyond what can be learned in a textbook. I am thankful to both professors and to my fellow air pollution graduate students, for their friendship and comradery during my time as a graduate student at UF.

Special thanks to Dr. Joseph D. Wander, whose belief in the value of academic research is unparalleled, for providing the idea for this project, as well as for his help, friendship and advice all along the way. I am also thankful to Dr. W. Emmett Bolch, Jr., whose letter years ago convinced me to come to the University of Florida, and to Dr. Robert J. Hanrahan, to whom I credit the excellent performance of the experimental system.

I would like to acknowledge Colonel Robert A. Capell, USAF, BSC, who saw the need for a bioenvironmental engineer with a Ph.D. in air pollution. Finally, I would like to thank the Armstrong Laboratory/OL-EQS, Tyndall AFB, Florida for providing funding for this research project, and the U.S. Air Force and the Air Force Institute of Technology, for their confidence in selecting me for advanced education and for the financial support.

## TABLE OF CONTENTS

ACKNOWLEDGMENTS .....	iii
LIST OF TABLES .....	vii
LIST OF FIGURES .....	viii
ABSTRACT .....	xii
1. INTRODUCTION .....	1
Background .....	1
Properties and Health Effects of Nitrogen Oxides .....	1
Environmental Impacts of NO <sub>x</sub> .....	4
Sources .....	4
NO <sub>x</sub> Formation .....	7
Fuel NO <sub>x</sub> .....	7
Thermal NO <sub>x</sub> .....	8
Regulation of NO <sub>x</sub> Emissions .....	11
NO <sub>x</sub> Controls for Stationary Sources .....	13
Application of NO <sub>x</sub> Control Strategies .....	13
Modifications to Operating Conditions .....	14
Combustion Modifications .....	15
Exhaust Gas Treatment .....	16
2. CONTROL OF NO <sub>x</sub> THROUGH GAS-SOLID INTERACTION .....	18
Exhaust Gas Treatment Methods .....	18
Catalytic Methods .....	19
Non-Catalytic Methods .....	21
Jet Engine Test Cells .....	22
U.S. Air Force (USAF) Sponsored Research .....	25
Vermiculite-based Catalyst .....	26
Field Studies .....	30
Related Research .....	31
Gas-Solid Interaction .....	32

Generalized Non-Catalytic Gas-Solid Reactions .....	33
Mathematical Models .....	35
Progressive-Conversion Model .....	36
Shrinking Unreacted-Core Model .....	36
Grain Model .....	39
Analagous Gas-Solid Reaction System Research .....	41
SO <sub>2</sub> -CaO Reaction .....	42
SO <sub>2</sub> -Calcium Hydroxide Reaction .....	43
SO <sub>2</sub> -Calcium Carbonate Reaction .....	44
Other Acid-gas-Calcium-based-solid Reactions .....	45
General Applicability of the Shrinking Unreacted-Core Model .....	46
Research Justification .....	47
Research Objectives .....	47
 3. EXPERIMENTAL METHODS AND MATERIALS .....	 49
General Research Approach .....	49
Experimental Variables .....	50
MgO-Vermiculite Reactive Sorbent Material .....	50
Temperature .....	52
Pressure .....	52
Gas Composition .....	53
Gas Flow Rate(s) .....	54
Gas Reaction/Sorption/Desorption .....	55
Fixed-Bed Reactor System .....	55
General Experimental Considerations .....	55
Experimental Arrangement .....	58
Tubular Fixed-bed Reactors .....	58
Experimental Procedures .....	63
Gas Analyses .....	70
Sorbent Surface Area Determination .....	76
Sorbent Particle Size Determination .....	77
 4. RESULTS AND DISCUSSION .....	 78
Intrinsic Kinetic Studies .....	78
Limitation of Gas-Film-Mass-Transfer Resistance .....	79
Solid Sorbent Characterizations .....	82
Surface Area Analyses .....	82
Particle Size Distributions .....	83
NO <sub>x</sub> Removal by Mg(NO <sub>3</sub> ) <sub>2</sub> -coated Vermiculite .....	86
NO <sub>x</sub> Removal by Sorbent Material .....	86
NO Removal by Sorbent Material .....	87
NO <sub>2</sub> Removal by Sorbent Material .....	89
Effects of Operational Variables .....	94

Effects of NO <sub>2</sub> Concentration . . . . .	94
Effects of Oxygen . . . . .	99
Effects of Bed Temperature . . . . .	105
Activation Energy Determination . . . . .	112
Effects of Water . . . . .	120
Effects of Residence (Reaction) Time . . . . .	122
Sorbtech-Supplied Sample Results . . . . .	123
Pressure Drop Characteristics . . . . .	124
Magnesium Nitrate Surface Decomposition . . . . .	127
Sorbent "Lifetime" and Regeneration . . . . .	130
Proposed Reaction Mechanism . . . . .	132
Application of the Shrinking Unreacted Core/Grain Model . . . . .	133
Diffusion-Through-Gas-Film-Control . . . . .	134
Chemical-Reaction-Control . . . . .	137
Diffusion-Through-Inert-Product-Layer-Control . . . . .	140
Derivations of the Shrinking Unreacted-Core Model . . . . .	144
Correlation Between Gas-Phase Concentration and Solid Conversion . . . . .	146
Local-Equilibrium Theory . . . . .	146
Application of Shrinking Unreacted-Core/Grain Model to Experimental Data . . . . .	149
50 ppm NO <sub>2</sub> at a Reaction Temperature of 423 K . . . . .	149
20 ppm NO <sub>2</sub> at a Reaction Temperature of 373 K . . . . .	165
200 ppm NO <sub>2</sub> at a Reaction Temperature of 473 K . . . . .	169
General Applicability of the Shrinking Unreacted-Core Model . . . . .	178
 5. PRACTICAL CONSIDERATIONS . . . . .	 182
Constraints on MgO–Vermiculite Sorbent Usage . . . . .	182
 6. CONCLUSIONS AND RECOMMENDATIONS . . . . .	 185
Conclusions . . . . .	185
Recommendations for Further Research . . . . .	188
 LIST OF REFERENCES . . . . .	 192
 BIOGRAPHICAL SKETCH . . . . .	 201

## LIST OF TABLES

<u>Table</u>	<u>page</u>
1-1. Physical properties of nitrogen oxides ( $N_xO_y$ ) . . . . .	2
1-2. Emission factors for nitrogen oxides ( $NO_x$ as $NO_2$ ) . . . . .	6
2-1. Physical properties of selected Mg-containing inorganic compounds . . . . .	28
3-1. USAF F110 turbine engine emissions data (as reported) . . . . .	54
4-1. BET surface areas of selected samples of laboratory-prepared MgO-vermiculite sorbent . . . . .	82
4-2. Intrinsic first-order rate coefficients ( $s^{-1}$ ) for $NO_2$ removal by MgO-vermiculite sorbent ( $[O_2]=0\%$ ) . . . . .	100
4-3. Intrinsic first-order rate coefficients ( $s^{-1}$ ) for $NO_2$ removal by MgO-vermiculite sorbent ( $[O_2]=10\%$ ) . . . . .	106



## LIST OF FIGURES

<u>Figure</u>	<u>page</u>
2-1. Schematic representation of a jet engine test cell (JETC) . . . . .	24
2-2. Schematic representation of the shrinking unreacted-core model . . . . .	38
2-3. Schematic representation of the grain model . . . . .	40
3-1. Experimental arrangement for packed-bed studies . . . . .	59
3-2. Example low-flow-rate rotameter calibration curves (Omega NO42-15ST Tube) . . . . .	61
3-3. Example high-flow-rate rotameter calibration curves (Omega NO92-04G Tube) . . . . .	62
3-4. Schematic representation of 316 stainless steel packed-bed reactor . . . . .	64
3-5. Schematic representation of internal sampling tube location and appearance . . .	65
3-6. Schematic representation of 316 stainless steel mixing or sampling manifold . . .	66
3-7. Typical chemiluminescent NO <sub>x</sub> analyzer calibration curve (for NO channel) . . .	74
3-8. Typical IR-2100 oxygen analyzer calibration curve . . . . .	75
4-1. Gas-film-mass-transfer resistance evaluation - NO <sub>2</sub> penetration ( $C_{out}/C_{in}$ ) versus bed exposure time ( $[NO_2]_{in}=200$ ppm, $T=473$ K, $[O_2]=0\%$ ) . . . . .	81
4-2. Log-probability plot of MgO-vermiculite sorbent particle size distribution . . . .	84
4-3. Log-probability plot of Akrochem Elastomag ® 170 MgO powder particle size distribution (manufacturer-provided data) . . . . .	85

4-4.	NO removal by humidified MgO-vermiculite sorbent ( $[\text{NO}]_{\text{in}}=210$ ppm, $T=423$ K, $[\text{O}_2]=11\%$ , 3% $\text{H}_2\text{O}$ vapor) . . . . .	88
4-5.	$\text{NO}_2$ removal versus residence time ( $T=473$ K, $[\text{O}_2]=9.9\%$ ) . . . . .	90
4-6.	First-order kinetic plot ( $[\text{NO}_2]_{\text{in}}=100$ ppm, $T=473$ K, $[\text{O}_2]=10\%$ ) . . . . .	92
4-7.	First-order kinetic plot ( $[\text{NO}_2]_{\text{in}}=100$ ppm, $T=473$ K, $[\text{O}_2]=10.5\%$ ) . . . . .	93
4-8.	$\text{NO}_2$ penetration vs bed exposure time ( $T=473$ K, $[\text{O}_2]=0\%$ ) . . . . .	95
4-9.	$\text{NO}_2$ penetration vs bed exposure time ( $T=423$ K, $[\text{O}_2]=0\%$ ) . . . . .	96
4-10.	$\text{NO}_2$ penetration vs bed exposure time ( $T=373$ K, $[\text{O}_2]=0\%$ ) . . . . .	97
4-11.	$\text{NO}_2$ penetration vs bed exposure time ( $T=473$ K, $[\text{O}_2]=10\%$ ) . . . . .	102
4-12.	$\text{NO}_2$ penetration vs bed exposure time ( $T=423$ K, $[\text{O}_2]=10\%$ ) . . . . .	103
4-13.	$\text{NO}_2$ penetration vs bed exposure time ( $T=373$ K, $[\text{O}_2]=10\%$ ) . . . . .	104
4-14.	$\text{NO}_2$ penetration vs bed exposure time ( $[\text{NO}_2]_{\text{in}}=200$ ppm, $[\text{O}_2]=0\%$ ) . . . . .	108
4-15.	$\text{NO}_2$ penetration vs bed exposure time ( $[\text{NO}_2]_{\text{in}}=100$ ppm, $[\text{O}_2]=0\%$ ) . . . . .	109
4-16.	$\text{NO}_2$ penetration vs bed exposure time ( $[\text{NO}_2]_{\text{in}}=50$ ppm, $[\text{O}_2]=0\%$ ) . . . . .	110
4-17.	$\text{NO}_2$ penetration vs bed exposure time ( $[\text{NO}_2]_{\text{in}}=20$ ppm, $[\text{O}_2]=0\%$ ) . . . . .	111
4-18.	$\text{NO}_2$ penetration vs bed exposure time ( $[\text{NO}_2]_{\text{in}}=100$ ppm, $[\text{O}_2]=10\%$ ) . . . . .	113
4-19.	$\text{NO}_2$ penetration vs bed exposure time ( $[\text{NO}_2]_{\text{in}}=50$ ppm, $[\text{O}_2]=10\%$ ) . . . . .	114
4-20.	$\text{NO}_2$ penetration vs bed exposure time ( $[\text{NO}_2]_{\text{in}}=20$ ppm, $[\text{O}_2]=10\%$ ) . . . . .	115
4-21.	Arrhenius plot of $\ln k$ versus $1000/T$ ( $T$ between 473 and 423 K, $[\text{NO}_2]_{\text{in}}=100$ ppm, $[\text{O}_2]=0\%$ ) . . . . .	116
4-22.	Arrhenius plot of $\ln k$ versus $1000/T$ ( $T$ between 473 and 373 K, $[\text{NO}_2]_{\text{in}}=20$ ppm, $[\text{O}_2]=0\%$ ) . . . . .	117
4-23.	$\text{NO}_2$ penetration versus bed exposure time (20 ml $\text{H}_2\text{O}$ added to 7 g MgO-vermiculite sorbent, $[\text{NO}_2]_{\text{in}}=100$ ppm, $[\text{O}_2]=0\%$ $T=473$ K) . . . . .	121

4-24. Predicted (Ergun equation) versus experimental pressure drop as a function of superficial velocity for a 0.1 m long bed of MgO-vermiculite sorbent (T=473 K) .....	126
4-25. Thermal decomposition of $\text{Mg}(\text{NO}_3)_2 \cdot 6\text{H}_2\text{O}$ on vermiculite (temperature increasing with time) .....	128
4-26. Thermal decomposition of used MgO-vermiculite sorbent (T=523 K) .....	129
4-27. Comparative bed outlet $\text{NO}_2$ and NO concentrations versus bed exposure time showing NO production .....	131
4-28. Graphical representation of the shrinking unreacted-core model under diffusion-through-gas-film control .....	135
4-29. Graphical representation of the shrinking unreacted-core model under chemical-reaction control .....	138
4-30. Graphical representation of the shrinking unreacted-core model under diffusion-through-inert-product-layer control .....	141
4-31. Shrinking unreacted-core model evaluation ( $[\text{NO}_2]_{\text{in}}=50$ ppm, T=423 K, $[\text{O}_2]=0\%$ ) .....	150
4-32. Shrinking unreacted-core chemical-reaction-control-equation evaluation, $\tau_r=397$ minutes, ( $[\text{NO}_2]_{\text{in}}=50$ ppm, T=423 K, $[\text{O}_2]=0\%$ ) .....	152
4-33. Shrinking unreacted-core product-layer-diffusion-equation evaluation, $\tau_d=820$ minutes, ( $[\text{NO}_2]_{\text{in}}=50$ ppm, T=423 K, $[\text{O}_2]=0\%$ ) .....	153
4-34. Shrinking unreacted-core chemical-reaction-control-equation evaluation, $\tau_r=205$ minutes, ( $[\text{NO}_2]_{\text{in}}=50$ ppm, T=423 K, $[\text{O}_2]=0\%$ ) .....	154
4-35. Shrinking unreacted-core product-layer-diffusion-equation evaluation, $\tau_d=957$ minutes, ( $[\text{NO}_2]_{\text{in}}=50$ ppm, T=423 K, $[\text{O}_2]=0\%$ ) .....	155
4-36. Cumulative mass $\text{NO}_2$ removed versus bed exposure time ( $[\text{NO}_2]_{\text{in}}=50$ ppm, T=423 K, $[\text{O}_2]=0\%$ ) .....	157
4-37. Cumulative mass $\text{NO}_2$ removed versus bed exposure time for a long-term run ( $[\text{NO}_2]_{\text{in}}=50$ ppm, T=423 K, $[\text{O}_2]=0\%$ , Gas samples collected from center of bed) .....	158

4-38. Plot of inverse first-order rate coefficient ( $1/k$ ) versus bed exposure time ([NO <sub>2</sub> ] <sub>in</sub> =47.5ppm, T=423 K, [O <sub>2</sub> ]=0%) . . . . .	163
4-39. Experimental versus predicted NO <sub>2</sub> concentration ([NO <sub>2</sub> ] <sub>in</sub> =47.5 ppm, T=423 K, [O <sub>2</sub> ]=0%, Gas samples collected from middle of bed) . . . . .	164
4-40. Shrinking unreacted-core model evaluation ([NO <sub>2</sub> ] <sub>in</sub> =20 ppm, T=373 K, [O <sub>2</sub> ]=0%) . . . . .	166
4-41. Shrinking unreacted-core chemical-reaction-control-equation evaluation, $\tau_r$ =1023 minutes, ([NO <sub>2</sub> ] <sub>in</sub> =20 ppm, T=373 K, [O <sub>2</sub> ]=0%) . . . . .	167
4-42. Shrinking unreacted-core product-layer-diffusion-equation evaluation, $\tau_d$ =1093 minutes, ([NO <sub>2</sub> ] <sub>in</sub> =20 ppm, T=373 K, [O <sub>2</sub> ]=0%) . . . . .	168
4-43. Experimental versus predicted NO <sub>2</sub> concentration ([NO <sub>2</sub> ] <sub>in</sub> =19.1 ppm, T=373 K, [O <sub>2</sub> ]=0%, Gas samples collected from middle of bed) . . . . .	170
4-44. Shrinking unreacted-core model evaluation ([NO <sub>2</sub> ] <sub>in</sub> =200 ppm, T=473 K, [O <sub>2</sub> ]=0%) . . . . .	171
4-45. Shrinking unreacted-core chemical-reaction-control-equation evaluation, $\tau_r$ =495 minutes, ([NO <sub>2</sub> ] <sub>in</sub> =200 ppm, T=473 K, [O <sub>2</sub> ]=0%) . . . . .	173
4-46. Shrinking unreacted-core product-layer-diffusion-equation evaluation, $\tau_d$ =1015 minutes, ([NO <sub>2</sub> ] <sub>in</sub> =200 ppm, T=473 K, [O <sub>2</sub> ]=0%) . . . . .	174
4-47. Experimental versus predicted NO <sub>2</sub> concentration ([NO <sub>2</sub> ] <sub>in</sub> =170.0 ppm, T=473 K, [O <sub>2</sub> ]=0%, Gas samples collected from middle of bed) . . . . .	175
4-48. Cumulative mass NO <sub>2</sub> removed versus bed exposure time for a long-term run ([NO <sub>2</sub> ] <sub>in</sub> =170 ppm, T=473 K, [O <sub>2</sub> ]=0%, Gas samples collected from center of bed) . . . . .	176
4-49. Comparative bed NO <sub>2</sub> and NO concentrations versus bed exposure time during long-term run showing NO production ([NO <sub>2</sub> ] <sub>in</sub> =170 ppm, T=473 K, [O <sub>2</sub> ]=0%, Gas samples collected from center of bed) . . . . .	177

Abstract of Dissertation Presented to the Graduate School  
of the University of Florida in Partial Fulfillment of the  
Requirements for the Degree of Doctor of Philosophy

HETEROGENEOUS-PHASE REACTIONS OF NITROGEN DIOXIDE WITH  
VERMICULITE-SUPPORTED MAGNESIUM OXIDE

By

Larry Thomas Kimm

August 1995

Chairperson: Eric R. Allen

Major Department: Environmental Engineering Sciences

Controlling nitrogen oxides ( $\text{NO}_x$ ) from a non-steady-state stationary source like a jet engine test cell (JETC) requires a method that is effective over a wide range of conditions. A heterogeneous, porous, high surface area sorbent material comprised of magnesium oxide powder attached to a vermiculite substrate has been commercially developed for this purpose. Data from extensive laboratory testing of this material in a packed-bed flow system are presented.  $\text{NO}_2$  removal efficiencies, kinetics, and proposed  $\text{NO}_2$  removal mechanisms over a range of representative JETC exhaust gas characteristics are described. Exhaust gas variables evaluated included:  $\text{NO}_2$  concentration, temperature, flow rate (retention time), oxygen content and moisture content. Availability of water and oxygen were found to be important variables. It is probable that water is necessary for the conversion of  $\text{MgO}$  to  $\text{Mg}(\text{OH})_2$ , which is a more reactive compound having thermal stability over the range of

temperatures evaluated. Gaseous oxygen serves to oxidize NO to NO<sub>2</sub>, the latter being more readily removed from the gas stream. The presence of oxygen also serves to offset thermal decomposition of NO<sub>2</sub> or surface nitrite/nitrate. Effective "lifetime" and regenerability of the exposed sorbent material were also evaluated. NO<sub>2</sub> removal efficiencies were found to greatly exceed those for NO, with a maximum value greater than 90 percent. The effective conversion of NO to NO<sub>2</sub> is a crucial requirement for removal of the former. The reaction between NO<sub>2</sub> and MgO-vermiculite is first-order with respect to NO<sub>2</sub>. The temperature dependence of the first-order rate coefficients provided evidence that data were collected in the region of chemical-reaction control. Activation energies associated with this reaction ranged from approximately 20 and 36 kJ/g-mol when oxygen was not present and 15 to 25 kJ/g-mol when oxygen was present in the system. The shrinking unreacted-core model was used to describe the physical and chemical mechanisms occurring in the removal of NO<sub>2</sub> from a flowing gas stream. It appeared that the reaction begins with control by chemical reaction and progressed to control by diffusion processes as reaction progressed. An empirical relationship was also developed which allowed for the prediction of NO<sub>2</sub> removal with increasing bed exposure time. The range of temperatures and concentrations evaluated, while valid for the representation of simulated jet engine test cell conditions, appeared to be a transition region making the absolute determination of rate-limiting mechanism(s) difficult. With impending regulations aimed at controlling JETCs as stationary sources of NO<sub>x</sub>, results from these studies will be useful to environmental engineers developing air pollution controls for similar sources. Knowledge of parameters affecting the efficiency and capacity of NO<sub>x</sub> control systems employing this medium is necessary to ensure compliance with regulations.

## CHAPTER 1 INTRODUCTION

### Background

The combustion of carbonaceous jet fuels during jet engine testing produces significant quantities of nitrogen oxides ( $\text{NO}_x$ ). Besides direct negative impacts on human health, nitrogen oxides have been linked to other detrimental effects on air quality and the environment. The latter include interactions with hydrocarbons to produce photochemical oxidants and smog, and contribution to the phenomenon of acid precipitation through nitric acid formation. Nitric oxide emissions may also contribute to the degradation of visibility and aesthetics by direct emission of high NO levels in elevated plumes followed by atmospheric oxidation to  $\text{NO}_2$  and fine particulate aerosols resulting from by-products of  $\text{NO}_2$  reactions (Wark and Warner, 1981).

### Properties and Health Effects of Nitrogen Oxides

There are seven possible forms of nitrogen oxides ( $\text{N}_x\text{O}_y$ ). Two of the most abundant of these gaseous oxides of nitrogen, nitric oxide (NO) and nitrogen dioxide ( $\text{NO}_2$ ), are the predominant air pollutants of environmental and health concern. These two forms, however, are rapidly interchangeable in the atmosphere and are often grouped together and collectively

called "NO<sub>x</sub>." Some of the physical properties associated with gaseous nitrogen oxides (N<sub>x</sub>O<sub>y</sub>) are shown in Table 1-1. Nitrous oxide (N<sub>2</sub>O) is another oxide of nitrogen that is also present in the atmosphere at appreciable concentrations. Nitrous oxide is a gas with recognized anesthetic properties, which has also been suggested to be a product of combustion. Its ambient concentration is approximately 0.5 parts per million (ppm), well below the threshold concentration for biological effects. Fortunately, in the troposphere, it is balanced atmospherically by a cycle that is independent of the other oxides of nitrogen. Nitric oxide (NO) is a colorless gas whose ambient concentration is normally well below 0.5 ppm. At this concentration it produces minimal effects on human health. However, nitric oxide is a precursor to the formation of NO<sub>2</sub> and is an active compound in the formation of photochemical smog, initiating reactions that produce secondary air pollutants.

Table 1-1. Physical properties of nitrogen oxides (N<sub>x</sub>O<sub>y</sub>).

Species	Mol Wt (g/gmol)	Solubility in Water (mL/100g)	Melting Point (°C)	Boiling Point (°C)
NO	30.01	7.34	-163.6	-151.7
NO <sub>2</sub>	46.01	See Note 1	See Note 2	See Note 2
NO <sub>3</sub>	62.00	Soluble (ether)	Decomp. 20.0	Unavailable
N <sub>2</sub> O	44.02	130.0	-102.4	-89.0
N <sub>2</sub> O <sub>3</sub>	76.01	Soluble (ether)	-111.0	2.0
N <sub>2</sub> O <sub>4</sub>	92.02	130.52	-11.3	21.2
N <sub>2</sub> O <sub>5</sub>	108.01	Soluble	40.7	Sublimes 32.3

NOTES: 1. Reacts with H<sub>2</sub>O forming HONO<sub>2</sub> and/or HONO

2. Liquid and solid forms are primarily N<sub>2</sub>O<sub>4</sub>

Sources: Neal et al., 1981.; Lange's Handbook of Chemistry, 1973.



The most harmful effects of  $\text{NO}_x$  are primarily attributed to exposure to  $\text{NO}_2$ , the most toxic of these oxides.  $\text{NO}_2$  is a reddish-brown gas that is quite visible in sufficient concentration ( $> 0.25$  ppm).  $\text{NO}_2$  is not a primary pollutant in the sense that it directly affects human health, unless the exposure concentration is high.  $\text{NO}_2$  exerts its main toxic effects on the lungs via free-radical-mediated reactions and other mechanisms. Both  $\text{NO}$  and  $\text{NO}_2$  are free radicals that may produce lipid peroxidation reactions within human cells. The environmental hazard of  $\text{NO}_2$  is primarily associated with the pulmonary effects of the pollutant. Exposure to concentrations of  $\text{NO}_2$  from 0.7 to 5.0 ppm for 10 to 15 minutes have produced abnormalities in pulmonary airway resistance. Exposures to 15 ppm can cause eye and nose irritation, and pulmonary discomfort is noted at 25 ppm for exposures of less than one hour.

The greatest danger of exposure to  $\text{NO}_2$  is the delay in experiencing its full effect upon the respiratory system. The delayed effect of  $\text{NO}_2$  injury is made potentially more dangerous by two other factors. Human perception of the odor of  $\text{NO}_2$  is insufficient to warn against injury or even death. Additionally,  $\text{NO}_2$  quickly desensitizes an individual to its odor through olfactory fatigue, and if  $\text{NO}_2$  levels gradually rise, a person could unknowingly be exposed to concentrations high enough to cause permanent injury or death. Because of the low solubility of  $\text{NO}_2$  in water, it is only slowly removed from the lungs by circulating blood and may remain in contact with lung cells for prolonged periods of time. Given the same total dose, short-term exposure to high concentrations of  $\text{NO}_2$  is more injurious than long-term exposure to lower concentrations. The toxic effects of  $\text{NO}_2$  are often synergistic with or

additive to those of other environmental contaminants (Wark and Warner, 1981; Neal et al., 1981).

#### Environmental Impacts of NO<sub>x</sub>

In addition to the direct effects on health, nitrogen oxides may create other detrimental effects on air quality and the environment. These effects include interactions with hydrocarbons to produce photochemical oxidants and smog; contribution to acid precipitation through nitric acid formation; and degradation of visibility and aesthetics by formation of high NO<sub>2</sub> levels in elevated plumes and fine particulate aerosols resulting from by-products of NO<sub>x</sub> reactions (Organization for Economic Cooperation and Development, 1983).

#### Sources

Over 95 percent of all the man-made nitrogen oxides that enter the atmosphere in the United States are produced by the combustion of fossil fuels. As of 1990, over 55 percent of these emissions are attributed to stationary sources, such as utility and industrial boilers, gas turbines, and stationary engines. Approximately 40 percent are from mobile sources (transportation). The remaining fraction is from miscellaneous sources including industrial processes and waste disposal. On a global scale, the anthropogenic NO<sub>x</sub> emission rate is minor compared to natural emissions and formation in the environment. As a result, air pollution associated with NO<sub>x</sub> is mainly a local or regional problem (Cooper and Alley, 1994; Wark and Warner, 1981).

The level of effect of nitrogen oxides on the local environment is highly dependent upon the emission rates of sources and prevailing meteorological conditions and topological

features in the local area. At an emission source, the concentration of nitrogen oxides is much higher than ambient background levels. Emission rates vary widely depending on the type of source and type of fuel used, as well as on the type and quality of pollution control equipment employed. This variation in  $\text{NO}_x$  production rates for uncontrolled sources is quite evident in Table 1-2.

From Table 1-2, it can be seen that an individual aircraft appears to emit negligible amounts of nitrogen oxides when compared to much larger combustion sources. However, recent studies by Johnson et al. (1992) indicate that aircraft emissions into the troposphere at an altitude above 10 km produce increased concentrations of ozone, off-setting ozone depletion, but contributing to increased surface temperatures ("global warming"). Modeling suggests that the radiative forcing of surface temperature is about 30 times more sensitive to aircraft emissions of nitrogen oxides than surface emissions. In the vicinity of an airport or Air Force base, where ground operations (taxiing, take-offs, landings, and maintenance in engine test cells) are combined with flight operations for a large number of aircraft, the contribution of pollutants in the local area due to nitrogen oxides can be significant.  $\text{NO}_x$  standards have traditionally not been enforced for jet engine test cells, which qualify for regulation as stationary sources. Gas turbine engines operating as mobile sources also have not been regulated in the past. Evolving regulations including the 1990 Clean Air Act Amendments, the failure of existing controls on stationary industrial processes to significantly lower urban ozone concentrations, and a demonstrated correlation between ozone levels and

Table 1-2. Emission Factors for Nitrogen Oxides (NO<sub>x</sub> as NO<sub>2</sub>)

Source	Average Emission Factor (as NO <sub>2</sub> )
Coal	
Household and commercial	8 lb/ton of coal burned
Industry and utilities	20 lb/ton of coal burned
Fuel Oil	
Household and commercial	12-72 lb/1000 gal of oil burned
Industry	72 lb/1000 gal of oil burned
Utility	104 lb/1000 gal of oil burned
Natural Gas	
Household and commercial	116 lb/million ft <sup>3</sup> of gas burned
Industry	214 lb/million ft <sup>3</sup> of gas burned
Utilities	390 lb/million ft <sup>3</sup> of gas burned
Gas Turbines	200 lb/million ft <sup>3</sup> of gas burned
Waste Disposal	
Conical incinerator	0.65 lb/ton of waste burned
Municipal incinerator	2 lb/ton of waste burned
Mobile Source Combustion	
Gasoline-powered vehicle	113 lb/1000 gal of gasoline burned
Diesel-powered vehicle	222 lb/1000 gal of oil burned
Aircraft	
Conventional	23 lb/flight per engine
Fan-type jet	9.2 lb/flight per engine
Nitric Acid Manufacture	57 lb/ton of acid product

Source: Wark and Warner, 1981 (Based upon U.S. EPA AP-67, 1970).

NO<sub>x</sub> concentrations seem to point toward increased regulatory pressure to reduce NO<sub>x</sub> emissions from jet engine test cell activities in the near future.

### NO<sub>x</sub> Formation

If NO<sub>x</sub> standards for test cell emissions are to be considered, clearly those systems available for controlling these emissions must be thoroughly evaluated. To reduce NO<sub>x</sub> emissions, two primary actions can be taken. These are the direct control of the reaction(s) producing the pollutant (combustion process), or control of the process effluent. To understand the means of controlling NO<sub>x</sub> emissions, it is critical to examine the basic chemistry, thermodynamics, and kinetics of the formation reactions. Oxides of nitrogen formed by combustion processes are generally caused either by the conversion of chemically bound nitrogen in the fuel ("fuel NO<sub>x</sub>"), or by thermal fixation of atmospheric nitrogen in the combustion air ("thermal NO<sub>x</sub>").

The principal factors affecting the formation of nitrogen oxides in combustion processes are the amount of fuel-bound nitrogen, peak combustion temperature, oxygen level at peak temperature, and residence time in the combustion zone (Organization for Economic Cooperation and Development, 1983).

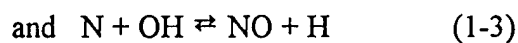
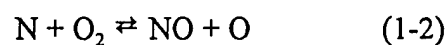
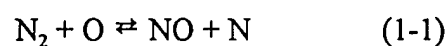
### Fuel NO<sub>x</sub>

When a fuel containing organically bound nitrogen is burned, the contribution of the fuel-bound nitrogen to total NO<sub>x</sub> can be significant. The N-C bond is much weaker than the N-N bond in molecular nitrogen, so fuel nitrogen can be more easily oxidized to NO by

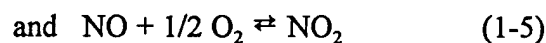
oxygen in the combustion gas. The mechanism of the conversion of fuel nitrogen is believed to proceed via a series of intermediates. One of the most important intermediates is hydrogen cyanide (HCN), which is fully converted from bound nitrogen in the reaction zone of the flame. Moving away from the reaction zone, the amount of HCN decreases as a result of its conversion into  $N_2$  and  $NO_x$ . Ammonia ( $NH_3$ ) may be detected along with  $N_2$ , HCN, and  $NO_x$  in the products of combustion of nitrogen-containing fuels in the presence of a deficiency of atmospheric nitrogen. The conversion of fuel nitrogen into HCN is rapid, and the rate-limiting stage in the formation of  $NO_x$  is the oxidation of HCN. The yield of  $NO_x$  is influenced by the content of nitrogen in the fuel, the amount of excess air, and, to a lesser extent, combustion temperature (Ismagilov et al., 1990; Cooper and Alley, 1994; Wark and Warner, 1981).

#### Thermal $NO_x$

Due to the extremely high temperatures in the combustion zones of aircraft jet engines (up to 2500 K), thermal nitrogen oxides are formed by the oxidation of atmospheric nitrogen. The accepted model for the chemical reactions responsible for  $NO_x$  formation in the post-combustion zone was developed by Zeldovich in 1946. The reactions in Zeldovich's model are as follows:



In presenting these reactions, it is assumed that the fuel combustion reactions (between C, H, and O) have reached equilibrium and that the concentrations of O, H, and OH can be described by equilibrium equations. Considering only the thermodynamics of NO<sub>x</sub> formation, the two overall reactions of concern are those which produce NO and NO<sub>2</sub>. The relevant equilibrium reactions are



The equilibrium constants for reactions (1-4) and (1-5) ( $K_{p1}$  and  $K_{p2}$ , respectively) are

$$K_{p1} = \frac{(P_{\text{NO}})^2}{(P_{\text{N}_2})P_{\text{O}_2}} = \frac{(Y_{\text{NO}})^2}{(Y_{\text{N}_2})Y_{\text{O}_2}} \quad (1-6)$$

$$K_{p2} = \frac{(P_{\text{NO}_2})}{P_{\text{NO}}(P_{\text{O}_2})^{1/2}} = \frac{(P_T)^{-1/2}(Y_{\text{NO}_2})}{Y_{\text{NO}}(Y_{\text{O}_2})^{1/2}} \quad (1-7)$$

where:  $K_p$  = equilibrium constant,

$P_i$  = partial pressure of component  $i$  (atm),

$Y_i$  = mole fraction of component  $i$ ,

and  $P_T$  = total pressure (atm).

An analysis of values for  $K_{p1}$  and  $K_{p2}$  at various temperatures indicates that thermodynamically, the forward reaction in (1-5) is favored over the forward reaction in (1-4) at low temperatures, with very little NO formed at temperatures below 1000 K. Hence, the

formation of  $\text{NO}_2$  is favored at low temperatures, but  $\text{NO}_2$  dissociates back to  $\text{NO}$  at higher temperatures. The rate of equilibrium  $\text{NO}$  formation increases rapidly with increasing temperature. As the combustion zone temperature rises above 1000 K, the formation of  $\text{NO}_2$  becomes less likely under equilibrium conditions. Kinetically, however, the  $\text{NO}$  formation reaction is a slow one, which affects the availability of reactant to form  $\text{NO}_2$ .  $\text{NO}$  formation by reaction (1-1) has a very high activation energy (317 kilojoules/mole) and is most likely the rate-controlling reaction (Ismagilov et al., 1990).

It has been observed experimentally that  $\text{NO}$  concentrations in the combustion flame zone are significantly higher than those predicted by the Zeldovich mechanism. This "prompt"  $\text{NO}$  formation is attributed to super-equilibrium radical concentrations that are likely in hydrocarbon flames. It has been suggested that the intermediate,  $\text{HCN}$ , is formed when  $\text{N}_2$  reacts with a hydrocarbon radical.  $\text{HCN}$  combines with  $\text{OH}$  to form  $\text{CN}$ , and then  $\text{CN}$  is oxidized to  $\text{NO}$ . Based upon experimental data, MacKinnon (1974) developed a model that predicts the concentration of  $\text{NO}$  formed during combustion as a function of temperature,  $\text{N}_2$  and  $\text{O}_2$  concentrations, and time. At a total pressure of one atmosphere, the model equation is:

$$C_{\text{NO}} = 5.2 \times 10^{17} (\exp -72000/T) Y_{\text{N}_2}(Y_{\text{O}_2})^{1/2} t \quad (1-8)$$

where:  $C_{\text{NO}}$  =  $\text{NO}$  concentration (ppm),

$T$  = absolute temperature ( $^{\circ}\text{K}$ ),

$Y_i$  = mole fraction of component  $i$ ,

and  $t$  = time (seconds).



Consideration of equation (1-8) allows insight into the effect of temperature on NO formation, particularly in the hot flame zone. Once exhaust gases move away from this zone, they cool rapidly, reducing the reaction rates by orders of magnitude. If excess oxygen is present as the gas cools, the conversion of NO to NO<sub>2</sub> (reaction (1-5)) is favored. Thermodynamics predicts that the cooled gas will consist primarily of NO<sub>2</sub>. In reality, although the favored ambient form of NO<sub>x</sub> is NO<sub>2</sub>, flue gases from combustion contain predominantly NO. Approximately 90 to 95 percent of NO<sub>x</sub> emitted from combustion processes appears as NO, that is thermodynamically unstable in the environment as its temperature drops. However, the decomposition of NO into N<sub>2</sub> and O<sub>2</sub> and the reaction of NO with O<sub>2</sub> to form NO<sub>2</sub> are kinetically limited. Thus, the high concentrations of NO formed at high temperature in the combustion zone are "frozen in" and are carried out with exhaust gases into the atmosphere. From equation (1-8), therefore, it is seen that, with respect to the reduction of thermal NO<sub>x</sub>, combustion control strategies could be developed that are aimed at a reduction in peak temperature, a reduction in gas residence time at peak temperature, and a reduction of oxygen concentration in the high-temperature zone (Cooper and Alley, 1994; Wark and Warner, 1981; Organization for Economic Cooperation and Development, 1983).

### Regulation of NO<sub>x</sub> Emissions

The federal primary air quality standard for NO<sub>2</sub> is presently 0.05 ppm, based upon an annual arithmetic mean. Emission and performance standards for various stationary sources of NO<sub>x</sub> have also been established. Although the exhaust from jet engine test cells

(JETCs) is regulated for soot opacity, JETCs currently operate under implicit exemption from  $\text{NO}_x$  regulations, although they qualify as stationary sources. If jet engine testing operations are conducted in an ozone non-attainment area or where photochemical smog is already a significant problem, they become obvious targets for environmental regulation. Mobile sources are regulated under Title II of the Clean Air Act Amendments of 1990. Part B of these amendments addresses aircraft emission standards. A jet engine in a test cell could be considered to be a stationary source under Title I, and may be included for regulation under Title IV, Acid Deposition Control (Quarles and Lewis, 1990). In anticipation of these possibilities, the Administrator of the EPA and the Secretary of Transportation, in concert with the Secretary of Defense, have commissioned an investigation into the implications of regulating jet engine test cells. Some of the issues studied included the impacts of not controlling nitrogen oxides, the existence of appropriate control technologies, costs associated with these technologies and their effects on safety, design, structure, and operation or performance of aircraft engines and performance tests in test cells (EPA-453/R-94-068). After the recommendations of this study are evaluated,  $\text{NO}_x$  emission standards for jet engine test cells may be promulgated and enforced in the near future. A review of the most common  $\text{NO}_x$  control methods for stationary sources is useful for the consideration of their applicability to JETC exhaust control.

## NO<sub>x</sub> Controls for Stationary Sources

### Application of NO<sub>x</sub> Control Strategies

Based upon well characterized chemical and thermodynamic principles that control the formation of fuel and thermal NO<sub>x</sub>, several combustion modifications or changes to operating conditions can be used for these purposes. In power generation and some waste disposal applications, "low NO<sub>x</sub>" burners have been developed whose designs inhibit NO<sub>x</sub> formation by controlling the mixing of fuel and air. While some research is being conducted on jet engine designs to reduce NO<sub>x</sub> production (Beard, 1990), this approach needs to be evaluated for its applicability in light of strict and specialized military engine performance requirements and standards. Combustion modifications can reduce NO<sub>x</sub> formation by lowering one or more of the parameters: peak temperature, gas residence time, or oxygen concentration in the flame zone. It is difficult to employ these controls in a JETC application due to the changing power settings associated with test and acceptance runs and associated combustion exhaust fluctuations. Additionally, strict performance standards required during engine testing limit the applicability of combustion modifications which may make test results unrepresentative.

### Modifications to Operating Conditions

Several modifications to stationary and mobile source operating conditions have been developed that can be used to reduce  $\text{NO}_x$  formation from combustion. These include 1) low-excess-air firing; 2) off-stoichiometric combustion; 3) flue gas recirculation; 4) reduced air preheat; 5) reduced firing rates; and 6) water injection. Excess air is the amount of air that is in excess of the amount stoichiometrically required for 100 percent combustion of the fuel. Due to imperfect mixing of air and fuel in the combustion zone, there must be some excess air present at all times to reduce fuel waste and to prevent smoke formation. As excess air decreases,  $\text{NO}_x$  follows, while using less fuel. Off-stoichiometric combustion (also called staged-combustion) burns the fuel in two or more steps. The initial flame zone is fuel-rich, and the following zone(s) is (are) fuel-lean. Combustion with remaining air in the resulting fuel-rich regions in the primary flame zone are controlled by heat transfer. Although the overall air/fuel ratio is near stoichiometric, the primary  $\text{NO}_x$  formation zone of the flame is operated in a low- $\text{NO}_x$  condition.

Rerouting some of the flue gas back to the burner primary combustion zone is called flue gas recirculation. This process not only reduces the peak flame temperature, but also lowers the partial pressure of available oxygen at the burner, thereby decreasing  $\text{NO}_x$  formation. Reducing the amount of combustion-air preheat lowers the peak temperature in the primary combustion zone, decreasing thermal  $\text{NO}_x$  production. Since JETCs operate using ambient air as combustion air, this technique is obviously not applicable to these operations. Likewise, reduced firing rates to reduce heat release per unit volume cannot be

implemented under the strict protocols of jet engine testing. Water or steam injection into the fuel, combustion air, or combustion zone is very effective at reducing  $\text{NO}_x$  formation by reducing combustion temperatures (Cooper and Alley, 1994). Introducing additives into jet engine combustion zones or fuels, however, is a potential problem due to losses in output (which is closely monitored during testing) or physical damage to the engine or turbine blades. Some research has been conducted on other fuel or combustion zone additives as applied to jet engine test cells, which will be discussed in the following sections.

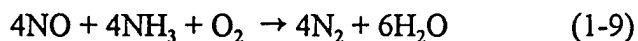
#### Combustion Modifications

Combustion modifications can reduce  $\text{NO}_x$  formation by lowering one or more of the parameters peak temperature, gas residence time, or oxygen concentration in the flame zone. Peak temperatures can be reduced by 1) using a fuel-rich primary flame zone; 2) increasing the rate of flame cooling; or 3) decreasing the adiabatic flame temperature by dilution (exhaust gas recirculation). Gas residence time in the primary flame zone can be reduced by 1) changing the shape of the flame zone; or 2) using the steps listed in the previous strategy. Oxygen concentration in the flame zone can be reduced by 1) decreasing the overall excess air rates; 2) controlling the mixing of fuel and air; and 3) using a fuel-rich primary flame zone (Cooper and Alley, 1994). In general, it is difficult to employ these controls in a jet engine test cell application due to the changing power settings associated with test and acceptance runs and associated performance fluctuations. Additionally, the strict performance standards required during military jet engine testing limit the applicability of combustion modifications.

### Exhaust Gas Treatment

Exhaust gas treatment appears to be the most applicable method of controlling NO<sub>x</sub> emissions due to the difficulty in using combustion/operations modifications with JETCs and the priority placed on unperturbed engine performance during testing. The high volume of exhaust from a military jet engine, combined with the need for higher levels of NO<sub>x</sub> reduction, makes the selection of the optimal exhaust gas treatment a difficult task. There are two main types of exhaust gas treatment processes, wet and dry processes. Wet processes typically employ the absorption of NO<sub>x</sub>. The main disadvantage of wet absorption is the low solubility of NO. Additionally, these processes often create liquid waste that may require proper disposal at significant cost. For these reasons, dry processes are generally preferred. These include selective or non-selective catalytic reduction, selective non-catalytic reduction, irradiation, and dry sorption (Cooper and Alley, 1994).

In selective catalytic reduction, only the NO<sub>x</sub> species are reduced (to N<sub>2</sub> gas), leaving free oxygen unreacted. With a suitable catalyst (typically a precious metal, although a variety of other catalysts have been studied) ammonia (NH<sub>3</sub>), hydrogen (H<sub>2</sub>), carbon monoxide (CO), or hydrogen sulfide (H<sub>2</sub>S) can be used as the reducing gas. NH<sub>3</sub> is the most commonly used gas. A number of stoichiometries have been proposed for this reaction. For example, Davini (1988) suggested



Although the selective catalytic reduction process is very effective and is capable of achieving NO reduction rates exceeding 90 percent in controlling steady-state processes, its

application to JETCs is expensive and involved compared to other treatments. At temperatures from 900 to 1000 C,  $\text{NH}_3$  will reduce  $\text{NO}_x$  to  $\text{N}_2$  without a catalyst; however,  $\text{NO}_x$  reduction efficiencies are only 40-60 percent. If the temperature is too low, unreacted  $\text{NH}_3$  will be emitted ("ammonia slip"), and if the temperature is too high,  $\text{NH}_3$  can be oxidized to NO. Thus both of these situations are obvious problems. Dry sorption techniques have the advantage of simplicity of operation and minimization of waste effluent. Relatively high  $\text{NO}_x$  reduction rates have been documented (Nelson et al., 1989; Lyon, 1991).

## CHAPTER 2

### CONTROL OF NO<sub>x</sub> THROUGH GAS-SOLID INTERACTION

#### Exhaust-Gas Treatment Methods

A significant amount of research has been conducted over the past two decades to determine a means of treating flue gases to reduce nitrogen oxide emissions. Some of the most extensive research has been conducted in Japan, which was one of the first countries to enact strict NO<sub>x</sub> emission regulations. In general, three classes of catalytic methods have been evaluated. The first class involves mixing the waste gas with methane (CH<sub>4</sub>) or other gaseous fuels/reducing agents before exposing the mixture to a catalyst; the second involves mixing the effluent with ammonia before exposure to a catalyst; and the third involves exposure to a catalyst or adsorbent with or without methane (or other fuel) or ammonia additions. Numerous materials have been proposed as catalysts, and a number of these have been patented, however, those receiving the most attention have been platinum or other precious metals or metallic oxides from the alkaline earth group (Nelson et al., 1989; Klimisch and Larson, 1975; Meubus, 1977).



### Catalytic Methods

Cohn [U.S. Patent 3,118,727 (1964)] has been issued a patent that describes a process for purifying waste gases containing nitrogen oxides by mixing them with a fuel (such as  $\text{CH}_4$ ) and passing the mixture over a platinum- or rhodium-containing catalyst at an initial reaction temperature of 690-780 F. Acres and Hutchings [U.S. Patent 3,806,582 (1974)] describe a similar process. Childers, Ellis, and Ryan [U.S. Patent 2,910,343 (1959)] describe a methane process involving two catalyst beds in series, one containing platinum or alumina and the second containing nickel or alumina. Vanadium oxide, molybdenum oxide and/or tungsten oxide catalysts on alumina or silicic acid substrates were used in combination with  $\text{CH}_4$  as described by Nonnenmacher and Kartte [U.S. Patent 3,279,884 (1966)]. Such base metal catalysts as iron, cobalt, nickel and copper dispersed on a refractory support were used by Reitmeier [U.S. Patent 2,924,504 (1960)]. Other patents relating to the use of methane and precious metal catalysts for the removal of  $\text{NO}_x$  from waste or tail gases include those of Andersen and Green [U.S. Patent 2,970,034 (1961)]; Romeo [U.S. Patent 3,425,803 (1969)]; Newman [U.S. Patent 3,467,492 (1969)]; Kandell and Nemes [U.S. Patent 3,567,367 (1971)]; Andersen, Romeo, and Green [U.S. Patent 3,098,712 (1963)]; and Hardison and Barr [U.S. Patent 3,402,015 (1968)] (Nelson et al., 1989; Lewis, 1975).

The use of ammonia as a reducing gas in the presence of a catalyst was described earlier. Baiker et al. (1987a, 1987b) and Chen et al. (1990) describe the selective catalytic reduction of nitric oxide with ammonia upon catalysts comprised of mono- and multi-layers of vanadia supported on titania, and mono-layers of vanadia immobilized on titania-silica

mixed gels. Davini (1988) studied the reduction of nitrogen oxide with ammonia in the presence of carbonaceous soots from industrial boilers. Lee and Kline [U.S. Patent 3,864,451 (1975)] describe a method for removing NO in the presence of sulfur dioxide by mixing ammonia with the flue gas in the presence of a catalyst selected from the group of platinum and transition metals and oxides and mixtures of these. Andersen and Keith [U.S. Patent 3,008,796 (1961)] have described the use of  $\text{NH}_3$  in combination with cobalt, nickel, or iron supported on alumina, silica, silica gel, or diatomaceous earth. Lyon (1987) describes an improved method using ammonium injection in a tightly controlled noncatalytic process. A problem with this method is the formation of ammonium salt particulate matter. Other patents relating to the use of ammonia and precious metal or other catalysts for the removal of oxides of nitrogen from a waste or tail gas include those of Cohn, Steele, and Andersen [U.S. Patent 2,975,025 (1961)] and Keith and Kenah [U.S. Patents 3,245,920 (1966); and 3,328,155 (1967)] (Nelson et al., 1989).

Control of nitrogen oxides is also attainable by several processes that do not utilize methane or ammonia, because the latter may be difficult to control. Additionally, the desired ammonia reaction occurs only within a narrow range of temperatures. One process that received great attention was the "RAPRENO<sub>x</sub>" selective reduction reaction first developed by Perry and Siebers (1986). In this process, cyanuric acid (non-toxic) is mixed with NO<sub>x</sub>-containing exhaust gases from which the NO<sub>x</sub> concentration (as NO) is significantly reduced (NTIS Tech Notes, 1987). Heap et al. (1988) combined this technology with combustion modification techniques to further improve the reduction of NO<sub>x</sub>. Unfortunately, it appears that this reaction is negatively affected by the presence of free oxygen (Wicke et al., 1989).

It has been determined that various alkali metal oxides and silicate materials can reduce nitrogen oxides without additional methane or ammonia. Harris, Morello, and Peters [U.S. Patent 3,459,494 (1969)] have successfully evaluated  $\text{CaO}$ ,  $\text{SrO}$ ,  $\text{BaO}$ ,  $\text{K}_2\text{O}$ ,  $\text{Na}_2\text{O}$  and others supported on Alundum cement, porcelain, silica, extended alumina, or alumina beads. Heavy-metal catalysts (copper, silver, nickel, molybdenum, palladium, and cobalt), supported on alumina were patented by Ryason [U.S. Patent 3,454,355 (1969)]. The catalytic properties of copper for the reduction of  $\text{NO}_x$  without added methane or ammonia are described by various investigators, including Gehri and Frevel [U.S. Patent 3,718,733 (1973)] and Kressley [U.S. Patent 3,682,585 (1972)]. Kranc and Lutchko [U.S. Patent 3,576,596 (1971)] employed a combination of copper and chromium impregnated on carbon supports to remove both  $\text{NO}$  and  $\text{CO}$  from a waste gas.

#### Non-Catalytic Methods

Many problems associated with catalytic control methods often make the use of non-catalytic methods more appealing. The most common problems with catalytic techniques include catalyst fouling or poisoning, and a narrow range of operating temperatures. These problems can be avoided by using non-catalytic controls. A number of dry sorption techniques that do not employ catalysts have also been evaluated as they apply to the control of nitrogen oxides. Ganz (1958) evaluated activated carbon, aluminosilicate, silica gel, manganese dioxide, copper dioxide, and coke for the removal of high concentrations of  $\text{NO}_2$  and found aluminosilicate to be the most suitable sorbent. Kyollen [U.S. Patent 3,498,743 (1970)] described a process employing either sodium carbonate, calcium carbonate, or

calcium oxide, that was highly dependent upon temperature and humidity conditions. Kitagawa [U.S. Patent 3,382,033 (1968)] developed a dry method that utilizes inorganic salts such as  $\text{PbSO}_4$ ,  $\text{KMnO}_4$ ,  $\text{KClO}_3$ ,  $\text{NaClO}$ ,  $\text{Na}_2\text{MO}_4$ ,  $\text{K}_2\text{S}_2\text{O}_3$ , and  $\text{Na}_2\text{HPO}_4$  and inorganic oxides like  $\text{AsO}_3$  and  $\text{PbO}_2$  as suitable adsorbents. Collins [U.S. Patent 3,674,429 (1972)] derived a two-stage process involving silica gel and an activated crystalline zeolitic molecular sieve. The use of activated carbon to adsorb nitrogen oxides has been studied extensively (Badjai et al., 1958 (Wark and Warner, 1981)). Its high surface area, adsorption rate and capacity, and regenerability are well known. James and Hughes (1977) used calcined limestones and dolomites (MgO-containing) to remove NO at high concentrations with good results. Kikkinides and Yang (1991) reported some success in the simultaneous sorption of  $\text{NO}_2$  and  $\text{SO}_2$  using a weak-base macroreticular resin material.

### Jet Engine Test Cells

With all of the previous research that has been conducted for application to industrial processes and power generation equipment, relatively little has been done to specifically address the control of  $\text{NO}_x$  from jet engine test cells. In order to better understand the problems associated with  $\text{NO}_x$  control in jet engine test cells, it is useful to examine their general structure, purpose and characteristics. The Department of Defense operates approximately 180 cells, which are considered to be stationary sources by the U.S. EPA. The purpose of a jet engine test cell is to provide a structure to evaluate engine performance during controlled testing after maintenance to assure proper operation before returning the

jet engine to service. The engines are operated over their full range of thrust, representative of typical operational modes. Total test times can range from less than an hour to two to eight hours. The most common jet engine test cell design is shown in Figure 2-1. The engine to be tested is mounted horizontally in the U- or L-shaped enclosure and combustion air is drawn in through sound-deadening baffles. Unequal flow distributions are corrected by turning vanes to provide an undistorted airflow at the engine outlet at a specified velocity (often  $< 50$  feet per second). Exhaust gases are blown into a large, long tube (augmenter tube) with a convergent entrance section. The purposes of the augmenter are to draw air into the test cell and engine with equal air pressure at the inlet and outlet of the engine (Note venturi shape), to draw a portion of the air around the engine housing to provide cooling similar to that experienced during flight, and to dilute and cool engine exhaust to prevent damage to construction materials. Augmented gas temperatures can vary from about 200 to 2000 F (100-1100 C) depending upon engine firing rate and augmentation ratio. Generally, the temperature of these gases is less than 500 F (260 C). The augmentation ratio is varied by the placement of the engine relative to the augmenter throat. Some augmenter tubes contain cooling water sprays to further quench the exhaust gases. Exhaust gases exit the augmenter tube through a perforated basket, which helps to dissipate some jet engine exhaust momentum as well as acoustical energy. In some cases, this basket can be adjusted to reduce back pressure on the engine. Gases leaving the augmenter tube fill a blast room before exiting the test cell through a stack. Cooled exhaust is vented to the atmosphere through multiple channels within the stack to minimize noise (Johnson and Katz, 1990). Depending upon the engine being tested, the volume flow rate of gas leaving the cell can be

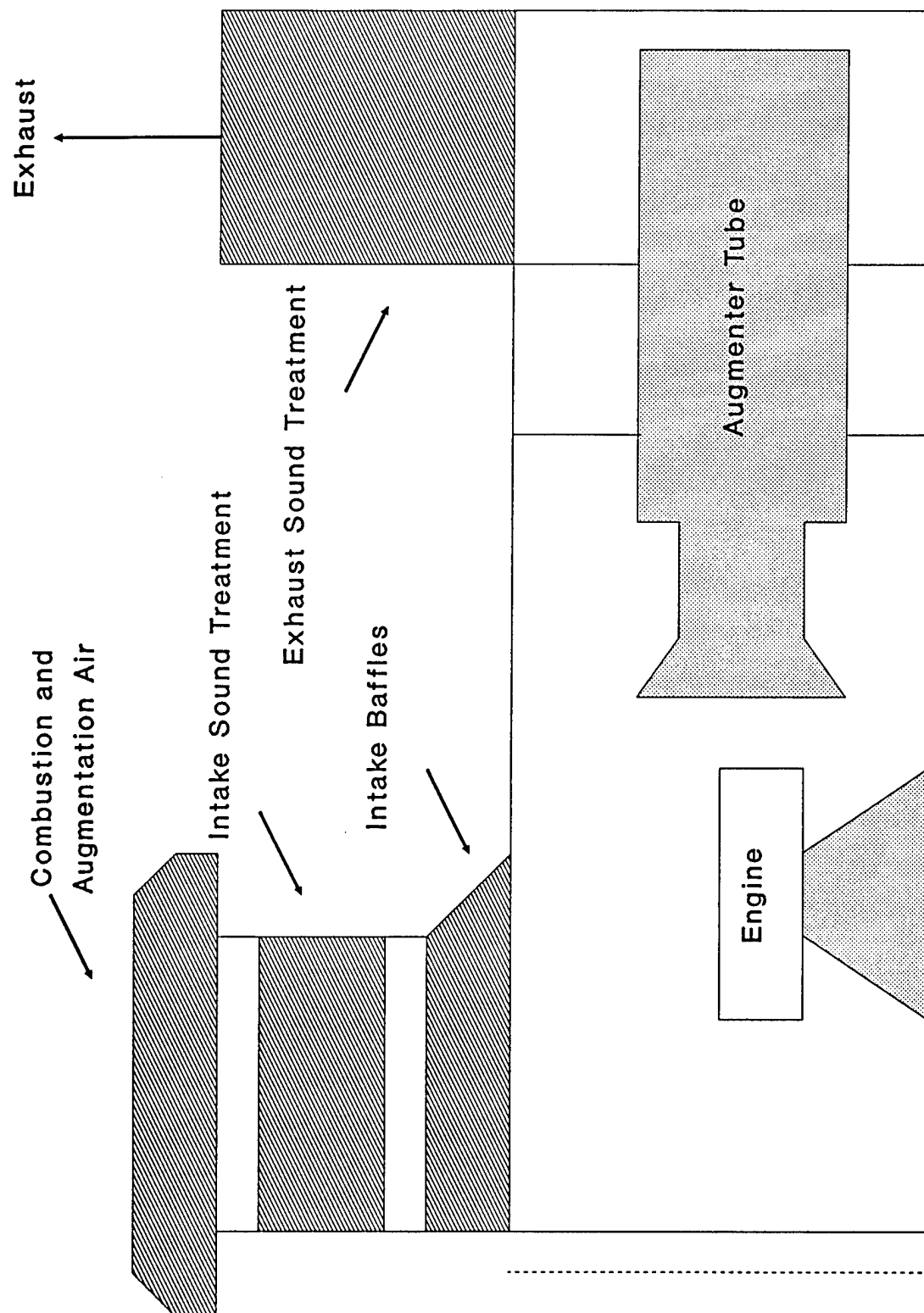


Figure 2-1. Schematic Representation of a Jet Engine Test Cell.

enormous. A unique feature of jet engine test cells is their highly variable test cycles (and  $\text{NO}_x$  production associated with varying peak flame temperature). Because of this variability, a  $\text{NO}_x$  control technology applicable to jet engine test cells must perform over a wide range of rapidly varying operating conditions.

#### Research Sponsored by the U.S. Air Force (USAF)

The Air Force (through the USAF Engineering and Services Center and USAF Civil Engineering Support Agency, now the Human Systems Center-Armstrong Laboratory, Tyndall AFB, Florida) has recently sponsored seven independent projects that specifically target the control of  $\text{NO}_x$  from JETCs. Johnson and Katz (1989) showed that reburning of exhaust with extra fuel was effective, but not economical. Ham et al. (1989) reported partial success with non-catalytic reduction using additives (ammonia, amines, and hydrazines) to simulated exhaust. Unfortunately, as temperature increased,  $\text{NO}_x$  production increased. A dual-bed mordenite-copper catalyst did offer some improvement in sensitivity to variable conditions over some better known selective catalysts (Kittrell, 1991). Berman et al. (1991) evaluated the photopromotion of NO thermal decomposition by various metallic oxides. This decomposition was very effective, but only in the absence of oxygen. Initial work reported by Petrik (1991) also found that  $\text{NO}_x$  reduction by ceramic-supported electrocatalysts was inhibited by even trace amounts of oxygen; however, continued development of these materials has produced catalytic ceramics that may be effective inside the jet engine (Gordon, 1994). Lyon (1991) evaluated  $\text{NO}_x$  reduction at the surface of heavier Group IIa oxides, but

the toxicity of these heavy metals is a detriment. The seventh study, which was selected for development, involved vermiculite and magnesium oxide (MgO)-coated vermiculite. NO<sub>x</sub> removal rates for this medium were appealing, and the technology has many other advantages including economics, simplicity, regenerability, and particularly, insensitivity to changes in exhaust gas conditions or composition (Nelson et al., 1989). The USAF has sponsored numerous studies in order to quantify emissions from jet engines. Seitchek (1985), Fagin (1988), and Spicer et al. (1990) have published jet engine emission values for many engines in the USAF-inventory operating on JP-4 jet fuel. Similar studies are underway for emissions associated with the combustion of JP-8 fuels. These documents describe NO<sub>x</sub> and other combustion by-product emission rates correlated with power setting or operational procedures. They are very useful for determining appropriate exhaust gas concentrations in order to simulate jet engine exhaust gas composition in the laboratory. Many lab-scale studies have used these data in their experimental design.

#### Vermiculite-based Catalyst

Vermiculite ((Mg,Fe<sup>m</sup>,Al)<sub>3</sub>(Al,Si)<sub>4</sub>O<sub>10</sub>(OH)<sub>2</sub>·4H<sub>2</sub>O, a thermally expanded form of a common aluminosilicate material) has been used as a carrier for other materials including nitrates and phosphates, in which the combinations are used as slow-release fertilizers. Evanshen [U.S. Patent 3,757,489 (1973)] describes the treatment of flue gases with polyvinylpyrrolidone with or without the addition of a catalyst of a nitrate or sulfate of copper or silver. He suggested suspending these materials on a carrier such as vermiculite. Sanitech, Inc., (now Sorbent Technologies Corporation, Twinsburg, Ohio) developed a new class of



sorbents originally designed for the control of  $\text{SO}_2$ , that were based upon  $\text{MgO}$  (an alkaline earth [IIa] metal oxide) coated onto vermiculite or perlite [Nelson, U.S. Patents 4,721,582; 4,786,484, 1988; and 4,829,036 (1989)].  $\text{SO}_2$  reduction is believed to occur primarily by reaction with  $\text{MgO}$ , forming complex sulfites or sulfates. It was assumed that  $\text{NO}_x$  could be removed in a similar manner, forming nitrites or nitrates. Sanitech researchers began evaluating expanded vermiculite as a catalyst in 1987. A patent describing the use of vermiculite as a selective reduction catalyst [US Patent 4,806,320] was granted to Sanitech in 1989.

In August 1988, the Air Force awarded Sanitech a Small Business Innovation Research (SBIR) project to further develop the new catalyst for application to jet engine test cells. Nelson et al. (1989) reported the results of a series of tests designed to establish the applicability and technical feasibility of using vermiculite as a catalyst to reduce  $\text{NO}_x$  from simulated jet engine exhaust. These studies, beginning as a selective-catalytic approach, evaluated how vermiculite variables (type and size), bed size, solid additives to vermiculite, flue gas variables (temperature, composition, flow rate) and the addition of methane or ammonia to the exhaust gases generally affected  $\text{NO}_x$  reduction.

Some initial regeneration studies were also performed. These screening studies indicated that a  $\text{MgO}$ -coated vermiculite material showed great promise as a  $\text{NO}_x$ -reducing agent for a wider variety of conditions than encompassed by commercial catalysts. Some of the major conclusions of this study included data indicating that vermiculite alone, without ammonia or methane additions, demonstrates the ability to reduce  $\text{NO}_x$  by 50 to 73 percent over the temperature range of 250-850 F. The use of gaseous ammonia only marginally

improved NO<sub>x</sub> reduction and increased the sensitivity of the process to temperature change. Vermiculite coated with MgO removed approximately 70 percent of NO<sub>x</sub> and the process was relatively insensitive to changes in waste gas composition, velocity and temperature.

It is believed that the NO<sub>x</sub> species were chemically adsorbed by the MgO/vermiculite product and attached at the surface as complex magnesium nitrites and/or nitrates. Tanabe and Fukuda (1974) found that MgO has a higher number of active (basic) sites compared to other alkaline earth metal oxides (i.e., CaO, SrO and BaO). Zhang et al. (1994) further attributed the activity of MgO surfaces to oxygen vacancies in the lattice structure. Some selected physical properties of MgO, Mg(OH)<sub>2</sub>, and magnesium nitrite and nitrates are shown in Table 2-1.

Table 2-1. Physical properties of selected Mg-containing inorganic compounds.

Species	Mol Wt (g/g-mol)	Density (g/cm <sup>3</sup> )	Mol Vol (cm <sup>3</sup> /g-mol)	Melting Point (°C)	Boiling Point (°C)
MgO	40.30	3.58	11.26	2852	3600
Mg(OH) <sub>2</sub>	58.32	2.36	24.71	See Note	-----
Mg(NO <sub>2</sub> ) <sub>2</sub> ·3H <sub>2</sub> O	170.36	-----	-----	Decomp 100	-----
Mg(NO <sub>3</sub> ) <sub>2</sub> ·2H <sub>2</sub> O	184.35	2.03	90.81	129	-----
Mg(NO <sub>3</sub> ) <sub>2</sub> ·6H <sub>2</sub> O	256.41	1.64	156.35	89	Decomp 330

Note: Loses water of hydration at 350 C.

Source: CRC Handbook of Chemistry and Physics, 73rd Edition, 1992.

Initial studies found that the sorbent material could be successfully regenerated with minor reduction in adsorption capacity of the regenerated material. Ruch et al. (1990) confirmed that the  $\text{MgO}$ –vermiculite/ $\text{NO}_x$  reaction is most likely due to chemisorption and that the vermiculite/ $\text{NO}_x$  sorption is a result of physical adsorption based upon hysteresis during limited adsorption/desorption tests. This observed hysteresis is most probably the result of the forces of chemisorption, generally involving electron transfer between the solid (adsorbent) and gas (adsorbate) molecules held at the surface. These forces are typically much stronger than the intermolecular van der Waals forces associated with physical adsorption (Kovach, 1978; Szekely et al., 1976). They also evaluated the surface areas of these products using  $\text{N}_2$  and water adsorption and Brunauer–Emmett–Teller (BET) theory and found the sorbent surface areas to be larger than would be expected from the collective surface areas of the vermiculite and  $\text{MgO}$ . This suggests that the vermiculite support effectively enhances the surface area development of the  $\text{MgO}$ . Reported nitrogen isotherm surface areas ranged from 16 to 55  $\text{m}^2/\text{g}$  for sorbents prepared at 550 C. Sieved samples had a maximum surface area of 36  $\text{m}^2/\text{g}$ . Fourier transform infrared (FTIR) solid spectra indicated the presence of  $\text{Mg}(\text{OH})_2$ , which disappeared as conditioning temperature increased. Nitrite was found in some samples exposed to low-concentration flue gases by FTIR solid and solution spectra, but results were determined to be inconclusive. X-ray diffraction interplanar spacings showed that  $\text{Mg}(\text{NO}_3)_2$  was present.

### Field Studies

Pilot-scale tests of this MgO-vermiculite sorbent were conducted on a JETC facility at Tyndall AFB, Panama City, Florida, between 9-11 June, 1992 and on 18 September, 1992. A two-stage filter bed design, consisting of four inches of virgin vermiculite in front of eight inches of MgO-coated vermiculite, was evaluated through four approximately 20 minute runs of subscale drone engines. An additional run was conducted through four inches of activated carbon, followed by the eight-inch MgO-vermiculite bed. NO<sub>x</sub> removal efficiencies for the first four tests were approximately 50 percent. This increased to approximately 80 percent with the addition of the activated carbon bed. Between June and September 1992, approximately 150 unmonitored engine tests took place. When the September 1992 test was conducted, NO<sub>x</sub> removal had decreased to 60 percent. Gas temperatures, velocities, and pressure drop through the beds were also measured. The Air Force sponsor had imposed a pressure drop limit of two inches of water on the bed, which was not exceeded. However, approximately two-thirds of the volumetric flow was allowed to bypass the filter to prevent overheating inside the JETC facility. Results showed that significant amounts of unburned (non-methane) hydrocarbons (primarily ethylene) passed through the beds that did not contain activated carbon (Nelson et al., 1992; Wander and Nelson, 1993).

More regeneration studies were conducted by Nelson et al. (1990) to attempt to optimize the regeneration of MgO-vermiculite after "saturation" with NO<sub>x</sub> (and SO<sub>2</sub>). The sorbents were alternately exposed to simulated jet engine exhaust and regenerated in reducing atmospheres for a number of treatment cycles to evaluate NO<sub>x</sub> sorption capabilities.

Performance during sorption/desorption cycles was evaluated on the basis of weight gain and loss. It appeared that there was a loss of surface area when the material was regenerated at excessively high temperatures ( $> 800$  C). Regeneration consisted of three steps: 1) drying; 2) heating to a temperature above  $550$  C (in the presence of  $N_2$ , or CO or  $CH_4$  to reduce off-gassing  $NO_x$ ); and 3) cooling. Of these, CO is the gas of choice. Heating during regeneration was accomplished using a rotary-kiln calciner, a vertical tube apparatus, and a horizontal conveyor kiln. Wickham and Koel (1988) have published an excellent review on the reduction of  $NO_x$  by CO.

#### Related Research

A review of current literature indicates that no research other than that already described has been conducted on this MgO-vermiculite sorbent. As a result, no data on intrinsic kinetics or reaction mechanism(s) exist. Significant amounts of related research, however, have been conducted on similar acid/acid anhydride gas-base/gas-solid systems. The results of these studies have been used to design and construct appropriate experimental systems to collect data for interpretation using proven and accepted sorption study techniques. A short review of some of the fundamentals of gas-solid interactions and chemisorption is necessary to better understand the complex phenomena involved in these heterogeneous systems.

### Gas-Solid Interaction

The smallest unit of a gas-solid system can be represented by the interaction between a single solid particle and a flowing gas stream. This representation is convenient and simple, and, in principle, may be generalized to more complex multi-particle systems, such as packed beds. These interactions can be catalytic, in which the solid functions as a catalyst -- often in the facilitation of a gas-phase reaction -- or non-catalytic, in which the surface acts to physically or chemically remove reactants from the gas phase.

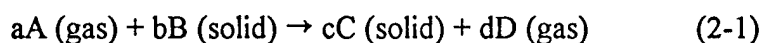
Adsorption occurs with a decrease in surface free energy and normally a decrease in entropy; as a result, it is generally an exothermic process. In physical adsorption, sorbed species are attracted and held at the solid surface by van der Waals dispersion forces. These forces are much weaker than chemical bonding forces; the heat evolved is small, generally between 1 and 10 kcal/g-mole (4-40 kJ/g-mole), approximately the heat of vapor condensation for relatively non-polar substances. Chemisorption is primarily responsible for gas-solid reactions and catalysis on solid surfaces. In chemisorption, the forces involved are of the same order of magnitude as those for chemical bonding, and the heat of chemisorption is often between 10 and 150 kcal/g-mole (40-600 kJ/g-mole). The process of physical adsorption, like condensation, has very little or no activation energy and as a result is assumed to occur rapidly. Chemisorption often displays a higher activation energy, implying a slow rate; however, chemisorption reactions having small activation energies are known. Unlike physisorption, chemisorption is specific to the gases and solids involved, just like chemical

reactions are. Chemisorption is also temperature dependent, occurring faster as temperature increases; however, the amount chemisorbed at equilibrium decreases with temperature (Hayward and Trapnell, 1964; Szekely et al., 1976 ).

Gas–solid reactions are inherently complex due to the number of simultaneous processes that occur throughout the course of reaction. Any equilibrium conditions reached are often dynamic rather than static in nature, since the system continues to change with time. In addition to mass transfer and diffusion processes, these reactions often include heat transfer and structural changes in the solid phase. Ideally, to properly describe a particular gas–solid reaction, all of these simultaneous and consecutive processes should be taken into consideration. In practicality, however, this would make for extremely complex mathematical models. A good engineering model should be one that closely approximates the real situation without too many mathematical complexities that will make it too cumbersome to use. The use of simplifying assumptions and the careful design of experiments, to reduce or limit the effects of variables on a given process so that it may be neglected, are often necessary to produce useable data and models.

#### Generalized Non-Catalytic Gas–Solid Reactions

A generalized non-catalytic gas–solid reaction may be represented by the following reaction scheme:



where A and B are gaseous and solid reactants, respectively, C and D are products, and a,b,c, and d are stoichiometric coefficients. This overall reaction may actually comprise several sequential or simultaneous steps, of which one is rate-controlling. The three basic steps in the generalized non-catalytic gas–solid diffusion-reaction process are

- 1) Gas-phase mass transfer via diffusion of the gaseous reactant from the bulk gas stream to the external surface of the solid sorbent particle.
- 2) Gas–solid interaction on or within the solid sorbent particle through
  - a) Diffusion of the gaseous reactant into the pores of the solid complex, which could consist of a combination of solid reactants and products.
  - b) Adsorption of the gaseous reactant on the surface of the solid complex.
  - c) Chemical reaction at the surface.
  - d) Desorption and diffusion of gaseous products, if any, from the surface and out of the pores of the solid complex.
- 3) Gas-phase mass transfer of any gaseous products from the external solid surface into the bulk gas stream

The number of diverse processes and steps involved makes the analysis of gas–solid reactions a potentially unwieldy problem. In general, each step provides resistance to chemical reaction, and these resistances are additive. When the processes occur in series, it is necessary to determine which step provides the major resistance to reaction, and ultimately controls the overall reaction rate. The resistances of the different steps can vary greatly from each other, so the step with the highest resistance can be considered to be the rate-controlling



step. A simplified expression for the rate-determining step can then be used to describe the overall process.

Three major processes are generally considered to be rate-controlling in non-catalytic gas–solid reactions:

- 1) Mass transfer of the gaseous reactant from the bulk gas phase through the stagnant film layer surrounding the particle to the surface of the solid sorbent. The rate of this step is most dependent upon the fluid dynamics of the gas flow around the solid particle.
- 2) Chemical kinetics of the reaction between the gaseous and solid reactants.
- 3) Mass transfer of the gaseous reactant or product by diffusion through any product layer at the surface of the solid or in the internal pore structure of the solid. The rate of this step is highly dependent on the extent of reaction and the physical properties of the product layer or solid sorbent.

### Mathematical Models

The classical Langmuir theory, which is based solely on available surface area, is often insufficient to account for the formation of a solid product layer on the surface of the solid reactant and associated surface changes. This theory assumes a uniform reactant surface, with reaction ceasing after all surface area is covered (Laidler, 1987). Related non-linear sorption models are not applicable to systems with porous sorbents where isotherms are favorable and chemical reaction and pore diffusion resistances can be significant (Biyani and

Goochee, 1988). In general, gas-solid reactions can be described by an ideal Langmuir isotherm only when there is exclusive and complete monolayer sorption, all active sites on the sorbent are equivalent and there is no interaction between adjacent adsorbate molecules (Comes et al., 1993). Solid structural changes resulting from the chemical change in the solid can be quite complex, but are generally classified as being either sintering (and resultant pore closure), swelling, softening, and cracking (Szekely et al., 1976). These changes may affect diffusivities of gaseous reactants as well. A number of mathematical models based upon these recognized physical and chemical phenomenon have been developed and described in the literature.

#### Progressive-Conversion Model

This model is a simplified, idealized model for the non-catalytic reaction of particles with a surrounding fluid. A basic assumption of this model is that the reactant gas enters and reacts throughout the particle at all times, although probably at different rates at different locations within the particle. This model obviously assumes a highly porous particle structure to allow for easy reactant diffusion with little intraparticle resistance to diffusion. With negligible diffusional (or mass transfer) resistance, the overall rate is controlled by chemical kinetics, which is generally slow in this case.

#### Shrinking Unreacted-Core Model

Evidence from a wide variety of situations indicates that the progressive-conversion model does not accurately approximate the behavior of real particles. Often, the reaction produces an inert product layer of converted solid reactant which can produce significant

resistance to diffusion. A mathematically simple model, that was developed by Yagi and Kunii in 1955, is often used to describe non-catalytic gas–solid reactions. This model, often called the shrinking unreacted-core model, is based upon the visualization that the reaction occurs first at the outer surface of an idealized spherical reactant particle (Yagi and Kunii, 1961). As reaction progresses, the reaction front (or zone) moves radially into the solid, often leaving behind completely converted material in the form of an inert solid product called "ash." A graphical representation of this model is shown in Figure 2-2.

The reaction steps in this model are the same as those previously described for a generalized non-catalytic gas–solid reaction, occurring sequentially, although in any given reaction, some steps may not occur. Effective diffusivity of the adsorbate through the solid product is assumed to be a constant. Various equations relating the radial position of the reaction zone (a measure of solid conversion) with reaction time have been developed. These equations will be described in following sections before they are applied to the present study. Although originally developed for application to non-porous solid reactants, the model has been successfully used to describe systems utilizing porous solid sorbents. The main physical difference between the two situations is that the reaction zone is diffuse in a porous solid as opposed to a sharp interface in a non-porous one. A variable-diffusivity shrinking-core-model was developed by Krishnan and Sotirchos (1993a). Their analysis revealed the strong effects of reaction temperature, gas-phase concentration, and product layer thickness on effective diffusivity of the reactant gas through the solid reactant and "inert" product layer matrix.

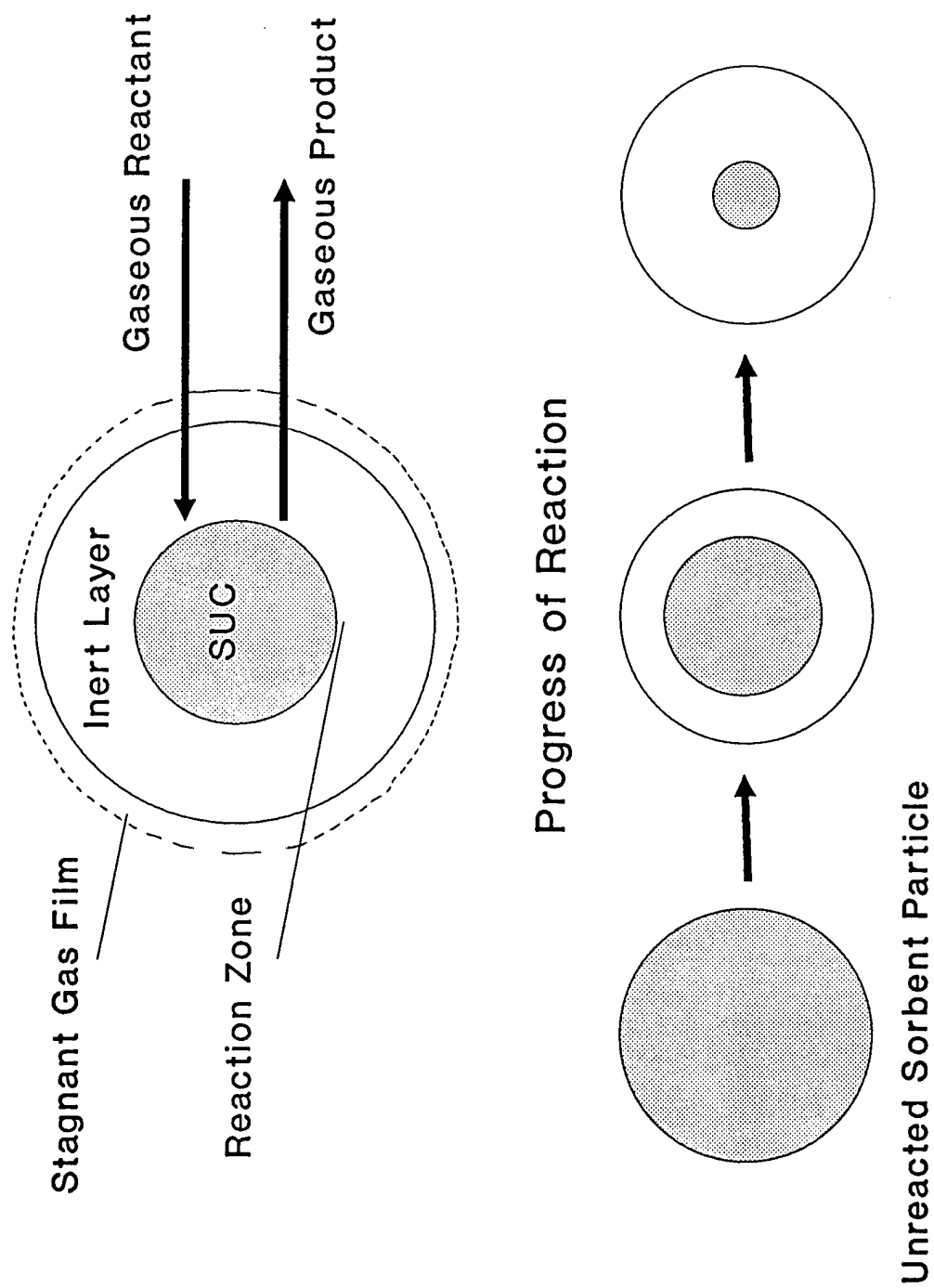


Figure 2-2. Schematic representation of the shrinking unreacted-core model.

### Grain Model

To account for sorbent porosity, Szekely and Evans (1970) first improved upon the basic shrinking unreacted-core model by further defining the structure of the idealized sorbent pellet or particle. The particle is assumed to be made up of compacting individual grains of uniform size and shape. A schematic representation of the grain model is shown in Figure 2-3. While in reality, this assumption may not be entirely accurate, the model presents a means of accounting for the effects of particle and grain shapes on reaction rates. Each grain still reacts following the shrinking unreacted-core model. A shape factor for one of three idealized predominant shapes (either a sphere, cylinder, or flat plate) enters the relevant shrinking unreacted-core model equations. This shape factor can be used to qualitatively discern information about the sorbent surface physical structure as it affects sorption behavior.

This model has been further modified by Hartman and Coughlin (1976), among others, to account for increased diffusional resistance to chemical reaction in the product layer. This effect is greatly compounded when the molar volume of the product is significantly larger than that of the solid reactant, causing coverage or blockage of potentially available intergrain pore surface area. This may cause a discrepancy between the theoretical solid-surface conversion-versus-time behavior, as predicted by the model, and actual experimental results. Ramachandran and Smith (1977) took the model a step further in modeling the single-pore behavior in a porous pellet to predict the conversion versus time relationship for gas-solid non-catalytic reactions. Their model accounts for the influence of pore diffusion, diffusion through the product layer, and surface reaction. A key parameter useful in

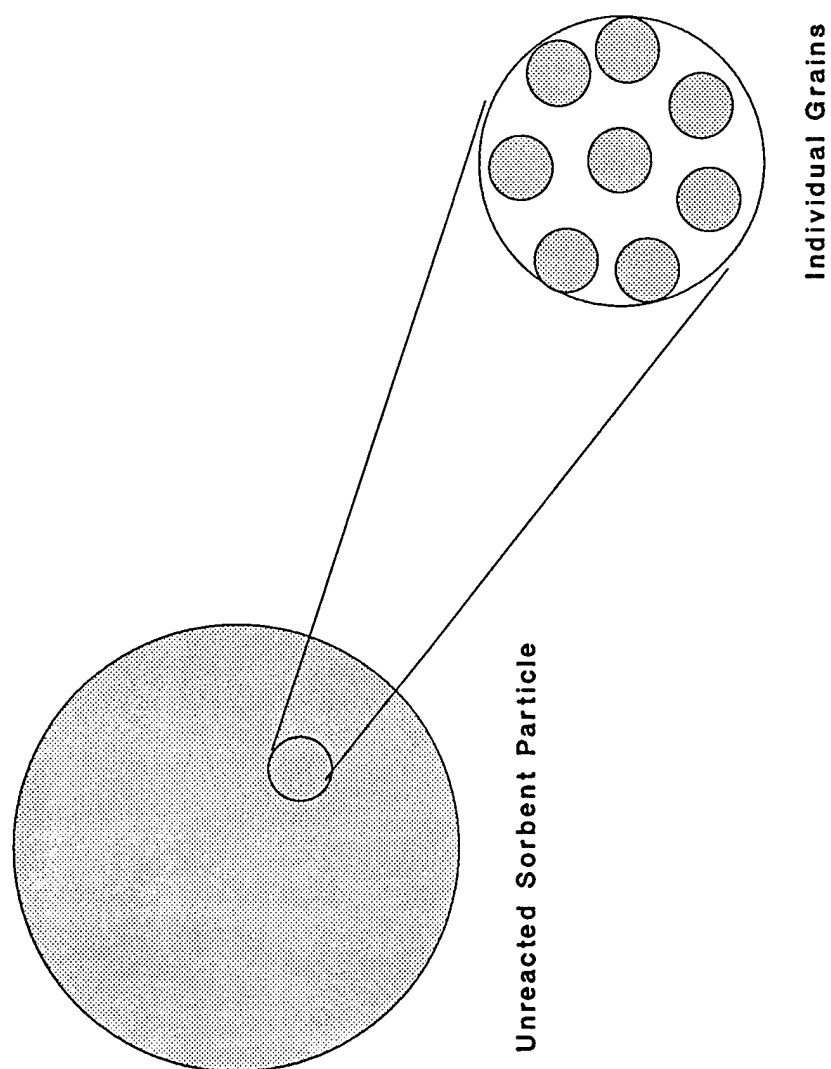


Figure 2-3. Schematic representation of the grain model.

describing the observed discrepancy between theoretical and observed solid conversion is the effective diffusivity through the product layer. Incomplete conversion, which decreases with an increase in intrapellet diffusional resistance, is predicted using the random pore model developed by Bhatia and Perlmutter (1981a). A unique feature of this model is that solid pores are not assumed to be of uniform size, so smaller pores are more easily blocked when a dense or large-volume product is formed on the surface. Dam-Johansen et al. (1991) used physical parameters of a chalk sorbent to modify the grain model down to the micrograin level. While this provides a physical description of the reaction occurring at the sub-grain level, the reaction taking place still follows the shrinking unreacted-core mechanism.

#### Analogous Gas-Solid Reaction System Research

The most similar gas-solid reaction systems discussed in current literature describe the reactions between sulfur dioxide ( $\text{SO}_2$ ) and lime/calcium oxide ( $\text{CaO}$ ), calcium hydroxide ( $\text{Ca}(\text{OH})_2$ ), or limestone (calcium carbonate ( $\text{CaCO}_3$ )). Reactions of acidic gases with calcined limestone have been closely studied because of their industrial importance. The high porosities of various forms of  $\text{CaO}$  (nominally over 50 percent) makes them quite suitable for tests of the numerous forms of the shrinking unreacted-core model. Although these models have been used quite successfully, the fundamental rate-controlling processes are still not well understood (Borgwardt et al., 1986). Data on reactions between other acid gas/acid anhydride gases and other carbonate rocks are also available. In these processes,  $\text{SO}_2$ -containing gases are contacted with lime or limestone, either as a wet slurry or dry solid.  $\text{SO}_2$  is generally collected on the solid surface for reuse or disposal. Regeneration may produce

reusable sulfuric acid or in some cases, elemental sulfur. A magnesium oxide process similar to lime or limestone scrubbing is sometimes used where MgO is hydrated to  $\text{Mg}(\text{OH})_2$  which reacts with  $\text{SO}_2$  forming  $\text{MgSO}_3/\text{MgSO}_4$  solids. These can be heated, generating  $\text{SO}_2$  and MgO. The  $\text{SO}_2$  can normally be recovered as a sulfuric acid product (Cooper and Alley, 1994).

#### $\text{SO}_2$ -CaO Reaction

Borgwardt (1970) investigated the reaction of  $\text{SO}_2$  with calcined limestones and found a first-order chemical reaction to be the predominant process with resistance limiting  $\text{SO}_2$  sorption by small particles. He found that the reaction rate decreased rapidly as CaO conversion increased. Some of the solids contained significant quantities of MgO, which did not readily react with  $\text{SO}_2$  at the elevated temperatures evaluated. Wen and Ishida (1973) found, through an application of the grain model, that the overall reaction rate between  $\text{SO}_2$  and CaO was highly temperature dependent, particularly at lower temperatures where it was controlled by chemical kinetics. They reported that various kinetic studies have indicated that reaction rates may vary considerably (more than an order of magnitude) depending upon the type of limestones used. This variability is a common problem inherent in the study of heterogeneous sorbents.

The previously mentioned study by Hartman and Coughlin (1976), which improved the applicability of the grain model, also described the  $\text{SO}_2$ -CaO reaction. The strong relationship between surface area and the reactivity of CaO toward  $\text{SO}_2$  was analyzed via the shrinking unreacted-core model by Borgwardt and Bruce (1986). The surface area is



apparently very sensitive to the presence of water vapor, which reduces porosity (Borgwardt, 1989). A graphic representation of the shrinking unreacted-core model was depicted in a series of energy dispersive X-ray analysis micrographs of calcined limestone chalk and  $\text{SO}_2$  (Dam-Johansen and Ostergaard, 1991a). The associated data were fitted with a grain model of the shrinking unreacted-core mechanism (Dam-Johansen, 1991b). Bjerle et al. (1992) reported useful experimental techniques for describing this reaction as well. They were able to use the shrinking unreacted-core model to describe the various stages of reaction as conversion progressed. Sotirchos and Zarkanitis (1992) found that the sulfation rates of  $\text{MgO}$  were comparable to those for  $\text{CaO}$ . A simple grain model was also used to interpret data describing a furnace sorbent slurry injection process, in which a limestone slurry was calcined for use in  $\text{SO}_2$  removal (Damle, 1994).

#### $\text{SO}_2$ -Calcium Hydroxide Reaction

Flue-gas desulfurization through spray drying of a  $\text{Ca}(\text{OH})_2$  slurry has recently become an important alternative to the traditional wet lime or limestone scrubbing techniques. In spray drying,  $\text{SO}_2$ -containing flue gases are contacted in a dryer with finely atomized lime slurry that absorbs the  $\text{SO}_2$ . As water evaporates from the slurry droplets, reacted solids and unreacted  $\text{Ca}(\text{OH})_2$  remain and are collected on bag filters. This accumulated residual  $\text{Ca}(\text{OH})_2$  serves to remove considerable quantities of unreacted  $\text{SO}_2$  from the inside of the bags as well as in the ducts. Ruiz-Alsop and Rochelle (1988) used a bench-scale fixed-bed reactor to study this reaction. The shrinking unreacted-core model was applied to their results. Among the many factors evaluated, relative humidity of the gas was determined to

be the most important variable affecting sorption behavior. Chu and Rochelle (1989) examined the simultaneous removal of  $\text{SO}_2$  and  $\text{NO}_x$  (as NO) by  $\text{Ca}(\text{OH})_2$  and in some cases additives, including fly ash,  $\text{CaSO}_3$ , and NaOH. These additives improved  $\text{NO}_x$  removal. Another bench-scale evaluation of the removal of  $\text{SO}_2$  and NO by  $\text{Ca}(\text{OH})_2$  was conducted by Jozewicz et al. (1990). NO was not very reactive toward  $\text{Ca}(\text{OH})_2$  relative to  $\text{SO}_2$ , but adding  $\text{Mg}(\text{OH})_2$  did improve NO removal somewhat.

#### $\text{SO}_2$ -Calcium Carbonate Reaction

Pigford and Sliger (1970) noted the effects of increased product layer diffusional resistance in the reaction between  $\text{SO}_2$  and  $\text{CaCO}_3$ . The overall reaction rate was governed by both diffusion of  $\text{SO}_2$  through a layer of solid reaction product, progressively formed on the active solid surface, and diffusion of  $\text{SO}_2$  through pores in the solid. The direct sulfation of  $\text{CaCO}_3$  was studied by Hajaligol et al. (1988) via thermogravimetric analyses and a bench-scale fluidized bed setup. The product layer diffusion controlled shrinking unreacted-core model was used to fitted to the experimental data, using a correction factor for product layer volume, although chemical kinetics were still important to determining the overall reaction rate. Snow et al. (1988) also evaluated the direct sulfation of limestone under conditions that did not decompose  $\text{CaCO}_3$  to CaO. Their results were similar to those of Hajaligol et al. (1988). As previously mentioned, a variable diffusivity shrinking unreacted-core model was successfully applied to the direct sulfation of  $\text{CaCO}_3$  by Krishnan and Sotirchos (1993b). Effective gas diffusivity through the solid product layer was found to be a strong function of gas temperature and  $\text{SO}_2$  concentration in the bulk gas-phase.

### Other Acid-gas–Calcium-based-solid Reactions

Other sorption studies employing the shrinking unreacted-core model and its derivations have been conducted to study the control of other acid gases. The reaction of hydrogen chloride (HCl) with CaO is of interest for the control of acid vapors emitted from municipal and hazardous waste incineration operations. Gullett et al. (1992) used a specialized fixed-bed reactor to study this reaction and determine the controlling mechanism and kinetics. They examined the relative importance of chemical reaction and product layer diffusion control using the combined resistance shrinking unreacted-core model. Their research also provided data on how operating parameters like reaction temperature and gas-phase concentration affect sorption. The strong resistance to chemical reaction provided by solid-state diffusion was proved to follow a grain model by Weinell et al. (1992). Pakrasi (1992) performed kinetic studies of HCl removal by hydrated lime powder in a bench-scale fixed-bed reactor. His studies included a thorough examination of the chemical kinetics and possible mechanism associated with the HCl–CaO reaction. Relative humidity played a key role in determining HCl removal rate and the extent of solid sorbent conversion. Other relevant variables such as gas concentration and temperature were also examined. Incomplete conversion (compared to that theoretically predicted stoichiometrically or by the shrinking unreacted-core model), was the result of increased diffusional resistance in the product layer. Both the shrinking unreacted-core model and an empirical model were used to interpret observed conversion versus time data.

The process of coal gasification often produces significant quantities of hydrogen sulfide ( $\text{H}_2\text{S}$ ). Limestones (either calcined or uncalcined) have been investigated as sorbents for the removal of these gases through the direct sulfidation of the solids via thermogravimetric analyses (Krishnan and Sotirchos, 1994). The shrinking unreacted-core model was employed both quantitatively and qualitatively to derive kinetic parameters and to provide a description of the rate-limiting mass transfer processes. In this case, since the product, calcium sulfide ( $\text{CaS}$ ) is more porous and less voluminous than the  $\text{CaCO}_3$  reactant, diffusional resistances were limited.

#### General Applicability of the Shrinking Unreacted-Core Model

From the previous discussion, it is readily seen that the shrinking unreacted-core model and its derivations are useful tools for describing the complex chemical and physical processes associated with gas–solid reactions. If the required physical parameters are known, much detail about the physical rate-controlling mechanisms can be gleaned from a reaction under study using these models. Combined with the traditional chemical kinetics principles for determining intrinsic kinetic parameters, data can be collected which can ultimately be used to improve the use of a gas–solid reaction to control gaseous pollutants.

### Research Justification

No other research has been reported that would delineate the intrinsic chemical kinetic parameters associated with the reactions of  $\text{NO}_x$  with  $\text{MgO}$ –vermiculite sorbents. Likewise, the probable reaction mechanism has not yet been determined, including the identification of rate-controlling step(s). A chemico-physical model like the shrinking unreacted-core model may be used to explain sorbent performance characteristics and provide useful information related to the optimization of a process employing this novel sorbent for removing  $\text{NO}_x$  from jet engine test cell exhaust, or even other combustion sources. Reviewing the effects of other operating parameters such as gas concentration, temperature, flow rate, moisture, and oxygen can provide a more complete picture of the sorptive phenomena occurring. All of these will be useful to the engineer or scientist who may attempt to employ this medium in an air pollution control situation in the future.

### Research Objectives

Based upon the justification for this basic research, the objectives of this study are to

1. Qualify and quantify  $\text{NO}_x$  sorption, singly and in combination, by  $\text{MgO}$ –vermiculite using appropriate isotherms. Determine appropriate kinetic parameters associated with the sorption reactions. Determine the controlling mechanism(s) and whether these are chemical reaction, diffusion, or mass transfer limited.

2. Evaluate saturation characteristics (lifetime) of the material. Develop a model to predict sorbent performance with time.
3. Evaluate the desorption and regeneration efficiencies of  $\text{NO}_x$  on MgO-vermiculite.
4. Evaluate the pressure-drop characteristics of the material over time as gas collection progresses.

## CHAPTER 3 EXPERIMENTAL METHODS AND MATERIALS

### General Research Approach

A fixed-bed reactor system was designed, constructed and used to collect the relevant data to meet the established research objectives. The present study systematically addressed individual exhaust gas components, focusing primarily on  $\text{NO}_x$ , under strictly controlled conditions to delineate the nature of the sorption rates and mechanisms. Processes and rates for removal of  $\text{NO}_2$  and  $\text{NO}$  by  $\text{MgO}$ –vermiculite sorbent were independently evaluated. Moistened sorbent and/or humidified gases were used to evaluate the  $\text{NO}_x$  removal characteristics of  $\text{Mg}(\text{OH})_2$ . A variety of test conditions were used to determine important operating parameters and limitations. By combining gaseous components, their interactions in the presence of the sorbent material could be evaluated. Intrinsic and overall kinetic parameters were determined. A complete description of the kinetics of gas–solid reactions is very complicated, especially for systems involving solid products, for which the processes at both the gas–solid interface and the reaction interface between the reactant and product solids must be considered. Although the rate expressions can be quite complex, the reactions between adsorbate and adsorbent can often be described by first-order kinetics (Szekely et al., 1976). Data were mathematically interpreted using the shrinking unreacted-core model

and its variations, as well as empirically. These models provided a chemico-physical basis for explaining sorbent performance and probable reaction mechanisms.

### Experimental Variables

#### MgO—Vermiculite Reactive Sorbent Material.

This material (approximately 45% MgO to 55% vermiculite substrate by weight) was prepared according to a process patented by the inventor (U.S. Patent 4,721,582, Sorbent Technologies Corporation, (Sorbtech), Twinsburg, Ohio, 1988). Commercial-grade magnesium oxide was used (98% volatile-free MgO) with a manufacturer-reported surface area of 170 m<sup>2</sup>/g (Elastomag ® 170, Akrochem Corporation, Akron, Ohio). While the process of preparing the sorbent is described in detail in the patent, a more general descriptive process is presented here for informative and comparative purposes. Sorbent was prepared in small batches, by necessity, in stainless steel pans in the laboratory. A quantity of coarse vermiculite was weighed out in the pan, to which a 4:1 mass ratio of deionized water was added. This is the maximum ratio allowed in the patent, but is greater than the 2:1 ratio reported by Sorbtech in the preparation of a sample provided by them for experimental use. Trial-and-error practice in the laboratory indicated that sufficient water was necessary to attach the majority of the MgO particles to the surface of the vermiculite. Since the vermiculite is highly hydrophilic, it readily absorbs the extra water. The sorbent is subsequently heat-treated, during which process any excess water will be driven off. The water and vermiculite were mixed to ensure complete absorption.



Magnesium oxide powder was prepared for addition to the mixture by sieving with a 28-mesh Tyler Standard sieve (600  $\mu\text{m}$  opening). Forty-five grams MgO per 55 grams dry vermiculite was added to the wet vermiculite while the mixture was manually stirred using a stirring tool. This ratio was the same as that reported by Sorbtech and is less than the 60:40 maximum mass ratio described in the patent. The same ratio was used so that the two sorbents could be compared. Sorbtech is able to prepare large batches of material using mechanical stirring, perhaps allowing them to use less water, while more evenly coating the sorbent with the  $\text{Mg}(\text{OH})_2$  slurry.

After thorough mixing, the sorbent was allowed to air dry overnight until the individual particles were again "free-flowing." The pans of sorbent were then placed in a preheated muffle furnace set at 550 C and "conditioned" for 30 minutes. It is believed that this process increases sorbent surface area by expanding the particles as a result of driving out interior water vapor via heating. This process also dehydrates the  $\text{Mg}(\text{OH})_2$  formed by previously hydrating the MgO powder.

Since only small batches of MgO-coated vermiculite could be made in the laboratory, this process had to be repeated a number of times to produce a sufficient quantity of sorbent for experimental purposes. All of these individual batches were combined in an air-tight polyethylene container and mixed together. While the preparation procedures were carefully followed in making each batch, some variation could be expected in the sorbent from batch to batch. The sorbent itself is inherently heterogeneous, however, so it was hoped that these variations could be minimized by mixing the various batches. Samples of the combined batch mixture were randomly selected for comparative surface area analyses as a measure of this

variation, as well as for comparison with data from the Sorbtech samples to ensure that the sorbent was properly prepared.

The sorbent material was incorporated into a packed-bed arrangement in a non-reactive 316 stainless steel tubular reactor in a controlled temperature (tube furnace) environment, which will be described later. A single batch of material was used for all experiments. Limited surface area/composition analyses of the material were performed to establish baseline values. Comparative experiments were conducted using sorbent samples provided by Sorbtech.

#### Temperature

Reaction temperatures were controlled using a tube furnace (Model 421135, Thermolyne, Dubuque, Iowa) to contain the reaction vessel. Sorption study temperatures of 373, 423, and 473 K were used. These temperatures were chosen because they represent a reasonable range expected for augmented/cooled exhaust gases. Gases were preheated before entering the furnace to ensure that they were at or above reaction temperature (+ 20 °C) when they entered the bed, so they would not need additional heating.

#### Pressure

All runs were conducted at atmospheric pressure. The bed outlet gases were exhausted to the atmosphere through a laboratory ventilation system. Pressure drop versus exposure time was evaluated through the bed, using a U-tube manometer connected to ports at the bed inlet and outlet. Pressure drop versus gas velocity was evaluated via an empirical correlation.

### Gas Composition

To quantify emissions from jet engines, the USAF has sponsored numerous studies and has published jet engine emission values for many engines in the USAF inventory. These documents describe  $\text{NO}_x$  and other combustion by-product emissions correlated with power setting or operational procedures (Spicer et al., 1990). These studies are very useful for determining appropriate exhaust gas concentrations to simulate jet engine exhaust gas composition in the laboratory. Many lab-scale studies have used these data in their experimental design. Gas composition was kept constant for each run. Major components of JETC exhaust were evaluated individually (mixed in  $\text{N}_2$  or air):  $\text{NO}$  (5-200 ppm),  $\text{NO}_2$  (20-200 ppm), and  $\text{O}_2$  (0-10%). Gas concentration ranges relate to representative values at four common engine settings (nominally, idle, 30%, 75% and 100% power) for the USAF F110 turbine engine. Actual engine emissions data are shown in Table 3-1. Water vapor (3-5% by volume at temperature) was evaluated in cohort with other gaseous components. Water vapor may hydrate the  $\text{MgO}$ , forming a reactive hydroxide.

It is seen from this table that jet engine exhaust contains significant quantities of unburned hydrocarbons, carbon monoxide ( $\text{CO}$ ) and carbon dioxide ( $\text{CO}_2$ ). Particulate matter in the form of soot or condensation aerosols will also most likely be present in real exhaust. All of these exhaust components have the potential to affect the  $\text{NO}_x$  sorption performance of the sorbent. For the purposes of this study, these variables were not included to allow for the evaluation of the basic  $\text{NO}_x$ -sorbent reaction(s).

Table 3-1. USAF F110 Turbine Engine Emissions Data (as reported)

Power Setting	THC (ppmC)	NO <sub>x</sub> (ppmv)	NO (ppmv)	CO (ppmv)	CO <sub>2</sub> (%)
Idle	7	13.8	11.2	85	0.98
30 Percent	6	30	28	23	1.25
63 Percent	3	97	92	13	2.35
Intermediate (High Mach)	3.5	243	227	15	3.17
105% Afterburner -Augmented	335	21.5	3.7	178	0.42

Source: Spicer et al., 1990, page 27.

#### Gas Flow Rate(s)

Gas flow rate(s) were kept constant for each run. However, flow rates/gas velocities were varied to produce two contact times of 0.5 and 1.0 second, keeping pressure drop to a minimum. Contact times were calculated by dividing bed length by superficial gas velocity. This is only an approximation of the true distribution of contact times since the actual gas velocity may be based upon a more tortuous pathway through the packed bed volume, increasing or decreasing the contact time of an individual reactant gas molecule. These superficial velocities correspond to nominal space velocities of 3,600 and 7,200 per hour.

Since mass transfer limitations from the gas phase to the solid surface can obscure intrinsic chemical kinetics, it is important to limit this resistance to chemical reaction. A sufficiently high gas velocity will effectively decrease the thickness of the stagnant gas film

layer surrounding the sorbent particle. Practical constraints on pressure drop will likely limit gas velocity in the application of this control technology to jet engine test cells. Comparative experiments and mathematical evaluations were performed to ensure that this source of error was effectively minimized. Results will be presented in a subsequent section.

#### Gas Reaction/Sorption/Desorption

Gas reaction/sorption was measured by the change in concentration of the test gas(es) with bed residence and exposure times. Gases were sampled at the inlet and outlet of the sorbent bed, and also from three points within the bed (of nominal 0.1-m length). Both short-term (to dynamic equilibrium) and long-term results (taking the bed to "saturation," a function of bed exposure time) were collected. Concentration-versus-time data from within the bed were used to evaluate intrinsic chemical kinetics. Overall kinetic data were derived from progressive removal efficiencies and were used to model overall sorbent performance with increasing bed exposure times.

#### Fixed-Bed Reactor System

#### General Experimental Considerations

Many gas–solid reactions are studied using individual sorbent particles or pellets. These individual particles are placed in a controlled environment and exposed to the adsorbate of interest. Sorption behavior is determined gravimetrically using a microbalance and mass balance calculations. An increase in sorbent mass is directly related to solid sorbent conversion via stoichiometry. Some fundamental gas–solid studies employ either thin films

of solid sorbent reactant, or fine particles dispersed within an inert material bed such as quartz silica sand or glass beads. While these types of studies are valuable for collecting data on fundamental reactions occurring between the phases, in this study, by necessity, the use of the prepared sorbent was a fundamental limitation. Experimental results may or may not be transferable to the basic reactions between  $\text{NO}_x$  gases and  $\text{MgO}$  or  $\text{Mg}(\text{OH})_2$  solids. It is possible that the process of making the sorbent promotes sorption through the enhancement of available surface area. It is also possible, however, that the inefficient transfer of  $\text{Mg}(\text{OH})_2$  slurry to the vermiculite substrate before calcination may create dense agglomerates or otherwise make  $\text{MgO}$  unavailable for reaction with  $\text{NO}_x$ . The effects on ultimate sorbent conversion and bed utilization will be discussed later.

Often, particularly in chemical or materials engineering studies of gas-solid reactions, the emphasis is on the solid sorbent surface and its conversion as reaction progresses. Experiments are designed for the purpose of optimizing the solid sorbent itself. Solid conversion is generally measured directly through chemical analyses, including spectroscopic and chromatographic methods. Physical properties of the sorbent can be evaluated using X-ray diffraction or electron microscopy, for example. While these previously discussed studies are invaluable, in environmental engineering and particularly, in air pollution control, the focus is often on the gas-phase concentration and the effective removal of the pollutant of interest. This applied engineering approach is the result of the unavoidable fact that environmental regulations mandate the reduction of emissions to specified limits and compliance with regulations is determined through air sampling. It is still crucial, however, that gas-phase concentrations be correlated with solid conversion through an appropriate

chemico-physical model to adequately explain the removal of gaseous contaminants. A means for accomplishing this correlation using local equilibrium theory and assumptions regarding constant-pattern behavior for mass transfer in a fixed-bed will be detailed later.

The basic principles that govern chemical kinetics and diffusion phenomena in single particles are normally unaffected by the presence of other particles in an arrangement like a packed bed. Changes in the flow field due to the packed bed arrangement likewise do not invalidate these principles (Szekely et al., 1976). In this way, a fixed-bed experimental system may be used to extend the information obtainable from single particles to multiple-particle systems. Multiple-particle systems are obviously of more interest since practical systems must be of this type. Since the sorbent material is highly heterogeneous, data reproducibility between samples is very important. This was evaluated by comparing results for the same experimental conditions between different samples of sorbent material.

While the basic principles of single gas-solid interaction will still apply, the physical characteristics of any experimental fixed-bed reactor can markedly affect chemical kinetics and overall sorption behavior. It is critical that such a system be carefully designed, to ensure that any experimental data collected are scientifically valid and defensible. Often, practical constraints such as temperature and, particularly, gas velocity and its effect on pressure drop through the bed, must be incorporated into the experimental design. Such other factors as particle fluidization velocity and the potential for temperature and concentration gradients must be accounted for as well. In this research, MgO will be attached to its vermiculite substrate. Results, however, may be different from those for individual MgO particles due to this arrangement.

### Experimental Arrangement

The experimental arrangement for sorption and desorption/regeneration employed in this study is shown in Figure 3-1. Nitrogen oxides (mixed in  $N_2$ ) were supplied from separate certified standard cylinders (Bi-Tec Southeast, Inc., Tampa, Florida) to ensure reliability of concentrations and to minimize contaminant concentrations. Initially,  $NO_2$  mixtures were generated using a  $NO_x$  generator (Model 100, Thermo Environmental Instruments, Franklin, Massachusetts) as a source of  $NO_2$ . This generator produces  $NO_2$  by mixing ozone generated from UV irradiation of air with NO. While the system could easily and efficiently convert high concentrations of NO to  $NO_2$ , two major problems resulted from its use. First, it is extremely difficult to perfectly titrate ozone with NO using this system, without leaving excess ozone. The flow controls in the unit are insufficient for this purpose. A related but more important variation was the ultraviolet lamp output used to generate ozone appeared to vary from one test to the next for a given voltage setting. The presence of ozone was unwanted in the experimental study since it could complicate data interpretation by oxidizing  $NO_x$  to other species not readily measurable with the instrumentation used.

As a result, it was necessary to use standard cylinder gas as an  $NO_2$  source. Since this is actually  $N_2O_4$  under pressure, there is a small potential for the gas to decay with time. While total  $NO_x$  was the same as certified, some NO "contamination" is generally present in the cylinder gas. The NO contamination in the  $NO_2$  cylinders was always less than two to five percent. Similar impurity values were noted in the  $NO_2/NO$  ratio in the NO cylinders. This



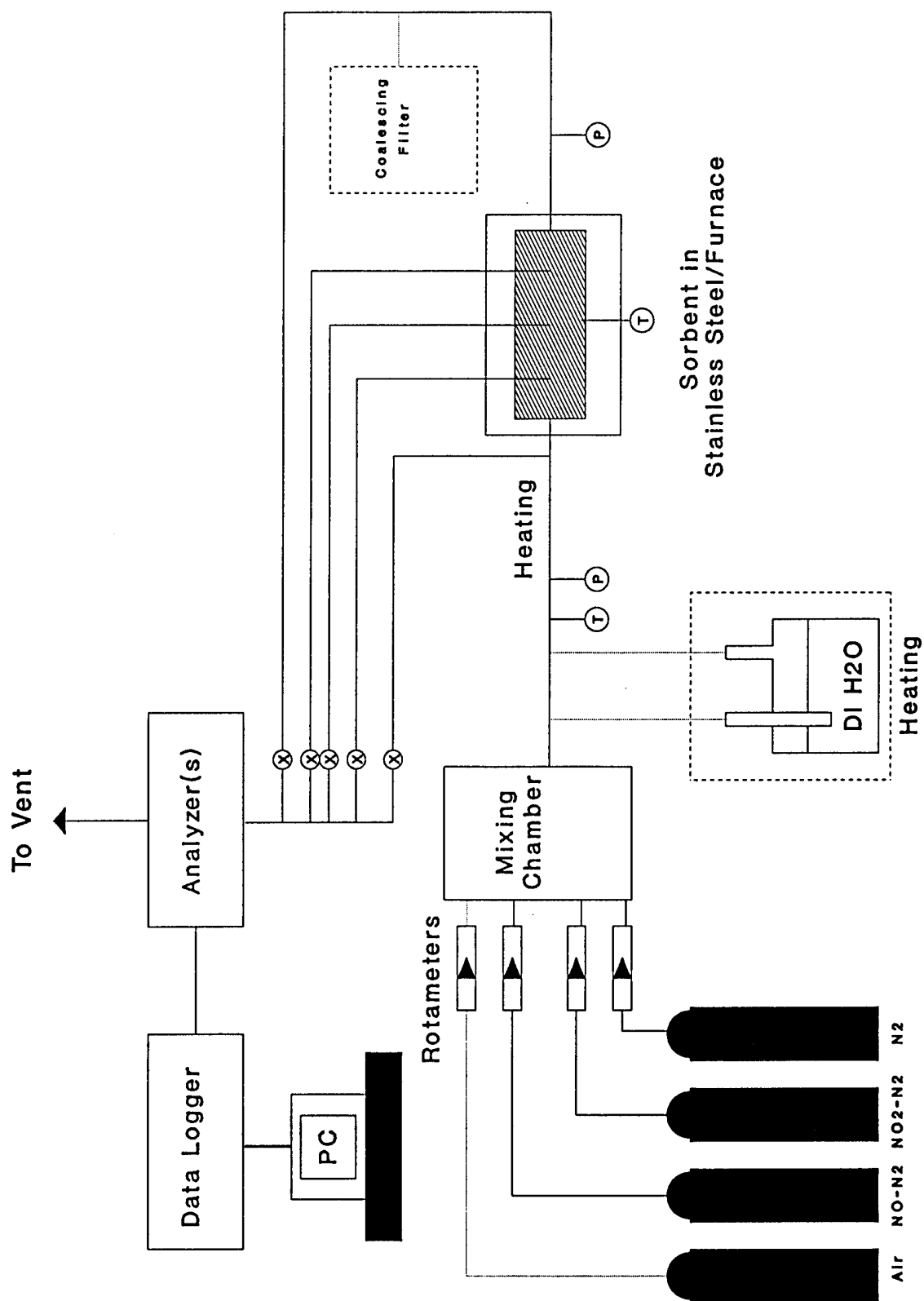


Figure 3-1. Experimental arrangement for packed-bed studies.

is a problem with attempting to use "pure"  $\text{NO}_2$  (or  $\text{NO}$ ) in gas-solid sorption studies employing cylinder gases. These gases were diluted with dry air or prepurified  $\text{N}_2$  to the appropriate concentration(s). Cylinder gas flow rates were measured using precision rotameters (Omega Engineering, Inc., Stamford, Connecticut) with only glass and/or stainless steel wetted parts. While the manufacturer provided calibration data, all rotameters (both high- and low-flow-rate tubes) were independently calibrated in the laboratory using a primary airflow standard (Gilibrator, Gilian Instrument Corporation, Wayne, New Jersey). These calibrations were extremely important for accurate gas flow rate measurements, particularly when using low-flow-rate tubes, which have non-linear calibration curves. Good agreement was reached between the calibration curves, as can be seen in the example comparative calibration curves, Figures 3-2 and 3-3. Laboratory calibration curves were used to measure gas flow rates in this study.

All system components were made of either 316 stainless steel or Pyrex <sup>TM</sup> glass to reduce the potential for  $\text{NO}_x$  removal by system reactivity. Inert gas transfer lines were made from Teflon <sup>TM</sup> tubing of minimal lengths to minimize transfer losses. Most connections were through 316 stainless steel compression fittings (Swagelok, Inc., Solon, Ohio). Where pipe thread connections were necessary, Teflon <sup>TM</sup> tape was used to prevent leakage. Before experiments were initiated, the entire system was leak-checked and  $\text{NO}_x$  decay (reactivity) measurements were made for the system. Each system component was isolated and evaluated separately. Overall  $\text{NO}$  and  $\text{NO}_2$  removal as a result of system reactivity were estimated at less than one percent. In this way, any changes in  $\text{NO}_x$  concentration with time could be attributed solely to the presence of the sorbent material in the fixed-bed reactor.

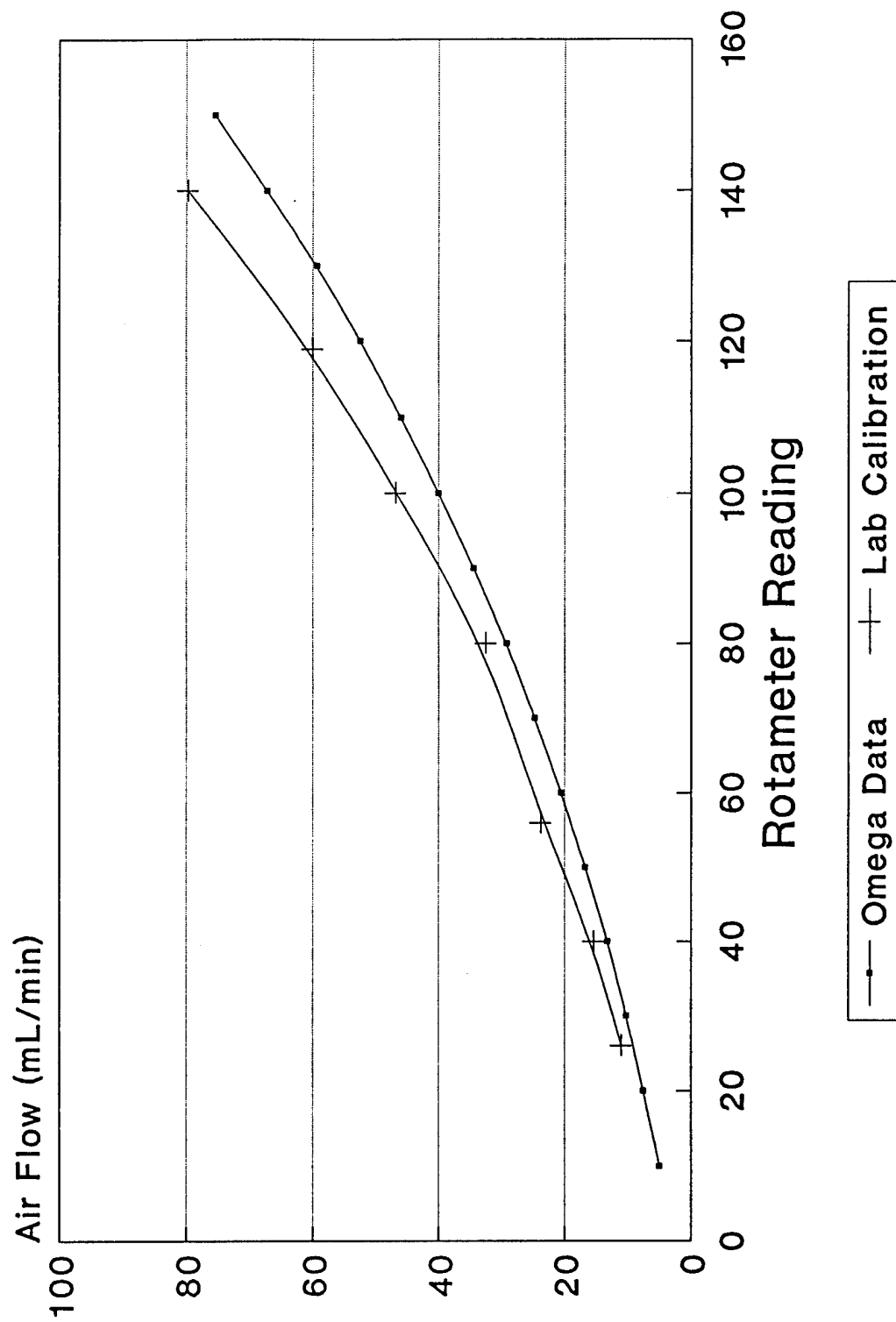


Figure 3-2. Example low-flow-rate rotameter calibration curves (Omega NO42-15ST Tube).

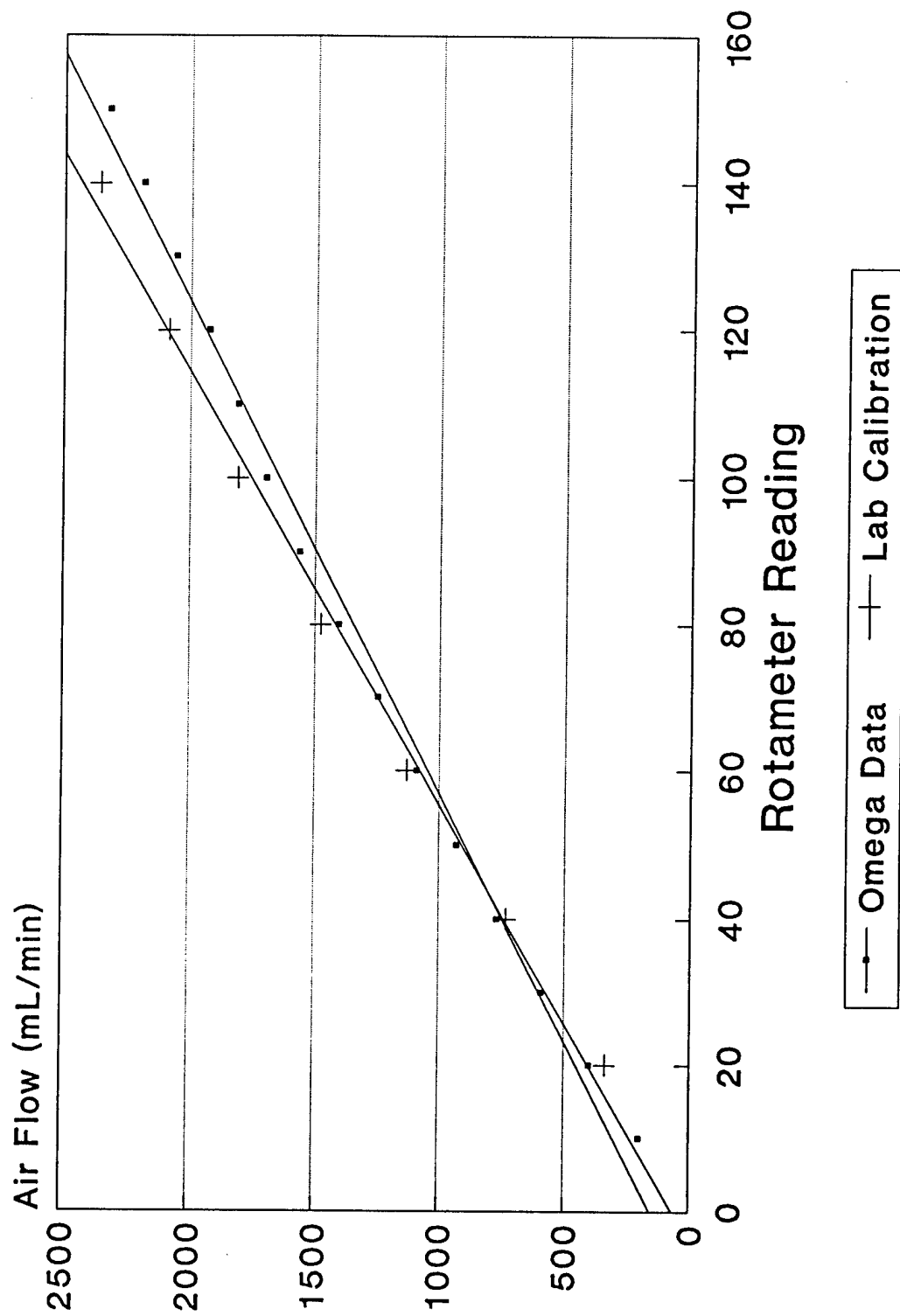
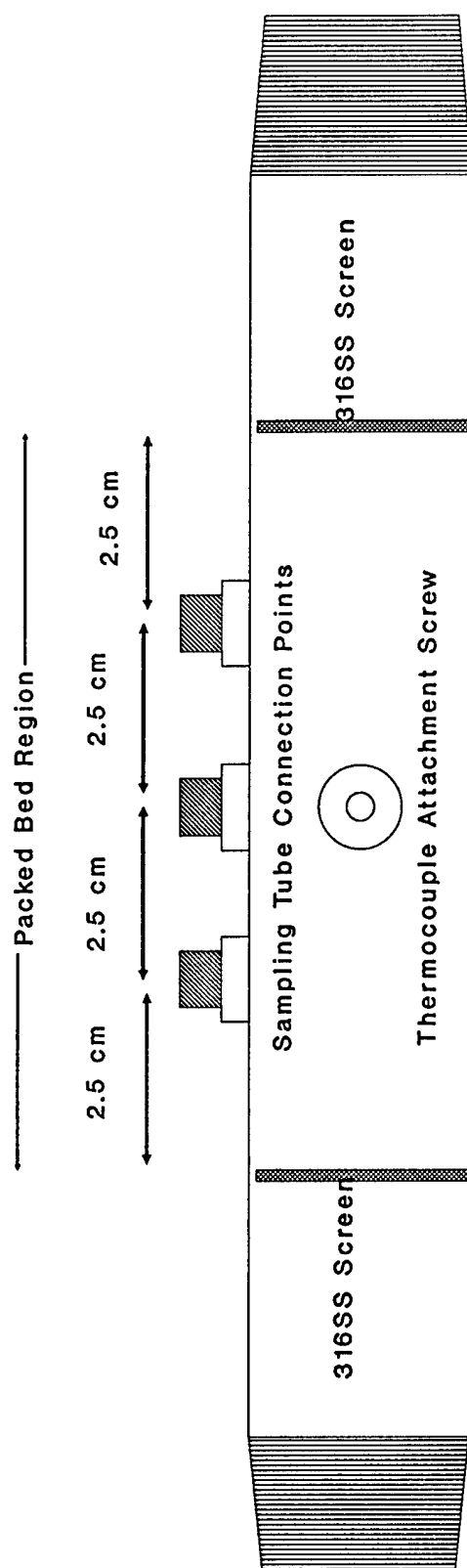


Figure 3-3. Example high-flow-rate rotameter calibration curves (Omega NO92-04G Tube).

### Tubular Fixed-bed Reactors

The reactors, and mixing and sampling manifolds were machined from 316 stainless steel seamless pipe stock (2.54 cm ID) (T.M.R. Engineering, Micanopy, Florida). Schematic representations of the reactors, sample lines, and mixing and sampling manifolds are shown in Figures 3-4, 3-5, and 3-6, respectively. While it is often standard practice and may be sufficient to use only inlet and outlet concentrations from a fixed-bed to determine overall conversion efficiency, this is obviously inadequate for the determination of intrinsic chemical kinetics. For this reason, the reactors were designed to allow for the collection of samples from three points within the packed bed. Using data collected from these points, a more accurate depiction of the concentration versus time profile within the bed can be discerned. This leads to the calculation of valid intrinsic chemical kinetic parameters. An Arrhenius-type expression was used to determine corresponding activation energies.

Sampling lines were connected to the reactor via permanently welded 316 stainless steel compression fittings (Swagelok, Inc., Solon, Ohio) and could be easily removed between runs. One-eighth inch diameter internal sampling lines were used to minimize the cross-sectional area blocked by the lines which could disrupt flow through the bed. The fractional area blocked by the cross-section of a sampling line was approximately 16 percent. A total of 12 holes (0.1 cm diameter) were drilled in the sampling lines. As shown in Figure 3-5, these holes were placed in three places, located at the centroids of two concentric circles of equal area within the reactor diameter. Each sampling location was from three sets of two pairs of holes, the latter offset by  $90^\circ$  from each other.



316 SS Fixed-bed Reactor Schematic (Not to Scale)

Total Length Approximately 47 cm.

Figure 3-4. Schematic representation of 316 stainless steel packed-bed reactor (end connections not shown).

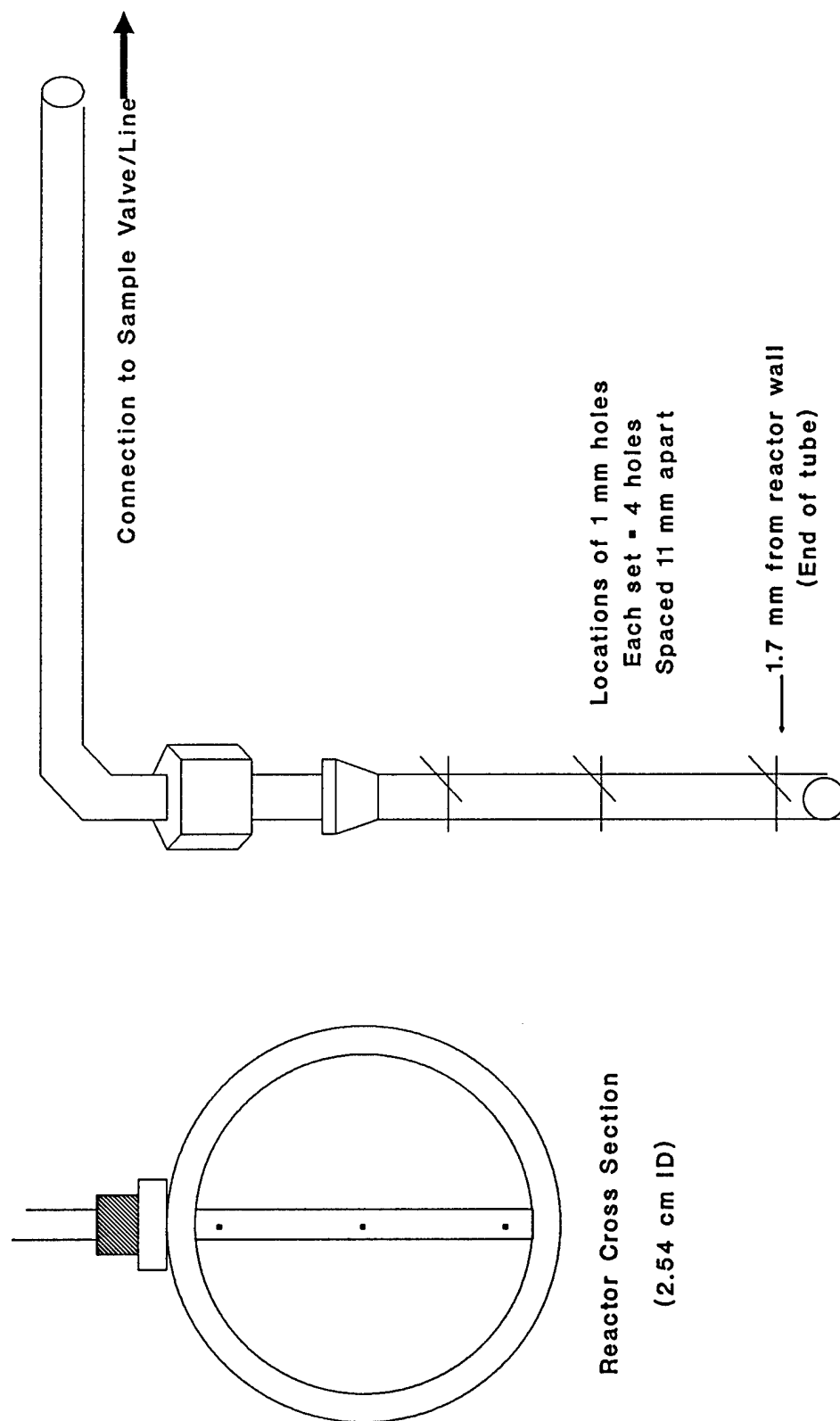
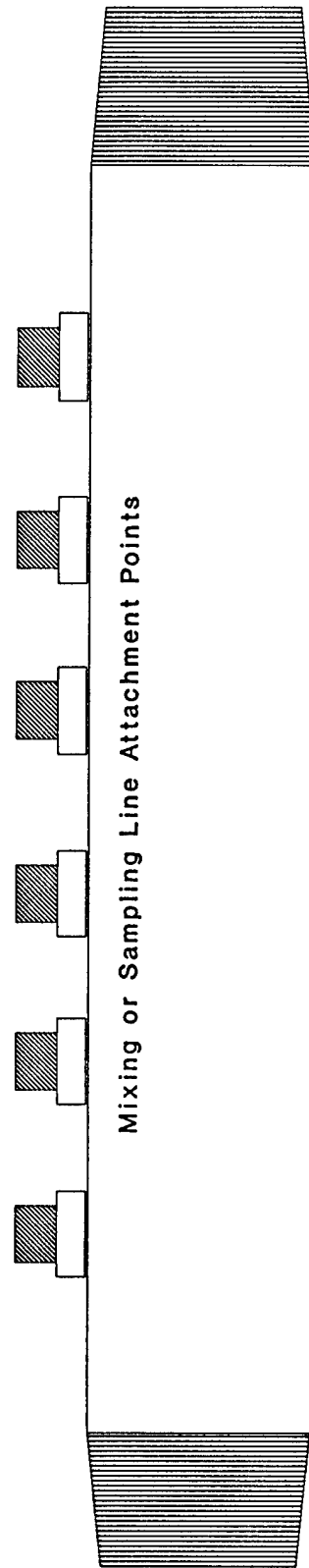


Figure 3-5. Schematic representation of internal sampling tube location and appearance.



316 SS Mixing or Sampling Manifold

Total Length Approximately 47 cm.

Figure 3-6. Schematic representation of 316 stainless steel mixing or sampling manifold.



This arrangement was chosen to ensure that a representative sample of gas was collected from any given location within the bed, avoiding the potential bias caused by any flow disturbances through the packed bed, or by reactor wall effects. The number of holes and perpendicular placement were intended to prevent inconsistencies due to hole blockage during the course of a run, although this did not appear to be a problem. A thermocouple attachment screw mounting was placed on the outside of the reactor(s) to allow for the independent measurement of reaction temperature for comparison with the indicated furnace temperature. The mixing and sampling manifolds were simply sections of 316 stainless steel pipe, approximately 70 cm long (28 inches), with six permanently emplaced 316 stainless steel compression fittings for the connection of gas transfer lines and/or valves, as appropriate.

Before use, machined parts were cleaned and degreased with methanol, followed by acetone and a deionized water rinse. Cleaning all parts with deionized water between runs was sufficient during the normal conduct of experiments. For a nominal bed length of 10 cm, the bulk volume of a packed bed was approximately 51 cm<sup>3</sup>. Individual sorbent samples were measured out using a graduated cylinder filled to a loosely packed volume of approximately 51 cm<sup>3</sup>. These samples were transferred to preweighed sealable polyethylene sample containers and weighed (approximate mass 7-7.5 g/sample). Since MgO comprised approximately 45% of the total sorbent by mass, each bed contained approximately 3 g MgO. After sampling lines were inserted into the reactor, the bed was packed between circular 316 stainless steel screens (12x12 mesh) at the center of the clean tube using a marked steel ram rod to ensure that the bed was properly located. End connections were replaced and a Type K (Nickel–Chromium versus Nickel–Aluminum) thermocouple (Model XCIB-4-4-3, Omega

Engineering, Inc., Stamford, Connecticut) and meter were attached to the outside of the reactor.

### Experimental Procedures

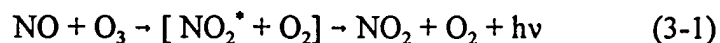
The packed reactor was placed inside the tube furnace with the bed centered within the furnace and the tube element mounted vertically on the furnace control base. The vertical arrangement was chosen to optimize gas-solid contact by avoiding the potential for solid settling and channeling of the gas stream through the bed volume. The middle 15 cm of the furnace was reported to be completely temperature-controlled by the manufacturer, providing a sufficient length for isothermal experimental conditions. Once the reactor was in place, sampling lines were individually connected to two-way stainless steel valves (Model W-1188, Whitey Co., Highland Heights, Ohio) at the sampling manifold. Gas lines entering the tube furnace were wrapped in high-temperature heating tapes. These had been previously calibrated using a Type K thermocouple to measure surface temperature at various settings on the variable voltage controller. Depending on the reaction temperature of interest, the heat tape voltage controller was set to produce a gas preheat temperature approximately 20 °C above reaction temperature. The tube furnace was turned on and allowed to heat up for approximately one hour to achieve temperature control, while the bed was simultaneously being flushed with approximately 2 sLpm dry N<sub>2</sub>. After this conditioning period, thermocouple readings for the tube furnace and independent reactor thermocouple were

compared and averaged to determine actual experimental reaction temperature. This reaction temperature was used to calculate the actual flow rate through the bed, which could then be used to determine residence time at any given sampling point within the bed. It was assumed that the sorbent bed was at the same temperature as the reactor surface after sufficient equilibration time.

When gas humidification was used, a secondary preheating heat tape was used before the gases entered the humidification vessel, which consisted of an impinger apparatus mounted inside a modified 3-liter Pyrex™ flask (Southern Scientific, Inc., Micanopy, Florida) containing deionized water. The flask was placed in a heated flask mantle connected to a separate voltage controller. Various temperature/flow rate combinations were evaluated to allow for 3-5% water vapor to be picked up by the flowing gas stream. The humidified gases were then reheated to ensure that they were approximately 20 °C above reaction temperature. The actual water vapor content of the gases was determined by weighing collected condensed water from a stainless steel coalescing filter (Model 41S6, Balston, Inc., Haverhill, Massachusetts) at the bed outlet. Water vapor was removed from the sample gas stream before analysis through condensation in the sampling manifold. Gas flow rate was always corrected for the presence of water vapor. The effect of moisture on reaction was sometimes evaluated simply by adding sufficient deionized water to a virgin bed to convert all MgO into  $\text{Mg}(\text{OH})_2$ . This was verified by the presence of water vapor at the bed outlet. Once converted,  $\text{Mg}(\text{OH})_2$  is stable over the range of temperatures evaluated (Sidgwick, 1952).

### Gas Analyses

All reactions were monitored by selectively removing gas samples from the stainless steel tubular reaction vessel through selected valves connected to the sampling manifold system. NO<sub>x</sub> concentrations were analyzed using a chemiluminescent analyzer (Model 42H, Thermo Environmental Instruments, Franklin, Massachusetts) based upon the reaction of NO with O<sub>3</sub>, following reduction of NO<sub>2</sub> to NO. The feasibility of the commercial chemiluminescent analyzer was established in 1970 by Fontijn et al. and the first prototype was developed in 1972 (Steffenson and Stedman, 1974). The method is now widely used, in fact, the use of a chemiluminescent method is required for the measurement of NO<sub>2</sub> in the atmosphere (40 CFR, Part 50, Appendix F). The principle of operation of the chemiluminescent analyzer is based upon the chemiluminescent reaction between NO and ozone (O<sub>3</sub>). This reaction is as follows:



where  $h\nu$ , which represents the quantity of light energy emitted by an electronically excited intermediary (NO<sub>2</sub><sup>\*</sup>), is simply Planck's constant ( $h$ ) multiplied by the frequency of the emitted radiation ( $\nu$ ), in this case with a wavelength greater than 600 nm. A sample of gas is drawn from a selected point in the system by an external pump. The sample is mixed with ozone generated by an internal ozonator inside a reaction chamber. The resultant reaction produces a characteristic luminescence with an intensity directly proportional to NO concentration, since O<sub>3</sub> is provided in excess, and its concentration can be considered a

constant in the reaction. This light energy is detected by a photomultiplier tube, which generates an electronic signal that is then converted to a NO concentration reading.

Nitrogen dioxide is measured by difference through its thermal conversion into NO. A solenoid valve is used to switch to the NO<sub>x</sub> mode, where all NO<sub>2</sub> in the gas sample is converted to NO, based upon the thermodynamic principles previously explained, and is combined with NO originally in the sample. In the NO mode, gas does not pass through the thermal converter and therefore contains both NO and NO<sub>2</sub>, with only the NO capable of reacting with ozone to produce light energy. Thus, the NO<sub>2</sub> concentration of the sample is determined by subtracting the signal from the NO mode from the larger signal obtained in the NO<sub>x</sub> mode since:

$$[\text{NO}_x] - [\text{NO}] = [\text{NO}_2] \quad (3-2)$$

The instrument specifications, as reported in the manufacturer's manual, indicate several scales providing an overall measurement range from zero to 5,000 ppm, with a limit of detection of 50 ppb (0.050 ppm). Background noise level is 25 ppb (0.025 ppm), well below the detection limit. The instrument exhibits linearity in response of  $\pm 1\%$  of full scale, with a zero drift (24-hour maximum) of 50 ppb (0.05 ppm), and a span drift (24-hour maximum) of  $\pm 1\%$  of full scale. The separate scales are linear over their entire ranges, which was verified by multiple-point calibrations with certified gases. While the interference of HNO<sub>3</sub> and HONO with NO<sub>2</sub> measurements in chemiluminescent analyzers is well documented (Spicer et al., 1994; Joseph and Spicer, 1978), the concentrations of these interferents were expected to be low in the system employed. When sufficient moisture was present to form

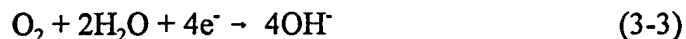
acids, they were ultimately collected in the coalescing filter or condensed out in the sampling manifold prior to analysis.

Similarly, the presence of water vapor itself can interfere with  $\text{NO}_x$  measurements directly by  $\text{NO}_2$  absorption, as well as via third-body quenching of chemiluminescence (Trdona et al., 1988; Campbell et al., 1982). Therefore, it is important to minimize contact-time of the gas with water vapor in sampling lines. Any  $\text{NO}_2$  removed by gas humidification is accounted for by the fact that bed inlet gases were sampled after this point in the system. The analyzer reaction chamber is maintained at a vacuum of approximately 29 inches of mercury (98 kPa) to minimize third-body quenching effects. Another common interference with  $\text{NO}_x$  measurements in the atmosphere is caused by the presence of such other nitrogen-containing compounds as peroxyacetyl nitrate (PAN), which can be converted into NO in the thermal converter. Again, these species are not suspected to be present in the experimental procedures used in this study.

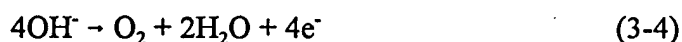
To prevent particulate matter contamination of the chemiluminescent analyzer, a 0.5  $\mu\text{m}$  pore size Teflon™ filter (Gelman Sciences, Ann Arbor, Michigan) was placed in the sample line at the analyzer sample inlet. This filter was found to be essentially non-reactive to  $\text{NO}_x$ . Without such a filter, it is quite easy to experience blockage of internal capillary tubing. Deposits could also form on the glass filter that separates the reaction chamber from the photomultiplier tube, causing a loss in instrument sensitivity (Klapheck and Winkler, 1985).

A continuous gas analyzer (Model IR-2100, Infrared Industries, Inc., Santa Barbara, California) was used to electrochemically measure  $\text{O}_2$  concentrations. The principle of

operation upon which this instrument is based is a simple coulometric process in which oxygen in the sample gas stream is reduced in an electrochemical cell. The gas stream enters the cathode cavity, with any oxygen being metered to the cathode through a diffusion barrier. At the cathode, oxygen is electrochemically reduced via the reaction



An electrolyte solution in the cathode cavity contains potassium hydroxide (KOH), which facilitates migration of the generated hydroxyl ions to an anode, where they are oxidized back to oxygen. This occurs following the reaction



The resulting cell current is directly proportional to the oxygen concentration in the sample gas stream. This current is measured electronically and is converted into an indicated concentration value. The instrument measures oxygen concentration between zero and 25%, with a manufacturer-reported accuracy of  $\pm 2\%$  of full-scale on all ranges. When using this instrument, one must keep the sample inlet pressure and flow rate within the specified limits to ensure accuracy of the measurement.

Multiple-point calibrations were performed on all instruments following procedures outlined in the appropriate instrument manuals. Certified standard gases were used as transfer standards whose composition is traceable to the National Institute of Standards and Technology, and appropriate calibration curves were determined by challenging the instruments with known standard mixtures. Typical calibration curves for the  $\text{NO}_x$  and  $\text{O}_2$  analyzers are shown in Figures 3-7 and 3-8, respectively. Daily zero and span checks were performed on each analyzer, and quality control charts were produced. Running sample

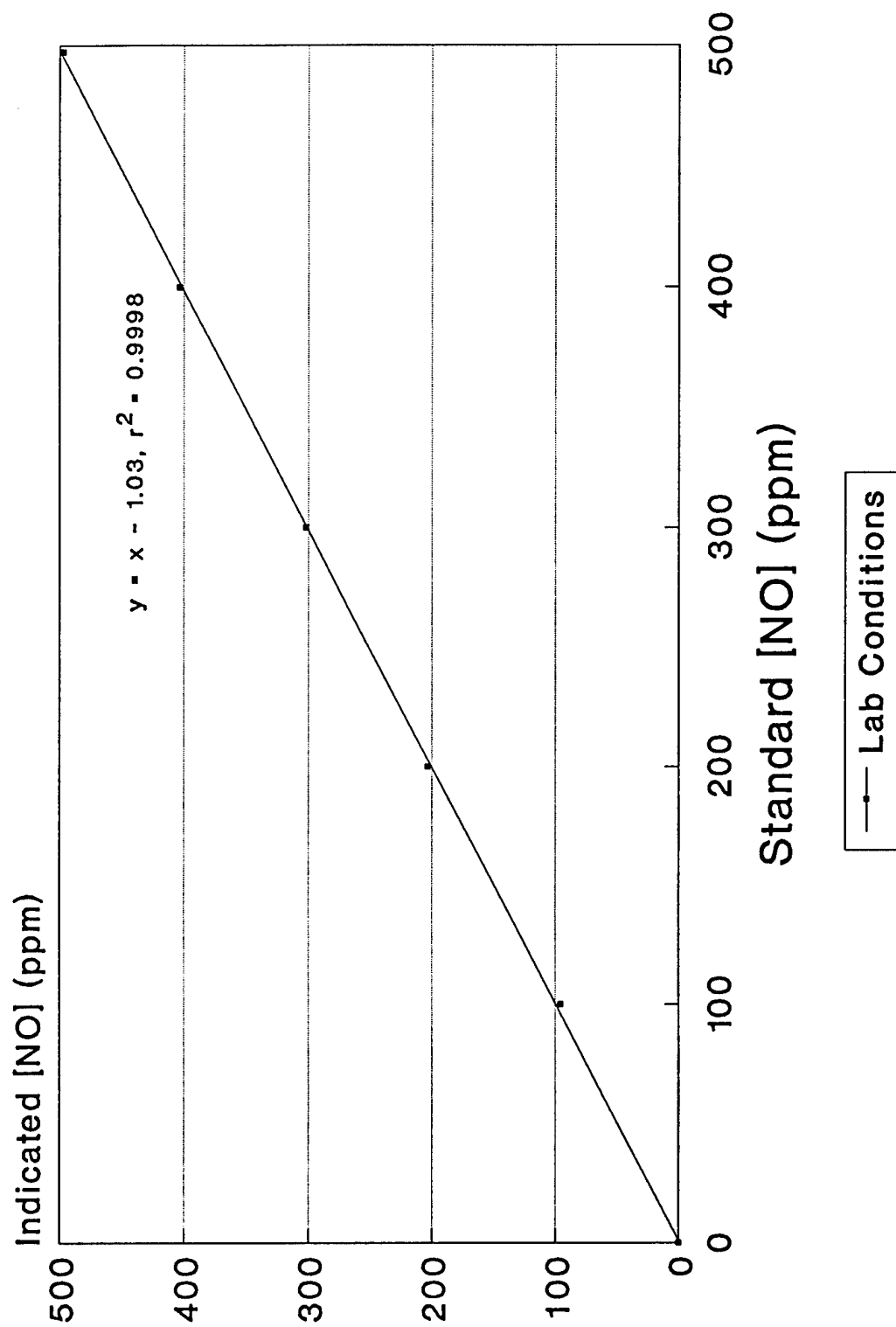


Figure 3-7. Typical chemiluminescent NO<sub>x</sub> analyzer calibration curve (for NO channel).



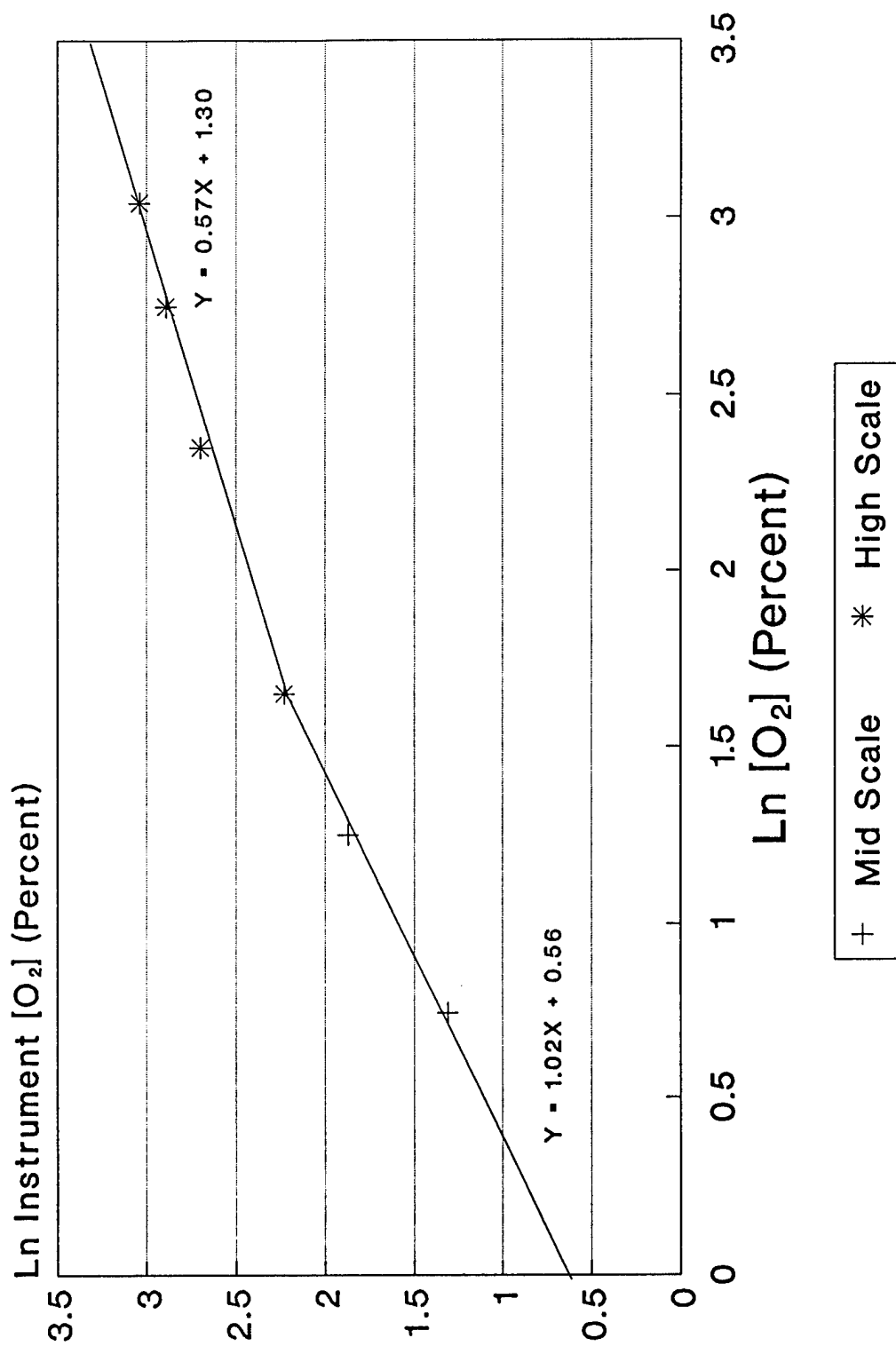


Figure 3-8. Typical IR-2100 oxygen analyzer calibration curve.

means and standard deviations were shown on the control charts. Based upon control chart results, instruments were recalibrated when necessary. Quality assurance was maintained by showing that all quality control systems were in good order.

As the NO/NO<sub>x</sub> chemiluminescent analyzer has a flow bypass system installed to ensure that samples are always collected at ambient pressure, all experimental measurements were made at the same bypass flow rate used during the initial calibration. Failure to do so can result in gas concentration measurement errors as great as 10 percent from one end of the bypass flow scale to the other. Additionally, a NO<sub>x</sub> generator (Model 100, Thermo Environmental Instruments, Franklin, Massachusetts) was used to determine the actual analyzer NO<sub>x</sub> converter efficiency and ensure that the efficiency exceeded 95%.

#### Sorbent Surface Area Determination

In preparation for packed-bed studies, BET surface areas of selected samples of laboratory-prepared MgO-vermiculite sorbent, Sorbtech-supplied sorbent, and raw coarse vermiculite were determined using a Micromeritics ASAP 2000 automated surface-area and pore size analyzer. Duplicate samples were run to verify the validity of the data. Small samples of sorbent (approximately one gram) were first degassed at an absolute pressure of 10 to 15 mm Hg at 623 K for approximately eight hours. Nitrogen gas (in helium) was sequentially added to the sample tube at a temperature of 77 K. The volumes of nitrogen adsorbed at various partial pressures between approximately 0.1 and 0.3 atmosphere were

recorded by the analyzer. These data were plotted according to the BET model to determine the total surface area of the sample. Initial screening results were used as an indication of the best preparation method to use in making the sorbent. Based upon these results, a large quantity of sorbent was prepared following the procedure already described. Five additional samples were taken and analyzed using the BET method for precision estimates.

#### Determination of Sorbent Particle Size

The MgO-vermiculite sorbent is inherently a highly heterogeneous material. As a result, the range of particle sizes in a given sorbent sample can be great. Samples of MgO-vermiculite sorbent were sieved using a standard ASTM sieving apparatus. Cumulative mass collected at each stage was plotted against particle diameter using a log-probability chart to determine the mass median particle diameter. This median size was used in all calculations for which sorbent particle diameter was required to determine flow characteristics through the packed bed. It was noted that this value may or may not be the most accurate value, since sieving the sorbent material likely causes a decrease in particle size through mechanical abrasion. The true size is probably somewhat larger. Data for magnesium oxide powder particle size was plotted similarly using a manufacturer-provided mass distribution. Once the MgO powder has been applied to the surface of the vermiculite, any agglomeration would tend to create larger size particles. It is not known, however, how the application of  $\text{Mg}(\text{OH})_2$  slurry affects particle size. Results of these determinations are presented in the following chapter.

## CHAPTER 4 RESULTS AND DISCUSSION

### Intrinsic Kinetic Studies

Experiments were conducted to collect data that provide insights into relevant parameters controlling NO<sub>x</sub> removal efficiencies, potential reaction mechanism(s) and reaction kinetics. Duplicate runs were conducted for every set of conditions to generate the data necessary for the determination of kinetic parameters. A comparison of results between duplicate runs under similar conditions showed remarkable reproducibility (statistical error < 5%). To determine intrinsic reaction kinetics, NO<sub>x</sub> concentrations were followed with increasing bed exposure time from a selected sampling valve, which represented a specific bed residence time. This was necessary because of a system artifact that created a lag-time of approximately 3-4 minutes to allow for line flushing until a stable instrument reading was reached after a sampling valve was selected. To explain further, for a given set of conditions, four separate runs would be necessary to collect data for all five sampling points; bed inlet, three points within the bed, and bed outlet. Bed inlet values were checked on all runs, before and after the other data were collected. Every 10 seconds, the three NO<sub>x</sub> analyzer channels displayed 10-second average NO, NO<sub>2</sub>, and NO<sub>x</sub> concentration values ([NO<sub>2</sub>] calculated by difference). Data were collected every minute throughout the run. From these data,

concentration versus bed residence time curves could be plotted. Values for the same bed exposure time were used to plot concentration of interest versus residence time, which was a function of sampling point location and, thus, reaction time.

### Limitation of Gas Film Mass Transfer Resistance

In the conduct of intrinsic chemical kinetic studies of gas–solid reactions in packed-bed reactor systems, it is critical that gas film mass transfer resistance to reaction be minimized. The following description of the limitation of this resistance is based upon the work of Fogler (1992) and Szekely et al. (1976). The mass flux from a fluid to a solid surface is the product of a mass transfer coefficient and the concentration driving force. When gas film mass transfer is rate-limiting, the extent of reaction or fractional solid conversion is linear with respect to time. In a packed-bed system, the concentration driving force is the difference between reactant concentration at the void space at a point in the bed and the concentration at the surface of the sorbent particle adjacent to this point. Gas film mass transfer resistance can generally be minimized by using small sorbent particles and high superficial gas velocities. At low velocities, the stagnant gas film boundary layer thickness is large – at high velocities this thickness is decreased, reducing the mass transfer limitation through increased convective mass transfer.

Operating at lower reaction temperatures also helps to reduce gas film mass transfer limitations. When a reaction is gas film mass transfer limited, it will generally be insensitive to increases in temperature. Since gas film mass transfer is not an activated process, while

chemical reactions can have substantial activation energies, operating at lower temperatures should lead to control by chemical kinetics, making intrinsic kinetic data collected in this range more valid. The effects of gas film mass transfer resistance were evaluated by varying flow rate through the bed at the highest reaction temperature and graphically evaluating its effect on initial reaction rate. Figure 4-1 is an example of this type of study. The definition of  $\text{NO}_2$  penetration is the fraction of inlet  $\text{NO}_2$  concentration that exits the bed at a given time, i.e.,  $C_{\text{out}}/C_{\text{in}}$ . While superficial gas velocity was varied by an order of magnitude, this did not greatly affect the initial rates. The absolute variation in associated rate constants determined during this type of evaluation was generally less than ten percent. Because increasing flow rate through the packed-bed by an order of magnitude did not significantly affect the reaction rate, the lowest flow rate was used for the majority of experimental runs to conserve cylinder gases.

It will be shown later that, in most cases, the initial chemical kinetics were affected by an increase in temperature, providing more evidence that gas film mass transfer was not rate limiting. Using the mass-transfer correlation of Ruthven (1968), the ratio of superficial velocity to sorbent particle diameter is sufficient to minimize mass-transfer resistance, within the temperature range evaluated. Because flow through a packed-bed is a highly complex phenomenon and the intricate details relative to the gas-solid reaction mechanism and the physical characteristics of the solid sorbent are not fully understood, it is possible that some gas-film resistance to reaction exists. However, based upon the preceding discussion, it does appear that this resistance has been effectively minimized in this experimental research study.

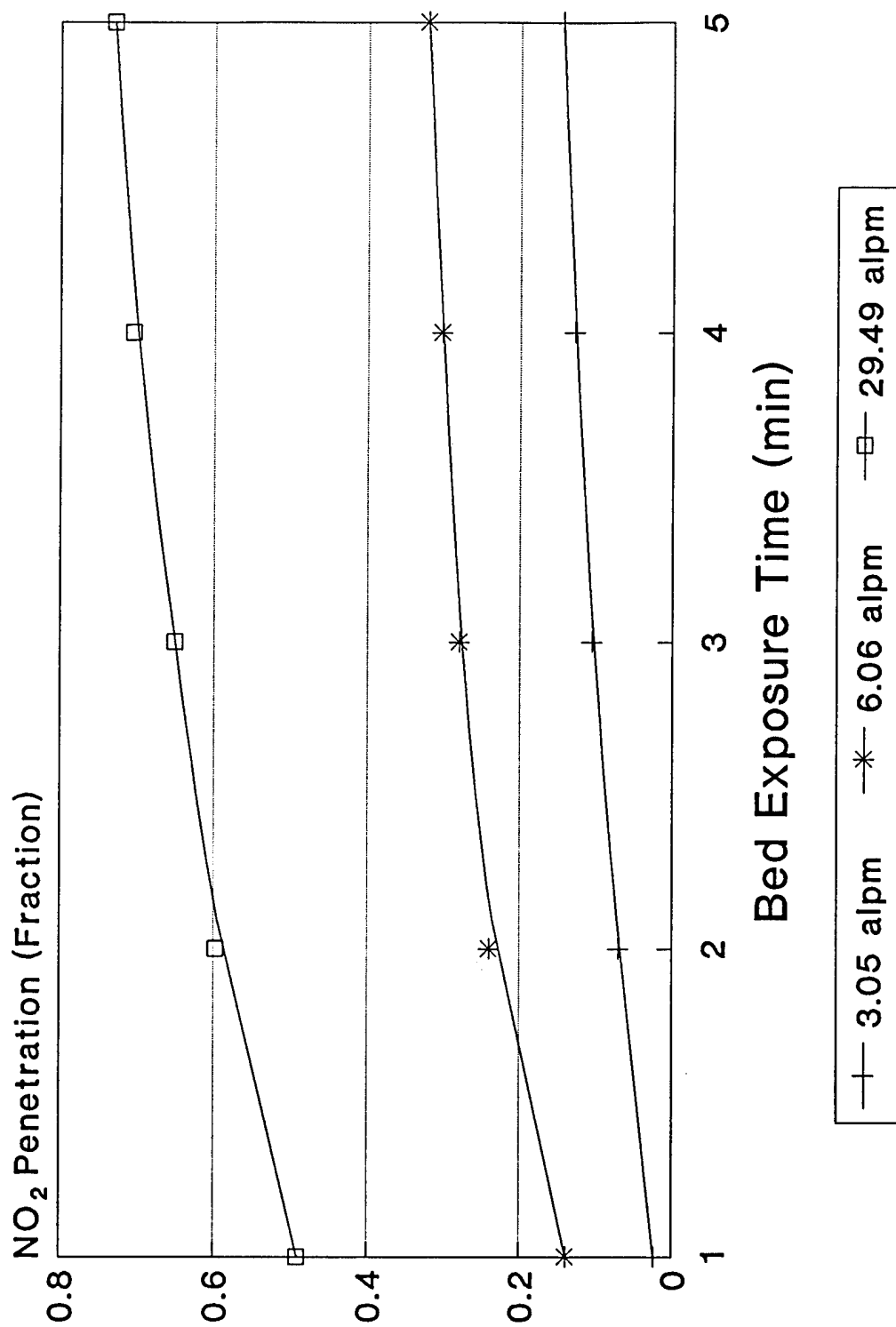


Figure 4-1. Gas film mass-transfer resistance evaluation - NO<sub>2</sub> penetration ( $C_{out}/C_{in}$ ) versus bed exposure time ( $[NO]_{in}=200$  ppm,  $T=473$  K,  $[O_2]=0\%$ ).

### Solid Sorbent Characterizations

#### Surface Area Analyses

Five samples of the composite batch of MgO-coated vermiculite were randomly selected for BET-specific surface area analyses. The intent was to look at the variability in surface area between smaller batches of material prepared in the laboratory. If the variation between samples is small enough, the mean surface area and sample standard deviation can be used to establish confidence limits for sorbent sample surface area. Results are shown in Table 4-1.

Table 4-1. BET surface areas of selected samples of laboratory prepared  
MgO-vermiculite sorbent.

Sample	BET Surface Area (m <sup>2</sup> /g)
A	41.92 + 0.19
B	36.08 + 0.15
C	37.93 + 0.11
D	39.20 + 0.17
E	42.10 + 0.17
Mean	39.45
Sample Standard Deviation	2.59



### Particle Size Distributions

A sample of MgO-vermiculite sorbent was sieved, as previously described, and results were plotted on a log-probability graph, shown in Figure 4-2. Since many particle size data are log-normally distributed, this type of plot should produce a linear representation from which relevant statistical parameters -- most importantly, the mass median diameter and geometric standard deviation -- can be determined. From Figure 4-2, it can be seen that the distribution is fairly linear between the 10th and 90th percentiles, so these data were used for this purpose. From the distribution, the mass median diameter (MMD) is approximately 1.7 mm, and the geometric standard deviation ( $\sigma_g$ ) is approximately 1.5. Since the sorbent particles were mechanically abraded during the sieving process, the true MMD is probably somewhat larger, perhaps in the range of 2 to 3 mm. The median diameter determined here, however, can be used for calculating flow characteristics for a packed bed filled with this type of sorbent.

A log-probability graph for the manufacturer-supplied size-distribution data on the MgO powder used to prepare the combination sorbent is shown at Figure 4-3. From this graph, the MMD for the MgO powder used is approximately 1.3  $\mu\text{m}$ , and  $\sigma_g$  is equal to approximately 2.5. Since the chemical reaction occurs at the surface of the MgO particles, this distribution can provide useful data for use in determining physical parameters via the shrinking unreacted-core model. The MMD is probably not the most appropriate dimension to use for these purposes, however, since the reactions occurring

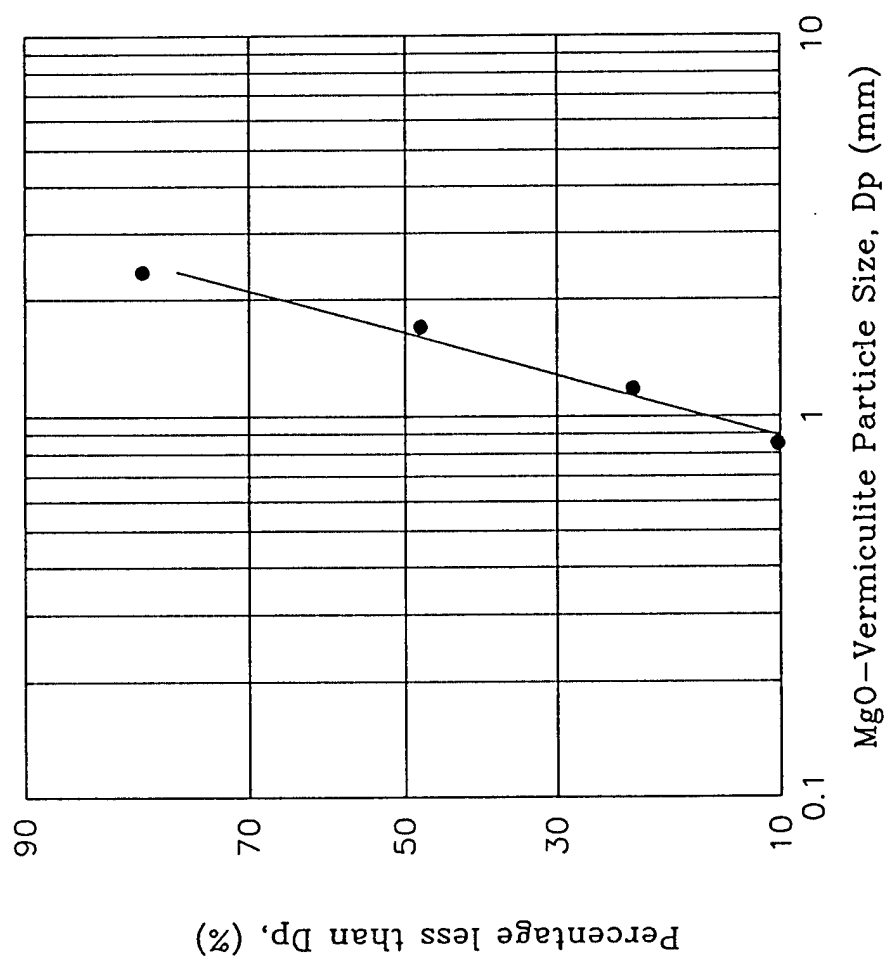


Figure 4-2. Log-probability plot of MgO-vermiculite sorbent particle size distribution.

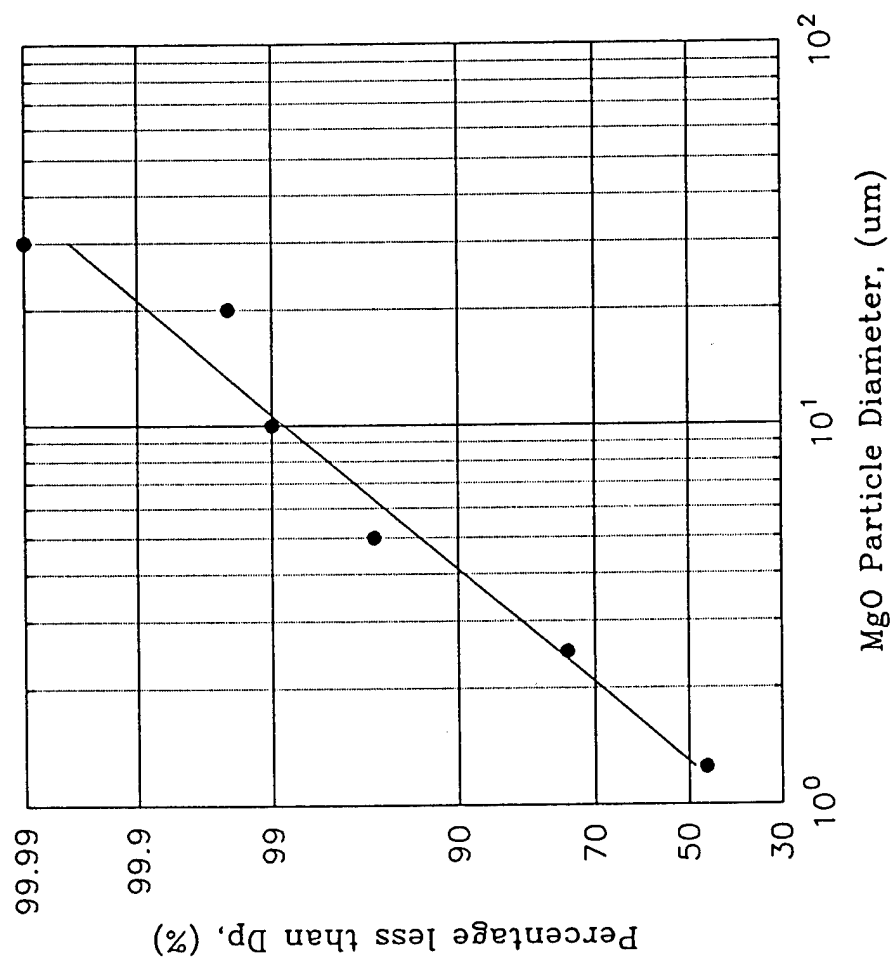


Figure 4-3. Log-probability plot of Akrochem Elastomag ® 170 MgO powder particle size distribution (manufacturer-provided data).

on the particles are a function of particle surface area. The MgO particle surface median diameter can be calculated from the log-probability distribution using the well-known Hatch-Choate equations (Hinds, 1982). A calculated count median diameter of approximately 0.1  $\mu\text{m}$  led to the determination of a value of approximately 0.6  $\mu\text{m}$  for the surface median diameter using these equations.

#### NO<sub>x</sub> Removal by Mg(NO<sub>3</sub>)<sub>2</sub>-coated Vermiculite

Results for Mg(NO<sub>3</sub>)<sub>2</sub>-coated vermiculite were similar to those for the plain heat-treated vermiculite. Removals of NO<sub>2</sub> were less than five percent over the range of temperatures (373 to 473 K) and concentrations (20 to 200 ppm) evaluated. NO removal efficiencies were much lower, and approached zero. The results of these tests were useful in verifying that if magnesium nitrate is formed on the solid surface during the course of the MgO (Mg(OH)<sub>2</sub>) reaction with NO<sub>2</sub>, and all the remaining MgO (or Mg(OH)<sub>2</sub>) is utilized or is otherwise unavailable for reaction, then these results preclude the further removal of NO<sub>x</sub> from the gases supplied to the bed, and reaction/removal should cease.

#### NO<sub>x</sub> Removal by Sorbent Material

It was found to be more difficult to remove NO than NO<sub>2</sub> by reaction with MgO, the former being generally less reactive than the latter. The removal of each species was independently affected by the experimental variables evaluated. Specific results are described in the following paragraphs.

### NO Removal by Sorbent Material

NO removal by MgO-coated vermiculite sorbent appeared to depend on inlet NO concentration and bed temperature. At low inlet NO concentrations ( $< 10$  ppm), NO removal efficiencies varied from initial values of approximately 60 percent to over 90 percent. In general, initial NO removal efficiency was greater at 373 K than at 423 or 473 K, indicating removal by physisorption rather than by chemisorption. The presence of water or water vapor did improve the removal efficiency of NO, but overall rates of removal were still low. As previously described, apparent NO removal was enhanced by the presence of oxygen, through the formation of  $\text{NO}_2$ . In their evaluation of NO removal by  $\text{Ca}(\text{OH})_2$  solids, Chu and Rochelle (1989) found that the gas- or solid-phase oxidation of NO to  $\text{NO}_2$  played an important role in the removal of the former. At higher NO concentrations ( $> 100$  ppm), the overall removal efficiencies were lower (less than 30 percent). Jozewicz et al. (1990) found no NO (from a 400 ppm NO gas stream concentration) removal by  $\text{Ca}(\text{OH})_2$  solids without the presence of oxygen at temperatures between 70 and 180 C. Carbon monoxide (CO) has been widely used as a probe molecule in surface science studies because it is one of the simplest adsorbate-adsorbent systems. Mejias et al. (1995) found the interaction of CO on MgO to be weak and of electrostatic origin, without noticeable chemical contributions. Since CO and NO are similarly non-reactive, this observation suggests that there may be a fixed NO sorption capacity, possibly the result of limited surface area available for physisorption.

Figure 4-4 is a representative concentration profile for NO removal by a MgO-vermiculite sorbent bed, without a significant quantity of  $\text{NO}_2$  present. As can be seen

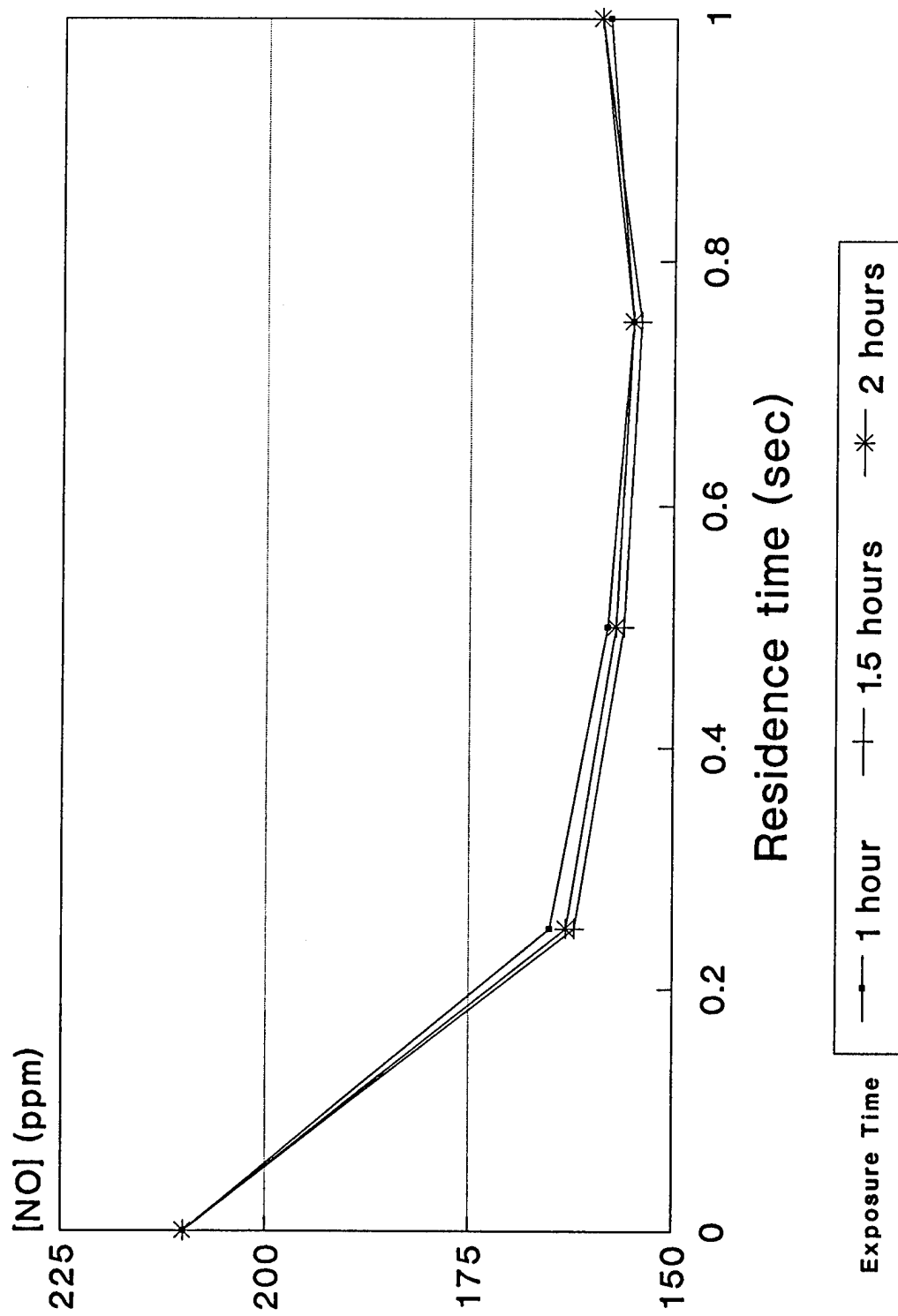


Figure 4-4. NO removal by humidified MgO-vermiculite sorbent ( $[\text{NO}]_{\text{in}}=210$  ppm,  $T=423$  K,  $[\text{O}_2]=11\%$ ,  $3\%$   $\text{H}_2\text{O}$  vapor).

from the figure, the bed did not remove a large amount of NO from the flowing gas stream, even in this case, with both water vapor and oxygen present. The observed NO removal may be the result of its oxidation to form NO<sub>2</sub>, which is removed by the bed. Since the gases were humidified, it is reasonable to assume that the MgO on the sorbent surface was hydrated to the hydroxide form. In general, when NO<sub>2</sub> was present, NO was no longer removed after a specific exposure time and was actually produced after sorption of sufficient NO<sub>2</sub>. The latter observed effect will be discussed later.

#### NO<sub>2</sub> Removal by Sorbent Material

Overall NO<sub>2</sub> removal efficiencies were found to greatly exceed those for NO. Initial NO<sub>2</sub> removal efficiencies were always greater than 90 percent. As bed exposure time to NO<sub>2</sub> progressed, NO<sub>2</sub> removal efficiency decreased, suggesting a "saturation" phenomenon. After approximately one hour of exposure time, NO<sub>2</sub> removal efficiency approached a stable value that was much greater than zero. Typical plots of NO<sub>2</sub> concentration versus residence time data are shown in Figure 4-5. In all of the cases evaluated, an intrinsic first-order kinetic dependence was observed:

$$-dC/dt = kC \quad (4-1)$$

where C= NO<sub>2</sub> concentration in ppm, t=residence time in seconds, and k=first-order rate constant in sec<sup>-1</sup>. Integrating equation (4-1) produces:

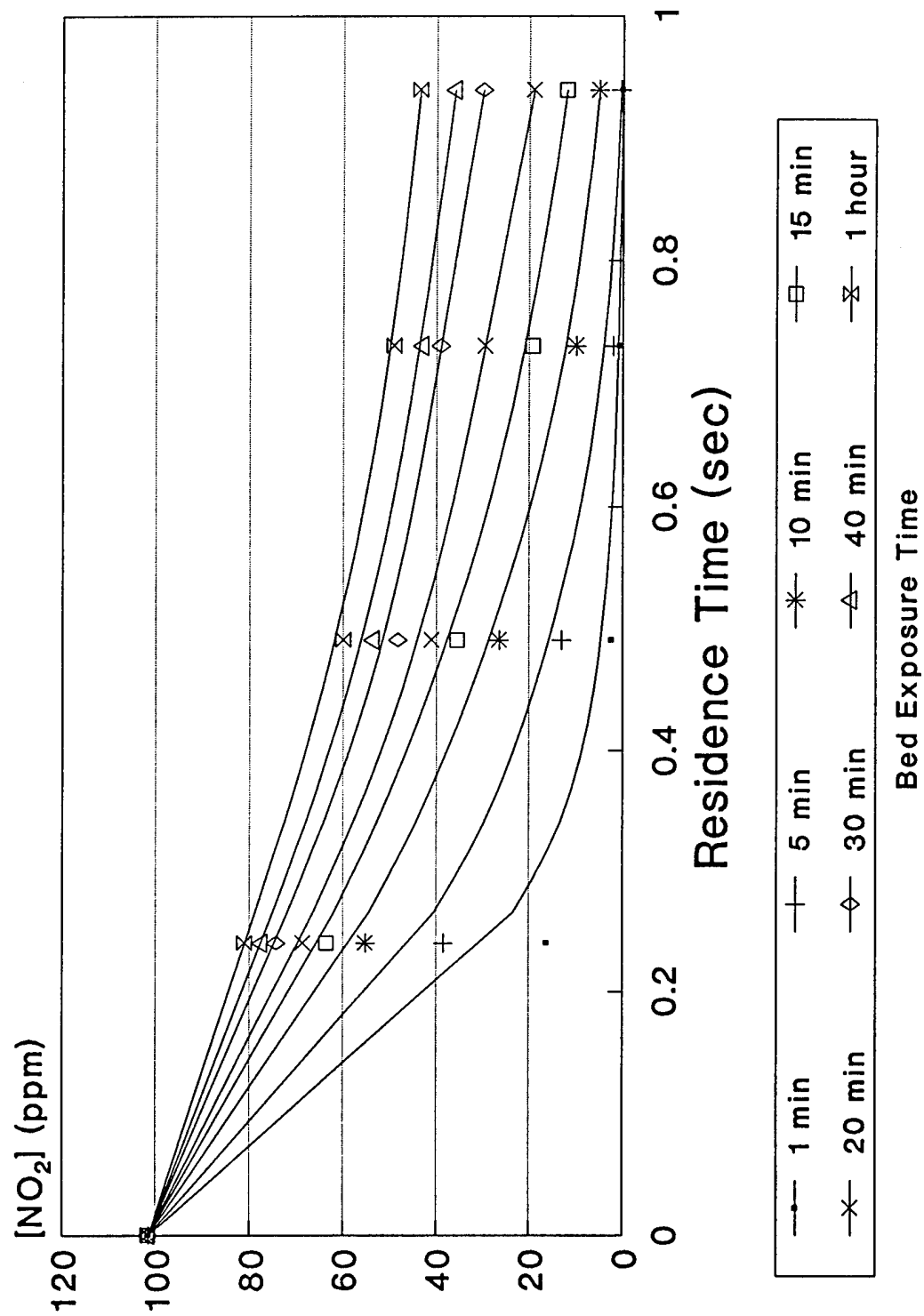


Figure 4-5.  $\text{NO}_2$  removal versus residence time ( $T=473\text{ K}$ ,  $[\text{O}_2]=9.9\%$ ).



$$C = C_o \exp(-kt) \quad (4-2)$$

where  $C_o$  = Inlet  $\text{NO}_2$  concentration in ppm and  $t$  = bed residence time in seconds.

From Equation (4-2) it can be seen that a plot of  $\ln(C/C_o)$  versus  $t$  should be linear, with a slope of  $-k$ , if the reaction is first-order. Data from Figure 4-5 are plotted in this way in Figure 4-6. A first-order kinetic expression appeared to describe  $\text{NO}_2$  removal and was used as a basis to model  $\text{NO}_2$  decay. Plots similar to that shown in Figure 4-6 were used to determine rate coefficients for different experimental conditions. Having established in all earlier runs evaluated that data from five sampling points produced sufficiently linear first-order plots, only three points were used to determine rate constants in subsequent runs, concentrations at the inlet and outlet and at a point within the bed.

Since the bed surface nature is changing with time during runs, values for  $k$  also change with time. Figure 4-7 is a representative figure showing the decrease in  $k$ -values as reaction (exposure) progresses. Also, as reaction progresses, the rate of change in rate coefficient values between readings decreases. This decrease in first-order rate coefficients with increasing bed exposure time may be associated with a change in activation energy, possibly indicative of a transition from one rate-limiting mechanism to another. Noticing this trend allowed for the derivation of a predictive empirical relationship between the first-order rate constant value and bed exposure time, which will be presented later. In the context of the shrinking unreacted core model, this may represent the transition from chemical reaction kinetics control (with significant associated activation energy) to a diffusion-controlled process, which would be a slow process. It was found that an (dynamic) equilibrium

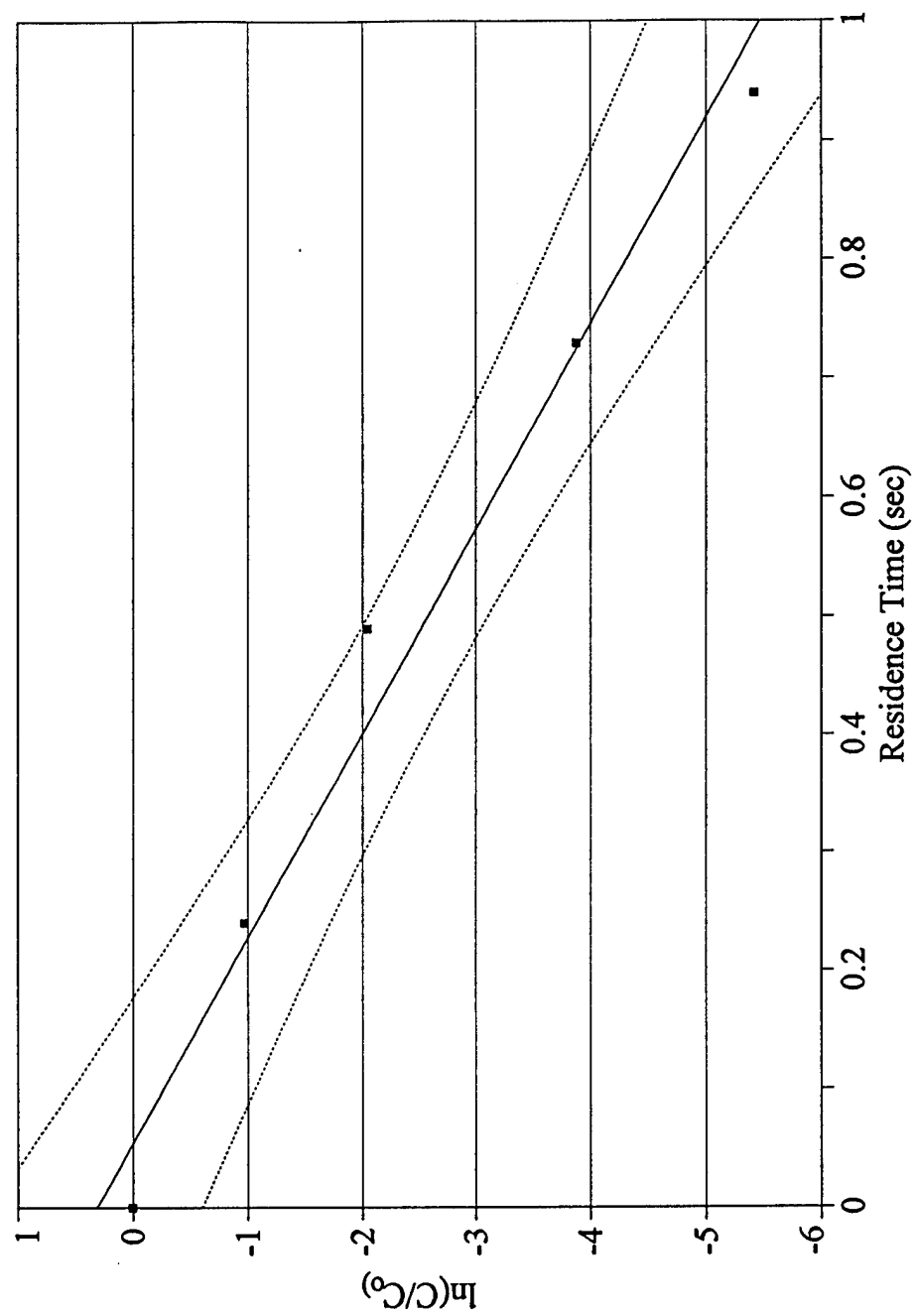


Figure 4-6. First-order kinetic plot ( $[\text{NO}_2]_m = 100$  ppm,  $T = 473$  K,  $[\text{O}_2] = 10\%$ ). Dashed lines represent 95% confidence limits.

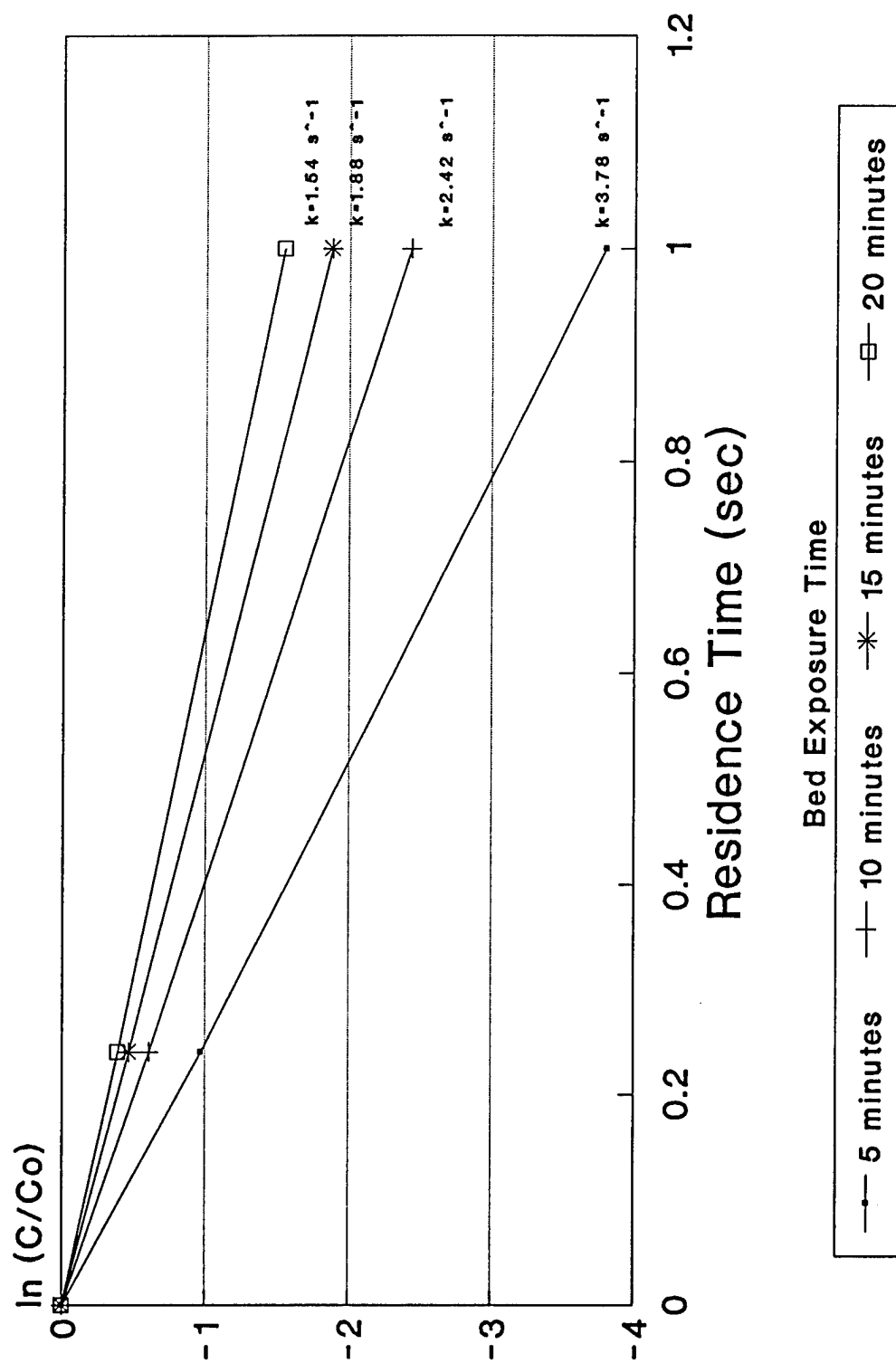


Figure 4-7. First-order kinetic plot ( $[NO_2]_{in} = 100$  ppm,  $T = 473$  K,  $[O_2] = 10.5\%$ ).

condition occurred after approximately 5-10 minutes of bed exposure time, providing the most reliable results for subsequent experiments and data analyses. While these data were most useful for the prediction of sorbent behavior with time, it made the accurate determination of intrinsic (or apparent) activation energies more difficult. Data on the activation energies associated with  $\text{NO}_x$  removal by surface reaction with the  $\text{MgO}$ -vermiculite sorbent will be presented in the following section, in which the effects of reaction temperature are described.

### Effects of Operational Variables

Numerous experiments were conducted to thoroughly evaluate the effects of operational variables of primary importance, such as reactive gas concentrations, humidity, reaction temperature, and gas flow rate. The combination of these results provided a clear picture, from which conclusions regarding probable reaction mechanisms and the dominant factors governing the  $\text{NO}_x$  removal capabilities of the sorbent material were drawn.

#### Effects of $\text{NO}_2$ Concentration

The effects of  $\text{NO}_2$  concentration on overall removal rates were dependent upon the bed temperature at which data were collected. Figures 4-8 through 4-10 show representative  $\text{NO}_2$  penetration versus bed exposure time data as a function of inlet  $\text{NO}_2$  concentration for the three reaction temperatures evaluated.  $\text{NO}_2$  penetration is defined as the percentage (fraction) of inlet  $\text{NO}_2$  exiting the bed at any given bed exposure or reaction time, or  $C_{\text{out}}/C_{\text{in}}$ . Obviously, this value is (in percent) 100% minus the  $\text{NO}_2$  removal efficiency percentage. In

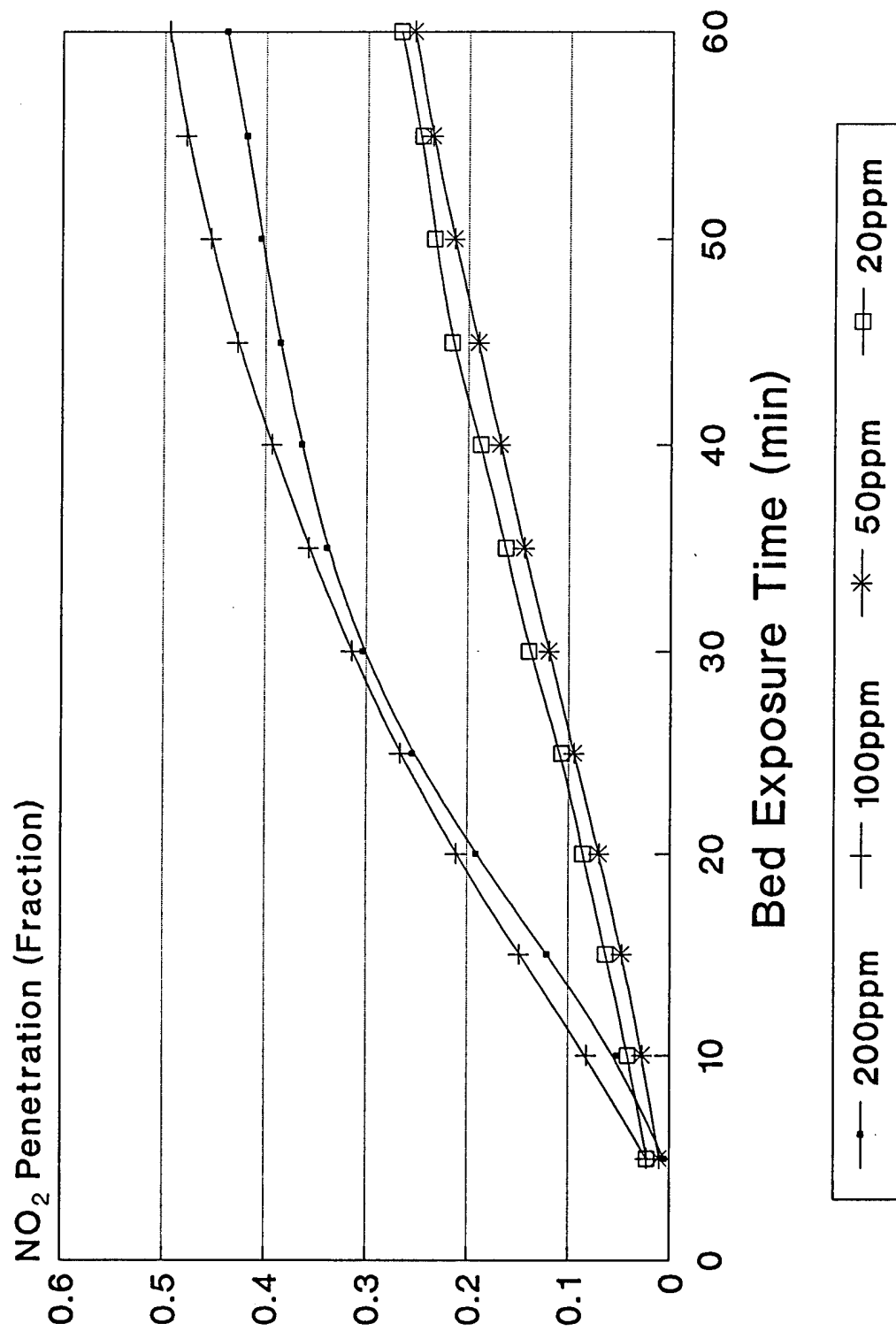


Figure 4-8. NO<sub>2</sub> penetration vs bed exposure time (T=473 K, [O<sub>2</sub>]=0%)

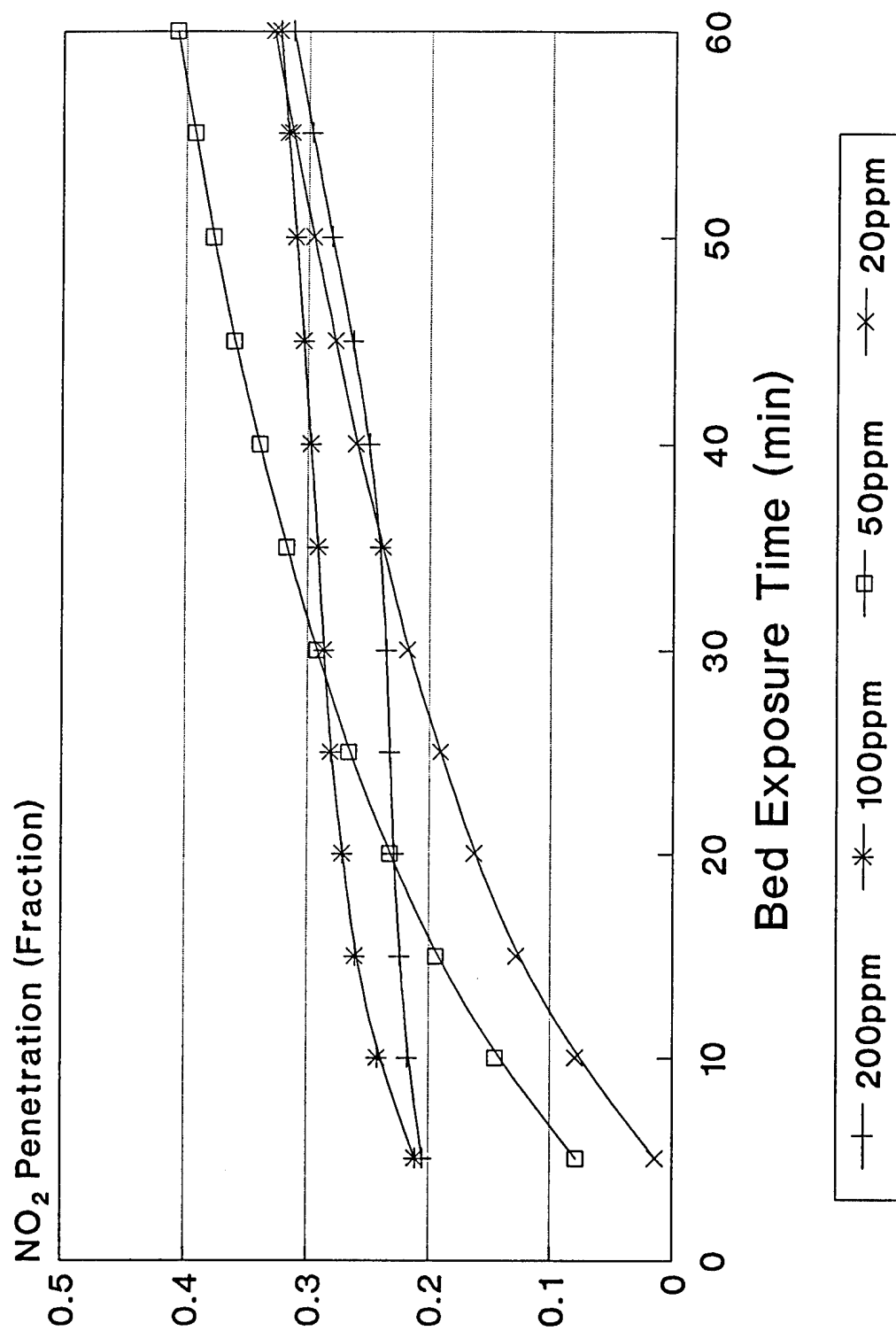


Figure 4-9. NO<sub>2</sub> penetration vs bed exposure time (T=423 K, [O<sub>2</sub>]=0%)

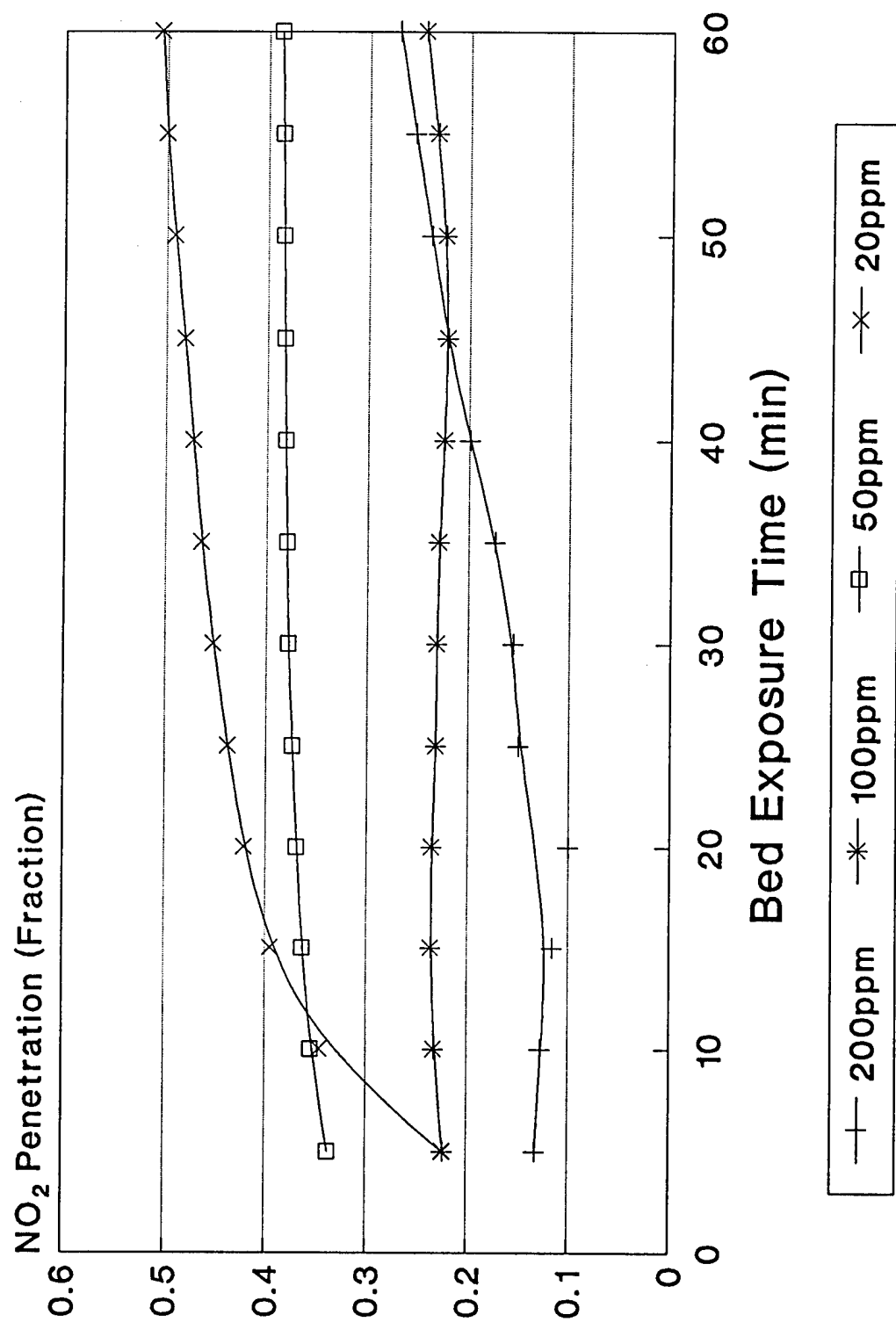


Figure 4-10. NO<sub>2</sub> penetration vs bed exposure time (T=373 K, [O<sub>2</sub>]=0%).

general, higher  $\text{NO}_2$  concentrations ( $\geq 100$  ppm) were removed more efficiently and more rapidly than lower  $\text{NO}_2$  concentrations, particularly at elevated temperature. This finding validates the use of a concentration-dependent chemical reaction model. The higher concentrations of  $\text{NO}_2$  may provide more opportunity for contact with active sites on the sorbent surface area at which the chemical reaction(s) take place. In some cases, this may mean that the external sorbent particle surface becomes covered by an "inert" ( $\text{Mg}(\text{NO}_3)_2$ ) product layer, leading to rate limitation by a diffusion-controlled process following the shrinking unreacted core mechanism. A higher concentration gradient would provide a driving force to facilitate pore diffusion and diffusion through the inert ( $\text{Mg}(\text{NO}_3)_2$ ) product layer to available remaining reactive  $\text{MgO}$  surface area in the interior portions of the sorbent particles.

Representative  $\text{NO}_2$  penetration data presented in Figure 4-8 shows that at a reaction temperature of 473 K, initial  $\text{NO}_2$  penetration was low (less than one percent), suggesting that the  $\text{NO}_2$  removal efficiency was greater than 99%, for all concentrations evaluated. After an initial conditioning period of approximately 10 minutes, there is a distinct diversion between the curves representing 20 and 50 ppm and the curves representing 100 and 200 ppm.  $\text{NO}_2$  penetration increased to approximately 45-50% for the latter, while it remained at approximately 25% for the former. Also, the rate of change of penetration was significantly higher for the higher  $\text{NO}_2$  concentrations. Kinetically, the fast initial reaction suggested that significantly more  $\text{NO}_2$  was removed at higher concentrations in a shorter period of time than at lower concentrations. It is possible that the decreases in  $\text{NO}_2$  removal rates at approximately 25 minutes for the two higher concentrations correspond to the completion of the "inert" surface-product-layer shell, whereas for the two lower concentrations, the exterior



surface is still being converted into an inert product layer after the same period of exposure time.

From Figure 4-9, at a reaction temperature of 423 K, initial  $\text{NO}_2$  penetration is lowest for the two lower inlet concentrations. Since there is less energy being supplied via heat energy to overcome the activation energy barrier, it may be that only a limited number of molecules can be removed. After approximately 25 minutes of bed exposure time have elapsed, the overall penetration numbers again converged toward a value between approximately 30 and 40 percent. At a reaction temperature of 373 K (Figure 4-10), there was no discernible pattern observe for the initial penetration values, although the value for an inlet  $\text{NO}_2$  concentration of 20 ppm remained the lowest. Toward the end of the bed exposure time period, however,  $\text{NO}_2$  penetrations were lowest for the two highest concentrations. This may be an indication of the higher concentration gradient serving to facilitate  $\text{NO}_2$  removal in promoting diffusion of the  $\text{NO}_2$  molecules toward available  $\text{MgO}$  interior reaction surfaces. Intrinsic first-order rate constants for these data are shown in Table 4-2.

#### Effects of Oxygen

Like  $\text{NO}$  removal, initial  $\text{NO}_2$  removal efficiencies were improved when oxygen was present. Since some  $\text{NO}$ , present as impurity in the  $\text{NO}_2$  gas supplied, is oxidized to  $\text{NO}_2$ , the actual  $\text{NO}_2$  removal rate may be higher than observed, particularly at lower temperatures. It is possible that  $\text{NO}$ , which is physisorbed on the sorbent surface, is eventually oxidized to  $\text{NO}_2$  before being sorbed to form a nitrite or nitrate compound. Since  $\text{O}_2$  concentrations were at the percent level, they are considered to be in great excess relative to  $\text{NO}_2$

Table 4-2. Intrinsic first-order rate coefficients ( $s^{-1}$ ) for  $NO_2$  removal by MgO-vermiculite sorbent ( $[O_2]=0\%$ )

NO <sub>2</sub> Concentration : Reaction Temp (° K):	200 ppm			100 ppm			50 ppm			20 ppm		
	473	423	373	473	423	373	473	423	373	473	423	373
1 minute	3.78	1.98	2.18	7.33	2.45	2.42	7.25	6.27	1.20	7.63	6.05	3.89
2 minutes	2.68	1.73	2.07	6.12	1.73	2.37	6.14	4.11	1.15	7.62	6.01	2.78
5 minutes	1.96	1.57	1.81	3.83	1.26	2.20	4.85	2.61	1.02	5.81	4.47	1.55
10 minutes	1.69	1.51	1.81	2.53	1.07	1.87	3.79	1.98	0.98	4.70	2.65	1.10
15 minutes	1.58	1.48	1.85	1.93	1.00	1.53	3.19	1.68	0.95	4.06	2.16	0.96
20 minutes	1.52	1.46	1.94	1.58	0.94	1.52	2.78	1.49	0.94	3.65	1.90	0.89
30 minutes	1.37	1.44	1.95	1.17	0.86	1.54	2.23	1.26	0.92	2.98	1.59	0.82
40 minutes	1.19	1.38	1.70	0.94	0.79	1.57	1.87	1.11	0.90	2.70	1.41	0.78
60 minutes	0.98	1.15	1.38	0.71	0.70	0.95	1.44	0.92	0.89	2.32	1.16	0.71

concentrations. For this reason, the apparent first-order kinetics was not affected by the presence of  $O_2$  in exhaust gases.

Representative plots of  $NO_2$  penetration versus bed exposure time, similar to those shown for experimental runs where oxygen was present, are shown at Figures 4-11 through 4-13. In Figure 4-11, at a reaction temperature of 473 K, initial  $NO_2$  penetration values were less than 1% for all three  $NO_2$  concentrations evaluated. In this case, an inlet  $NO_2$  concentration of 200 ppm was not evaluated, since the  $NO_2$  cylinder contained only 200 ppm gas, and therefore, dilution with air would have decreased this concentration. The shapes of the penetration curves are similar to those seen in Figure 4-8, with  $NO_2$  penetration remaining low (and removal efficiency remaining high) for an inlet  $NO_2$  concentration of 20 ppm. Overall  $NO_2$  penetrations for runs with oxygen present remained lower at a reaction temperature of 473 K when compared to runs conducted without oxygen. The presence of oxygen may facilitate the continued  $NO_2$  removal by the sorbent.

This distinction between  $NO_2$  penetration in the presence and absence of  $O_2$  did not apply for all  $NO_2$  concentrations at a reaction temperature of 423 K (Figure 4-12).  $NO_2$  penetration after a bed exposure time of one hour was actually higher for an inlet  $NO_2$  concentration of 100 ppm when oxygen was present compared to when oxygen was absent. At 50 ppm  $NO_2$ , the penetrations were approximately the same and were less at 20 ppm. At this temperature (423 K), oxygen may aid in the removal of low concentrations of  $NO_2$ . At a reaction temperature of 373 K (Figure 4-13) the  $O_2$  effect trend was reversed. Similar to the effect seen in Figure 4-10, at the lowest temperature evaluated, it appears that a sufficient gas-solid concentration gradient must exist to provide the driving force for reaction to occur.

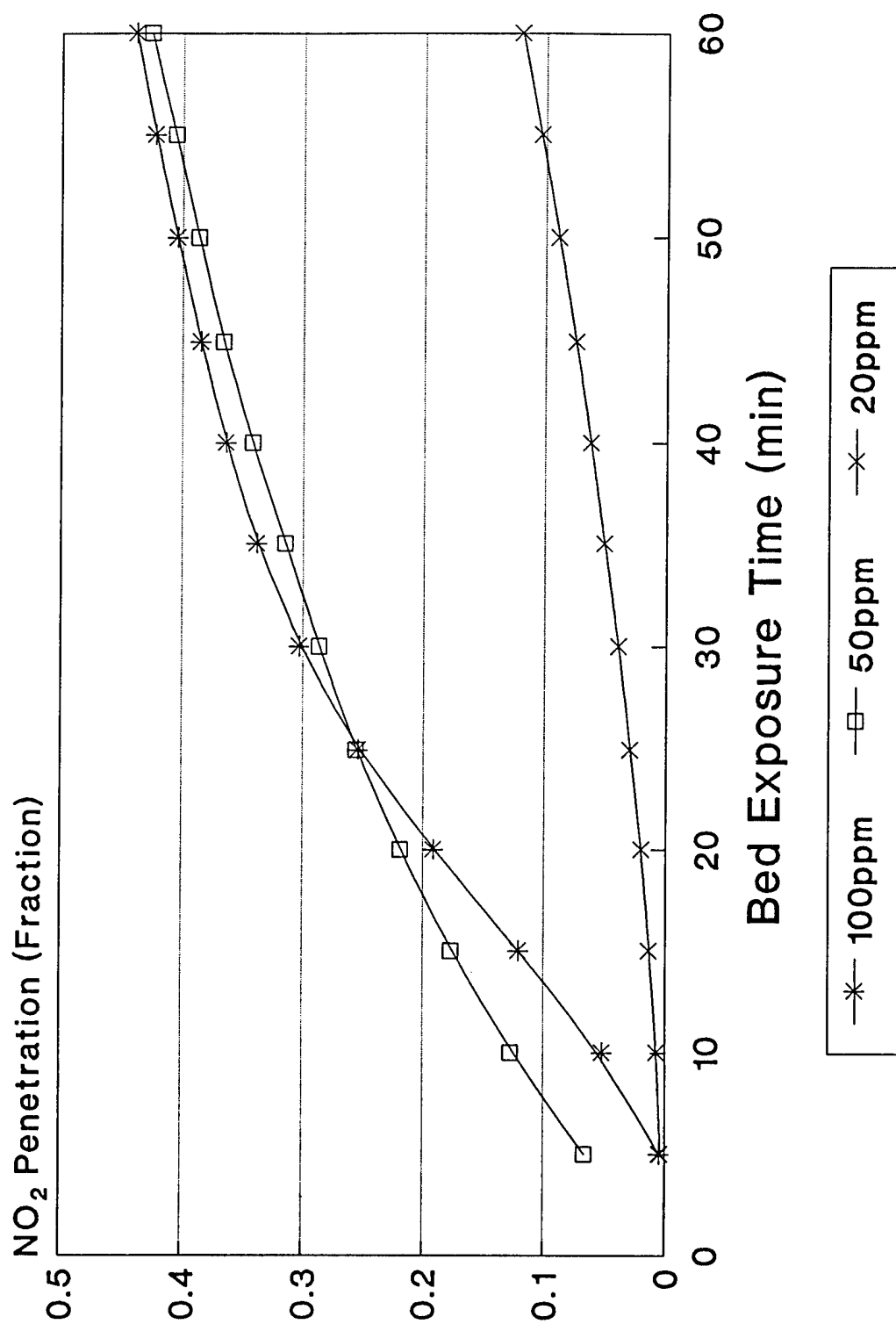


Figure 4-11. NO<sub>2</sub> penetration vs bed exposure time (T=473 K, [O<sub>2</sub>]=10%).

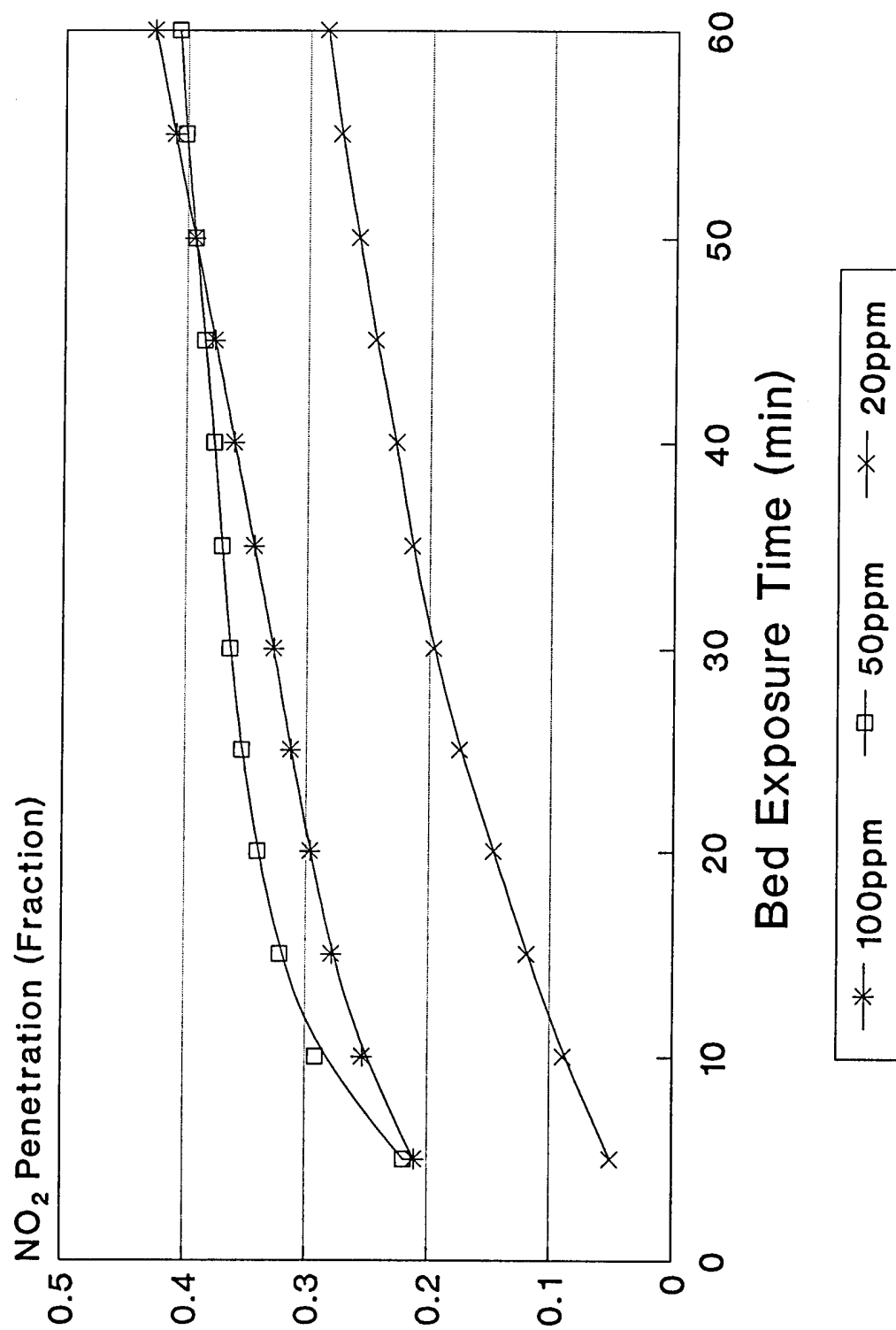


Figure 4-12. NO<sub>2</sub> penetration vs bed exposure time (T=423 K, [O<sub>2</sub>]=10%).

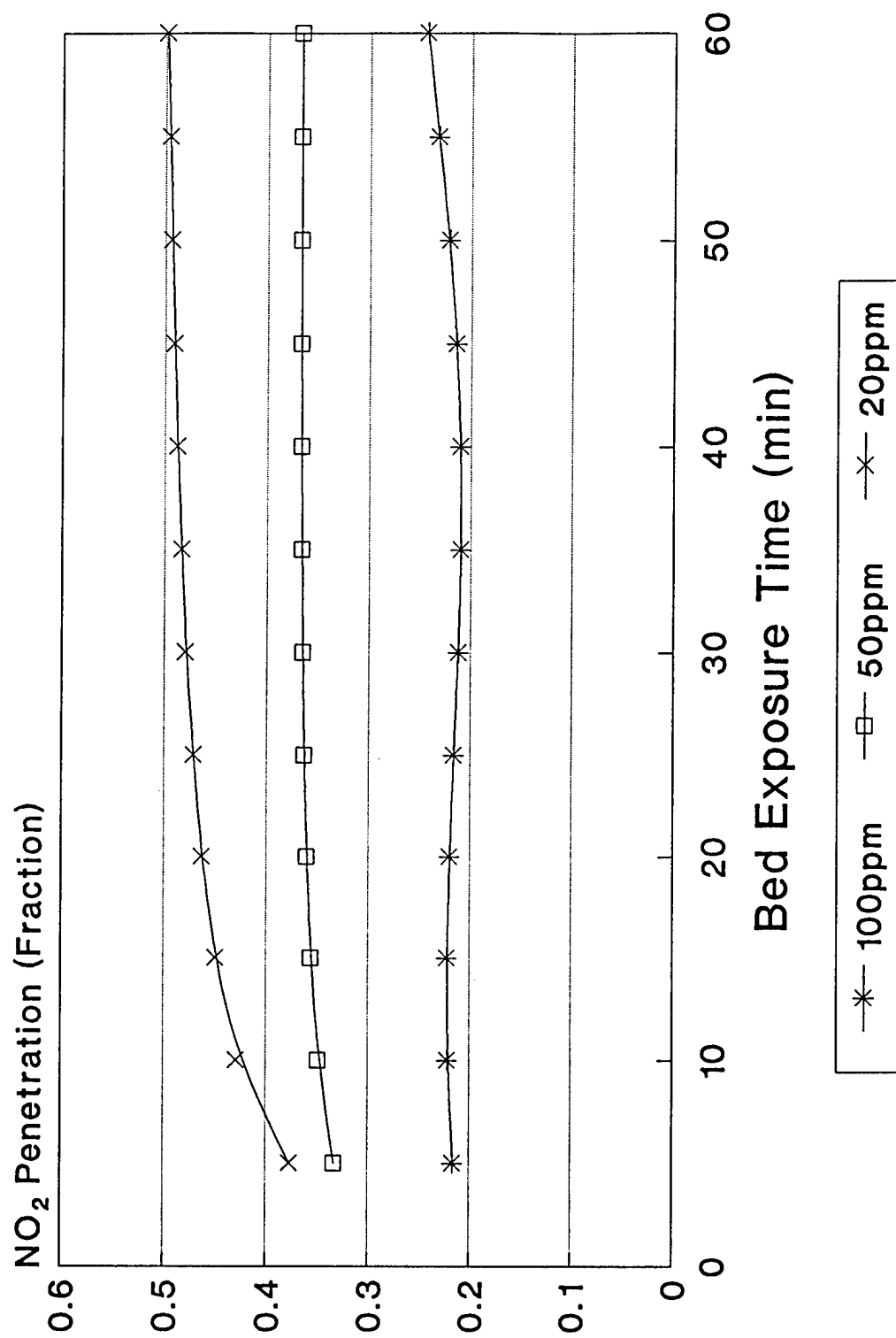


Figure 4-13. NO<sub>2</sub> penetration vs bed exposure time (T=373 K, [O<sub>2</sub>]=10%).

While initial  $\text{NO}_2$  penetration was lowest for an inlet  $\text{NO}_2$  concentration of 20 ppm, it rapidly increased and reached a value of approximately 50%. This short initial period of efficient removal may represent the small quantity of  $\text{NO}_2$  molecules initially physically adsorbed on the surface of the sorbent, or a chemical reaction induction period which occurs before dynamic equilibrium conditions are achieved.

From all of these data, it seems apparent that the range of reaction temperatures evaluated encompass a transition region where sorbent  $\text{NO}_2$  removal characteristics in the presence of oxygen are changing. The significance of the effects of temperature variation on  $\text{NO}_2$  penetration and the difficulty in distinguishing between these effects at the two lower temperatures will be examined in a later section. Table 4-3 contains intrinsic first-order rate coefficient data obtained with  $\text{O}_2$  present, which can be compared to the values displayed in Table 4-2 as a means of estimating the significance of oxygen in its effect on  $\text{NO}_2$  removal by the sorbent.

#### Effects of Bed Temperature

There appeared to be a  $\text{NO}_2$  reaction rate dependence on bed temperature when temperatures exceeded 423 K. In the range from 373 to 423 K, initial first-order  $\text{NO}_2$  removal rate coefficients were often approximately the same. When temperatures greater than 423 K were used, there was a much greater difference in first-order rate coefficient values. As expected, with all other variables kept constant, higher bed temperatures produced higher rate coefficient values. Additionally, as temperature increases, theoretically, more adsorbate molecules with sufficient activation energy for reaction to occur will strike the

Table 4-3. Intrinsic first-order rate coefficients ( $s^{-1}$ ) for  $NO_2$  removal by  $MgO$ -vermiculite sorbent ( $[O_2]=10\%$ )

NO <sub>2</sub> Concentration : Reaction Temp (° K):	100 ppm			50 ppm			20 ppm		
	473	423	373	473	423	373	473	423	373
1 minute	4.74	2.81	1.74	4.94	3.25	1.55	6.94	7.46	2.39
2 minutes	4.87	2.18	1.64	3.98	2.28	1.25	6.55	4.58	1.45
5 minutes	3.78	1.57	1.55	2.84	1.50	1.09	5.71	3.01	1.01
10 minutes	2.42	1.38	1.53	2.16	1.21	1.05	5.02	2.45	0.88
15 minutes	1.88	1.29	1.52	1.81	1.11	1.03	4.33	2.15	0.83
20 minutes	1.54	1.22	1.53	1.59	1.06	1.02	3.92	1.94	0.80
30 minutes	1.09	1.13	1.57	1.31	1.00	1.00	3.24	1.65	0.76
40 minutes	0.87	1.04	1.58	1.13	0.96	1.00	2.77	1.50	0.75
60 minutes	0.65	0.88	1.43	0.90	0.88	1.00	2.11	1.27	0.72



sorbent surface. Figures 4-14 through 4-17 are typical plots, similar to those presented in the previous sections, in which the effect of reaction temperature can more readily be seen. These figures depict sorbent performance when oxygen was not present in the system. Similar plots for those experiments where oxygen was present in the system are shown at Figures 4-18 through 4-20.

When the  $\text{NO}_2$  inlet concentration was 200 ppm (without oxygen), initial  $\text{NO}_2$  penetration was lowest at a bed reaction temperature of 473 K (Figure 4-14). Penetrations for the lower temperatures were somewhat higher initially. This separation in penetration remained until a bed exposure time between 20 and 25 minutes had elapsed, when  $\text{NO}_2$  penetration at 473 K exceeded the values at the other temperatures. If diffusion through the inert product layer controls the reaction at high conversion levels, an increase in temperature would increase the diffusion rate since effective diffusivity can be temperature dependent and improved diffusivity would be expected. This would cause higher reaction rates and overall conversion levels (Marsh and Ulrichson, 1985). While the initial rate of change in  $\text{NO}_2$  penetration versus time was low, it rapidly increased before beginning to taper off toward the end of the run. This coincides with a relative increase in  $\text{NO}_2$  penetration rate for the two lower temperatures evaluated. This delay in increasing  $\text{NO}_2$  penetration most likely represents the added time required to complete formation of the outermost product layer due to the decreased temperatures employed.

Similar curves are seen for an  $\text{NO}_2$  inlet concentration of 100 ppm (Figure 4-15). For inlet  $\text{NO}_2$  concentrations of 20 and 50 ppm (Figures 4-16 and 4-17, respectively), initial penetrations were low for all temperatures, but it appears that a higher temperature was

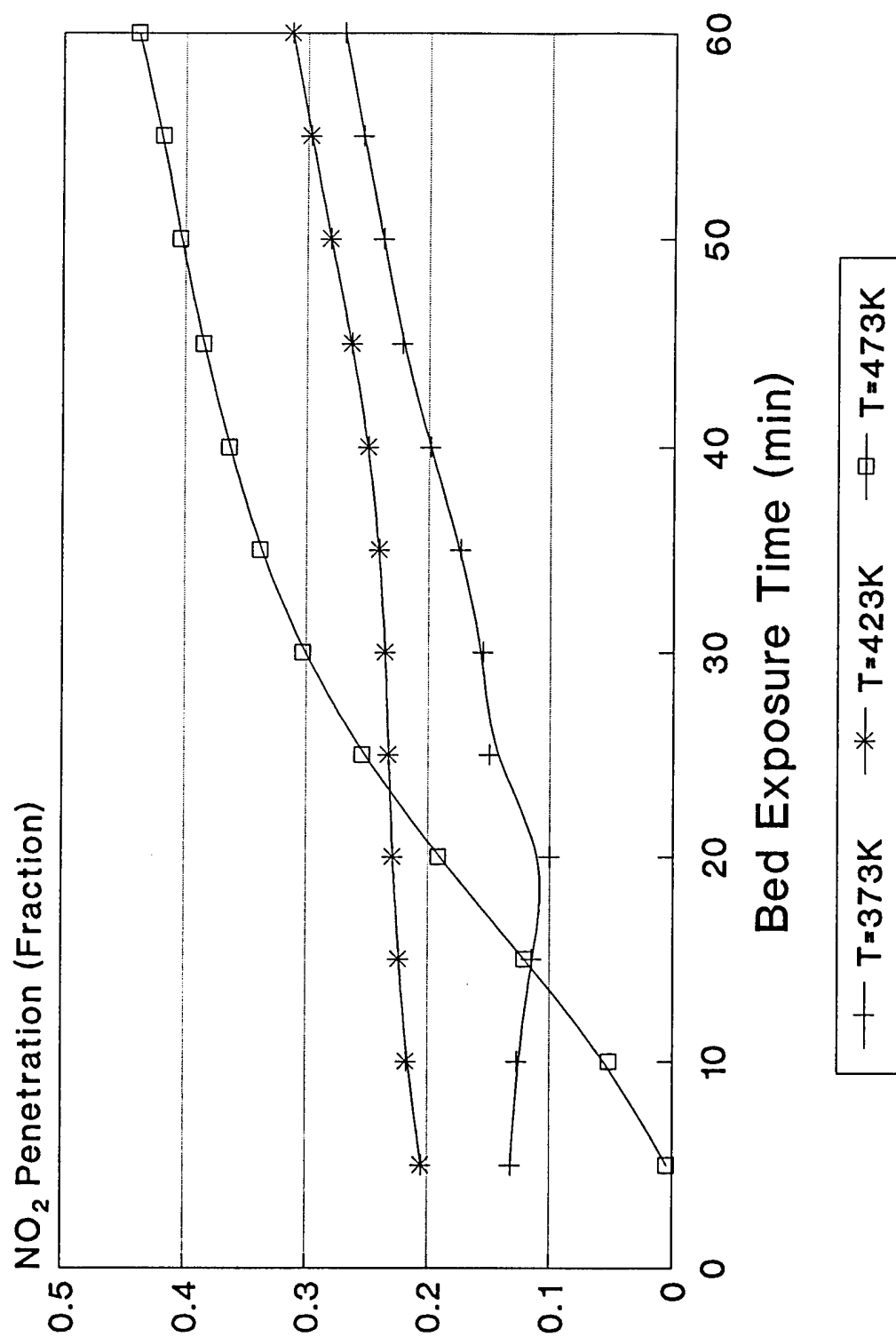


Figure 4-14. NO<sub>2</sub> penetration versus bed exposure time ([NO<sub>2</sub>]<sub>in</sub> = 200 ppm, [O<sub>2</sub>] = 0%).

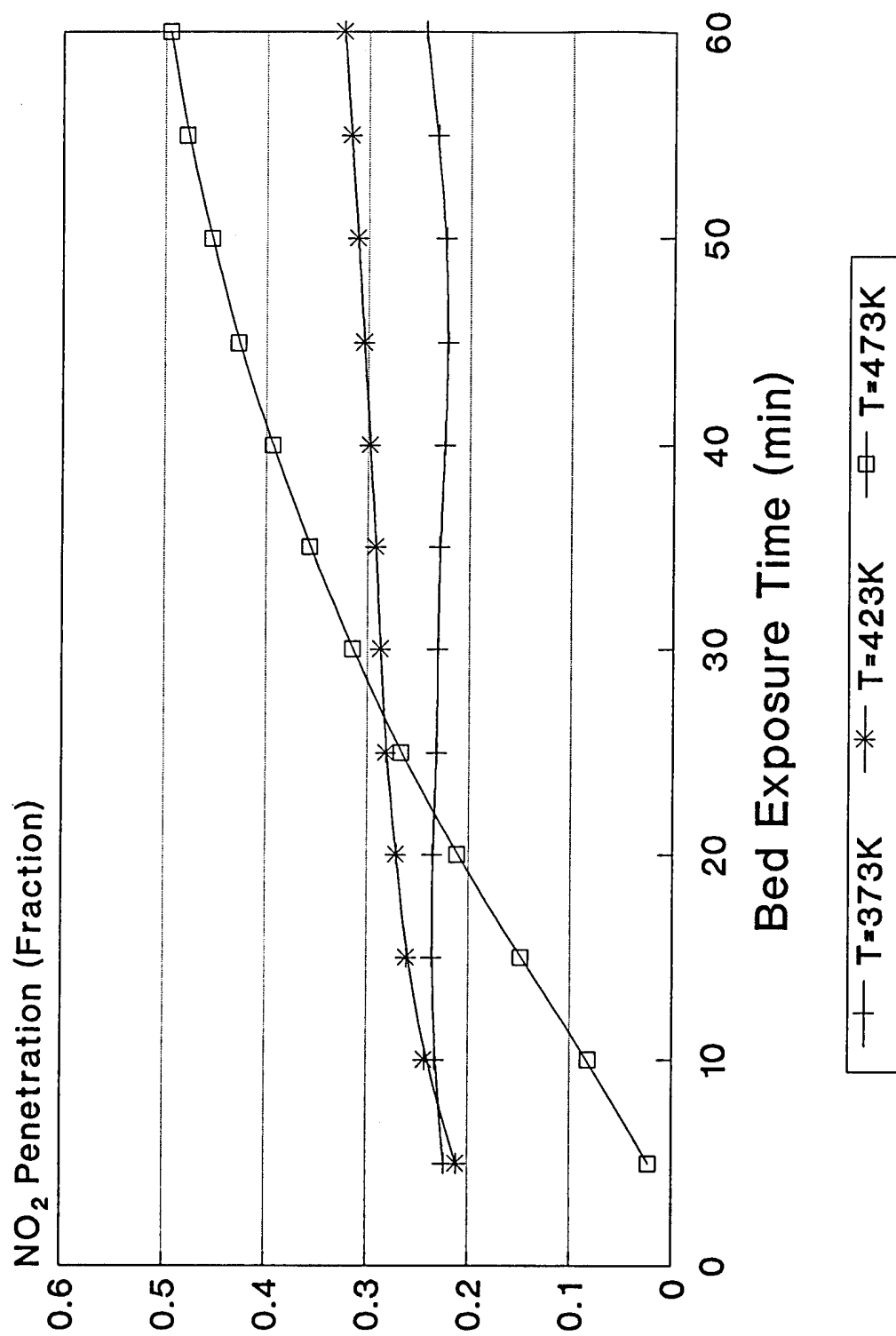


Figure 4-15. NO<sub>2</sub> penetration versus bed exposure time ([NO<sub>2</sub>]<sub>in</sub>=100 ppm, [O<sub>2</sub>]=0%).

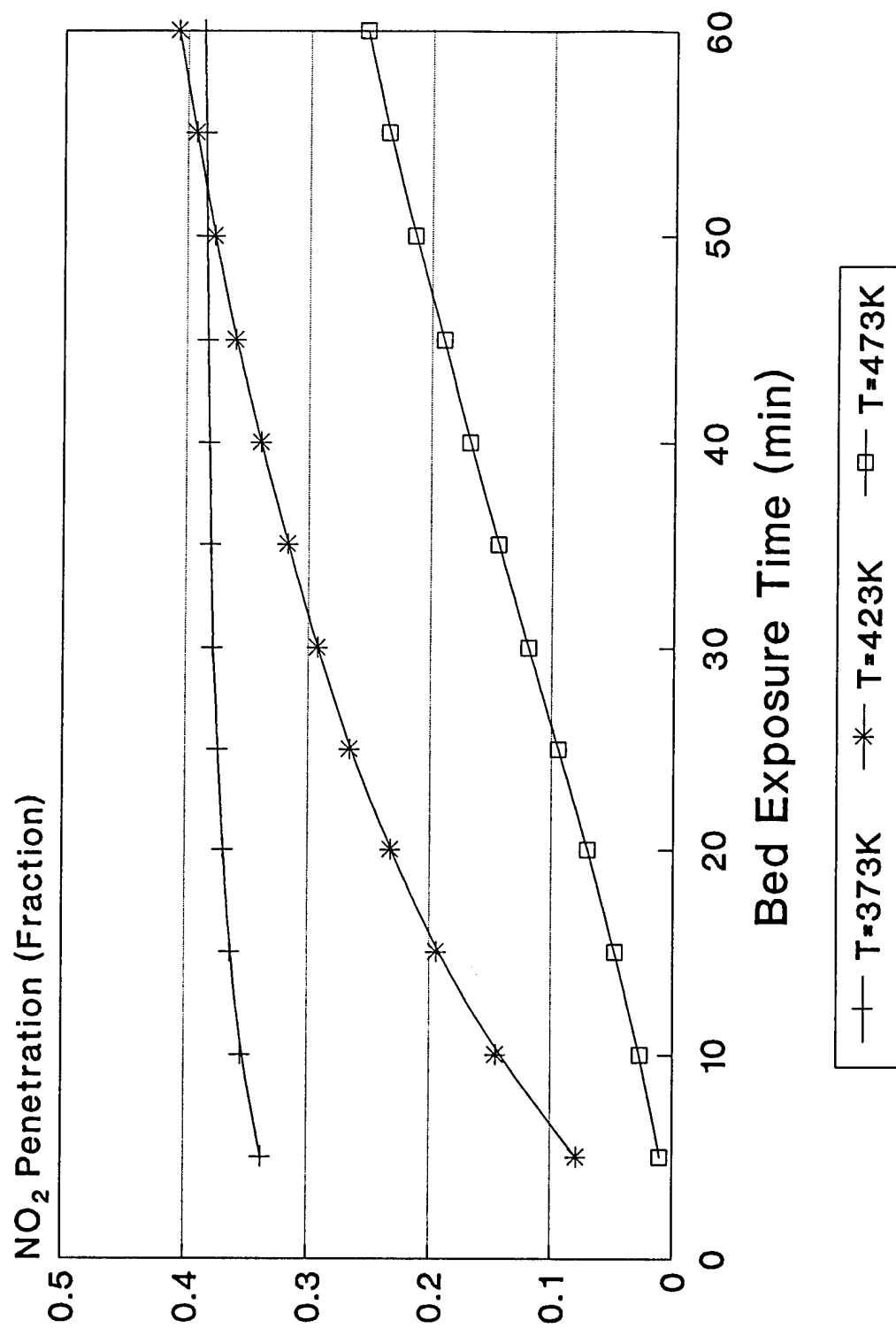


Figure 4-16. NO<sub>2</sub> penetration versus bed exposure time ([NO<sub>2</sub>]<sub>in</sub>=50 ppm, [O<sub>2</sub>]=0%).

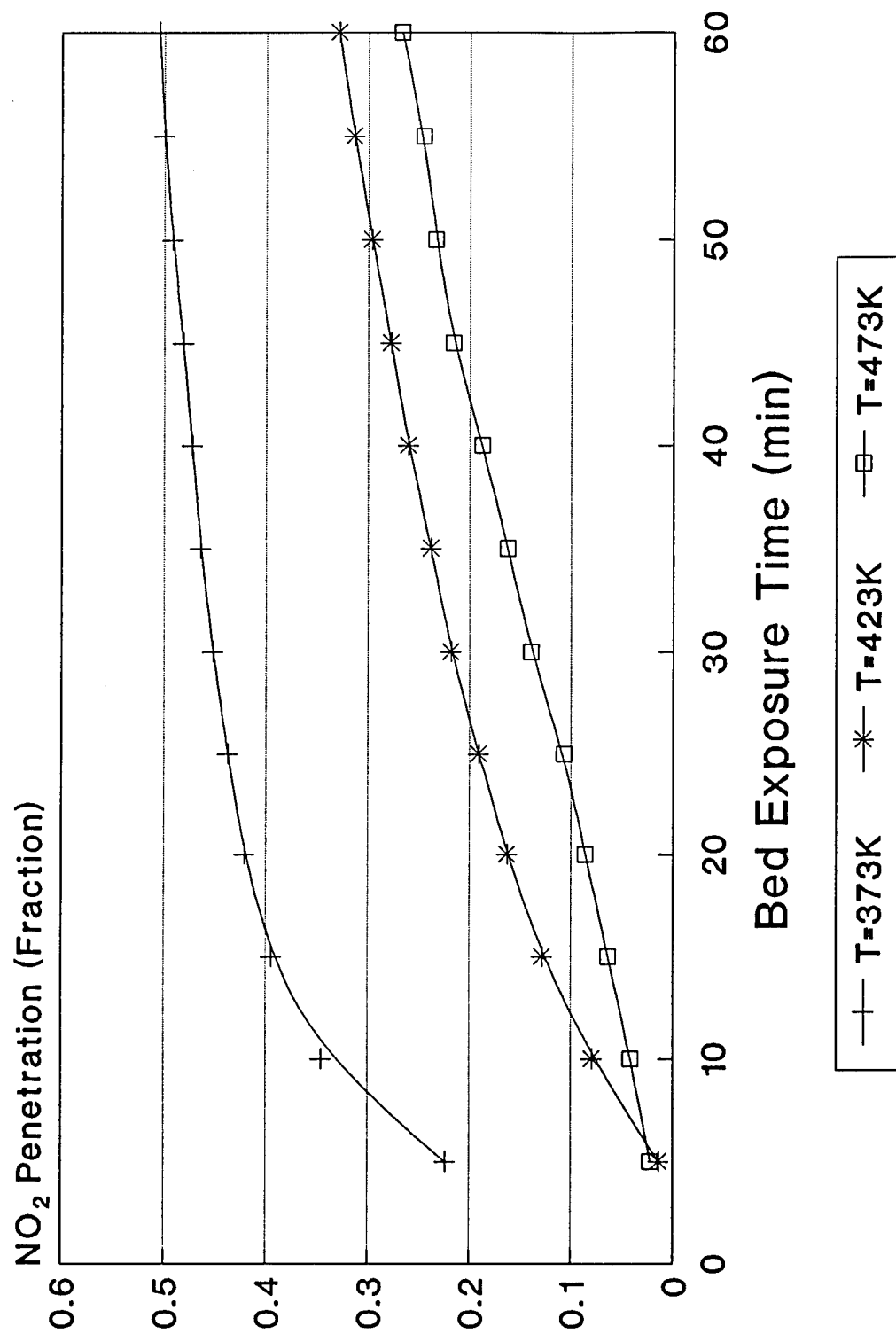


Figure 4-17. NO<sub>2</sub> penetration versus bed exposure time ( $[NO_2]_m = 20$  ppm,  $[O_2] = 0\%$ ).

required to maintain a reasonable amount of  $\text{NO}_2$  removal from the gas stream. When oxygen was present in the system, it had a less noticeable effect when comparing the temperature effects for a given inlet  $\text{NO}_2$  concentration as can be seen in Figures 4-18 through 4-20. Again, initial  $\text{NO}_2$  penetration was lowest at the highest temperature for all concentrations, but it increased more noticeably for the higher concentrations. For an inlet  $\text{NO}_2$  concentration of 20 ppm, penetration stayed below 10% for an exposure time of nearly an hour.

#### Activation Energy Determination

To determine experimental activation energies, Arrhenius plots of the natural logarithm of the bed-exposure-time-specific first-order rate coefficients versus the reciprocal of the absolute reaction temperature were prepared. The rate of removal of  $\text{NO}_2$  was sometimes less temperature-dependent between 373 and 423 K, as seen in Figure 4-21. When this was the case, data were collected at an intermediate temperature of approximately 450 K, since the plots were often more linear over the higher temperature range. A good example of linearity in the plot between 473 K and 373 K can be seen at Figure 4-22. From the slopes of these Arrhenius plots, the apparent activation energies can be determined. These were approximately 33 kJ/g-mol at 5 minutes bed exposure time and about 8 kJ/g-mol at 20 minutes bed exposure time for the example shown in Figure 4-21. The decrease in activation energy with bed exposure time suggests that a change in  $\text{NO}_2$  removal mechanism occurs with increasing bed exposure time. It is common, however, for Arrhenius plots of heterogeneous reaction parameters to show curvature (Clark, 1970).

Initial activation energies were often difficult to determine due to system fluctuations during the first 1 to 2 minutes of operation. This instability probably caused some of the

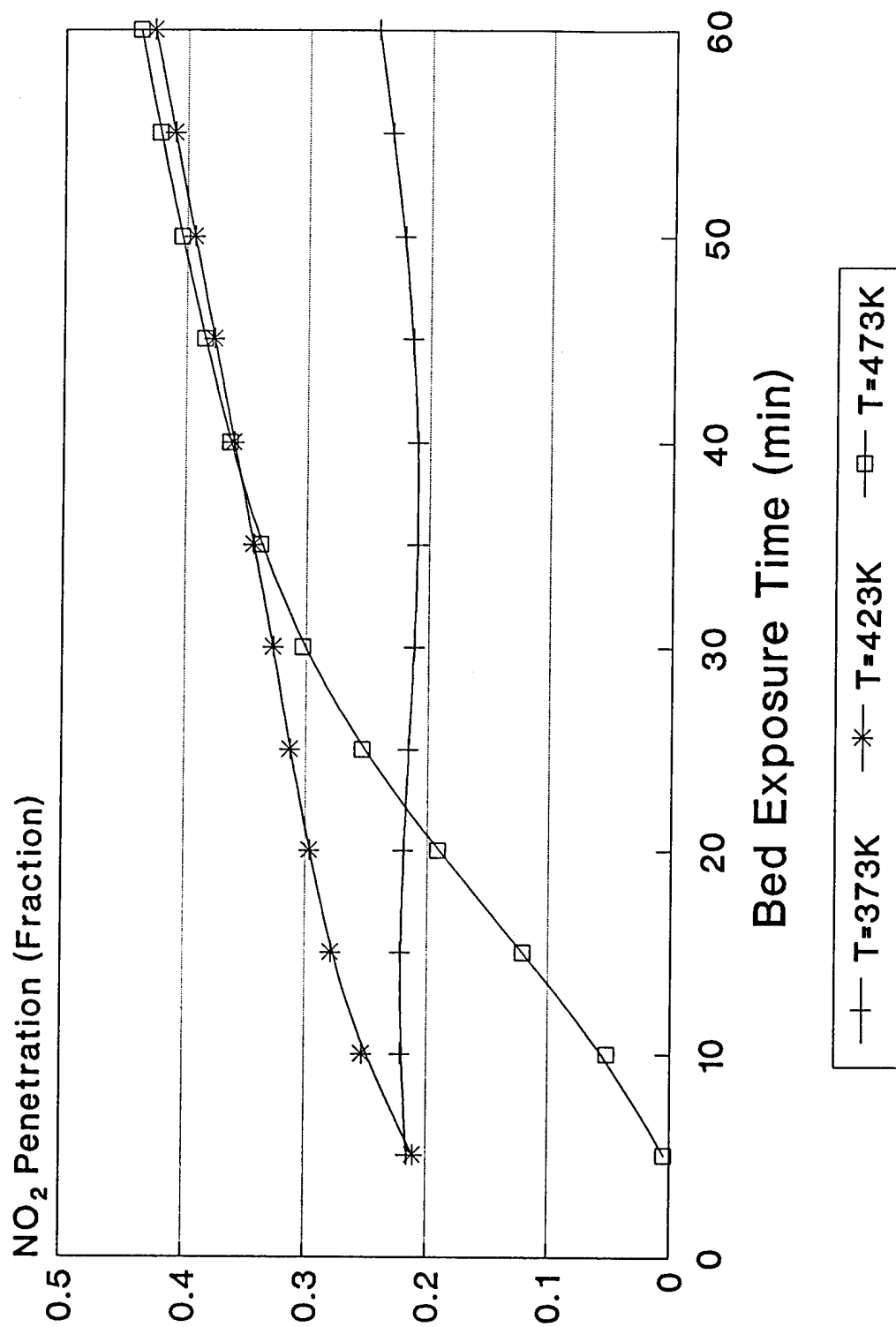


Figure 4-18. NO<sub>2</sub> penetration versus bed exposure time ( $[\text{NO}_2]_{\text{in}} = 100 \text{ ppm}$ ,  $[\text{O}_2] = 10\%$ ).

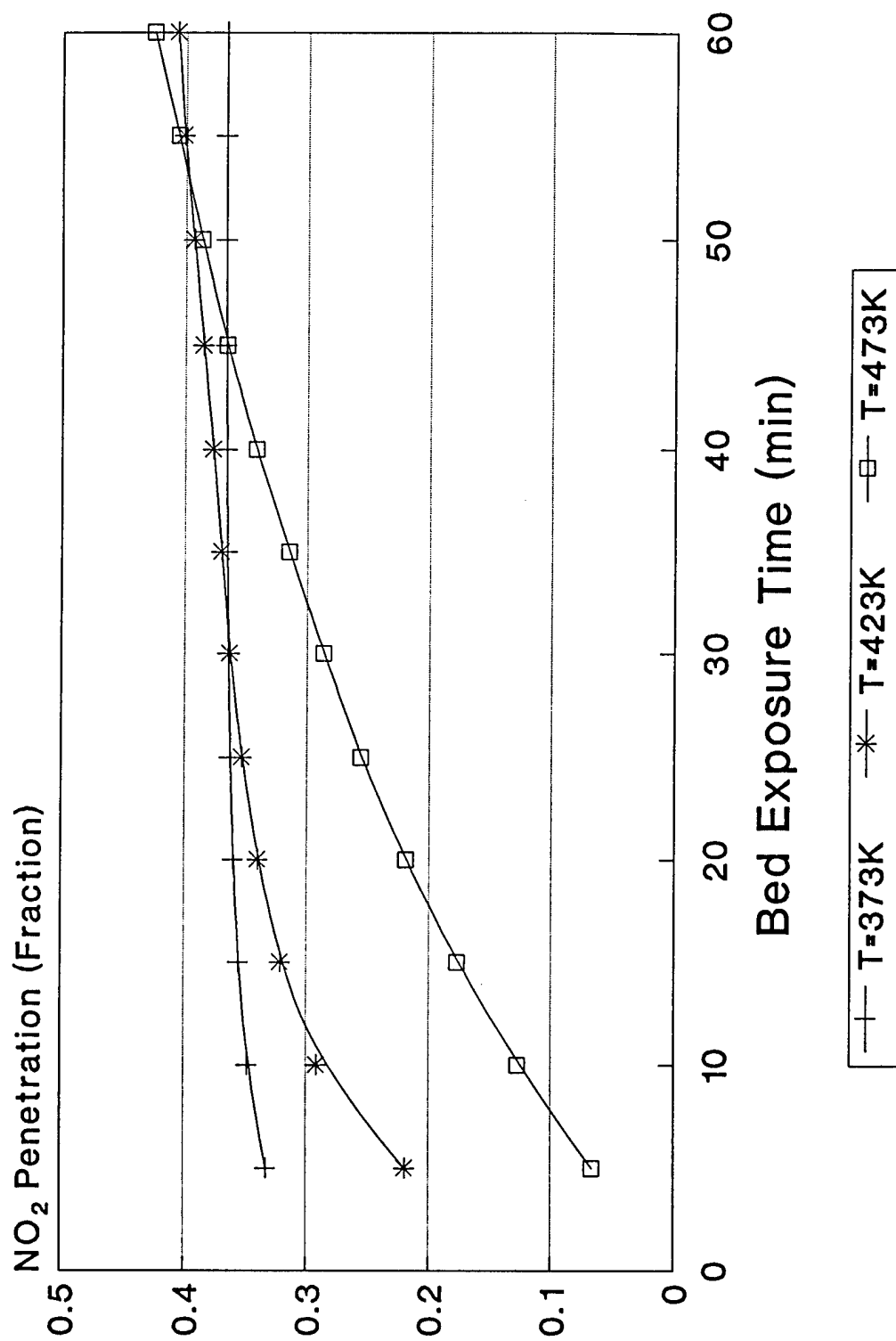


Figure 4-19. NO<sub>2</sub> penetration versus bed exposure time ( $[\text{NO}_2]_{\text{in}} = 50 \text{ ppm}$ ,  $[\text{O}_2] = 10\%$ ).



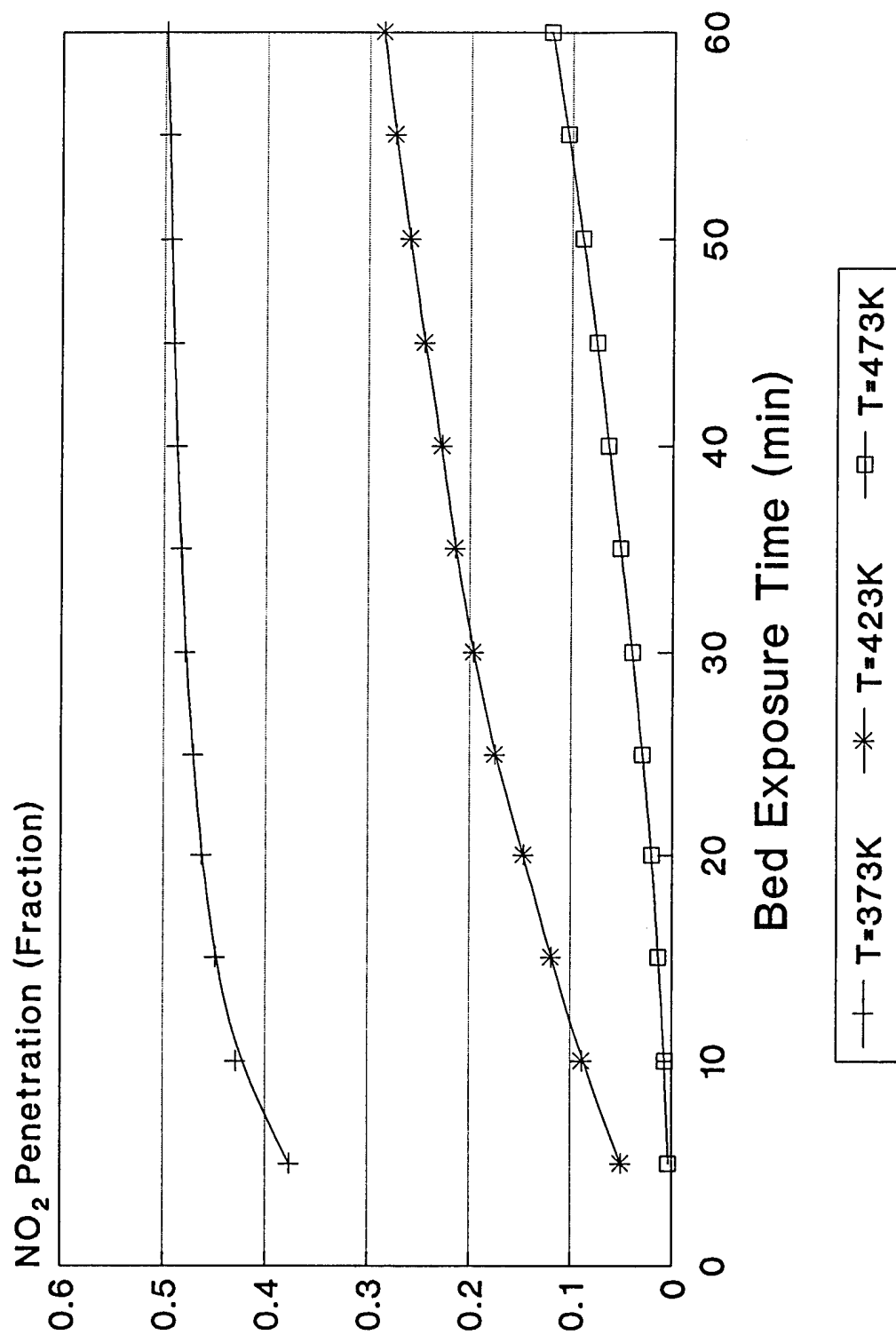


Figure 4-20. NO<sub>2</sub> penetration versus bed exposure time ([NO<sub>2</sub>]<sub>in</sub>=20 ppm, [O<sub>2</sub>]=10%).

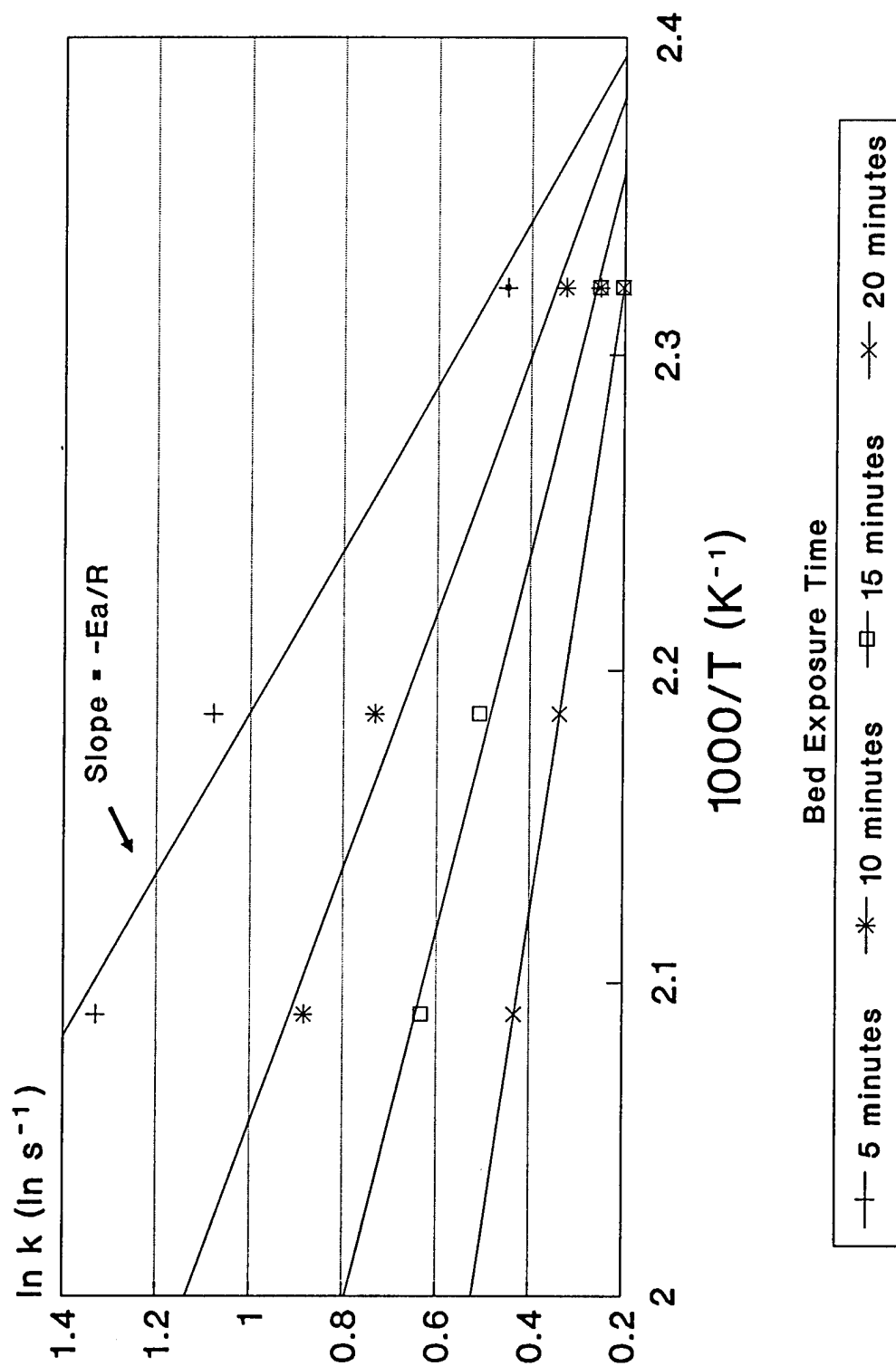


Figure 4-21. Arrhenius plot of  $\ln k$  versus  $1000/T$  ( $T$  between 473 and 423 K,  $[NO_2]_{in}=100$  ppm,  $[O_2]=0\%$ ).

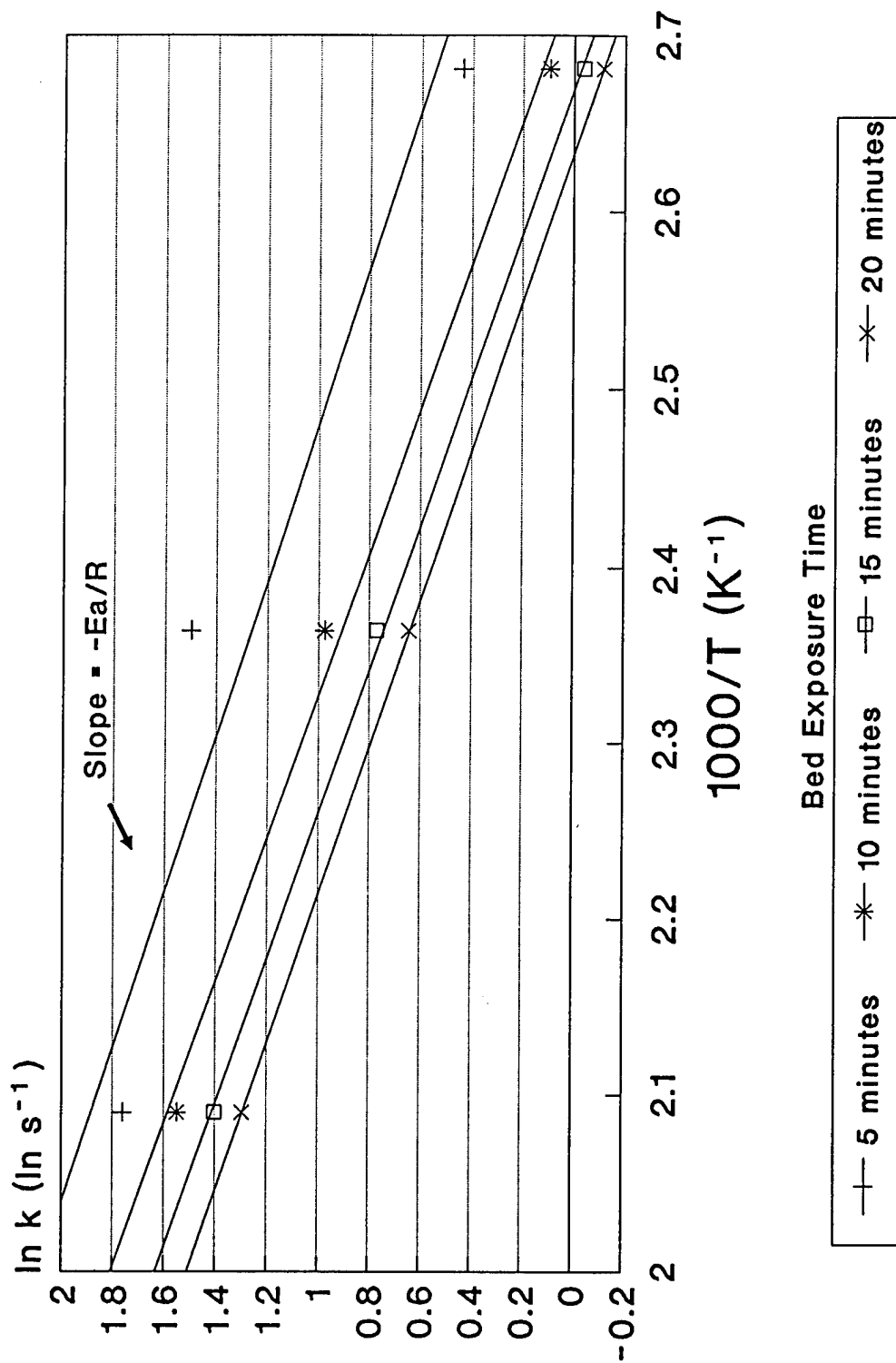


Figure 4-22. Arrhenius plot of  $\ln k$  versus  $1000/T$  ( $T$  between 473 and 373 K,  $[\text{NO}_2]_{\text{in}} = 20$  ppm,  $[\text{O}_2] = 0\%$ ).

discrepancies in the intrinsic first-order rate coefficients seen in the preceding tables. Best estimates of the Arrhenius activation energy associated with this sorption process are between 20 and 36 kJ/g-mol during the first few minutes of sorption without oxygen, and between 15 and 25 kJ/g-mol with oxygen present, for the range of  $\text{NO}_2$  concentrations and temperatures evaluated. These values are within the range of activation energies generally associated with chemisorption processes, as previously discussed.

When comparing activation energies for similar acid gas–alkaline solid reactions reported by different investigators, it must be noted that the values depend on the experimental arrangements used, the methods used in the analysis of experimental data, and the accuracy by which initial reaction rates can be measured. The chemical reaction rate coefficient usually influences only the initial stages of reaction, because once a product layer is formed, the local rate of reaction becomes diffusion controlled (Sotirchos and Zarkanitis, 1992). Hajaligol et al. (1988) determined the activation energy associated with the sulfation of CaO by  $\text{SO}_2$  to be approximately 146 kJ/g-mol. The activation energy calculated from initial rate data for the sulfation of CaO by Marsh and Ulrichson (1985) was 80 kJ/g-mole. Zarkanitis (1991) determined activation energies of the reaction of CaO with  $\text{SO}_2$  to be approximately 17 kJ/g-mole. The latter investigator determined this reaction to be less sensitive to reaction temperature than the reaction of  $\text{SO}_2$  with calcium carbonate. He also found that the sulfation of reagent-grade MgO proceeds at rates comparable to those for CaO. Sotirchos and Zarkanitis (1992) confirmed that the activation energy associated with the sulfation of CaO was 17 kJ/g-mol using an  $\text{SO}_2$  concentration of 2,000 ppm at reaction temperatures between 700 and 850 C. Borgwardt (1970) had previously reported that the

activation energy associated with the sulfation of CaO by a 3,000-ppm SO<sub>2</sub> gas stream at temperatures between 540 and 1100°C ranged from approximately 34 to 75 kJ/g-mol. Ruiz-Alsop and Rochelle (1988) estimated the activation energy of the reaction between SO<sub>2</sub> and Ca(OH)<sub>2</sub> to be approximately 12 kJ/g-mol. Obviously, there can be significant variations in the measurement of activation energies dependent upon experimental conditions.

Other studies of acid gas–solid reactions have produced results varying by a similar magnitude. Yang and Chen (1979) used a grain model to describe the reaction between 1.87% COS and CaO in the temperature range between 600 and 900 C. They determined an activation energy of approximately 18 kJ/g-mol associated with this reaction. The apparent activation energy for the reaction between 5,000 ppm HCl and CaO at temperatures between 150 and 350 C determined by Gullett et al. (1992) was approximately 28 kJ/g-mol. Activation energies determined by Krishnan and Sotirchos (1994) for the reaction between H<sub>2</sub>S and CaCO<sub>3</sub> ranged from 14 to 22 kJ/g-mol. The activation energy associated with the removal of H<sub>2</sub>S by zinc ferrite was 54 kJ/g-mol, which corresponded to a strong temperature dependence of the diffusion-controlled reaction (Karlegard and Bjerle, 1994).

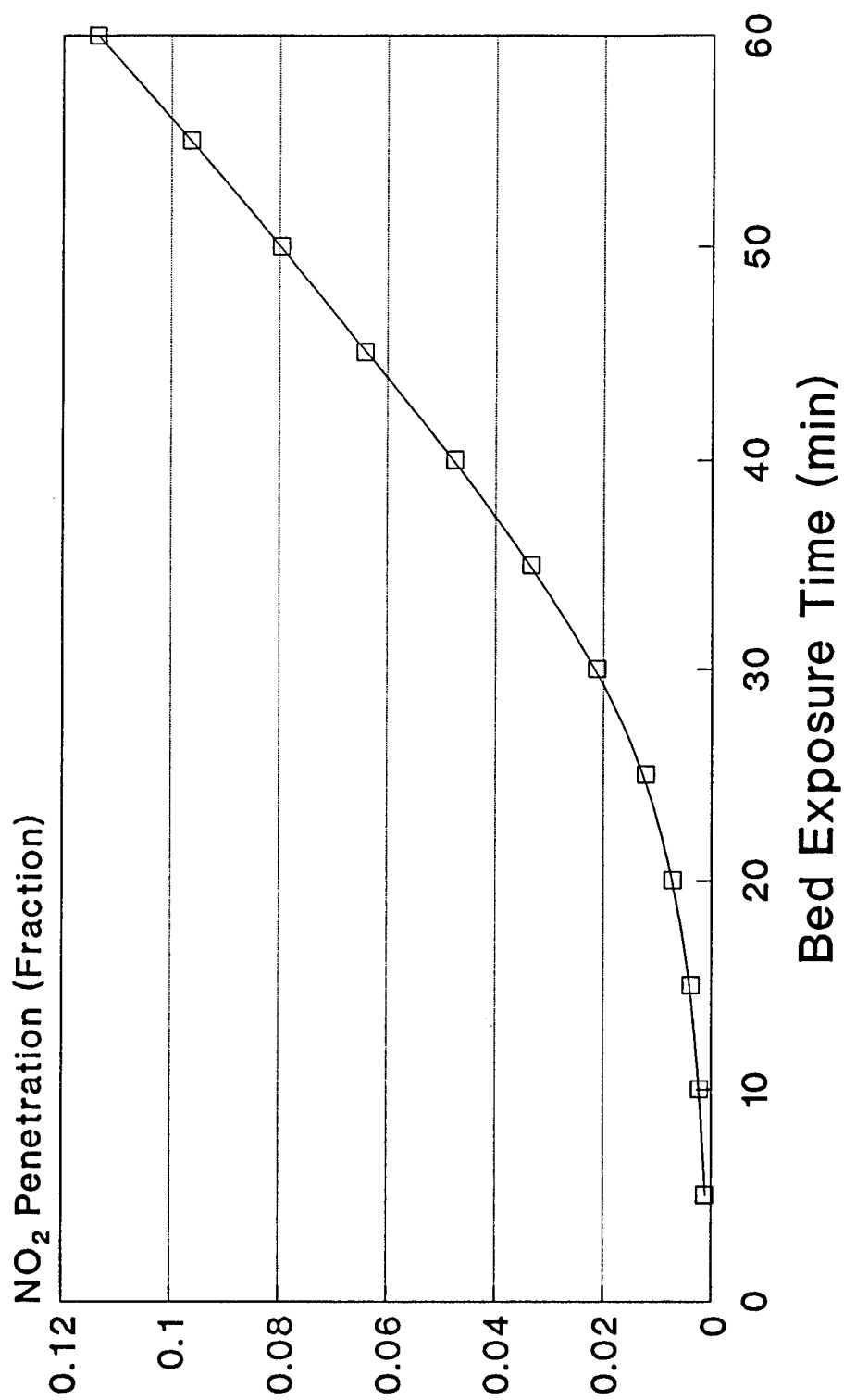
These activation energies associated with initial sorption kinetics that are reported here varied inversely with NO<sub>2</sub> concentration. Runs conducted with higher inlet NO<sub>2</sub> concentration had increasingly lower associated activation energies; in fact, it appeared that in some cases ( $[\text{NO}_2] \geq 100$  ppm) these energies were reduced to zero and sometimes became negative after 30 to 40 minutes. This finding would support a mechanistic transition from chemical kinetic control to diffusion control through a product layer, or intraparticle diffusion control. It is not known whether this is a function of increasing product layer thickness and

associated resistance to reaction or is simply a result of cumulative experimental error. Since the rate of reaction becomes very slow toward the end of the run, small errors in the determination of rate constants would become exaggerated in this range. It is also possible that there is more than one process controlling the reaction, or multiple reactions could be simultaneously taking place, obscuring the apparent activation energies measured.

#### Effects of Water

Water vapor carried by humidified gases greatly improved  $\text{NO}_2$  removal efficiency and overall sorption capacity. It is possible that this effect is due to the conversion of  $\text{MgO}$  into the more-reactive  $\text{Mg}(\text{OH})_2$ , which is thermally stable over the range of temperatures evaluated. Additionally, since  $\text{NO}_2$  is somewhat soluble in water, a small quantity may be removed in this way. This may cause the formation of nitrous and/or nitric acids, which are probably more reactive than  $\text{NO}_2$  and should be immediately neutralized by the basic sorbent, preventing any potential for corrosion problems.

Intrinsic first-order rate coefficients (and  $\text{NO}_2$  removal rates) for these experiments were generally comparable in the early stages of reaction, however,  $\text{NO}_2$  removal efficiency remained higher for an extended period of time when water was present in the system. Figure 4-23 is a typical example of an  $\text{NO}_2$  concentration versus bed exposure time profile utilizing moistened sorbent. The possible reasons for this effect include the increased reactivity of  $\text{Mg}(\text{OH})_2$  compared to  $\text{MgO}$ , the solubility of  $\text{NO}_2$  in water, and the lower molar volume ratio of  $\text{Mg}(\text{NO}_3)_2$  to  $\text{Mg}(\text{OH})_2$  compared to the molar volume ratio of  $\text{Mg}(\text{NO}_3)_2$  to  $\text{MgO}$ .  $\text{NO}_2$  solubility was avoided in experiments where the sorbent was wetted prior to exposure to flowing gases to convert the  $\text{MgO}$  on the surface into  $\text{Mg}(\text{OH})_2$ , leaving little free water.



—□— T=473K

Figure 4-23. NO<sub>2</sub> penetration versus bed exposure time (20 ml H<sub>2</sub>O added to 7 g MgO-vermiculite sorbent, [NO<sub>2</sub>]<sub>in</sub>=100 ppm, [O<sub>2</sub>]=0%, T=473 K).

When gas humidification was used, since  $\text{NO}_2$  concentrations were monitored directly at the bed inlet, chemical kinetics was not a function of  $\text{NO}_2$  absorbed in the humidification vessel. Since the molar volume ratio is smaller when starting with the hydroxide, more  $\text{NO}_2$  can be removed before the exterior surface becomes covered and  $\text{Mg}(\text{OH})_2$  is no longer readily available for reaction. This may mean that it takes longer to form a complete inert product layer shell when moisture is available in the system. After this layer is formed, however, the typical shrinking core behavior with product layer diffusion control would still be expected.

#### Effects of Residence (Reaction) Time

Studies varying gas flow rate and the resulting  $\text{NO}_x$  bed residence time showed an effect on  $\text{NO}_2$  removal efficiency, as expected. When whole-bed half-second residence time data were compared to data from the mid-point of the bed for a one-second residence time, they were found to be directly comparable. These results suggest that the chemical reaction is truly first-order with respect to  $\text{NO}_2$  and is essentially zero-order with respect to the solid,  $\text{MgO}$  "concentration." The total quantity of  $\text{NO}_2$  removed, however, would be a factor that would affect overall bed performance, particularly as surface "saturation" is approached. Better removal efficiencies were obtained with longer residence times. A residence time of one second produced very high initial removal efficiencies, often greater than 99%. This situation did not appear to be gas-film-mass-transfer-limited, as already discussed. Additionally, since longer residence times correspond to lower gas velocities, measured bed pressure drops were lower, which is preferable for JETC applications. Pressure drop results will be presented later.



### Sorbtech-Supplied Sample Results

Experimental results for samples of sorbent provided by Sorbtech were generally comparable to those for laboratory-prepared sorbent. Initial removal rates were greater than 99% for all cases evaluated; however, NO<sub>2</sub> penetration remained lower at the end of the run for these samples. Intrinsic first-order rate constants were approximately the same early in the reaction, but the decrease with extended bed exposure time was not as great. As discussed earlier, the Sorbtech samples actually showed lower average BET surface areas than the laboratory prepared sorbent. This difference in available surface area would generally indicate less activity for the Sorbtech samples in the removal of NO<sub>2</sub>, which apparently was not the case. It may be that the laboratory-prepared sorbent had higher porosity, which would contribute to a higher total surface area. The physical appearance of the Sorbtech sorbent was darker, with a more brown to tan color than the cleaner white appearance of the laboratory-prepared sorbent.

One distinct difference between the samples was that the Sorbtech sorbent was significantly more dense than the laboratory prepared sorbent, a bed volume of the Sorbtech sorbent weighed approximately 40% more than the laboratory sorbent. It was thought that the higher mass might be the result of the presence of water in the Sorbtech sorbent, which would also help to explain the improved NO<sub>2</sub> removal efficiency with time. Prewighed samples of both sorbents were heated in a muffle furnace to a temperature of 623 K for one hour to evaluate weight loss from dehydration. This proved to be insignificant, with the

laboratory samples losing approximately two percent mass, and the Sorbtech samples losing about three percent. The higher density material did not produce a higher surface area on a per bed basis, because there was little difference between the surface areas of laboratory-prepared samples and Sorbtech samples. In fact, laboratory prepared samples had, on average, 10% more surface area, which may be attributable to more microporosity, and may help in explaining the decreased performance since the high-surface-area micropores are more prone to blockage or plugging as reaction progresses and the nature of the sorbent surface changes.

### Pressure Drop Characteristics

The arrangement of particles in packed beds produces a complex geometry that makes the flow field difficult to define. For most practical problems, empirical relationships between pressure drop and the flow rate and characteristics of the fluid are used. When an empirical equation can be validated with experimental data, this is the best situation. Of numerous correlations proposed for relating pressure drop to flow rate, the Ergun equation is most widely accepted (Szekely et al., 1976):

$$\frac{\Delta P}{L} = 150 \frac{(1-\xi_v)^2}{\xi_v^3} \frac{\mu U_o}{(\varphi_s d_p)^2} + 1.75 \frac{(1-\xi_v)}{\xi_v^3} \frac{\rho_f U_o^2}{\varphi_s d_p} \quad (4-3)$$

where:  $\Delta P$ =pressure drop,  $L$ =bed depth,  $\xi_v$ =the void fraction,  $\mu$ =gas viscosity,  $\phi_s$ =a shape factor,  $d_p$ =sorbent surface area mean particle diameter (mass median diameter),  $\rho_f$ =gas density, and  $U_o$ =superficial gas velocity, all in appropriate absolute units.

It can be seen from equation (4-3), that at low fluid velocities the first (viscous) term predominates, and at high gas velocities that the second (inertial) term is dominant and the pressure drop is proportional to the square of gas velocity. The shape factor term,  $\phi_s$ , is defined as the ratio of the surface area of a sphere of equal volume to the particle to the surface area of the particle. The value of this term is obviously 1 for spherical particles and normally lies in the range from 0.5 to 0.9 for naturally occurring materials. The median sorbent particle diameter was approximately 2 mm. The value for  $\xi_v$  was determined by the mechanical compression of the sorbent to a point where gas would not flow through the bed, reducing the volume by approximately 30 percent ( $\xi_v=0.3$ ). Using water to fill void space in an average bed load produced an  $\xi_v$  value of approximately 0.6. Since vermiculite is highly hydrophilic, and bulk gas flow does not occur through the internal porosity of the particles, a value of 0.4 was used for  $\xi_v$ . Letting  $\phi_s=0.9$ , at 473 K, when  $U_o=0.1$  m/s,  $\Delta P$  is equal to 75 Pa; and when  $U_o=0.2$  m/s,  $\Delta P$  is equal to 163 Pa. These estimated values correspond well with average experimental  $\Delta P$  values of 75 and 125 Pa, respectively. Figure 4-24 depicts a comparison between experimentally measured pressure drop and the pressure drop predicted by the Ergun equation.

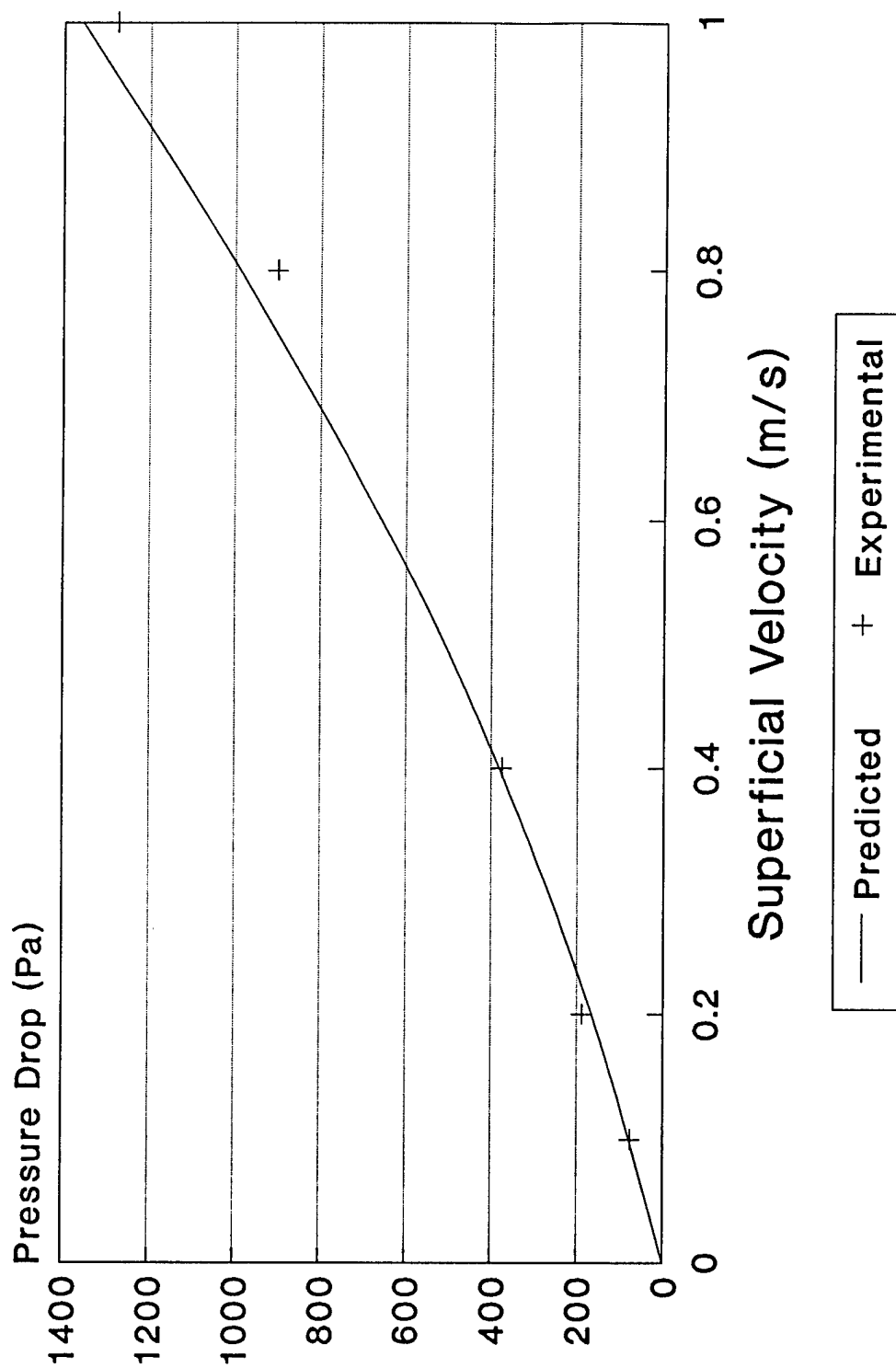


Figure 4-24. Predicted (Ergun equation) versus experimental pressure drop as a function of superficial velocity for a 0.1 m long bed of MgO-vermiculite sorbent ( $T=473$  K).

### Magnesium Nitrate Surface Decomposition

Solid  $\text{Mg}(\text{NO}_3)_2 \cdot 6\text{H}_2\text{O}$  (Certified A.C.S. grade, Fisher Scientific, Pittsburgh, Pennsylvania) was dissolved in deionized water and applied to heat-treated vermiculite, and the mixture was allowed to air dry. The mass ratio applied was approximately 15%  $\text{Mg}(\text{NO}_3)_2$ . This material was packed inside a clean reactor and 2 sLpm dry  $\text{N}_2$  was delivered to the bed. Bed outlet concentrations of NO and  $\text{NO}_2$  were followed over time as bed temperature was increased from ambient temperature to 373 K through 573 K in 50 °K steps. Results are plotted in Figure 4-25. From this figure, it can be seen that at temperatures used for sorption, little NO and  $\text{NO}_2$  were released compared to those emissions observed at much higher temperatures, 523 and especially 573 K. In either case, the ratio of  $\text{NO}_2/\text{NO}$  released was approximately between 10:1 and 16:1. Heating samples of used sorbent to a temperature of 523 K produced similar results (See Figure 4-26). This implies that  $\text{NO}_2$  is the predominant gaseous reactant in the forward reaction. Also, it is important to recognize that the decomposition of  $\text{Mg}(\text{NO}_3)_2$  is not a significant source of NO. Although it is obviously necessary to control NO emissions, these studies imply that NO production observed in  $\text{NO}_2$  sorbent removal studies must occur through a mechanism other than decomposition of  $\text{Mg}(\text{NO}_3)_2$ .

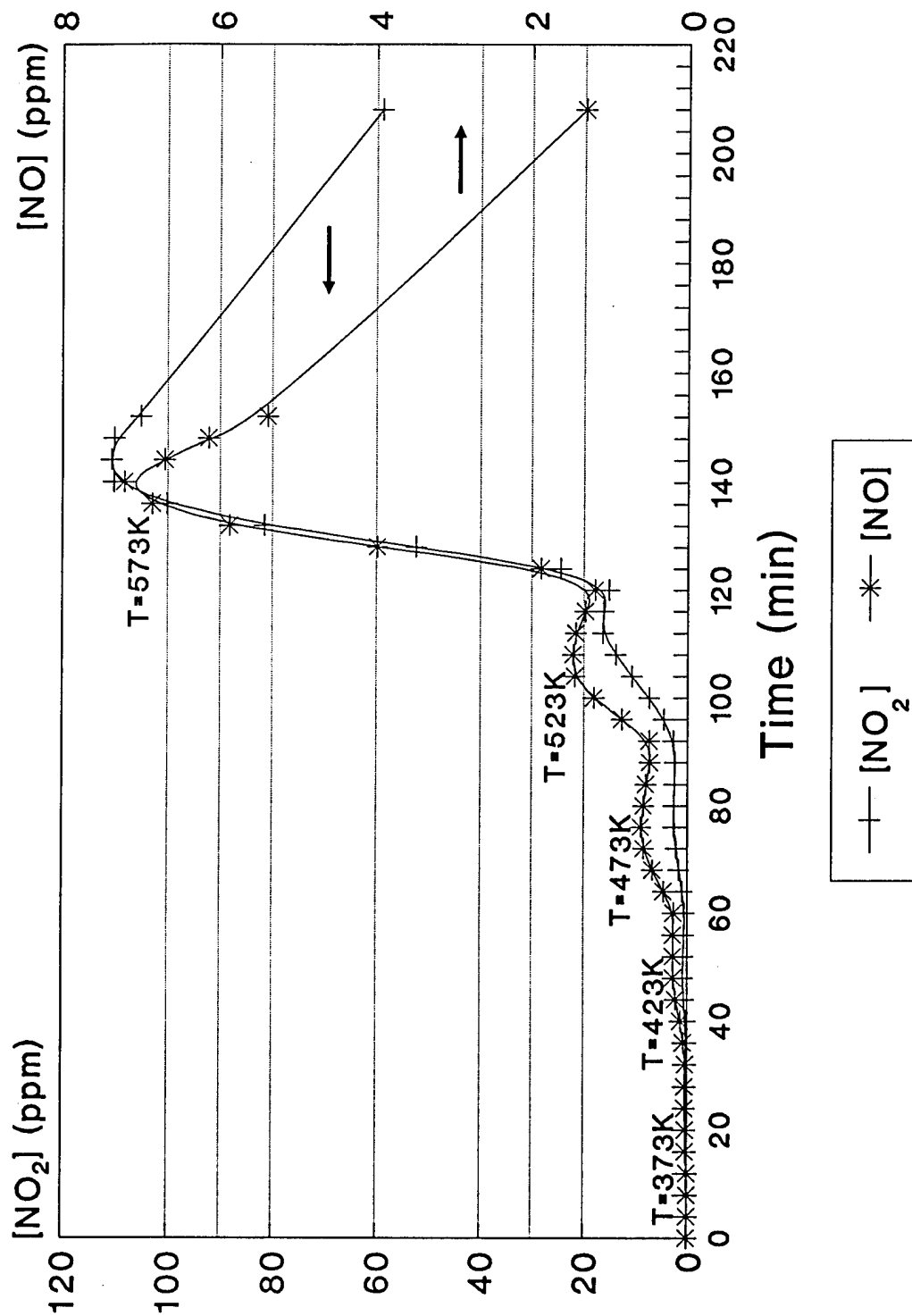


Figure 4-25. Thermal decomposition of  $\text{Mg}(\text{NO}_3)_2 \cdot 6\text{H}_2\text{O}$  on vermiculite (temperature increasing with time).

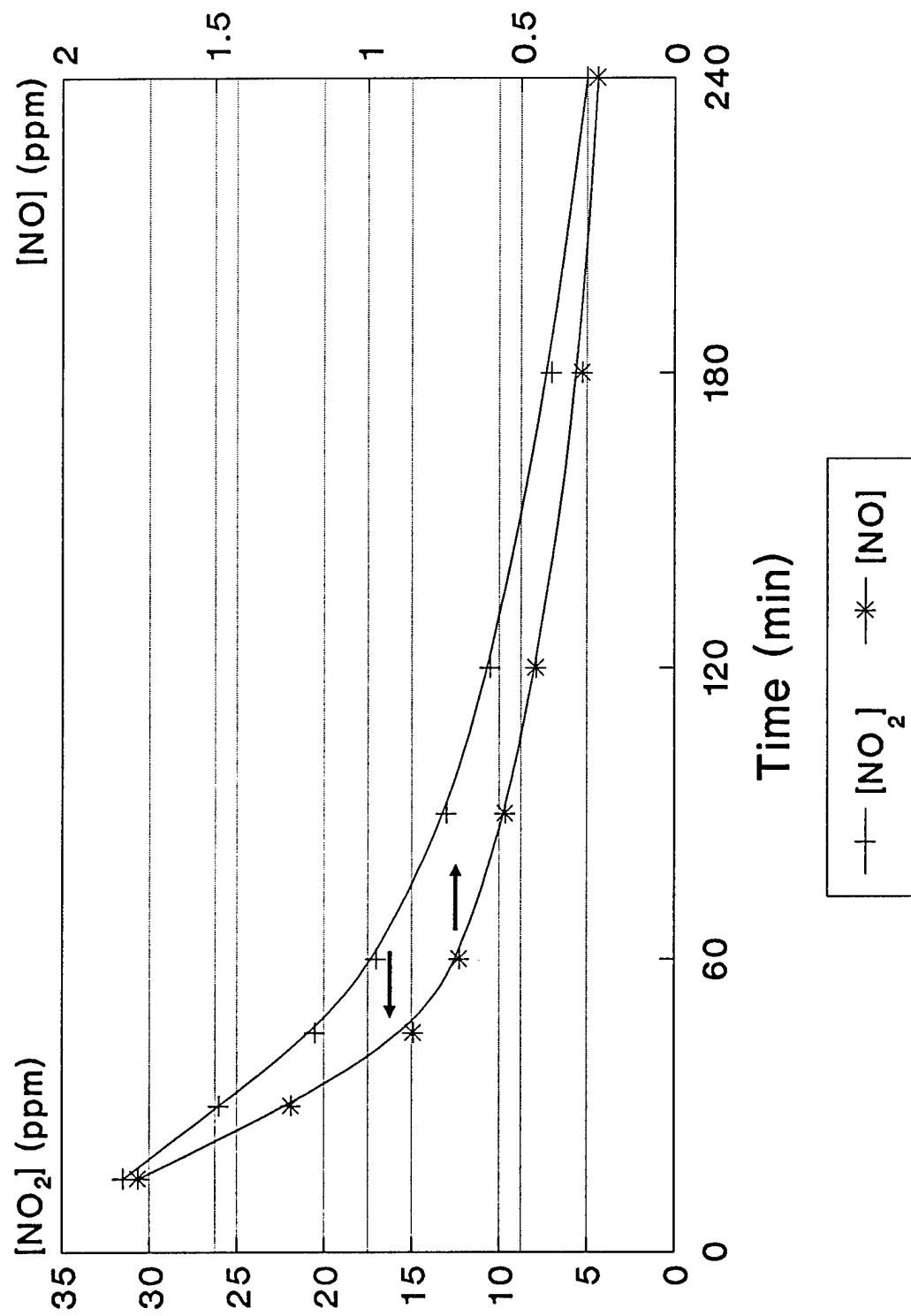


Figure 4-26. Thermal decomposition of used MgO-vermiculite sorbent ( $T=523\text{ K}$ ).

### Sorbent "Lifetime" and Regeneration

Whereas initial sorbent NO<sub>2</sub> removal rates were often greater than 90 percent fractional NO<sub>2</sub> removal decreased while NO<sub>2</sub> concentrations leaving the bed increased with bed exposure time (Figure 4-27). In this example, dynamic equilibrium was approached after approximately 20 minutes of bed exposure. At approximately the same time, NO outlet concentrations increased to values greater than NO inlet concentration. The NO produced was much greater than that which would result from nitrate decomposition, as previously described. Also, NO production through thermal NO<sub>2</sub> decomposition at temperatures below 500 K is minimal. These observations indicate that there must be another mechanism for NO production.

A consecutive multi-step chemical reaction of two or more molecules of NO<sub>2</sub> with MgO leading to the bed surface becoming saturated with Mg(NO<sub>3</sub>)<sub>2</sub> may be proposed. One step (which it is convenient to propose as the last) must be an oxidation process in which the equivalent of an oxygen atom is delivered to some intermediate product having the empirical formula MgN<sub>2</sub>O<sub>5</sub> (MgO + 2NO<sub>2</sub>). On a mass-ratio basis, this process appears to occur, on average, when approximately 3 mg NO<sub>2</sub> per gram of MgO are sorbed. While this corresponds to minimal utilization of the bed, significant capacity for NO<sub>2</sub> removal persists long after initiation of this final oxidation process, as NO<sub>2</sub> removal efficiencies of 50-60% can continue for hours. It may be that MgO or Mg(OH)<sub>2</sub> at the external particle surface is covered by a nitrated monolayer, so only internal oxide or hydroxide is available for reaction.



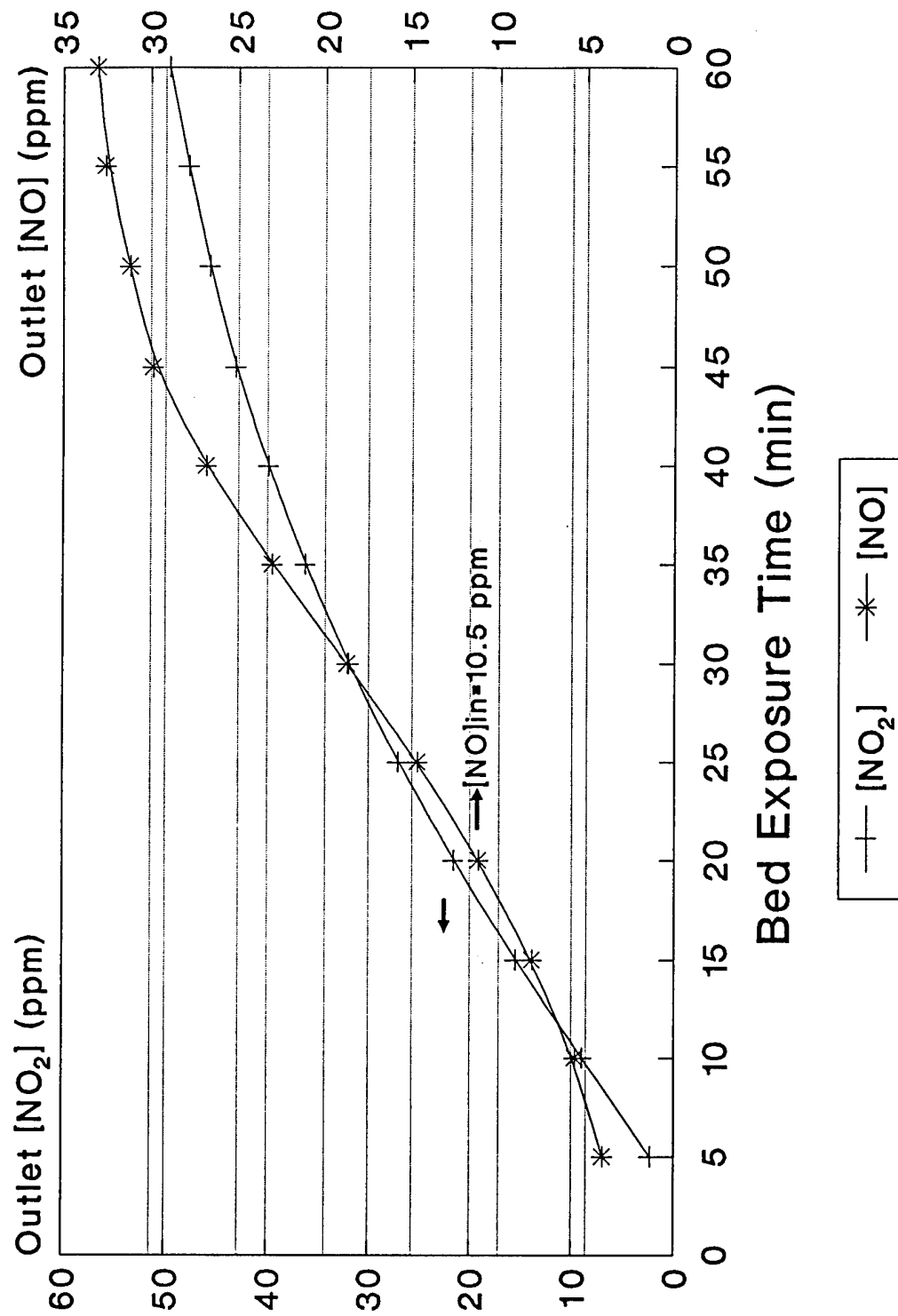


Figure 4-27. Comparative bed outlet  $NO_2$  and  $NO$  concentrations versus bed exposure time showing  $NO$  production.

It is also possible that the transformed surface catalyzes the continued oxidation (or reduction) of  $\text{NO}_2$ . A more descriptive discussion of sorbent lifetime within the context of the shrinking unreacted core model will be presented later.

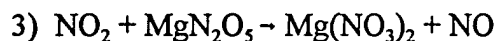
Beds regenerated through heating to approximately 550 K can be reused with little loss of performance. Obviously, regenerating solely through heating serves to release  $\text{NO}_x$  from the solid surface into the gas phase. This might defeat the purpose of using the sorbent to control  $\text{NO}_x$ . Introduction of a reducing gas (CO appears to be the reductant of choice) when regenerating the sorbent can alleviate this problem (Nelson et al., 1990).

#### Proposed Reaction Mechanism

While the exact reaction mechanism in this gas-phase interaction is unknown, the experimental data provide information that may be used to describe a possible mechanism. While the  $\text{NO}_2$  removal greatly exceeded NO removal, some NO was removed initially, presumably via a physisorption mechanism, as previously discussed. The finding of NO production during  $\text{NO}_2$  sorption led to an investigation of possible reaction mechanisms that would ultimately produce NO. A stepwise mechanism was envisioned, in which  $\text{NO}_2$  molecules are sequentially incorporated into intermediate products, ultimately forming  $\text{Mg}(\text{NO}_3)_2$ .

A simplified mechanism is proposed as follows:





It should be noted that  $\text{NO}_2$  is functioning as an oxidizing agent in the final step, to complete the formation of  $\text{Mg}(\text{NO}_3)_2$ , in the absence of oxygen. If oxygen were present, then it may competitively complete this last step, reducing NO formation. When  $\text{Mg}(\text{OH})_2$  is the solid reactant, the mechanism remains essentially the same, except that water may be liberated during the first step in forming  $\text{MgNO}_3$ . This first step is presumed to be the rate-limiting step since the other two steps are expected to be much faster.

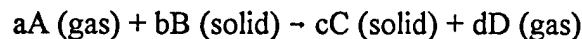
From a comparison of the ratio of the quantity of  $\text{NO}_2$  removed to NO produced as reaction progressed, some support for this mechanism was obtained. Initially, the absolute value of this ratio was very high, with much more  $\text{NO}_2$  being removed than NO being produced. As reaction progressed, however, this ratio often decreased to a point where 2 to 3 moles of  $\text{NO}_2$  were removed for every mole of NO produced. This value is appropriate given the proposed mechanism just shown. The time when this ratio was achieved was normally toward the end of the one hour experimental period. It is likely that even after the reaction becomes product-layer-diffusion-controlled, the other sequential steps are still occurring so that  $\text{NO}_2$  removal by the overall process is still apparent.

#### Application of the Shrinking Unreacted Core/Grain Model

The shrinking unreacted core model contains parameters that are useful for predicting the behavior of gas-solid reactions. Incorporating such physical parameters as the molar volume ratio of products to reactants (which can affect product layer formation and

subsequent product layer diffusional limitation of reaction rate) may further improve the utility of the model to describing reaction mechanism(s).

It is appropriate now to examine the equations for the three potential rate-limiting resistances affecting heterogeneous gas–solid reactions. The detailed derivations can be found in most standard texts on gas–solid reactions. The following is based on the descriptions reported by Szekely et al. (1976) and Levenspiel (1972). Using the generalized gas–solid reaction represented by equation (2-1)



to identify the only process acting, we can describe the rate of reaction with respect to conversion of the solid reactant for three idealized or limiting resistance situations: diffusion-through-gas-film control, chemical-reaction control, and diffusion-through-inert-product-layer control.

#### Diffusion-Through-Gas-Film Control

Whenever the stagnant gas film layer surrounding the sorbent particle produces significant mass transfer resistance to reaction, the gas-phase concentration profile for reactant A is as shown in Figure 4-28. From the figure, it is evident that no gaseous reactant is present at the solid surface, therefore, the concentration driving force [the quantity  $([A]_{\text{gas}} - [A]_{\text{solid}}) = ([A]_g - [A]_s)$ ] is a constant, having the value  $[A]_g$ . It is convenient to derive kinetic expressions for gas–solid reactions based on the external surface area of the sorbent particle,  $S = 4\pi R^2$ . From equation 2-1, we know that  $a(dN_B) = b(dN_A)$ , where  $N_A$  and  $N_B$  represent the number of moles of the reactants. Therefore, we can write

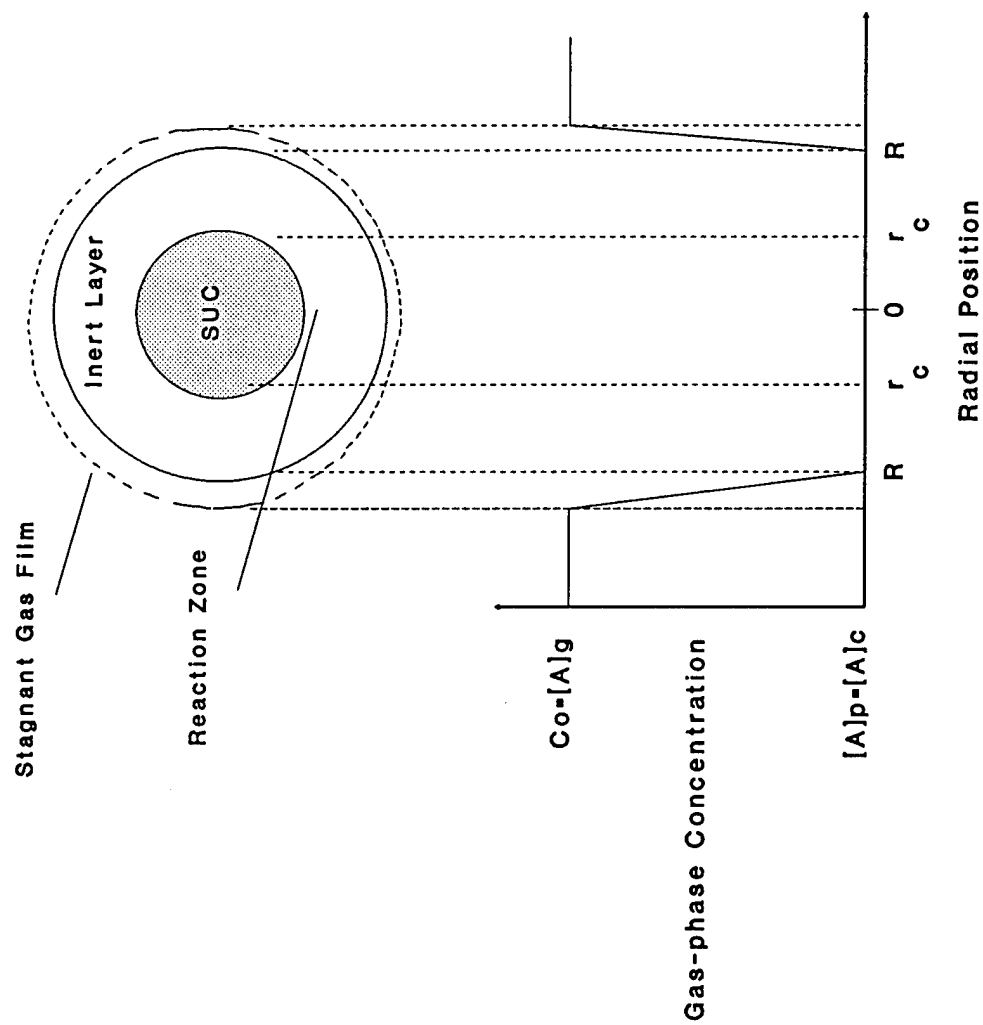


Figure 4-28. Graphical representation of the shrinking unreacted-core model under diffusion-through-gas-film control.

$$\frac{a}{S} \frac{dN_B}{dt} = -\frac{a}{4\pi R^2} \frac{dN_B}{dt} = -\frac{b}{4\pi R^2} \frac{dN_A}{dt} = bk_g([A]_g - [A]_s) = bk_g[A]_g \quad (4-4)$$

in which  $k_g$  is the mass transfer coefficient between the gas phase and the sorbent particle.

Letting  $\rho_B$  represent the molar density of  $B$  in the solid, and  $V$  be the particle volume, the number of moles of  $B$  present in the particle is:

$$N_B = \rho_B V \quad (4-5)$$

The decrease in the volume or radius of the shrinking unreacted core as a result of the reaction of  $a dN_B$  moles of solid and (or with)  $b dN_A$  moles of gas is given by the equation

$$-a dN_B = -b dN_A = -a \rho_B dV = -a \rho_B d(4/3 \pi r_c^3) = -4\pi \rho_B r_c^2 dr_c \quad (4-6)$$

Substituting equation 4-6 in equation 4-4 produces an expression for the rate of reaction in terms of the shrinking radius or unreacted core:

$$\frac{a}{S} \frac{dN_B}{dt} = -\frac{a \rho_B r_c^2}{R^2} \frac{dr_c}{dt} = bk_g[A]_g \quad (4-7)$$

By rearranging and integrating, an expression for how the unreacted core shrinks with time is derived:

$$-\frac{a \rho_B}{R^2} \int_R^{r_c} r_c^2 dr_c = bk_g[A]_g \int_0^t dt \quad (4-8)$$

Integration and rearrangement isolates the time of reaction:

$$t = \frac{a\rho_B R}{3bk_g[A]_g} \left[ 1 - \left( \frac{r_c}{R} \right)^3 \right] \quad (4-9)$$

Therefore, under gas-film-diffusion control,  $r_c = 0$ , and we will define  $\tau_f$  as the time for complete reaction of the particle:

$$\tau_f = \frac{a\rho_B R}{3bk_g[A]_g} \quad (4-10)$$

We can rewrite this equation in terms of fractional solid conversion ( $X$ ) by allowing:

$$1 - X = \left( \frac{\text{volume unreacted core}}{\text{total particle volume}} \right) = \frac{4/3 \pi r_c^3}{4/3 \pi R^3} = \left( \frac{r_c}{R} \right)^3 \quad (4-11)$$

Whence we can define the dependence of  $X$  upon  $t$ :

$$\frac{t}{\tau_f} = 1 - \left( \frac{r_c}{R} \right)^3 = X \quad (4-12)$$

Plotting solid conversion versus bed exposure or reaction time, as previously described, should reveal a linear relationship having a slope of  $1/\tau_f$  if gas-film-diffusion is rate-limiting.

#### Chemical-Reaction Control

From Figure 4-29, it can be seen that the concentration gradient, and the related progress of reaction, are unaffected by the presence of any inert layer(s) in this situation. The

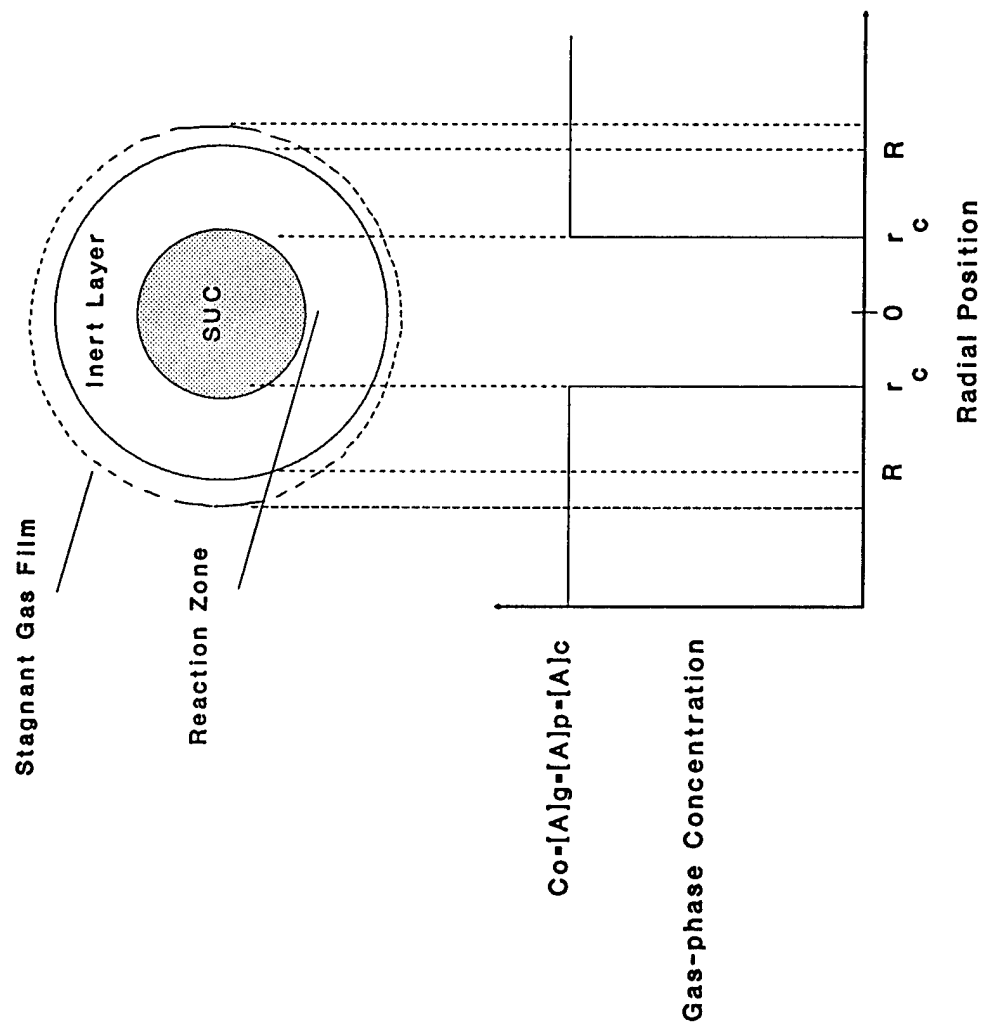


Figure 4-29. Graphical representation of the shrinking unreacted-core model under chemical-reaction control.



quantity of material reacting is proportional to the available surface area of the unreacted core (which at the beginning of the reaction would be the exterior surface of the particle as there is no inert product layer formed) and can be expressed in the same manner as equation 4-4:

$$-\frac{a}{4\pi r_c^2} \frac{dN_B}{dt} = -\frac{b}{4\pi r_c^2} \frac{dN_A}{dt} = bk_s[A]_g \quad (4-13)$$

Here  $k_s$  represents the intrinsic first-order rate coefficient for the surface reaction (cm/s).

Writing  $N_B$  in terms of the shrinking radius by analogy to equation 4-7:

$$-\frac{a}{4\pi r_c^2} \rho_B 4\pi r_c^2 \frac{dr_c}{dt} = -a\rho_B \frac{dr_c}{dt} = bk_s[A]_g \quad (4-14)$$

This may be rearranged and integrated to derive an expression describing how the unreacted core shrinks with time:

$$-a\rho_B \int_R^{r_c} dr_c = bk_s[A]_g \int_0^t dt \quad (4-15)$$

After integration,  $t$  may be isolated by rearrangement:

$$t = \frac{a\rho_B}{bk_s[A]_g} (R - r_c) \quad (4-16)$$

The time for complete conversion of the solid under chemical reaction control, defined as  $\tau_c$ , occurs when  $r_c=0$ :

$$\tau_r = \frac{a\rho_B R}{bk_s[A]_g} \quad (4-17)$$

An expression for the decrease in the radius of the shrinking core or the increase in fractional conversion of the solid particle surface then follows, including a substitution from equation 4-11:

$$g(X) = \frac{t}{\tau_r} = 1 - \frac{r_c}{R} = 1 - (1-X)^{1/3} \quad (4-18)$$

A linear plot of the right-hand side of the equation versus bed exposure time would allow for the prediction of  $\tau_r$  and identify chemical-reaction kinetics as the rate-controlling process.

#### Diffusion-through-Inert-Product-Layer Control

This analysis is somewhat more complicated since it requires a two-step process, first considering diffusion flux in a partially reacted particle, then letting the size of the unreacted core change with time. From Figure 4-30, both reactant  $A$  and the unreacted core radius move inward with time; however, the unreacted core shrinkage is slower than the flow rate of  $A$  toward the unreacted core by approximately three orders of magnitude (the order of the ratio of solid density to gas density), so a steady-state assumption regarding the dimension of the unreacted core is valid. This assumption greatly simplifies the mathematics, because it can now be assumed that the rate of reaction of  $A$  is equal to its rate of diffusion to the surface of the unreacted core:

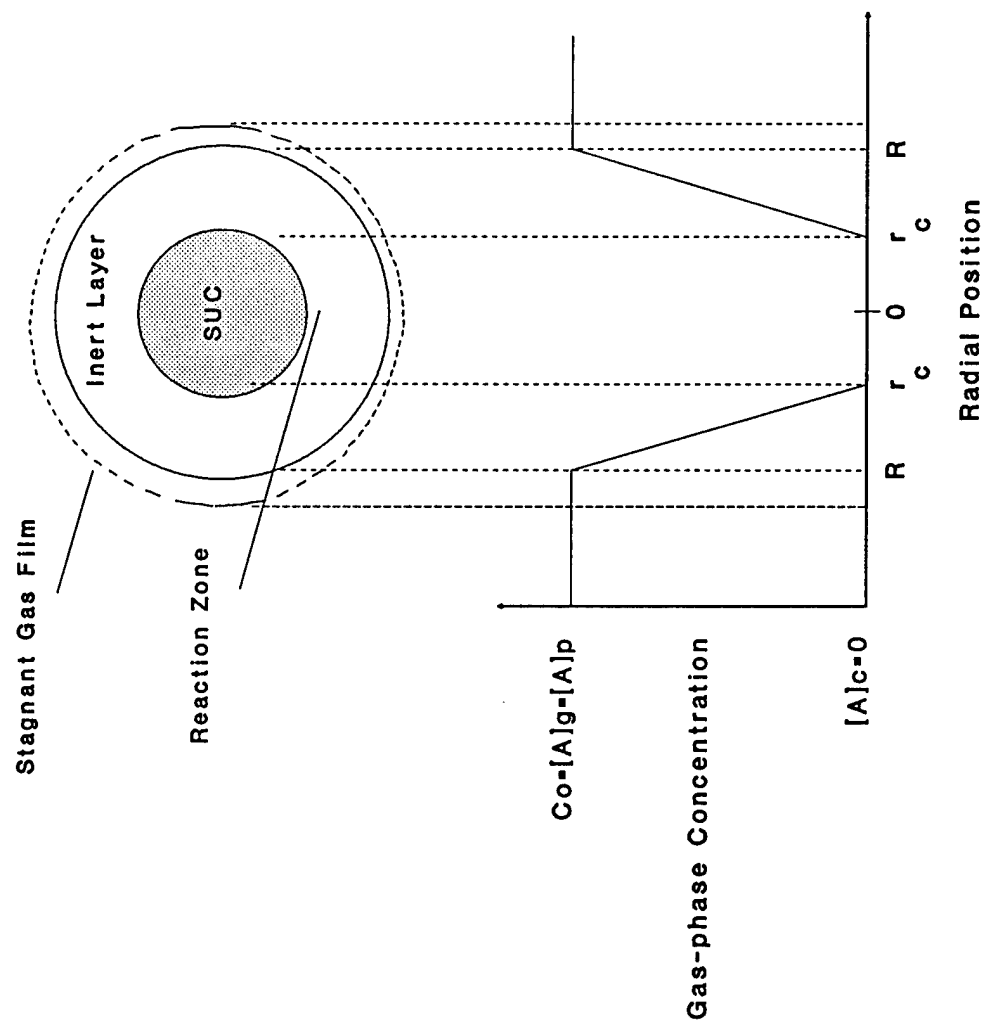


Figure 4-30. Graphical representation of the shrinking unreacted-core model under diffusion-through-inert-product-layer control.

$$-\frac{dN_A}{dt} = 4\pi r^2 Q_A = 4\pi R^2 Q_{AS} = 4\pi r_c^2 Q_{AC} = \text{Constant} \quad (4-19)$$

The flux of  $A$  within the inert layer is expressed by Fick's law for equimolar counterdiffusion: (Note that  $Q_A$  is positive.)

$$Q_A = D_e \frac{d[A]}{dr} \quad (4-20)$$

where  $D_e$  represents the effective diffusion coefficient of the gaseous reactant through the product layer ( $\text{cm}^2/\text{s}$ ). Owing to variations in the properties of the inert layer, the value of this coefficient is difficult to estimate and is generally determined experimentally. The effective diffusion coefficient can be obtained by adjusting  $D_e$  in the shrinking unreacted-core or grain model until the model predictions fit experimental data (Marsh and Ulrichson, 1985).

Equations 4-19 and 4-20 may be combined:

$$-\frac{dN_A}{dt} = 4\pi r^2 D_e \frac{d[A]}{dr} = \text{Constant} \quad (4-21)$$

Integrating through the inert layer :

$$-\frac{dN_A}{dt} \int_R^{r_c} \frac{dr}{r^2} = 4\pi D_e \int_{[A]_g}^{[A]_c} d[A] \quad (4-22)$$

therefore,

$$-\frac{dN_A}{dt} \left( \frac{1}{r_c} - \frac{1}{R} \right) = 4\pi D_e [A]_g \quad (4-23)$$

For a shrinking unreacted core of given size,  $dN_A/dt$  is constant, but the inert layer becomes thicker as the core shrinks, which decreases the diffusion rate of  $A$  through the layer. Before integrating equation 4-23, one of the variables must be eliminated. As in gas-film diffusion,  $N_A$  can be eliminated by writing it in terms of  $r_c$ . Substituting again from equation 4-6, and rearranging produces an integrable form:

$$- a\rho_B \int_{r_c=R}^{r_c} \left( \frac{1}{r_c} - \frac{1}{R} \right) r_c^2 dr_c = bD_e[A]_g \int_0^t dt \quad (4-24)$$

From this,

$$t = \frac{a\rho_B R^2}{6bD_e[A]_g} \left[ 1 - 3\left(\frac{r_c}{R}\right)^2 + 2\left(\frac{r_c}{R}\right)^3 \right] \quad (4-25)$$

Defining  $\tau_d$  as the time to complete conversion ( $r_c=0$ ) of the solid particle under product-layer-diffusion control :

$$\tau_d = \frac{a\rho_B R^2}{6bD_e[A]_g} \quad (4-26)$$

This leads to an expression for the progress of the reaction in terms of  $\tau_d$ :

$$\frac{t}{\tau_d} = 1 - 3\left(\frac{r_c}{R}\right)^2 + 2\left(\frac{r_c}{R}\right)^3 \quad (4-27)$$

This may also be expressed in terms of fractional solid conversion from equation 4-11:

$$p(X) = \frac{t}{\tau_d} = 1 - 3(1-X)^{2/3} + 2(1-X) \quad (4-28)$$

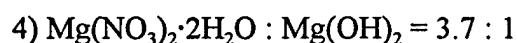
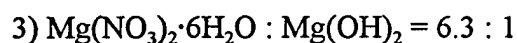
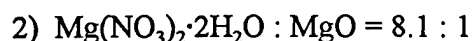
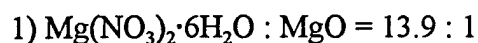
When product-layer diffusion is rate-controlling, a plot of the right-hand-side of equation 4-28 versus bed exposure time allows for the determination of  $\tau_d$ .

#### Derivations of the Shrinking Unreacted-Core Model

As reaction proceeds and a product layer is formed, the decreasing product layer diffusion rate can affect the overall rate. Equation 4-19 assumes a constant value of  $D_p$ , which may not be a valid assumption. Variation of the (decreasing) diffusion coefficient in the product layer may have to be taken into account to describe a reaction in which a more voluminous solid product forms (Krishnan and Sotirchos, 1993). More-elaborate models can be constructed allowing for changes in the controlling mechanism with time or solid-surface conversion. Often, a simple modification to the basic equations allows for an improved representation of the experimental data. When product-layer-diffusion is truly the rate-limiting process, the inclusion of the molar volume ratio (represented by  $Z$ ) in equation 4-28, as follows, may improve the fit (Szekely et al., 1976):

$$\frac{t}{\tau_d} = \frac{3[Z - (Z + (1 - Z)(1 - X))]^{2/3}}{Z - 1} - 3(1 - X)^{2/3} \quad (4-29)$$

This is especially true when the product layer molar volume is significantly larger (or smaller) than that of the solid reactant. Referring back to Table 2-1, four molar volume ratios are of interest in this research:



As all of these values are noticeably greater than one, the use of the Z-term is expected to aid in the interpretation of the experimental data collected in this study.

Szekely et al. (1976) also pointed out that the use of one or the other of the governing equations may not be sufficient to best describe the experimental data. Since the two equations are similar, it is often difficult to distinguish between chemical-reaction control and product-layer-diffusion control. In some cases, assuming gas-film diffusion is not rate-limiting, chemical-reaction and product-layer-diffusion may collectively control the reaction rate. In such cases, a term ( $\sigma^2$ ) representing the ratio of diffusional resistance to chemical-reaction resistance can be defined to apply the relative importance of each resistance to the reaction rate:

$$\sigma^2 = \frac{\tau_d}{\tau_r} = \frac{k_s R}{6D_e} \quad (4-30)$$

This term is applied via the equation:

$$\frac{2t}{\tau_r} = g(X) + \sigma^2 p(X) \quad (4-31)$$

### Correlation Between Gas-Phase Concentration and Solid Conversion

To use the shrinking unreacted-core model equations it is necessary to collect data describing solid conversion with time. This is normally done using thermogravimetric methods on single pellets, by way of real-time surface analyses, or post-sorption chemical analyses. As was previously explained, these data were not collected since they are less relevant to data directly indicative of the control efficiency of gaseous NO<sub>x</sub> pollutants. It is necessary to be able to correlate these data so that they can be used in the model equations to interpret sorption behavior. By invocation of assumptions related to constant-pattern behavior associated with the local-equilibrium theory of fixed-bed reactors, the previously displayed gas-penetration-versus-time data are made more amenable for this purpose.

### Local-Equilibrium Theory

While a detailed discussion of the local-equilibrium theory can be found in any standard text on adsorption in fixed beds, the following brief presentation is based upon descriptions by Sherwood et al. (1975) and Ruthven (1984). When there is efficient mass transfer between the gas and solid phases, the reactive gas travels through the packed bed as a wave without a significant change in concentration, other than that caused by reaction with



the sorbent surface. The wave front reaches a steady state and its width, as it moves through the bed, attains a "constant pattern." The constant-pattern approach is based on the assumption that the width of the concentration front tends toward a constant value as the concentration wave moves through a packed bed. The mass-transfer zone reaches a stable asymptotic form in this case (LeVan et al., 1988). According to Suzuki (1990), most adsorption isotherms are "favorable " and exhibit the non-linear Langmuir form. A favorable isotherm can be assumed for a single adsorbate with a high adsorption capacity, whose concentration decreases in the downstream flow direction (Frey, 1992). The asymptotic limit is reached when the fluid-phase front matches the adsorbed-phase front, and

$$\frac{q}{q_o} = \frac{C}{C_o} \quad (4-32)$$

in which  $q$  represents moles adsorbate sorbed per mole of reactant in the sorbent,  $q_o$  represents the largest number of moles of adsorbate that can be sorbed per unit mole of sorbent,  $C$  represents outlet gas concentration, and  $C_o$  represents inlet gas concentration. Constant-pattern behavior is the opposite limit to "unfavorable" or "proportional-pattern" behavior, in which the concentration front becomes diffuse and extended by mass transfer with the solid.

The differential-concentration driving force allows for mass transfer between phases. In the fixed-bed model, the simplified differential mass balance is represented by

$$-rate = \frac{\rho_B}{\epsilon_v} \frac{dq}{dt} \quad (4-33)$$

where  $\epsilon_v$  represents the void fraction of the bed. Correlation of this model with the shrinking unreacted-core model, using the assumption of constant-pattern behavior, produces

$$-rate = \frac{\rho_B}{\epsilon_v} \frac{dq}{dt} = C_o \frac{dX}{dt} \quad (4-34)$$

The rate equations obtained from the shrinking unreacted-core model can be used together with the fixed-bed model, but simple analytical solutions are hard to find and the determination of rate constants by the method of least squares is not possible. Some type of numerical procedure has to be used instead (Bjerle et al., 1992). The constant-pattern assumption allows the use of the relationship

$$X = \frac{q}{q_o} = \frac{C}{C_o} \quad (4-35)$$

Substituting the quantity  $(C/C_o)$  for  $X$  in the shrinking core equations allowed for the evaluation of their applicability to the experimental data collected. Karlegard and Bjerle (1994) used this approach in their study of the removal of  $H_2S$  by zinc ferrite. Other notable examples where the quantity  $(C/C_o)$  was used as an indication of solid conversion are the work of Wolff et al. (1993) who used  $\gamma-Al_2O_3$ -supported  $CaO$  to remove gaseous  $SO_2$ , and Dam-Johansen and Ostergaard (1991a), who examined the  $SO_2$ -limestone reaction.

### Application of Shrinking Unreacted-Core/Grain Model to Experimental Data

To determine the applicability of the shrinking unreacted-core model to the experimental data collected in this study, the respective governing equations were evaluated for various stages of the reaction. Three examples were chosen for presentation to show the range of applicability of the model to the reaction between  $\text{NO}_2$  and  $\text{MgO}$ . As an intermediate situation, the removal of 50 ppm  $\text{NO}_2$  at a reaction temperature of 423 K was chosen. For the evaluation of the extreme experimental conditions, the removal of 200 ppm  $\text{NO}_2$  at 473 K and the removal of 20 ppm  $\text{NO}_2$  at 373 K were evaluated. These three cases contain data collected in the absence of oxygen, using dry sorbent (no  $\text{Mg}(\text{OH})_2$ ). The relevance of the shrinking unreacted-core model to these situations will also be generally discussed. Each case will be presented separately, with a discussion of the specific applicability and considerations.

#### 50 ppm $\text{NO}_2$ at a Reaction Temperature of 423 K

Figure 4-31 represents the mathematical transformation of solid sorbent conversion data ( $X$  or  $\text{NO}_2$  penetration) into the values obtained from the shrinking unreacted-core equations. The left ordinate shows the chemical-reaction-control-equation values (Equation 4-18) and the right ordinate indicates the product layer diffusion control equation values (Equation 4-28). If an equation is representative of the mechanism occurring, then the plot will be linear with a slope of the inverse time to complete reaction,  $\tau_r$  or  $\tau_d$ , as previously discussed. From this figure, it visually appears that over the entire course of reaction

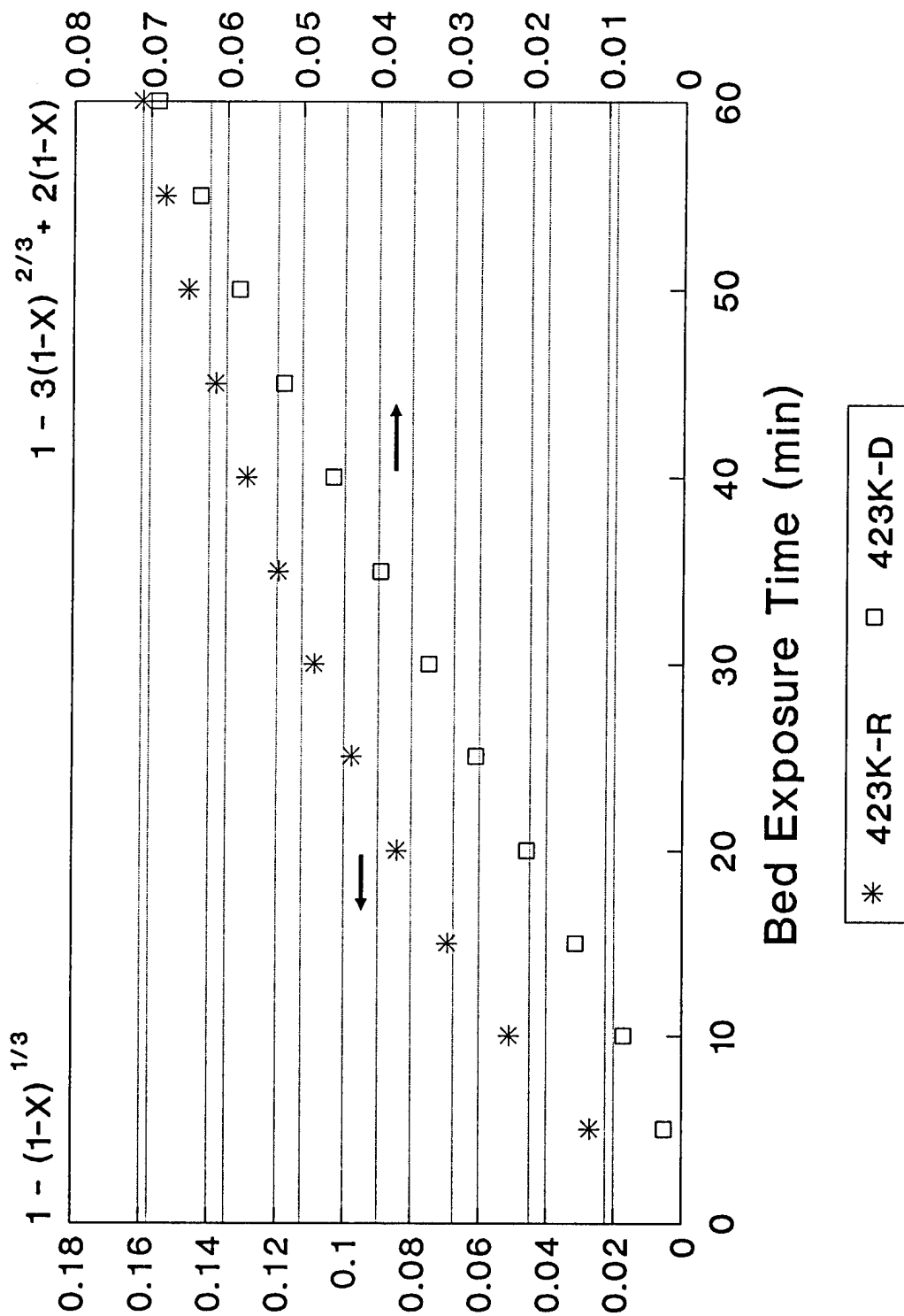


Figure 4-31. Shrinking unreacted-core model evaluation ( $[\text{NO}_2]_{\text{in}}=50$  ppm,  $T=423$  K,  $[\text{O}_2]=0\%$ ).

evaluated, the reaction-control-equation line shows noticeably greater curvature than the product-layer-diffusion-control-equation. To apply some statistical significance to the fit of these equations at various stages of the reaction, linear least-squares regressions of the data were performed, including the determination of 95% confidence intervals.

The two equations are separately evaluated as shown in Figures 4-32 and 4-33. From Figure 4-32, the equation of the least-squares linear regression line for the chemical-reaction-control-equation is  $y = 1 - (1-X)^{1/3} = 0.0025t + 0.0223$ , with an  $r^2$  value of 0.95. From this equation,  $\tau_r$  (the inverse of the slope of the regression line) is equal to 397 minutes. While the coefficient of determination's value is relatively high, there is obviously some curvature. A considerably better fit was obtained for the product-layer-diffusion-control equation, where both the  $r^2$  and F-statistic values are higher, as shown in Figure 4-33. Only the initial point falls outside the 95% confidence interval. From this fit,  $\tau_d$  is determined to be equal to 820 minutes, approximately twice as large as  $\tau_r$ , which would necessarily be smaller since chemical-reaction control assumes a more-rapid rate of reaction and, relatedly, a more-rapid solid conversion rate.

It is quite likely that both processes are simultaneously playing a role in the limitation of the reaction rate. It would be expected that chemical reaction control would be more important early in the reaction process. To test this, the first 15 minutes of data are replotted as shown in Figures 4-34 and 4-35. From these figures, the two mechanisms appear to be equally important in describing initial sorption behavior under these conditions. To test the combined resistance equation, the value of  $\sigma^2$  was calculated to be 2.5, which when used in Equation 4-31, produced a value of  $\tau_r$  equal to 357 minutes. As was previously discussed,

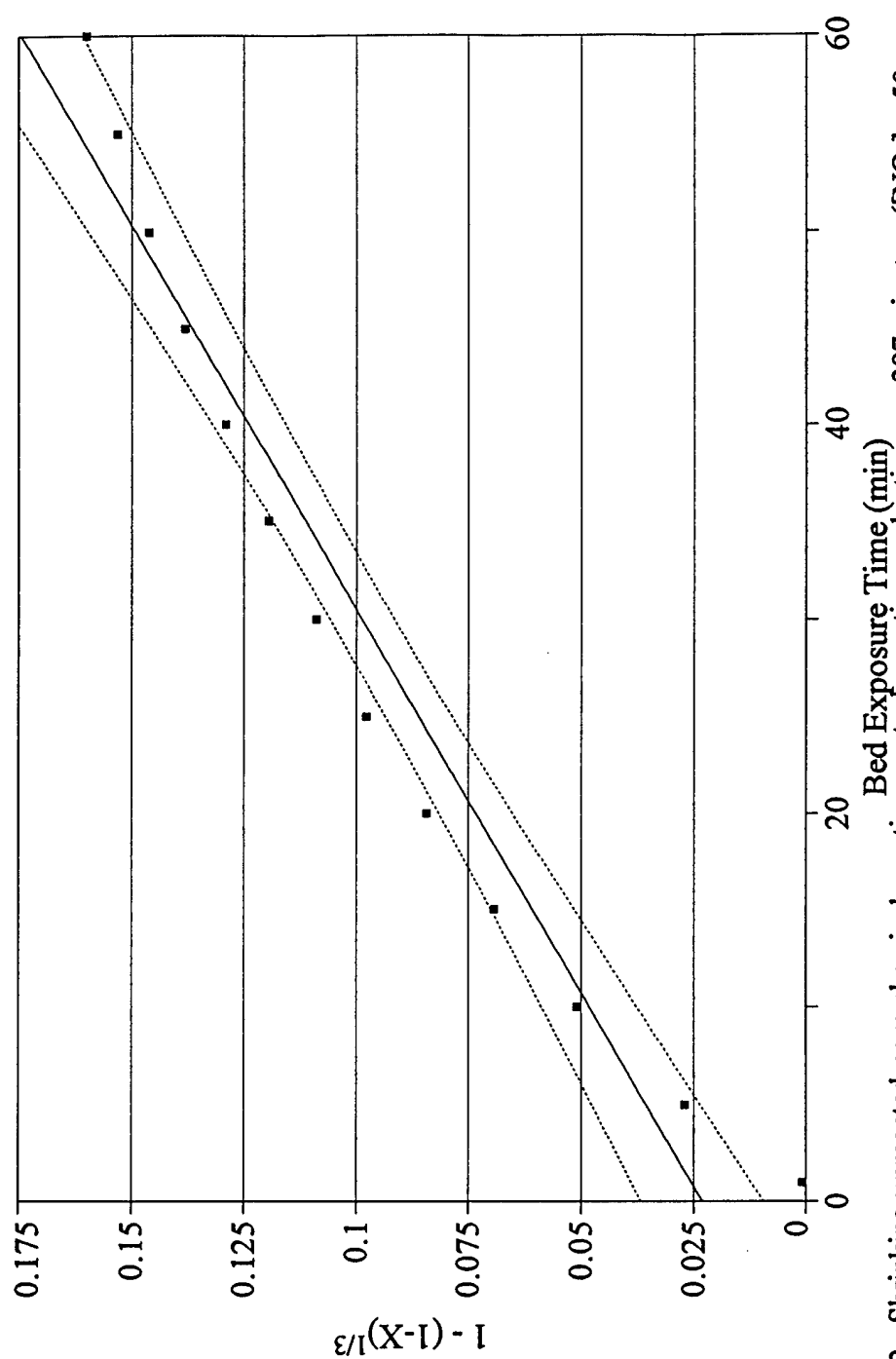


Figure 4-32. Shrinking unreacted-core chemical-reaction-control-equation evaluation,  $\tau_r=397$  minutes ( $[\text{NO}_2]_{\text{in}}=50$  ppm,  $T=423$  K,  $[\text{O}_2]=0\%$ ). [ $y = 0.003x + 0.023$ ,  $r^2=0.95$ , Fit Std Error = 0.012,  $F=208.1$ ].

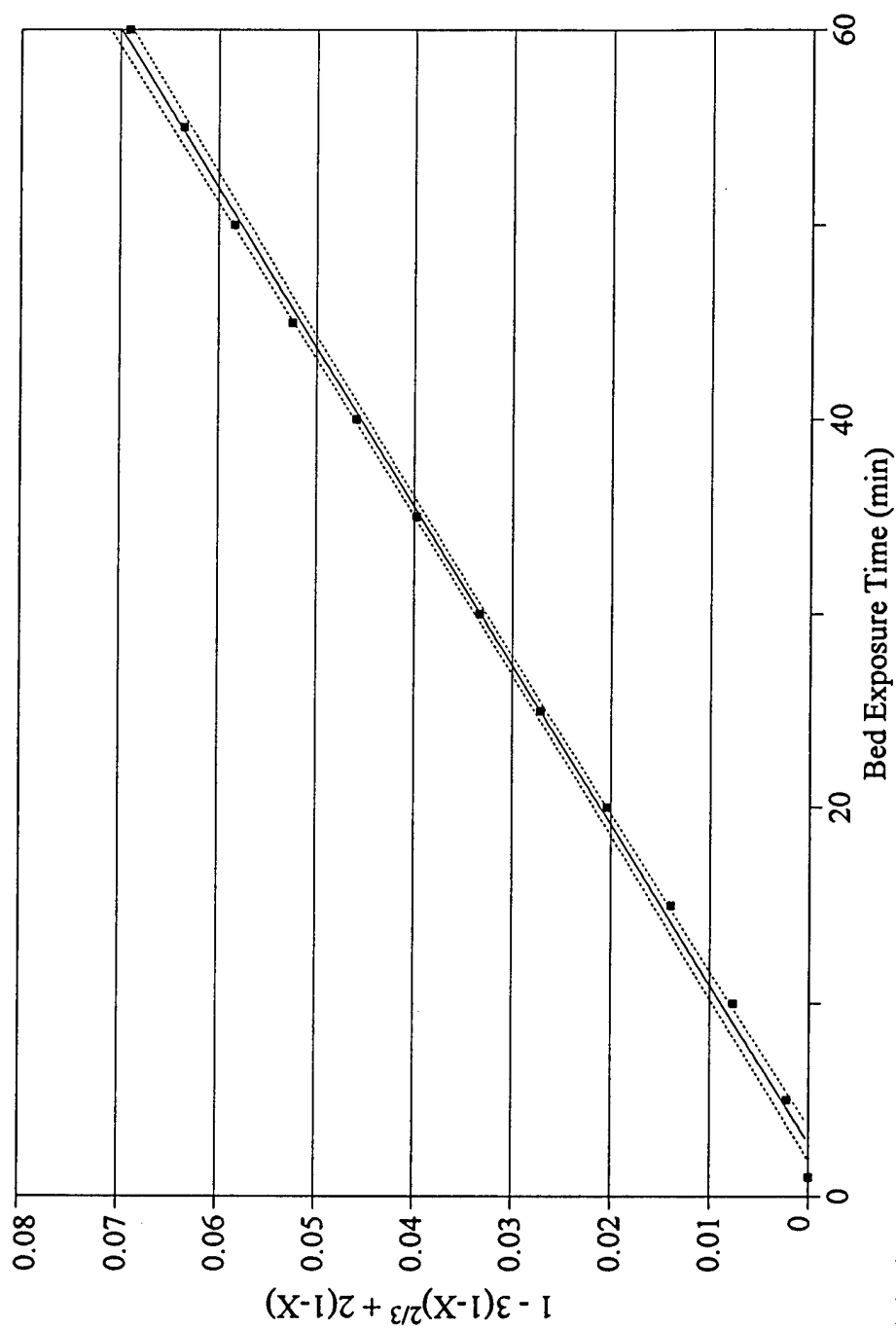


Figure 4-33. Shrinking unreacted-core product-layer-diffusion-control-equation evaluation,  $\tau_d=820$  minutes  $[NO_2]_m=50$  ppm,  $T=423$  K,  $[O_2]=0\%$ . [ $y = 0.001x + 0.003$ ,  $r^2=0.999$ , Fit Std Error = 0.001,  $F=7125.9$ ].

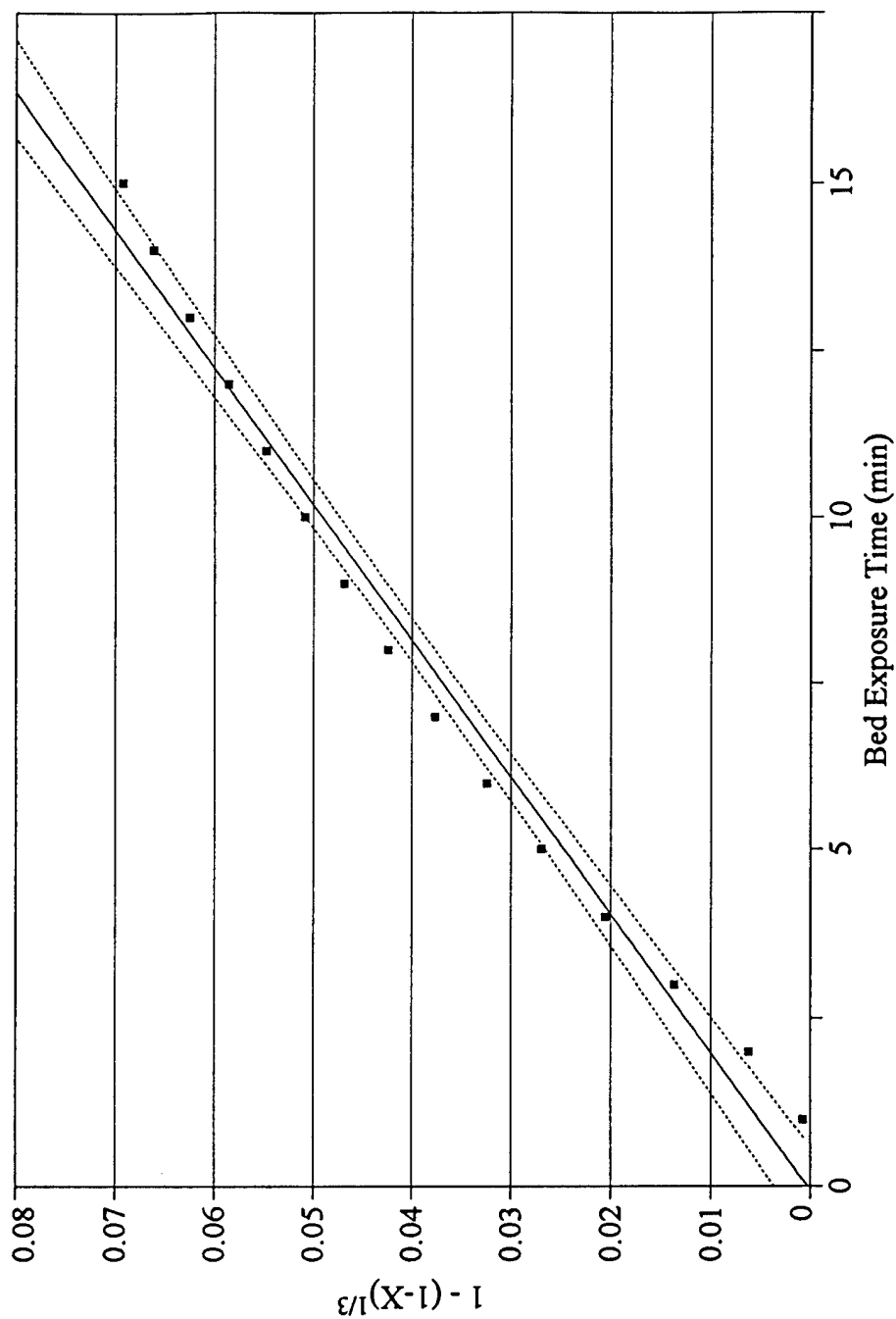


Figure 4-34. Shrinking unreacted-core chemical-reaction-control-equation evaluation,  $\tau_r=205$  minutes ( $[\text{NO}_2]_{\text{in}}=50$  ppm,  $T=423$  K,  $[\text{O}_2]=0\%$ ). [ $y = 0.005x + 0.0002$ ,  $r^2=0.98$ , Fit Std Error = 0.003,  $F=812.9$ ].



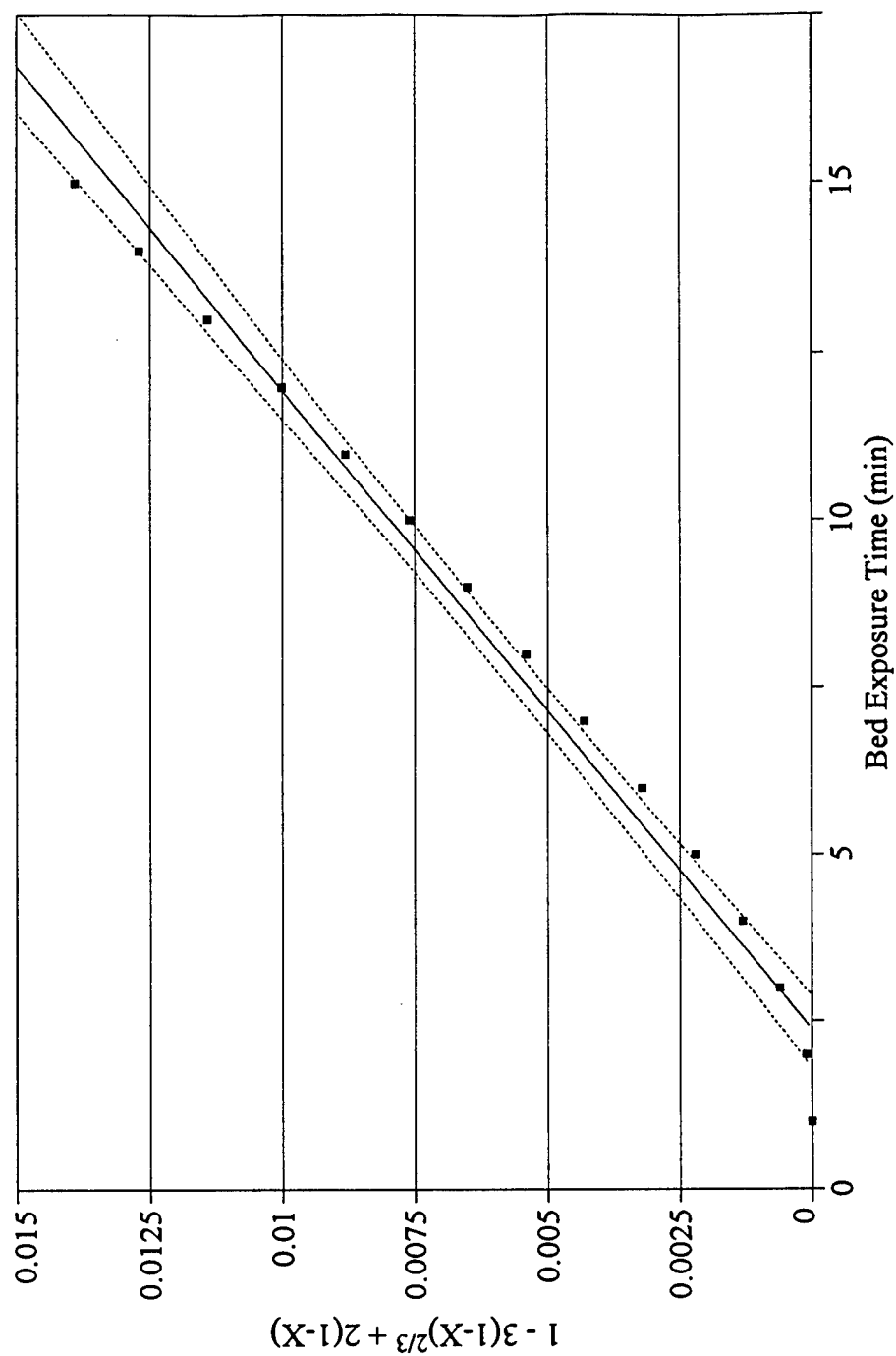


Figure 4-35. Shrinking unreacted-core product-layer-diffusion-control-equation evaluation,  $\tau_d=957$  minutes ( $[\text{NO}_2]_{\text{in}}=50$  ppm,  $T=423$  K,  $[\text{O}_2]=0\%$ ). [ $y = 0.001x + 0.003$ ,  $r^2=0.98$ , Fit Std Error = 0.0006,  $F=814.8$ ].

when the molar volume ratio of product to reactant is large, this may play a role in the ultimate determination of the overall rate as well as solid sorbent conversion efficiency. From the data in Table 2-1, the molar volume ratio of  $\text{Mg}(\text{NO}_3)_2$  (anhydrous) to  $\text{MgO}$ ,  $Z$ , is estimated to be approximately 3.7. Using Equation 4-29, a value of  $\tau_d$  equal to 330 minutes was calculated, a 60% smaller number than that calculated using Equation 4-28. It appears that the model predicts a significant effect from the molar volume ratio difference.

To put these numbers into perspective, the cumulative mass of  $\text{NO}_2$  removed by the sorbent bed was calculated using an iterative approach by multiplying the one-minute average  $\text{NO}_2$  removal rates by the  $\text{NO}_2$  mass flow rate for each minute of the run. These were added together to produce a cumulative mass of  $\text{NO}_2$  reacted at any given exposure time. It was assumed that all  $\text{NO}_2$  removed from the gas stream was taken up by the  $\text{MgO}$ -vermiculite sorbent bed. An example of these data collected from the middle of the bed is plotted in Figure 4-36. The middle of the bed was selected as the sampling point because it was assumed that the front half of the bed would become "saturated" more rapidly than the back half of the bed in a long-term run. It can be seen from this figure that the rate of cumulative mass removal is initially greater than later in the run. This trend is more evident in Figure 4-37, which shows data collected over a 7-hour period. This long-term run was conducted to evaluate the  $\tau$  values predicted by the model equations. Since samples were collected at the center of the bed, only half of the total bed mass was used for sorption up to this point, so  $\tau$  values should be divided by two for application to this reduced-sorbent-mass and associated surface area. Plots of the amount of  $\text{NO}_2$  mass adsorbed versus time were concave toward

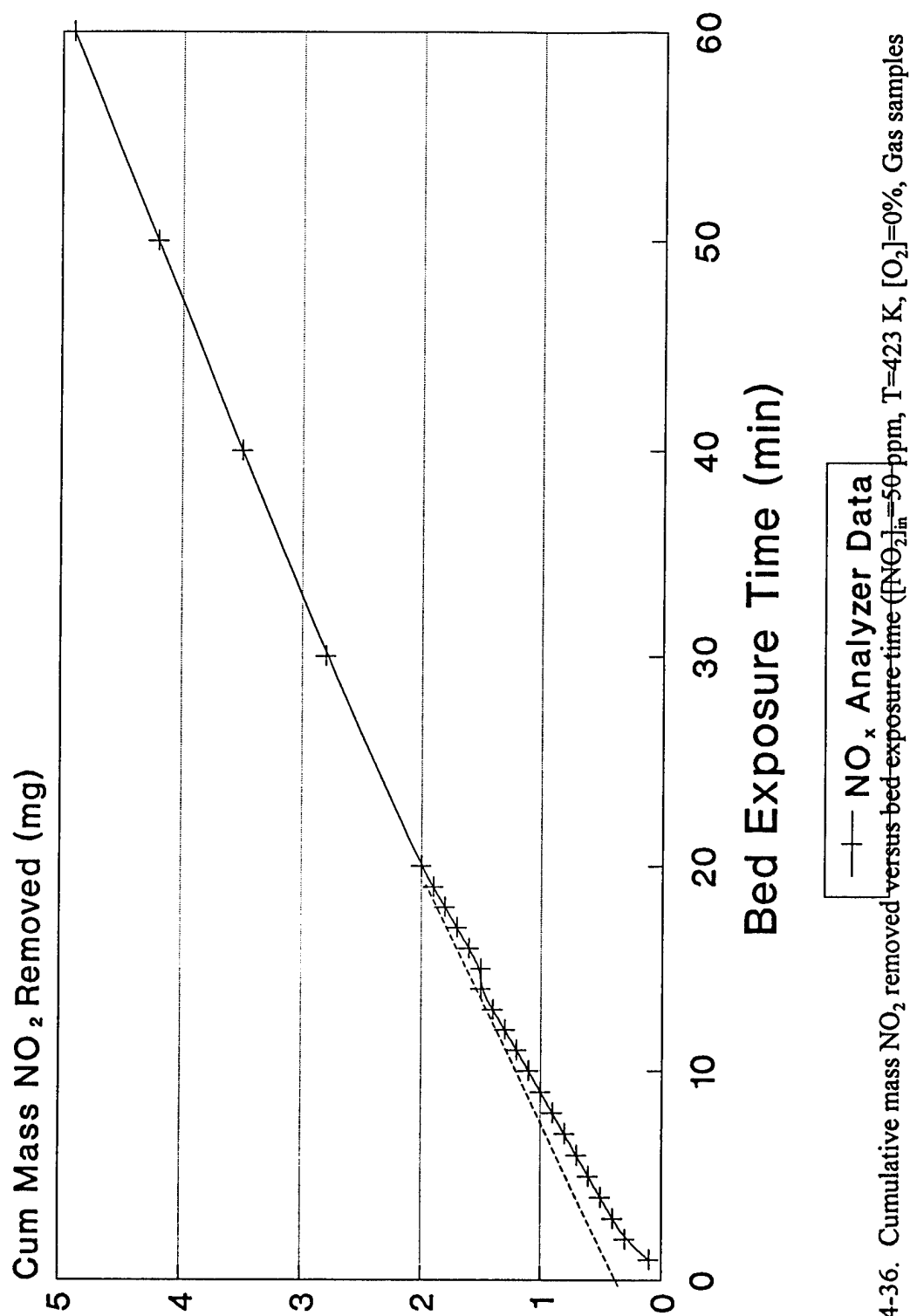


Figure 4-36. Cumulative mass  $\text{NO}_2$  removed versus bed-exposure time ( $[\text{NO}_2]_{\text{in}}=50$  ppm,  $T=423$  K,  $[\text{O}_2]=0\%$ , Gas samples collected from center of bed).

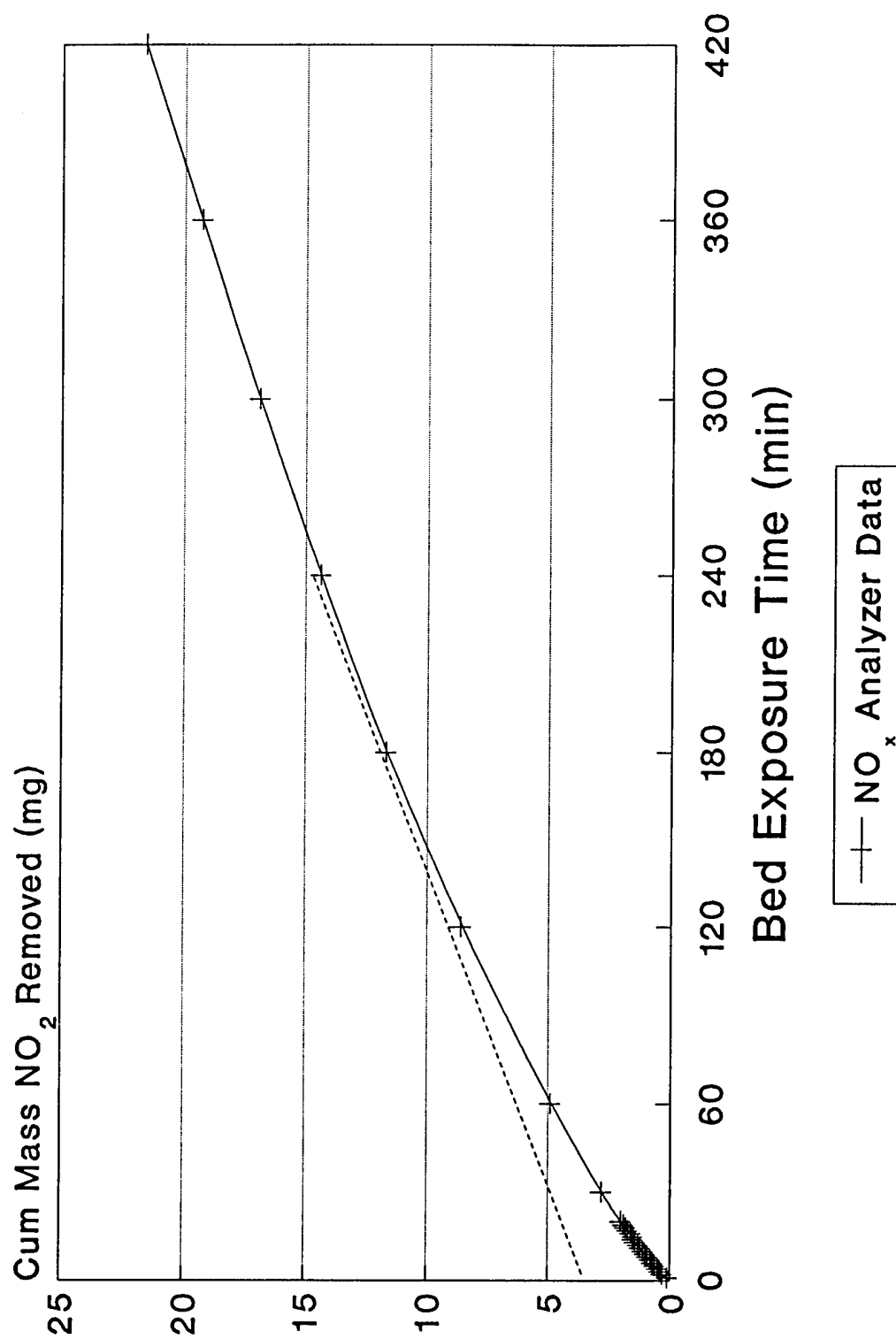


Figure 4-37. Cumulative mass NO<sub>2</sub> removed versus bed exposure time for a long-term run ([NO<sub>2</sub>]<sub>in</sub> = 50 ppm, T = 423 K, [O<sub>2</sub>] = 0%, Gas samples collected from center of bed).

the time axis, as in most diffusion-controlled processes in which the buildup of concentration inside the particle progressively reduces the driving force or the accumulation of product increases resistance (Pigford and Sliger, 1973).

From these figures, the mass removal rate does not appear to approach zero, even after an extended exposure period. The total mass of  $\text{NO}_2$  removed after 7 hours was only 21.6 mg or  $4.7 \times 10^{-4}$  moles. This is significantly less than the predicted stoichiometric capacity of the mass of  $\text{MgO}$  in the bed, corresponding to a utilization ratio of approximately 0.2%. It is interesting to note that the  $\text{NO}_2$  removal to  $\text{NO}$  production ration was approximately 4:1 after 3 hours, and was approximately 3:1 after 7 hours, supporting the previously proposed mechanism of removal. The low utilization ratio is believed to be a complex function of a number of important variables, including the low  $\text{NO}_2$  concentration in the bulk gas phase, the high product-to-reactant molar volume ratio, and reduced sorbent porosity.

Without a significant concentration-gradient driving force, formation of a layer of  $\text{Mg}(\text{NO}_3)_2$  on the exterior surface area of the sorbent will render the remaining available  $\text{MgO}$  relatively inaccessible for reaction with  $\text{NO}_2$ . The high product-to-reactant molar volume ratio means that a significant amount of surface area can become blocked from reaction as product is formed. For reactions accompanied by an increase in the volume of the solid phase, incomplete conversion may be expected with ultimate conversion decreasing with an increase in intrapellet diffusional resistance. In many gas-solid reactions, maximum solid conversion approaches a constant value less than 100%. The main reasons for this phenomenon are structural changes of the pores. Maximum conversion is reached when pore

closure occurs (Ramachandran and Smith, 1977). The reaction of  $\text{SO}_2$  with CaO or MgO forms a solid product,  $\text{CaSO}_4$  or  $\text{MgSO}_4$ , which occupies more space than the solid reactant. If there is no increase in the overall volume of the porous particles during reaction, the pore space may become completely filled with or covered by solid product. Once pores become plugged, the interior of the porous particles are practically inaccessible to gaseous reactants since diffusion through the solid product is an extremely slow process (Sotirchos and Zarkanitis, 1992). Bhatia and Perlmutter (1983) attributed the continued slow solid-surface conversion in gas-solid reactions to the effective closure of a narrow size range of small surface pores, leaving larger pores of smaller surface area available for reaction at a greatly reduced rate. Bhatia and Perlmutter (1981b) presented a correlation that allows for the calculation of maximum conversion based upon initial porosity ( $\epsilon_o$ ) and  $Z$ :

$$X_{\max} = \frac{\epsilon_o}{(Z-1)(1-\epsilon_o)} \quad (4-36)$$

Assuming an initial porosity value of 0.3, based upon values used for CaO by the authors, the calculated value for  $X_{\max}$  is approximately 16%. High initial sorbent porosity (and associated high surface area) can create the potential for internal diffusion limitations to chemical reaction. Marsh and Ulrichson (1985) found that grains of CaO obtained by calcining  $\text{Ca}(\text{OH})_2$  contained significant quantities of micropores, many of them around 22 Å in radius. Effective pore closure occurs when this radius decreases to approximately 5 Å. If intrapellet diffusional resistance is appreciable, pore closure may occur at the surface, significantly limiting diffusion into the particle interior and reducing ultimate MgO conversion within the

sorbent. In micropore diffusion, the diffusing molecules are "trapped" by the attractive forces near the pore walls in a process similar to surface diffusion, but steric effects are more important. Small differences in molecular size or shape can produce large differences in diffusivity (Ruthven, 1988). The simple grain model cannot realistically simulate porosities less than 26%, whereas initial porosities of calcined limestones can be greater than 50% (Damle, 1994).

Most experimental work published on  $\text{CaO-SO}_2$  reactions was conducted using  $\text{SO}_2$  concentrations in the tenths of a percent, one to two orders of magnitude greater than  $\text{NO}_2$  concentrations evaluated in this research. It is noted that Equation 4-36 does not have a gas-phase concentration term. At a given conversion level (or product layer thickness), Marsh and Ulrichson (1985) found that doubling the bulk gas-phase adsorbate concentration should double the overall reaction rate, consistent with the idea of a product layer surrounding the active surface area of the oxide. Another example is the degree of zinc ferrite utilization in the removal of 2,600 ppm  $\text{H}_2\text{S}$  at 500 to 600 C, as reported by Karlegard and Bjerle (1994), which varied from 5 to 11%.

A significant correlation between adsorbate concentration and solid conversion in the reaction between  $\text{SO}_2$  and  $\text{CaO}$  was reported by Simons (1988). Simons reported a utilization factor of approximately 0.6 for this effect, meaning a ten-fold increase in concentration produced a six-fold increase in effective utilization. Based upon this correlation, a ten-fold lower concentration would predict an  $X_{max}$  value of approximately 3%, and a hundred-fold lower concentration would predict an  $X_{max}$  value of approximately 0.4%. This may partially explain the low  $\text{NO}_2$  utilization rate by  $\text{MgO}$ . Since little is known about

the pore size distribution of the MgO-vermiculite sorbent, it is difficult to say what effect it may have on sorbent utilization. However, Simons also pointed out that small-pore plugging is dominant for 1- to 10- $\mu\text{m}$  particles, while pore-mouth plugging is dominant for 100- $\mu\text{m}$  particles. Rate limitations resulting from product-layer diffusion (prior to plugging or filling) are most evident for thick product layers occurring within the larger pores of larger particles. If pore plugging within the grains of the particle were occurring, lower conversion levels at higher temperatures would be expected.  $\text{NO}_2$  penetration curves with a sharp break to a flat curve would be expected if total pore closure occurs. However, positive slopes are seen even after a sharp drop in reaction rate (Marsh and Ulrichson, 1985). The calcination of  $\text{Ca}(\text{OH})_2$  to  $\text{CaO}$  results in highly porous particles with a theoretical porosity of approximately 50% (Newton et al., 1989). Depending upon the temperature used, the actual porosity can be lower, particularly for the calcination of  $\text{Ca}(\text{OH})_2$ . Virtually all of the surface area is in the internal pore structure. The increase in molar volume from solid reactant to product results in the filling of the pore structure and due to rapid reaction rates and pore diffusional resistances, may lead to plugging of the outer  $\text{CaO}$  layers, leaving the interior unreacted.

As was previously noted, the first-order kinetic rate coefficients decreased with time as reaction progressed. An empirical relationship between the inverse values of these coefficients and exposure time was noticed. After an initial period of adjustment to dynamic equilibrium conditions, a linear relationship between  $1/k$  and time appeared. Figure 4-38 displays an example of this relationship. This relationship allowed for the prediction of  $k$ -values at an extended bed exposure time, based upon the values obtained from the first hour of the experimental run. These predicted values were used in the first-order kinetic equation



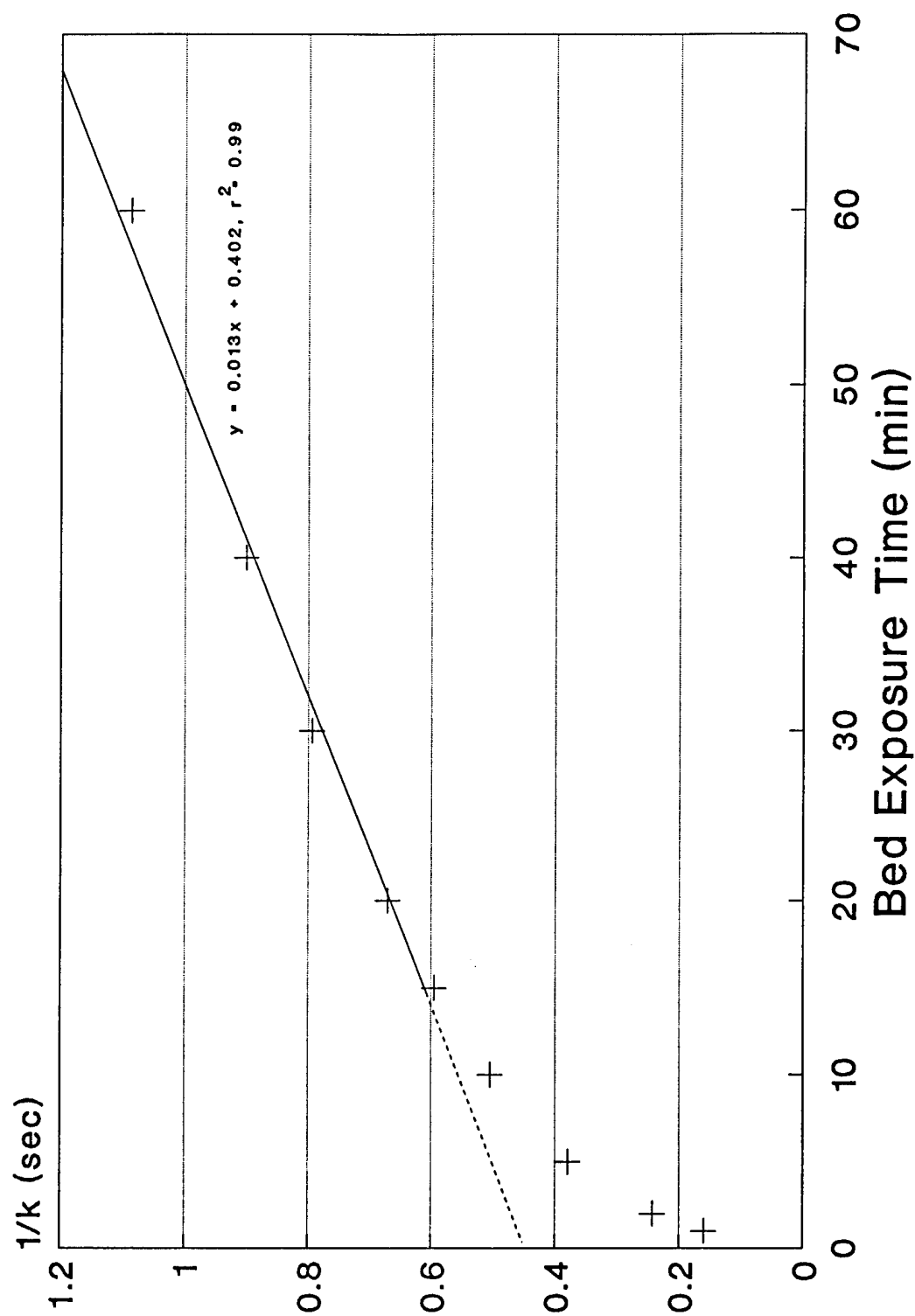


Figure 4-38. Plot of inverse first-order rate coefficient ( $1/k$ ) versus bed exposure time ( $[\text{NO}_2]_{\text{in}} = 47.5$  ppm,  $T = 423$  K,  $[\text{O}_2] = 0\%$ ).

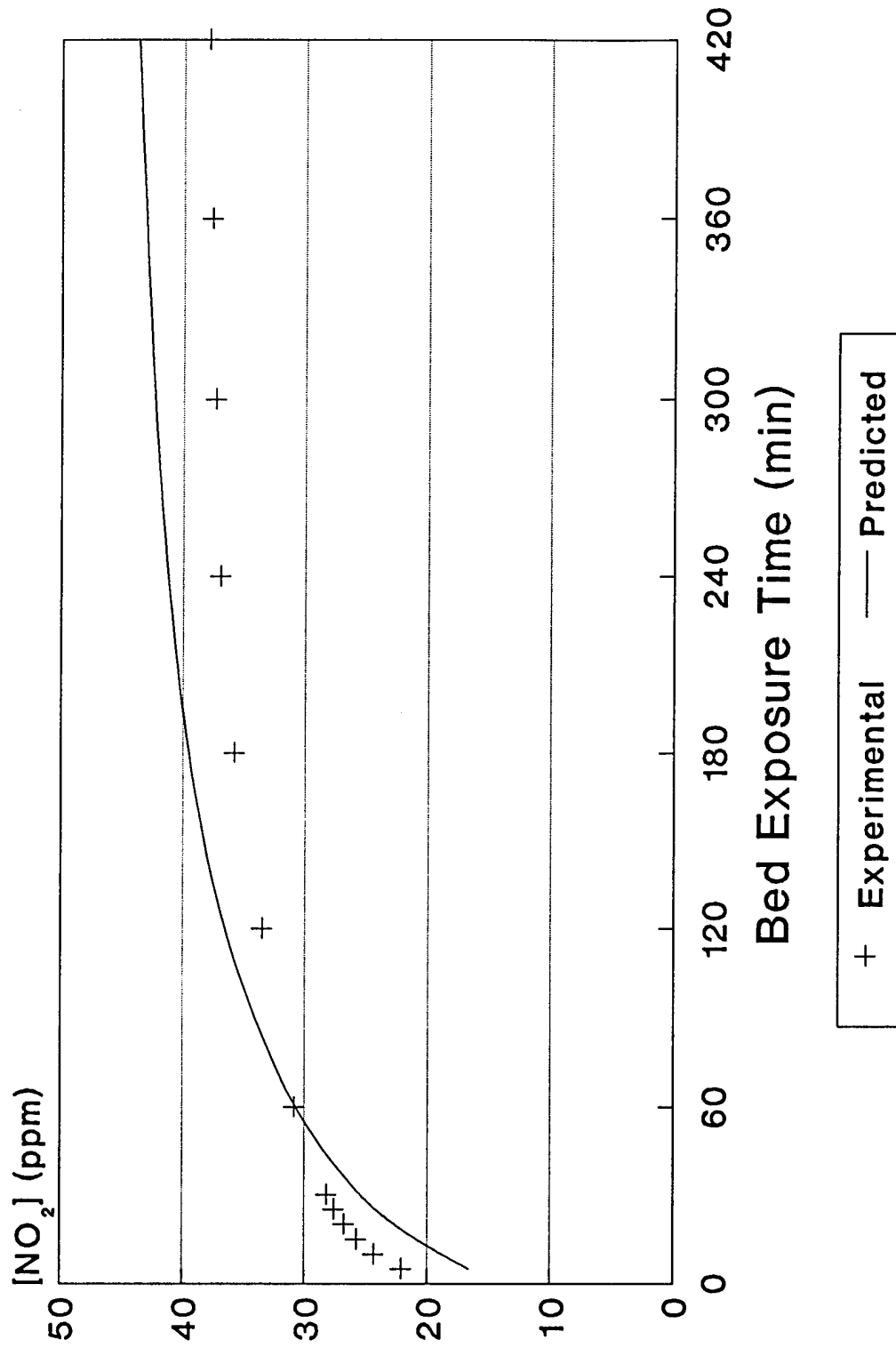


Figure 4-39. Experimental versus predicted  $NO_2$  concentration ( $[NO_2]_{in}=47.5$  ppm,  $T=423$  K,  $[O_2]=0\%$ , Gas samples collected from middle of bed).

to predict  $\text{NO}_2$  concentration at any given time. Predicted  $\text{NO}_2$  outlet concentration values are compared to experimental values for a long-term run, as shown in Figure 4-39.

To test the validity of  $\tau$  values predicted by the shrinking unreacted-core equations, the  $\text{NO}_2$  penetration (or fractional outlet concentration) versus time curves are useful. Based upon the shrinking unreacted-core model, "complete" conversion would be predicted to occur at approximately 180 minutes (one-half of approximately 360 minutes). Looking at Figure 4-39, effective  $\text{NO}_2$  removal has stabilized at a value of approximately 22% at this exposure time. Allowing the reaction to progress for four more hours,  $\text{NO}_2$  removal had only changed to 20%. The shrinking unreacted-core model can be used to reasonably predict "effective" complete conversion of the solid, and the time at which this will occur. This can be combined with the empirical model to predict what the  $\text{NO}_2$  removal rate will be when this occurs. The sorbent appears to continue to remove  $\text{NO}_2$  at a rate that is probably a function of the effective diffusivity through the product layer for subsequent removal by the abundant quantity of  $\text{MgO}$  available inside the particle.

#### 20 ppm $\text{NO}_2$ at a Reaction Temperature of 373 K

The controlling mechanism for this low-concentration, low-temperature extreme was difficult to discern. From Figure 4-40, there appears to be little difference between the chemical-reaction-control equation and the product layer diffusion equation. Progress of the reaction is visually more non-linear for both equations during the first 20 minutes than for the remainder of the curve. Fitting the equations to the longer-exposure-time data between 20 and 60 minutes produced a better fit. The results are shown in Figures 4-41 and 4-42. From

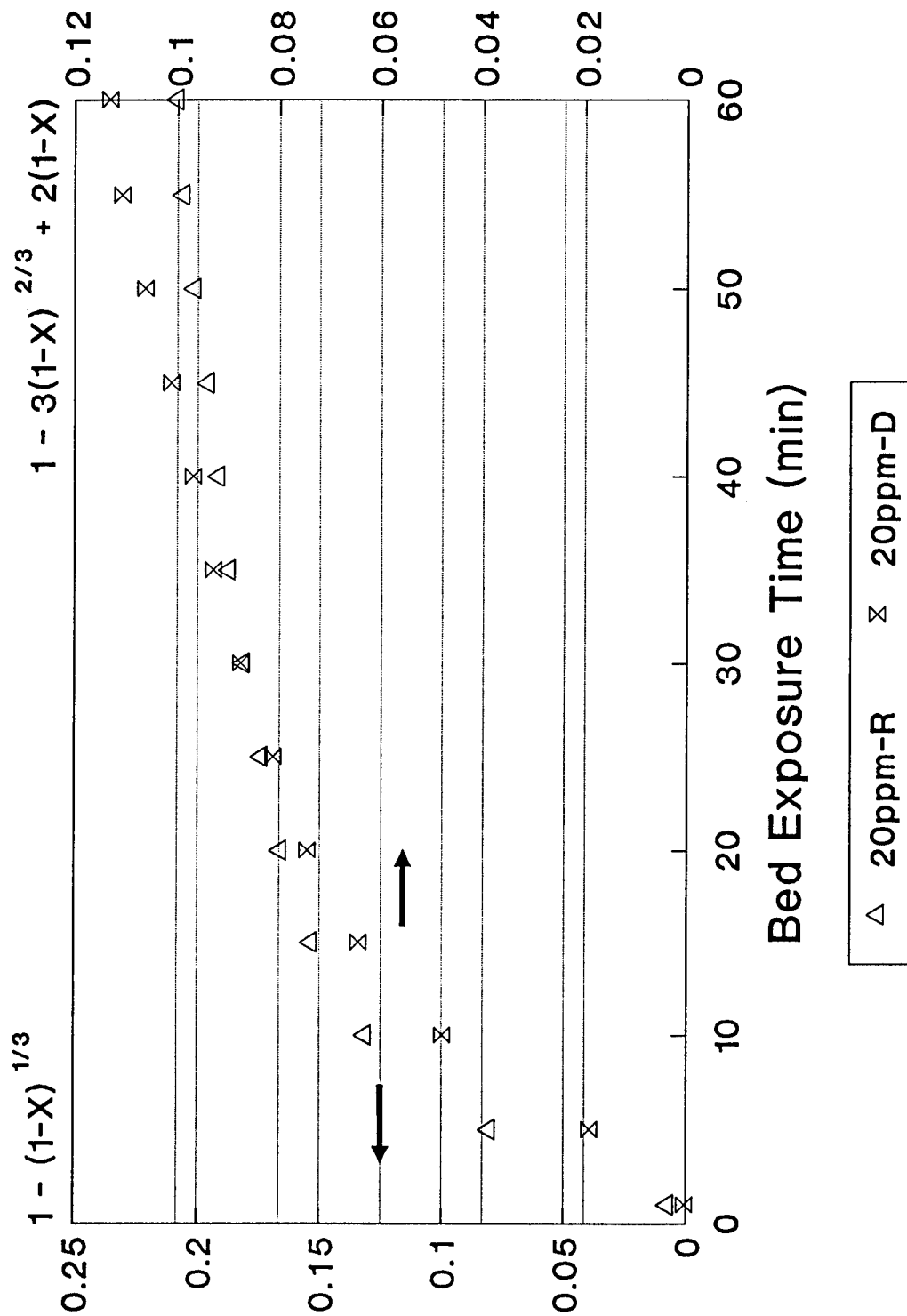


Figure 4-40. Shrinking unreacted-core model evaluation ( $[\text{NO}_2]_{\text{in}}=20$  ppm,  $T=373$  K,  $[\text{O}_2]=0\%$ ).

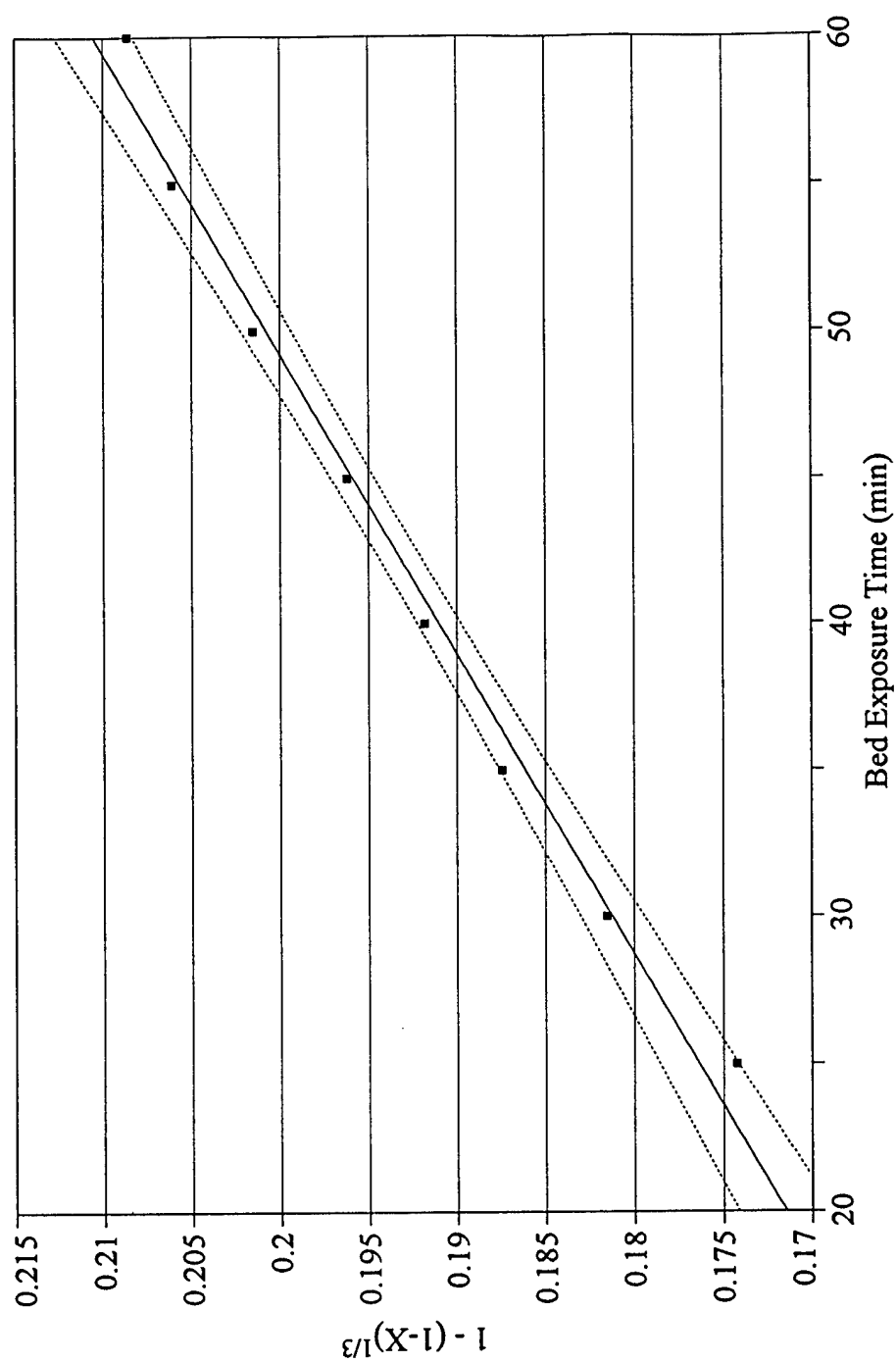


Figure 4-41. Shrinking unreacted-core chemical-reaction-control-equation evaluation,  $\tau_r=1023$  minutes ( $[\text{NO}_2]_{\text{in}}=20$  ppm,  $T=373$  K,  $[\text{O}_2]=0\%$ ). [ $y = 0.001x + 0.152$ ,  $r^2=0.99$ , Fit Std Error = 0.001,  $F=521.0$ ].

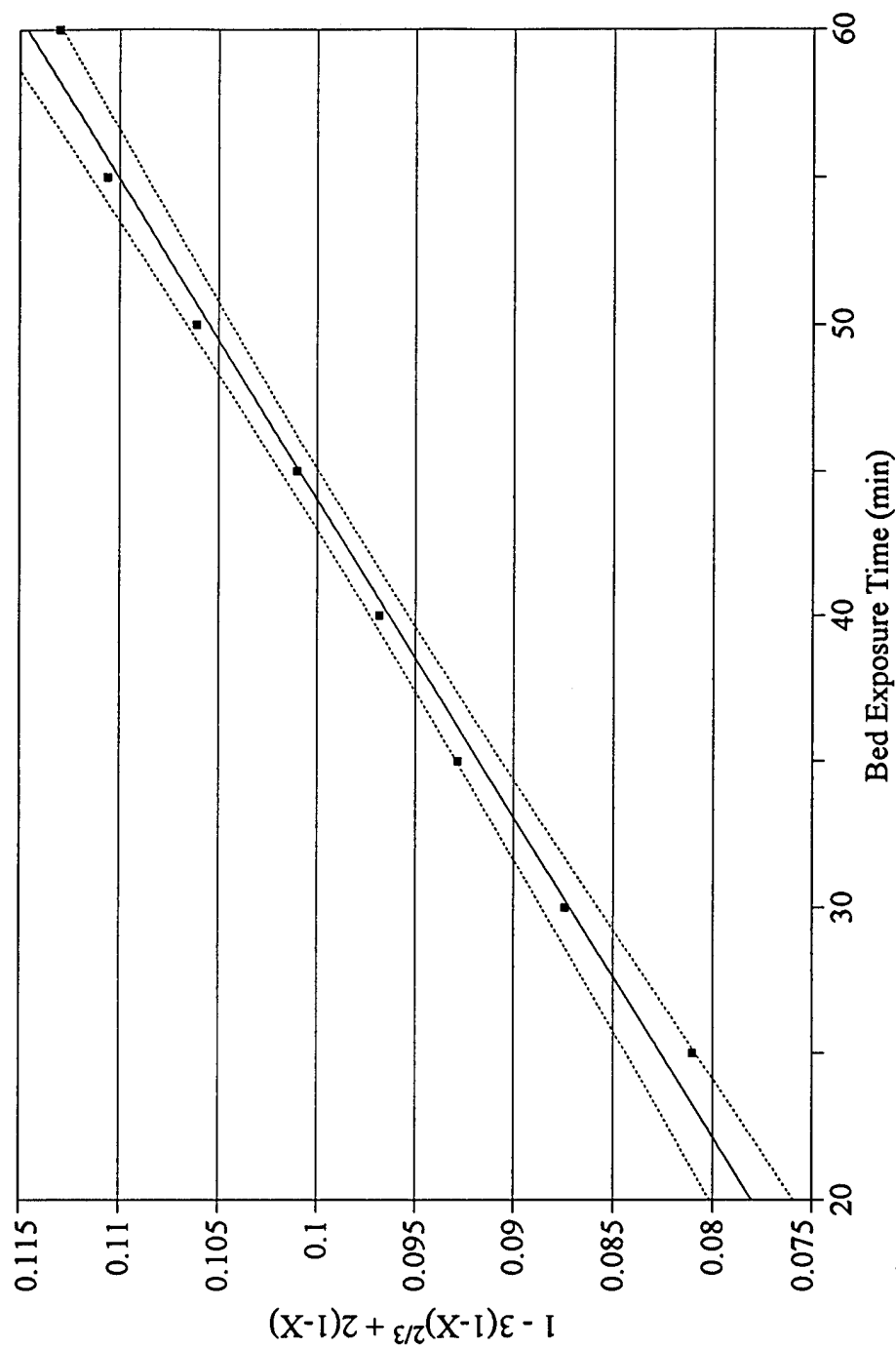


Figure 4-42. Shrinking unreacted-core product-layer-diffusion-control-equation evaluation,  $\tau_d=1093$  minutes ( $[\text{NO}_2]_{\text{in}}=20$  ppm,  $T=373$  K,  $[\text{O}_2]=0\%$ ). [ $y = 0.001x + 0.06$ ,  $r^2=0.99$ , Fit Std Error = 0.001,  $F=724.0$ ].

these curves,  $\tau_r$  is calculated to be 1023 minutes, and  $\tau_d$  is equal to 1093 minutes. Using the combination-of-resistances equation for the data between 20 and 60 minutes, a  $\tau_r$  value of 952 minutes was calculated. Using the differential molar volume equation, a  $\tau_d$  value of 515 minutes was calculated. At the mid-point of the bed, again, relative  $\tau$  values at this point would be approximately half of these values.

Results from a long-term run are presented at Figure 4-43. It appears from this figure that full "effective" utilization and achievement of dynamic equilibrium occurred closer to 500 minutes than to 250 minutes, indicating that the combination of resistances equation may be best-suited for describing sorption behavior in this situation. Chemical kinetics may be partially controlling due to the low  $\text{NO}_2$  concentration and associated limited reactant availability, and diffusion may be controlling due to the lack of concentration driving force to promote reaction. The ratio of  $\text{NO}_2$  removed to NO produced was approximately 3:1 after 7 hours exposure time. The total mass of  $\text{NO}_2$  removed at this time was approximately 10 mg, resulting in a very low utilization rate.

#### 200 ppm $\text{NO}_2$ at a Reaction Temperature of 473 K

The other extreme condition evaluated was the highest  $\text{NO}_2$  concentration at the highest reaction temperature. The shrinking unreacted-core model was used to fit these data as well. Figure 4-44 is a comparison of the two primary equations over the course of one hour. While the product-layer-diffusion-control equation is fairly linear over this entire period, the chemical-reaction-control equation shows a rapid increase in equation value, corresponding to a rapid increase in  $\text{NO}_2$  penetration early in the reaction. As expected, the

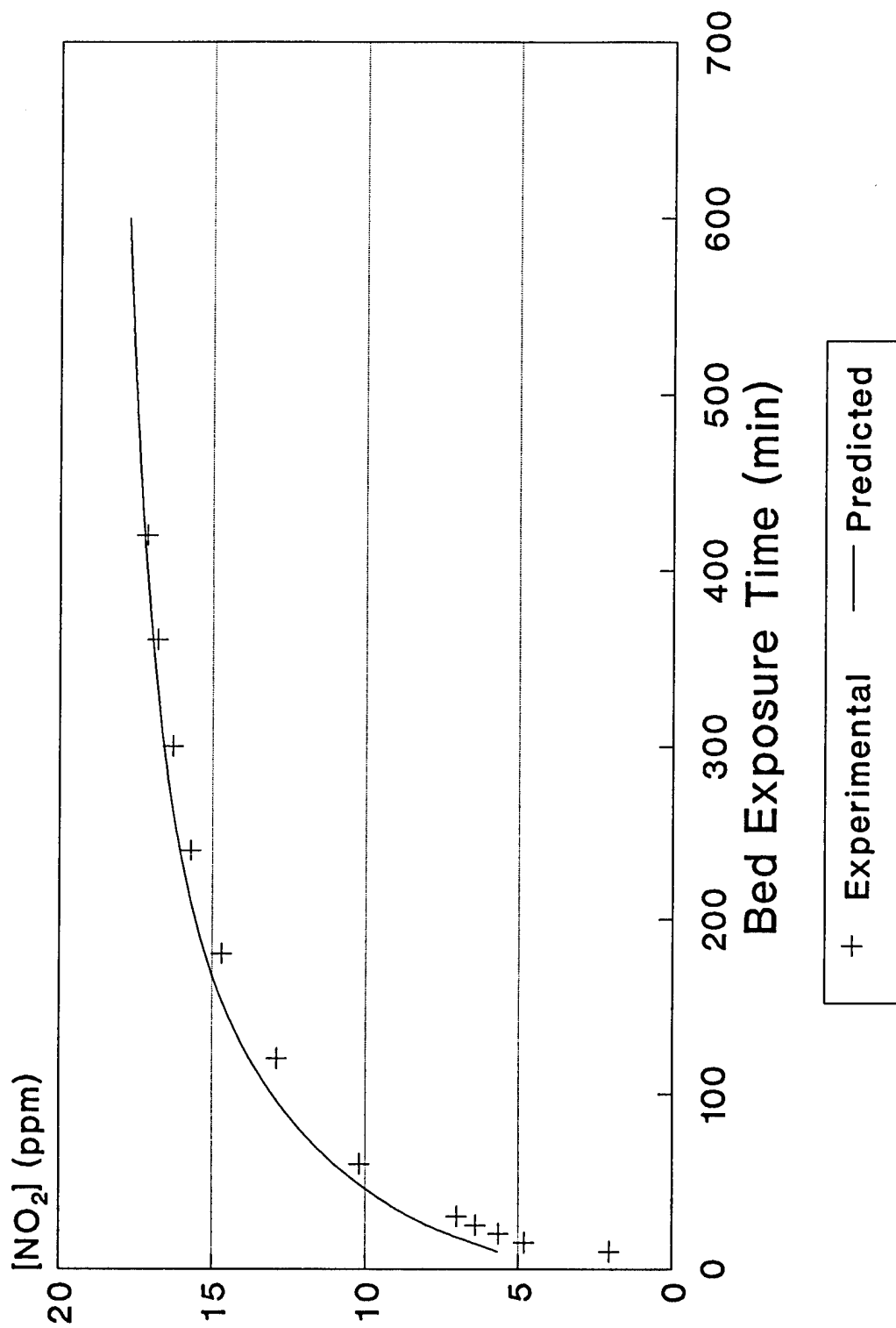


Figure 4-43. Experimental versus predicted  $\text{NO}_2$  concentration ( $[\text{NO}_2]_{\text{in}} = 19.1$  ppm,  $T = 373$  K,  $[\text{O}_2] = 0\%$ , Gas samples collected from middle of bed).



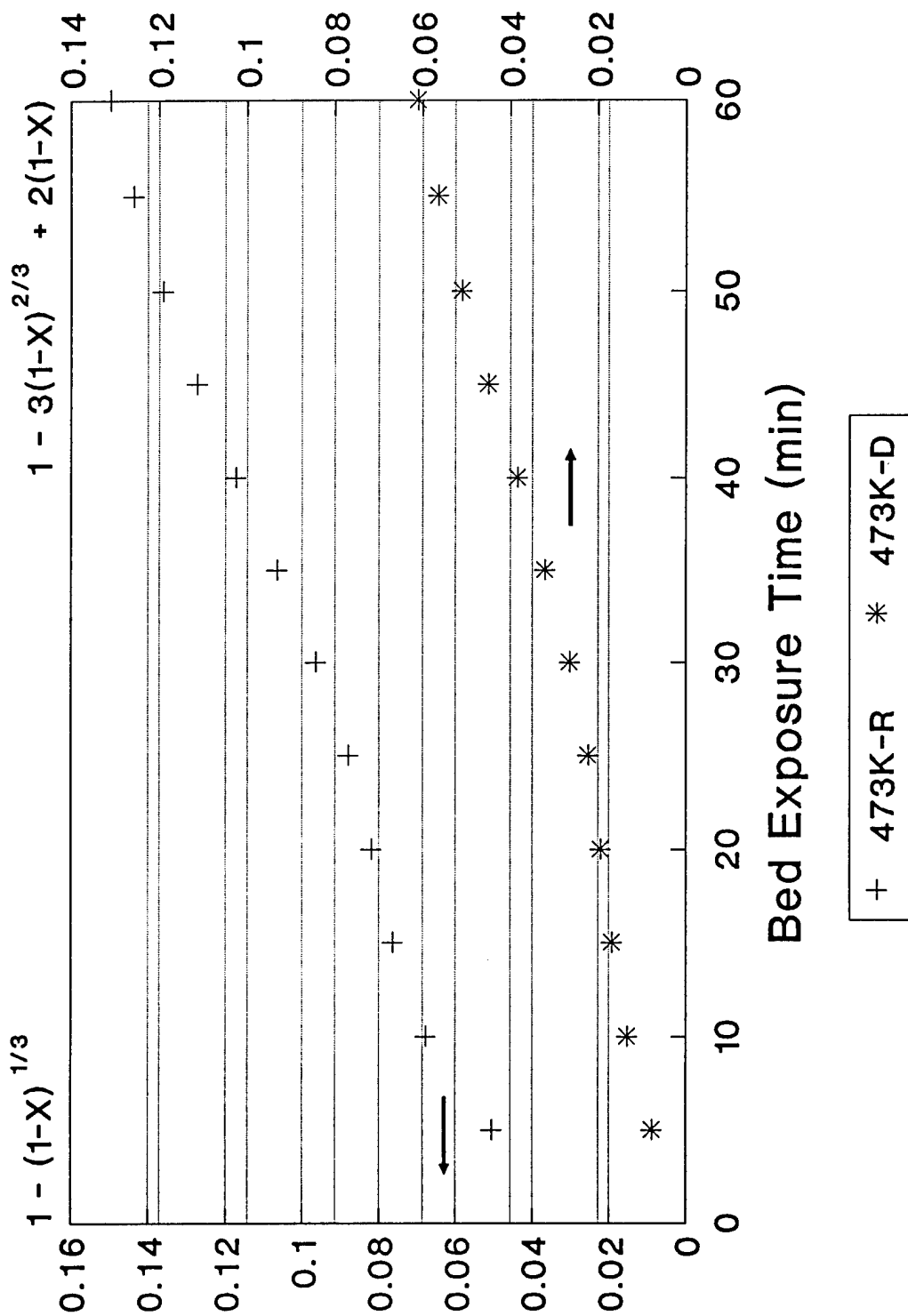


Figure 4-44. Shrinking unreacted-core model evaluation ( $[\text{NO}_2]_{\text{in}}=200$  ppm,  $T=473$  K,  $[\text{O}_2]=0\%$ ).

product-layer-diffusion-control equation seems more appropriate for describing the entire course of reaction over the first hour. Figures 4-45 and 4-46 depict linear least-squares fits to the chemical-reaction-control equation and product-layer-diffusion-control equation, respectively. From these figures, it is evident that statistically, the product-layer-diffusion-control-equation best represents the data, based upon the statistical parameters evaluated. There is some deviation outside the confidence intervals in the middle of the run, most probably the result of a transition from one mechanism to another. Both the combination of controlling-mechanism and increased-molar-volume equations predicted  $\tau$  values between approximately 400 to 500 minutes. To evaluate the predictability of sorption behavior at this (relatively) high concentration and temperature scenario, the empirical relationship between  $1/k$  and bed exposure time was used to produce the plot shown in Figure 4-47. Since this relationship is most predictable after an exposure time greater than approximately 30 to 40 minutes, it is likely that the rate coefficients predicted are for the slow-rate-diffusion process. For this reason, the model does not predict early sorption behavior well, leaving a gap between the experimental and predicted curves.

Figure 4-48 is a plot of cumulative  $\text{NO}_2$  mass removed versus bed exposure time, which clearly shows the decreased mass removal rate as reaction progressed and diffusional resistance increased. While a larger mass of  $\text{NO}_2$  was collected in this case,  $\text{MgO}$  utilization was still less than one percent. An interesting finding related to this slowdown in mass removal is depicted in Figure 4-49, which shows  $\text{NO}_2$  and  $\text{NO}$  concentrations as a function of time as measured at the middle of the bed. It can be seen that as the  $\text{NO}_2$  concentration increased toward the equilibrium product layer diffusion control situation at approximately

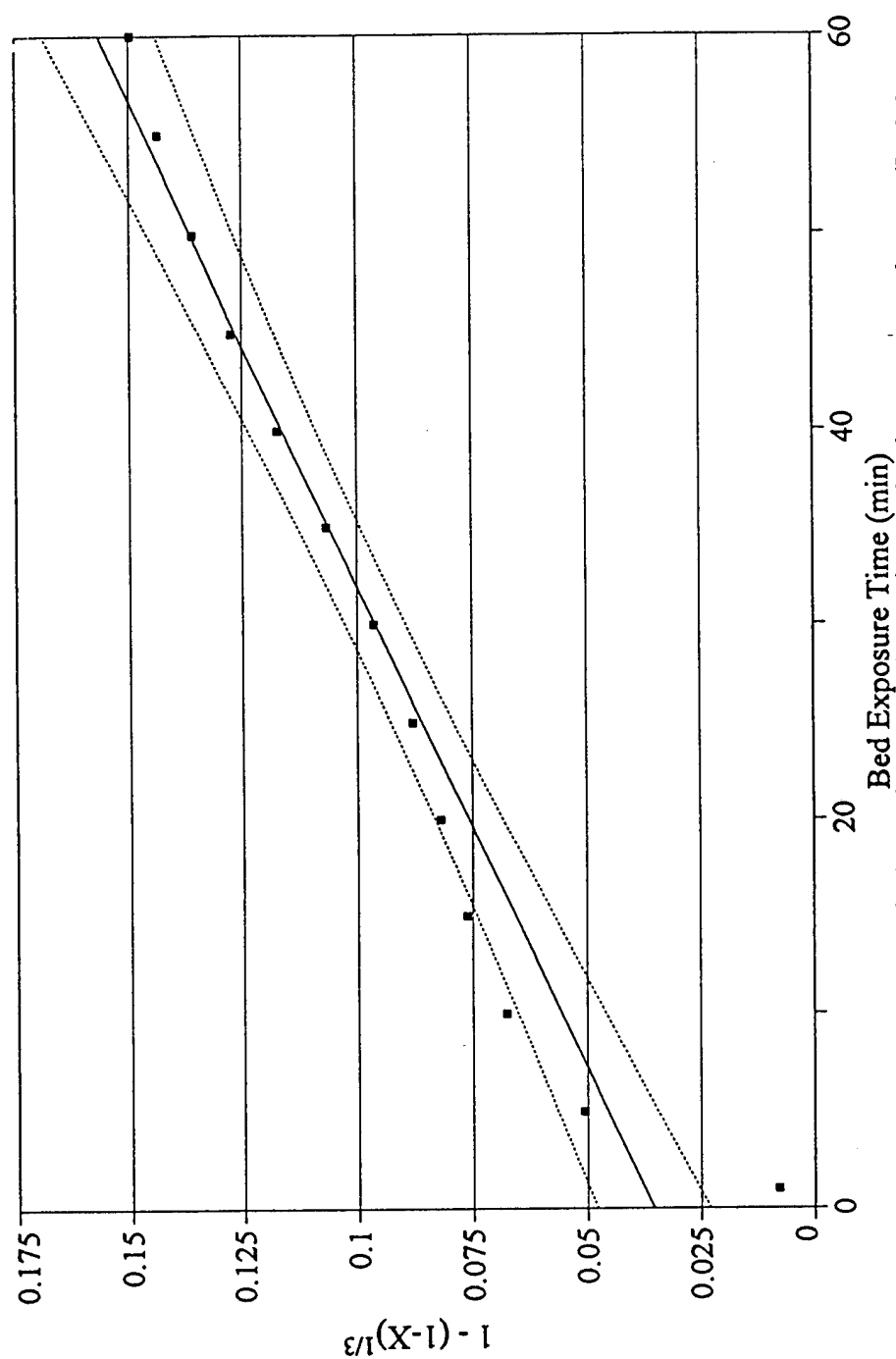


Figure 4-45. Shrinking unreacted-core chemical-reaction-control-equation evaluation,  $\tau_r=495$  minutes ( $[\text{NO}_2]_{\text{in}}=200$  ppm,  $T=473$  K,  $[\text{O}_2]=0\%$ ). [ $y = 0.002x + 0.035$ ,  $r^2=0.94$ , Fit Std Error = 0.011,  $F=159.7$ ].

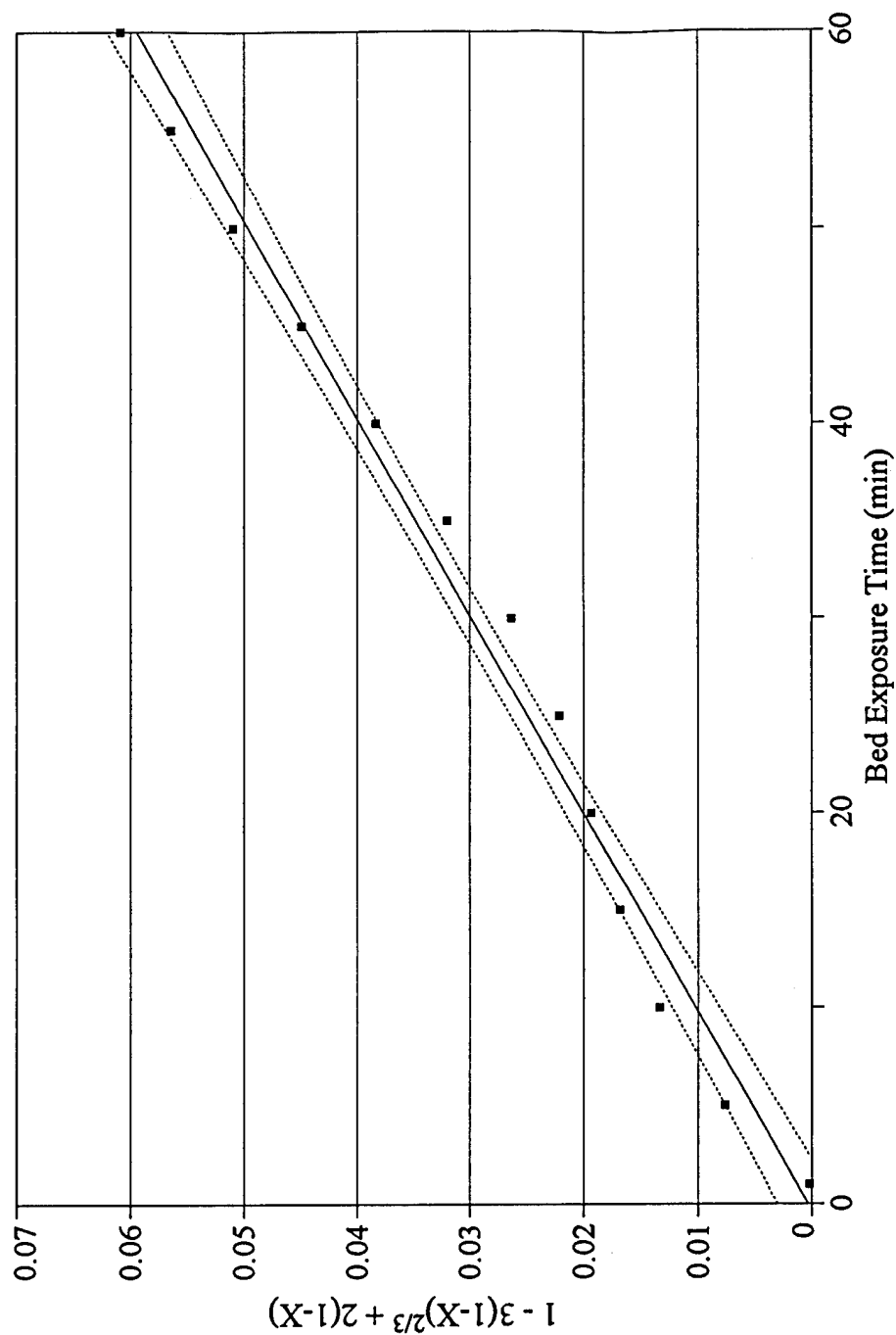


Figure 4-46. Shrinking unreacted-core product-layer-diffusion-control equation evaluation,  $\tau_d=1015$  minutes ( $[\text{NO}_2]_{in}=200$  ppm,  $T=473$  K,  $[\text{O}_2]=0\%$ ). [ $y = 0.001x + 0.0003$ ,  $r^2=0.99$ , Fit Std Error = 0.002,  $F=822.3$ ].

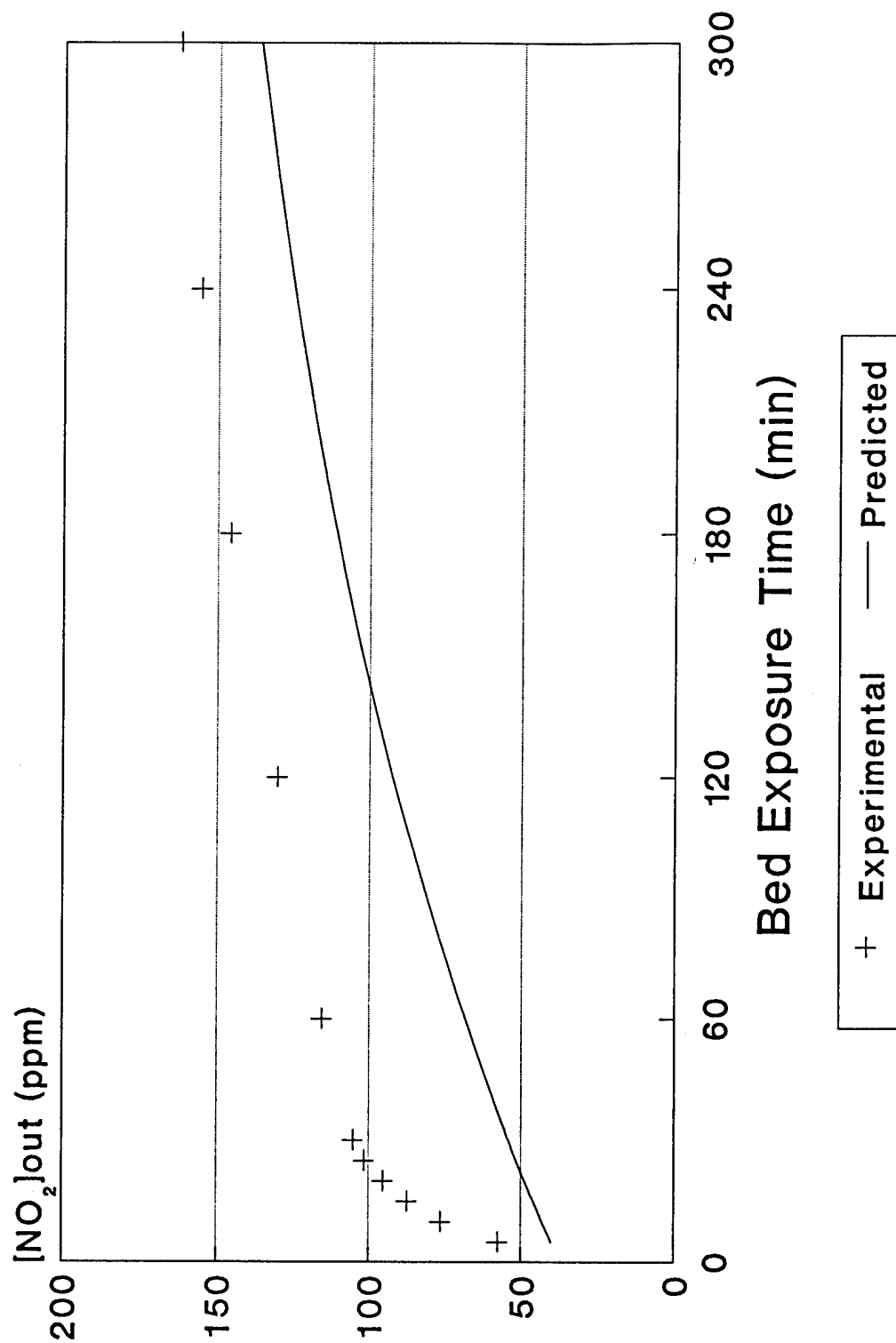


Figure 4-47. Experimental versus predicted  $\text{NO}_2$  concentration ( $[\text{NO}_2]_{\text{in}} = 170.0$  ppm,  $T = 473$  K,  $[\text{O}_2] = 0\%$ , Gas samples collected from middle of bed).

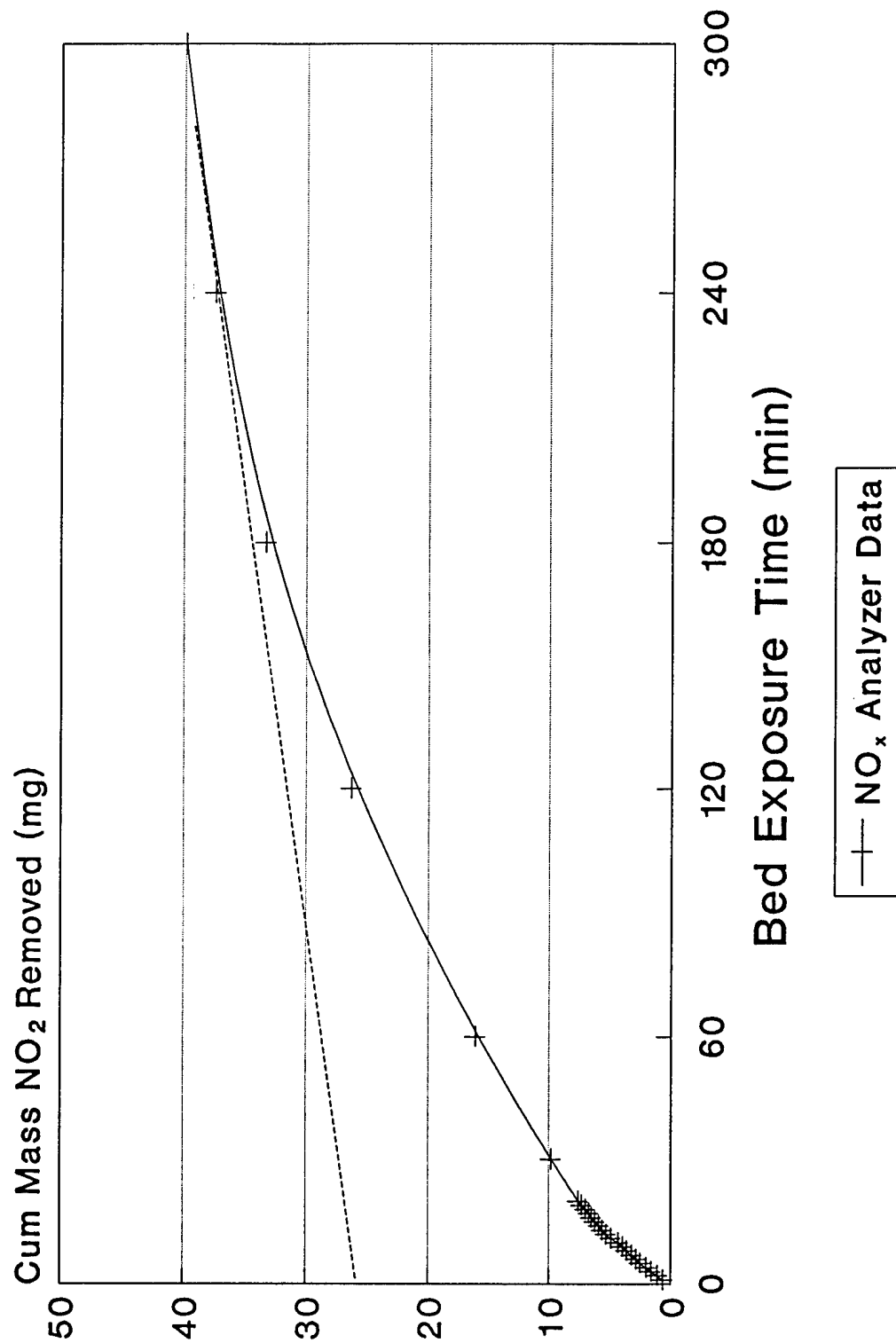


Figure 4-48 Cumulative mass NO<sub>2</sub> removed versus bed exposure time for a long-term run ( $[\text{NO}_2]_{\text{in}} = 170 \text{ ppm}$ ,  $T = 473 \text{ K}$ ,  $[\text{O}_2] = 0\%$ , Gas samples collected from center of bed).

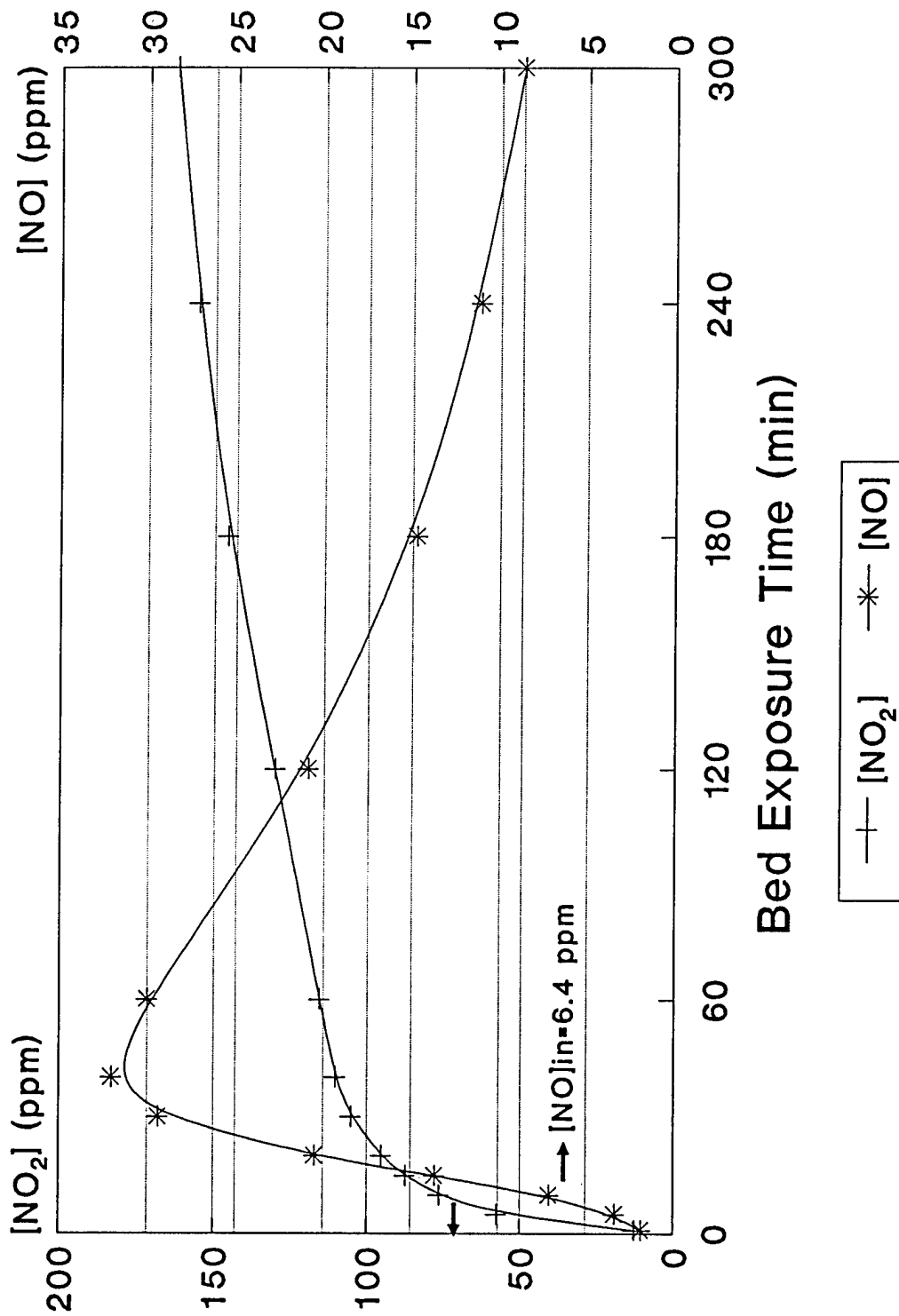


Figure 4-49. Comparative bed NO<sub>2</sub> and NO concentrations versus bed exposure time during long-term run showing NO production ( $[NO_2]_{in} = 170$  ppm,  $T = 473$  K,  $[O_2] = 0\%$ , Gas samples collected from middle of bed).

40 minutes, NO production was increasing toward a maximum. As NO<sub>2</sub> removal rate decreased due to the diffusional resistance, the rate of product formation (including NO) also decreased. After 300 minutes, NO<sub>2</sub> removal was approximately 5% and the NO concentration had almost reached its initial value. It is expected that when NO<sub>2</sub> was no longer removed, NO would no longer be produced and would indeed reach its initial bed inlet concentration.

#### General Applicability of the Shrinking Unreacted-Core Model

It appears from the cases just presented that the shrinking unreacted-core model provides a basis for chemically and physically describing the sorption behavior occurring during the removal of NO<sub>2</sub> by the MgO-vermiculite sorbent. Combined with the classical chemical kinetics evaluations performed, these results allow for the prediction of sorption behavior with time under a variety of conditions. The use of the local-equilibrium theory to describe the transition from packed-bed theories to the shrinking unreacted-core model was a key step in the process. While the local-equilibrium theory allowed for the determination of solid conversion as it relates to NO<sub>2</sub> penetration, it is apparent that this conversion is relative rather than absolute, based upon the low sorbent utilization rates found. These low utilization rates are certainly a complex function of many factors, however, such as the low NO<sub>2</sub> concentrations evaluated, as well as probable low porosities, which may produce intraparticle diffusional resistances, are key parameters. The high solid-product-to-reactant molar volume ratio is another mitigating factor in this situation. Dam-Johansen and



Ostergaard (1991b) attributed the rapid decrease in reaction rate during the sulfation of limestone particles to filling of micropores. The macroporous structure remaining may allow some sulfation to continue at a very slow rate. The degree of conversion decreases linearly from the particle surface inward to a certain distance from the surface where it goes to zero, forming a sharp front which moves inward with increasing exposure time. Larger samples with varying (CaO) thickness may lead to significant intraparticle diffusional limitations, which may intensify as the solid product forms particle agglomerations (Zarkanitis et al., 1990). While dynamic equilibrium conditions are achieved at a time equal to  $\tau$ , and effective conversion approaches a fairly constant value,  $\text{NO}_2$  is still being removed from the gas stream at a rate dependent upon its effective diffusivity through the product layer and/or porous structure of the sorbent. There remains a significant residual  $\text{NO}_2$  removal capacity, which continues at significant levels for extended periods of time.

The molar volume ratios of  $\text{Mg}(\text{NO}_3)_2$  products to  $\text{Mg}(\text{OH})_2$  reactants are approximately 50% smaller than the ratio to  $\text{MgO}$  reactants, which may partially account for the improved performance of hydrated sorbents. This results in more available surface area through unblocked pore-surface area on a normalized time basis. The shrinking unreacted-core model was used to interpret results under these conditions and, in general,  $\tau$  values were approximately twice as large. This means that hydrated sorbents can remove approximately twice as much mass from a gas stream with a given mass flow rate. Due to the inherent complications involved in the study of gas-solid reactions, chemical kinetics or the shrinking unreacted-core model alone can not completely describe the molecular processes that are occurring. A structural investigation of reactants and products may be helpful for this

purpose. The crystalline structure of MgO is the same as that of NaCl, while  $\text{Mg}(\text{OH})_2$  crystallizes with the  $\text{CdI}_2$  layer structure, in which every Mg atom is surrounded by six OH. Every OH forms three bonds to Mg atoms in its own layer, while contacting three OH of an adjacent layer (Wells, 1952). A larger bulk reactant would be comprised of relatively thin, irregularly shaped layers and may show more or less diffusional resistance as the lattice expands with reaction, forming a complex structure. Bamford et al. (1984) noted that lattice structure changes often associated with gas–solid reactions sometimes effectively eliminate oxygen vacancies, which have been reported to be relevant to the chemical reactivity of MgO.

It must be emphasized that while these models seem to have some utility in providing a chemico-physical basis for describing  $\text{NO}_2$  removal by the MgO–vermiculite sorbent under the range of experimental conditions studied, this applicability is limited by the experimental constraints placed upon these variables. Referring to the sulfation of CaO, Wen and Ishida (1973) stated that various kinetic studies indicate that reaction rates can vary significantly depending upon the type of limestones used, sometimes more than an order of magnitude. It is likely that MgO powder dispersed within a packed bed, or individual pure MgO pellets would behave quite differently from the combined MgO–vermiculite sorbent particles studied. The low  $\text{NO}_2$  concentrations used in this study probably have obscured the distinction between the controlling mechanisms, often making it difficult to absolutely distinguish one rate-determining mechanism from another.

It is apparent that the processes of pore closure, product-layer diffusion, and product sintering are important factors in this study, whose combination makes data analysis very difficult. To obtain a better understanding of how these mechanisms ultimately affect

conversion-versus-time behavior, more information is required on the solid structure and how it changes during the course of reaction (Marsh and Ulrichson, 1985). Because of the high diffusional resistance of the product layer, the concentration of gaseous reactant at the reaction interface, and consequently the reaction rate, may not be uniform even under the uniform temperatures and concentrations in the porous network. Structural properties depend not only on conversion, but also the relative rates of reaction (intrinsic kinetics) and mass transport in the product layer (Sotirchos and Yu, 1985). Gullett et al. (1992) compared the magnitude of the sum of squared errors as well as the coefficient of determination in defining the best-fitting shrinking-core-model equation in the reaction between HCl and CaO. They found that often either the chemical-reaction-control model or the product-layer-diffusion-control-model is sufficient to describe sorption, without the inclusion of both models simultaneously. The two main governing equations for chemical-reaction-control and product-layer-diffusion-control are themselves not uniquely distinct, particularly when the true solid sorbent conversion level is low. Therefore, care should be taken in using these modeling results to quantitatively derive physical parameters of the sorbent under the conditions evaluated, or in their extrapolation to different conditions under which MgO solids may be used to remove NO<sub>2</sub> from a flowing gas stream.

## CHAPTER 5 PRACTICAL CONSIDERATIONS

### Constraints on MgO–Vermiculite Sorbent Usage

Based upon the experimental results collected in this study, it is apparent that there may be some practical constraints on the effective employment of the MgO–vermiculite sorbent in the control of nitrogen oxides from jet engine test cells. The widely varying conditions produced by jet engine testing require a control medium that is effective over the entire range. While the sorbent effectively removed  $\text{NO}_2$  from a flowing gas stream, the ability of the sorbent to remove NO was minimal. The low concentrations of total  $\text{NO}_x$  emitted from a jet engine test cell make their removal by the sorbent more difficult, especially after a product layer has formed on the exterior surface of the sorbent particles. Depending upon the focus of any regulations related to jet engine test cells promulgated in the future, a 50% reduction in  $\text{NO}_x$  emissions may be sufficient.

This research has shown that the sorbent can continue to remove an average of approximately 50% of the total quantity of  $\text{NO}_2$  for a significant period of time, particularly from lower concentration gas streams ( $< 100$  ppm). To put some of the results into perspective, the mass of sorbent required for the removal of  $\text{NO}_2$  from a larger volume source can be calculated. Using the results from the conditions under which the bed was nearly

saturated (170 ppm  $\text{NO}_2$ , 473 K) the sorption capacity of the sorbent (after 5 hours) was approximately 40 mg  $\text{NO}_2$ /3.5 g sorbent bed. This corresponds to a mass loading ratio of approximately  $1.14 \times 10^{-2}$  g  $\text{NO}_2$  per gram sorbent, at an overall rate of  $2.3 \times 10^{-3}$  g  $\text{NO}_2$  /g sorbent-hour. While initial  $\text{NO}_2$  removal was greater than 90%, the average removal over the five-hour period was approximately 40%. Taking as an example a 10,000-acfm source of 200 ppm  $\text{NO}_2$  at 473 K, the volume of bed required to treat this source, with all other conditions remaining the same, and taking the bed to saturation after one hour, is approximately 3 m<sup>3</sup>, not an inordinately large size. Obviously, it is not practical to regenerate or replace the bed every hour, and the volume of gas to be treated may be larger, so a larger bed would be used. As was already pointed out, jet engine test cells are not steady state sources and the average test run may be much shorter than an hour in duration. After jet engine exhaust is augmented, the concentration of  $\text{NO}_2$  would also likely be less than 200 ppm, so the bed would last longer because it takes longer to form the product layer when reacting with lower concentrations of gases. Lower  $\text{NO}_2$  concentrations will produce lower removal rates, but the bed will last longer. When lower-concentration gases are expected, elevated temperatures can help to improve diffusivity through the product layer in the absence of a large concentration gradient driving force.

The effective conversion of NO to  $\text{NO}_2$  is a crucial element in the eventual successful employment of this  $\text{NO}_x$  control medium. Spicer et al. (1990) noted that exhaust augmentation can increase the  $\text{NO}_2$ -to-NO ratio from 1 or 2:10 to 7 or 8:10. While they attributed some of this oxidation to the presence of peroxy radicals in fuel-rich combustion, oxygen oxidation can be significant as well. Obviously there are a number of other variables,

including the presence of other exhaust gas components, that need investigation before one can truly predict what may happen on the sorbent surface.

As was noted by Wander and Nelson (1993), bed pressure drop is a potentially significant limiting factor in the use of the MgO-vermiculite sorbent in a packed-bed scenario. Nelson et al. (1993) evaluated the potential for NO<sub>x</sub> removal in a variety of flow-through bed arrangements in which the gases would make indirect contact with the sorbent at the wall of the container rather than physically passing through it. This did not work well, so it appears that direct contact is necessary for the removal of NO<sub>2</sub> from the gas stream. The Ergun equation describes the pressure-drop-versus-superficial-velocity relationship, so it can be used in the design of a packed bed in keeping pressure drop below established limits. An empty-bed residence time of approximately one second is recommended for efficient NO<sub>2</sub> removal, as well as in the minimization of pressure drop through the bed, although reduced times still allow for some removal of NO<sub>2</sub>. The physical dimensions of a unit designed for the control of nitrogen oxides from a jet engine test cell must be based upon these constraints in order to effectively remove the nitrogen oxides while minimizing the negative impacts on the jet engine testing operations that are producing the exhaust to be treated.

## CHAPTER 6 CONCLUSIONS AND RECOMMENDATIONS

### Conclusions

The gas–solid reactions between  $\text{NO}_2$  and NO and MgO–vermiculite sorbent were studied using a bench-scale packed-bed reactor and simulated operating conditions representative of jet engine test cells. The effects of primary variables including gas-phase concentrations, reaction temperature, moisture, and gas velocity were evaluated. The design of the packed-bed reactor allowed for the collection of gas samples from various points within the bed, which is an improvement over the common use of inlet and outlet measurements in the determination of intrinsic chemical kinetic parameters in packed-bed studies. First-order rate coefficients were determined for use in the determination of activation energies associated with this reaction using the Arrhenius relationship. Sorption behavior over time was interpreted using the shrinking unreacted-core model, as well as an empirical model, which described the chemical and physical processes occurring during the course of the reaction. It should be emphasized that the conclusions reached from this research study are specific to the sorbent studied and the operating conditions used. Based upon the results of the experiments conducted and the interpretation of data collected during the course of this study, the following conclusions can be drawn:

1. NO is not readily removed by MgO-vermiculite. Any removal probably occurs through limited physisorption and/or conversion into nitrogen dioxide by oxygen present in the augmented exhaust gas. The oxidation of NO to NO<sub>2</sub> is crucial to the successful employment of this medium.

2. Nitrogen dioxide removal efficiencies greatly exceed nitric oxide removal efficiencies, with maximum values greater than 90 percent. NO<sub>2</sub> continues to be removed by the sorbent at a greatly reduced rate for extended periods of time.

3. High concentrations of NO<sub>2</sub> were readily removed from the gas stream, rapidly converting MgO into Mg(NO<sub>3</sub>)<sub>2</sub>. The formation of a solid product layer slowed the reaction down as it progressed from control by chemical-reaction kinetics to diffusion control, a much slower process. The higher concentration gradients provided the larger driving forces for the continued removal of NO<sub>2</sub> through diffusion.

4. The reaction between NO<sub>2</sub> and MgO-vermiculite is first-order with respect to NO<sub>2</sub>. The temperature dependence of the first-order rate coefficients is evidence that data were collected in the region of chemical reaction control. Activation energies associated with this reaction were in the range from approximately 20 to 36 kJ/g-mol in the absence of oxygen and 15 to 25 kJ/g-mol when oxygen was present in the system. These values are indicative of a low-energy chemisorption process.

5. Wetted sorbent or humidified gases promote NO<sub>2</sub> removal, possibly by the conversion of MgO into Mg(OH)<sub>2</sub>, which appears to be more reactive and is thermally stable over the range of temperatures studied. Since the molar volume ratio of magnesium nitrate to magnesium hydroxide is lower than when compared to MgO, there is less potential for



active surface area coverage by the product, which improved sorption performance with time.

6. The presence of oxygen in the exhaust gas aided in the removal of NO by the oxidation of NO to NO<sub>2</sub>. It appeared that oxygen may have promoted the continued removal of NO<sub>2</sub> by the sorbent.

7. Temperature affected the reaction by increasing reaction rates both initially (chemical-reaction control) and by improving effective diffusivity. Reaction temperature must be kept below 523 K, since this is the temperature at which Mg(NO<sub>3</sub>)<sub>2</sub> begins to decompose.

8. The pressure drop versus superficial velocity relationship can be described using the Ergun equation. This equation should be used to design any system in which this sorbent will be employed since pressure drop is a limiting factor in a jet engine test cell application.

9. It is possible to regenerate the sorbent by heating for reuse. The initial NO<sub>2</sub> removal efficiency of regenerated sorbent is similar to fresh sorbent, but the extended performance decreases with time, probably the result of structural changes (i.e., reduced porosity/surface area, sintering, etc.).

10. A reaction mechanism has been proposed to explain the production of NO during the removal of NO<sub>2</sub>. NO may be produced during the final oxidation step of mixed nitrite–nitrate product to its final nitrate form. After the NO<sub>2</sub> removal rate decreases, NO production decreases accordingly.

11 The shrinking unreacted-core model was applied to NO<sub>2</sub> penetration data using the local-equilibrium theory to estimate solid-sorbent conversion. The model described the

sorption behavior over a variety of conditions, in particular showing a transition from chemical reaction control to product layer diffusion control. In some cases it appeared that both processes were simultaneously rate-limiting. It is evident that the range of concentrations and temperatures evaluated represented a transition region, which made it difficult to conclusively determine rate-limiting mechanisms. The possibility of simultaneous and sequential surface reactions makes modeling the  $\text{NO}_2$  removal a challenging problem.

12. An empirical equation was developed that allows for the prediction of  $\text{NO}_2$  removal over extended periods of time.  $\text{MgO}$  utilization rates are far below stoichiometrically predicted values, most probably the result of some combination of lost surface area due to pore blockage or reduced surface area due to coverage of available reactant by a higher-molar-volume product, and an insufficient concentration-gradient driving force for continued reaction.

#### Recommendations for Further Research

Based upon the conclusions presented above and the experiences gained during the conduct of this experimental study, a number of recommendations for further research in the area have become evident:

1. The oxidation of  $\text{NO}$  to  $\text{NO}_2$  is critical to the effective employment of this sorbent medium in the control of total  $\text{NO}_x$ . Options for the accomplishment of this oxidation should be investigated. This oxidation could be accomplished prior to entering the bed or within the bed, although residence times there may be too short. Contact with oxidizing agents like peroxide solutions, for example, may be a starting point. In practicality, oxygen

provided from exhaust-gas augmentation may accomplish some of this oxidation.

2. More MgO-vermiculite surface studies are necessary to better understand the nature of the surface and the role it plays in the removal of  $\text{NO}_2$  from a flowing gas stream. Pore size distributions and associated structural implications may be very useful in further explaining the rate-limiting processes involved in this reaction. The measurement of additional physical parameters is required for the strict mathematical interpretation of shrinking unreacted-core model results. Real-time surface analyses would allow for following the progress of reaction, which could be combined with post-sorption analyses for the quantification of solid conversion and product formation. A modified reactor design that would allow for the removal of all used sorbent after a run (without any loss) would be an improvement in this regard.

3. More traditional sorption studies, where the progress of reaction is followed using thermogravimetric methods and single sorbent pellets, may also assist in the application of the shrinking unreacted-core model to this reaction. This research is actually a step ahead in that regard, since the basic research on the reaction between  $\text{NO}_2$  and MgO powder (without vermiculite substrate) has not yet been conducted or reported. The use of pressed pellets of MgO would also be useful in this regard. Dispersing small quantities of MgO in an inert bed of quartz sand is another method that may allow for the collection of this type of data.

4. The range of experimental conditions studied should be extended to evaluate the application of this sorbent material to other combustion sources. The use of  $\text{NO}_x$  concentrations from one to two orders of magnitude greater than used here for the collection

of intrinsic kinetic data would be extremely useful in this regard. These data would also be useful in determining the true limits of MgO utilization by  $\text{NO}_2$  in the sorbent, and would most likely make the shrinking unreacted-core model results easier to interpret. The high temperature limit appears to be between 523 and 573 K, at which magnesium nitrate decomposition is significant.

5. Obviously, there are other exhaust gas components whose presence may affect the  $\text{NO}_2$  removal characteristics of this sorbent. These other components should be evaluated to determine their respective roles in the  $\text{NO}_2$  removal process. One major component includes the combustion aerosols, which would probably accumulate on the surface of the sorbent, possibly making MgO on the exterior surface of the particle unavailable for reaction. Some of the carbonaceous aerosols may themselves remove  $\text{NO}_2$ . The effect of this added layer on the effective diffusivity of  $\text{NO}_2$  inward toward unreacted MgO inside the particle would also need investigation.

6. More tests at all operating conditions, but at longer reaction times, should be conducted to provide more information on reaction rates and final conversions. Fully automated valve-switching and data-collection systems would be very useful when performing long-term runs. The predictability of  $\text{NO}_2$  penetration as it relates to MgO conversion is useful information in the design of any application that might employ this sorbent medium.

7. The role of water and water vapor needs further study to validate the findings of this research. It is essential to know if the improved  $\text{NO}_2$  removal capabilities found in the

presence of water are truly the result of the  $\text{Mg}(\text{OH})_2$  formed and the change in molar volume ratio, or are a result of an absorption process.

8. Studies similar to those reported here should be conducted using  $\text{SO}_2$  as the adsorbate gas as it is also effectively removed by this sorbent. The basic kinetic and mechanistic data on the reaction between  $\text{SO}_2$  and  $\text{MgO}$  have not yet been reported. The simultaneous exposure of the sorbent to  $\text{SO}_2$  and  $\text{NO}_x$  should also be evaluated since there is a reported synergistic effect on the combined removal when the two species are present together. The presence of  $\text{SO}_2$  may also help in the removal of  $\text{NO}$  by its reduction to nitrogen. Steciak et al. (1995) reported that the reaction:  $\text{MgO} + \text{SO}_2 + \text{NO} \rightarrow \text{MgSO}_4 + \frac{1}{2}\text{N}_2$  is thermodynamically feasible below 1030 C, but no kinetic data have been reported. An important point to be stressed here is that there are many other potential uses for this sorbent that could be investigated.

9. The use of high-purity  $\text{NO}_2$  from a permeation tube apparatus would avoid the problem of  $\text{NO}$  contamination in bed feed gas. This would allow for an improved evaluation of the  $\text{NO}$  formation seen during the course of reaction in this research. If there were no  $\text{NO}$  present in the samples that entered the bed, formation by chemical reaction on the sorbent surface would be easier to follow.

10. The application of this sorbent medium to ambient  $\text{NO}_2$  sampling should be investigated. Since low concentrations of  $\text{NO}_2$  can be effectively removed using this sorbent it may be feasible to attempt to collect low-level concentrations of  $\text{NO}_2$  from urban atmospheres for analysis if conditions were optimized.

## LIST OF REFERENCES

40 CFR 50, Appendix F., "Measurement Principle and Calibration Procedure for the Measurement of Nitrogen Dioxide in the Atmosphere (Gas Phase Chemiluminescence)."

Baiker, A.; Dollenmeier, P.; Glinksi, M.; and Reller, A., "Selective Catalytic Reduction of Nitric Oxide with Ammonia: Part I, Monolayer and Multilayers of Vanadia Supported on Titania," *Applied Catalysis*. 35:351-364, 1987a.

Baiker, A.; Dollenmeier, P.; Glinski, M.; and Reller, A., "Selective Catalytic Reduction of Nitric Oxide with Ammonia: Part II, Monolayers of Vanadia Immobilized on Titania - Silica Mixed Gels," *Applied Catalysis*. 35:365-380, 1987b.

Bamford, C.H.; Tipper, C.F.H.; and Compton, R.G., Comprehensive Chemical Kinetics, Volume 21, Reactions of Solids with Gases, Elsevier Publishers; Amsterdam, pp 131-134, 1984.

Beard, J., "Computer Modelling Makes Jet Engines Less Noxious," *New Scientist*. 30, 1990.

Berman, E.; Dong, J.; and Lichtin, N.N., Photopromoted and Thermal Decomposition of Nitric Oxide by Metal Oxides, ESL-TR-91-32, HQ AFESC, Tyndall AFB, Florida, 1991.

Bhatia, S. K. and Perlmutter, D. D., "A Random Pore Model for Fluid-Solid Reactions: II. Diffusion and Transport Effects," *AIChE Journal*. 27(2):247-254, 1981a.

Bhatia, S. K. and Perlmutter, D. D., "The Effect of Pore Structure on Fluid-Solid Reactions: Application to the SO<sub>2</sub>-Lime Reaction," *AIChE Journal*. 27(2):226-234, 1981b.

Bhatia, S. K. and Perlmutter, D. D., "Effect of the Product Layer on the Kinetics of the CO<sub>2</sub>-Lime Reaction," *AIChE Journal*. 29(1):79-86, 1983.

Biyani, P. and Goochee, C. F. "Nonlinear Fixed-Bed Sorption When Mass Transfer and Sorption Are Controlling," *AIChE Journal*. 34(10):1747-1751, 1988.

Bjerle, I.; Xu, F.; and Ye, Z., "Useful Experimental Technique for the Study of Heterogeneous Reactions," *Chemical Engineering Technology*. 15:151-161, 1992.

Borgwardt, R. H., "Kinetics of the Reaction of  $\text{SO}_2$  with Calcined Limestone," *Environmental Science and Technology*. 4(1):59-63, 1970.

Borwardt, R. H., "Calcium Oxide Sintering in Atmospheres Containing Water and Carbon Dioxide," *Industrial Engineering Chemistry Research*. 28(4):493-500, 1989.

Borgwardt, R. H. and Bruce K R, "Effect of Specific Surface Area on the Reactivity of  $\text{CaO}$  with  $\text{SO}_2$ ," *AIChE Journal*. 32(2):239-246, 1986.

Borgwardt, R. H.; Roache, N. F.; and Bruce, K. R., "Surface Area of Calcium Oxide and Kinetics of Calcium Sulfide Formation," *Environmental Progress*. 3(2):129-135, 1984.

Campbell, N.T.; Beres, G.A.; Blasko, T.J.; and Groth, R.H., "Effect of Water and Carbon Dioxide in Chemiluminescent Measurement of Oxides of Nitrogen," *Journal of the Air Pollution Control Association*. 32(5):533-535, 1982.

Chen, J. P.; Buzanowski, M. A.; Yang, R. T.; and Cichanowicz, J. E., "Deactivation of the Vanadia Catalyst in the Selective Catalytic Reduction Process," *Journal of the Air and Waste Management Association*. 40(10):1403-1409, 1990.

Chu, P. and Rochelle, G. T., "Removal of  $\text{SO}_2$  and  $\text{NO}_x$  from Stack Gas by Reaction with Calcium Hydroxide Solids," *Journal of the Air Pollution Control Association*. 39(2):175-179, 1989.

Clark, A., The Theory of Adsorption and Catalysis, Academic Press, New York, 1970, pp. 239-271.

Comes, P.; Gonzalez-Flesca, N.; Menard, T.; and Grimalt, J.O., "Langmuir-Derived Equations for the Prediction of Solid Adsorbent Breakthrough Volumes of Volatile Organic Compounds in Atmospheric Emissions Effluents," *Analytical Chemistry*. 65(8):1048-1053, 1993.

Cooper, C.D. and Alley, F.C. Air Pollution Control: A Design Approach, 2nd ed., Waveland Press, Inc.; Prospect Heights, Illinois, pp 485-513, 1994.

CRC Handbook of Chemistry and Physics, 73rd ed., CRC Press; Boca Raton, Florida, pp 4-72 - 4-73, 1993.

Dam-Johansen, K. and Ostergaard, K., "High-Temperature Reaction Between Sulphur Dioxide and Limestone - I. Comparison of Limestones in Two Laboratory Reactors and a Pilot Plant," *Chemical Engineering Science*. 46(3):827-837, 1991a.

Dam-Johansen, K. and Ostergaard, K., "High-Temperature Reaction between Sulphur Dioxide and Limestone - II. An Improved Experimental Basis for a Mathematical Model," *Chemical Engineering Science*. 46(3):839-845, 1991b.

Dam-Johansen, K.; Hansen, P.F.B.; and Ostergaard, K., "High-Temperature Reactions Between Sulphur Dioxide and Limestone - III. A Grain-Micrograin Model and its Verification," *Chemical Engineering Science*. 46(3):847-853, 1991.

Damle, A. S. "Modeling a Furnace Sorbent Slurry Injection Process," *Air and Waste*. 44:21-30, 1994.

Davini, P., "Reduction of Nitrogen Oxides with Ammonia: The Activity of Certain Soots," *Fuel*. 67:24-26, 1988.

Fogler, H.S., Elements of Chemical Reaction Engineering, P T R Prentice Hall; Englewood Cliffs, New Jersey, 1992.

Frey, D. D., "Mixed-Gas Adsorption Dynamics of High-Concentration Components in a Particulate Bed," *AIChE Journal*. 38(10):1649-1655, 1992.

Ganz, S. N., "Sorption of Nitrogen Oxides by Solid Sorbents," *Journal of Applied Chemistry of the USSR*. 31 (1):128-130, 1958.

Gullett, B. K.; Jozewicz, W.; and Stefanski, L. A., "Reaction Kinetics of Ca-Based Sorbents with HCl," *Industrial Engineering Chemistry Research*. 31(11):2437-2446, 1992.

Hajaligol, M.R.; Longwell, J.P.; and Sarofim, A.F., "Analysis and Modeling of the Direct Sulfation of  $\text{CaCO}_3$ ," *Industrial Engineering Chemistry Research*. 27(12):2203-2210, 1988.

Ham, D.O.; Moniz, G.; and Gouveia, Additives for  $\text{NO}_x$  Emissions Control from Fixed Sources, ESL-TR-89-24, HQ AFESC, Tyndall AFB, Florida, 1991.

Hansen, P.F.B.; Dam-Johansen, K.; Johnsson, J.E.; and Hulgaard, T., "Catalytic Reduction of NO and  $\text{N}_2\text{O}$  on Limestone During Sulfur Capture under Fluidized Bed Combustion Conditions," *Chemical Engineering Science*. 47(9):2419-2427, 1992.

Hartman, M. and Coughlin, R. W., "Reaction of Sulfur Dioxide with Limestone and the Grain Model," *AIChE Journal*. 22(3):490-498, 1976.

Hayward, D.O. and Trapnell, B.M.W., Chemisorption, 2nd ed., Butterworth and Co.; London, 1964.



Heap, M. P.; Chen, S. L.; Kramlich, J. C.; McCarthy, J.M.; and Pershing, D. W., "An Advanced Selective Reduction Process for NO<sub>x</sub> Control," *Nature*. 335:620-622, 1988.

Hinds, W.C., Aerosol Technology: Properties, Behavior and Measurement of Airborne Particles, John Wiley and Sons; New York, pp 69-100, 1982.

Ismagilov, Z. R.; Kerzhentsev, T. L.; and Susharina, T. L., "Catalytic Methods for Lowering the Amount of Nitrogen Oxides in Exhaust Gases on Combustion of Fuel," *Russian Chemical Reviews*. 59 (10):973-988, 1990.

James, N. J. and Hughes, R., "Rates of NO<sub>x</sub> Absorption in Calcined Limestones and Dolomites," *Environmental Science and Technology*. 11(13):1191-1194, 1977.

Johnson, C.; Henshaw, J.; and McInnes, G. , "Impact of Aircraft and Surface Emissions of Nitrogen Oxides on Tropospheric Ozone and Global Warming," *Nature*. 355:69-71, 1992.

Johnson, S.A. and Katz, C.B. Feasibility of Reburning for Controlling NO<sub>x</sub> Emissions from Air Force Jet Engine Test Cells, ESL-TR-89-33, HQ AFESC, Tyndall AFB, Florida, 1989.

Joseph, D. W. and Spicer, C. W., "Chemiluminescence Method for Atmospheric Monitoring of Nitric Acid and Nitrogen Oxides," *Analytical Chemistry*. 50(9):1400-1403, 1978.

Jozewicz, W.; Chang, J. C. S.; and Sedman, C. B., "Bench-Scale Evaluation of Calcium Sorbents for Acid Gas Emission Control," *Environmental Progress*. 9(3):137-142, 1990.

Karlegard, A. and Bjerle, I., "Kinetic Studies on High Temperature Desulphurization of Synthesis Gas with Zinc Ferrite," *Chemical Engineering Technology*. 17:21-29, 1994.

Kikkinides, E. S. and Yang, R. T. "Simultaneous SO<sub>2</sub>/NO<sub>x</sub> Removal and SO<sub>2</sub> Recovery from Flue Gas by Pressure Swing Adsorption," *Industrial Engineering Chemistry Research*. 30(8):1981-1989, 1991.

Kittrell, R.J., High Temperature NO<sub>x</sub> Control Process, ESL-TR-89-36, HQ AFESC, Tyndall AFB, Florida, 1991.

Klapheck, K. and Winkler, P., "Sensitivity Loss of a NO<sub>x</sub>-Chemiluminescence Analyzer Due to Deposit Formation," *Atmospheric Environment*. 19(9):1545-1548, 1985.

Klimisch, R. L. and Larson, J. G., The Catalytic Chemistry of Nitrogen Oxides, Plenum Press; New York, 1975.

Krishnan, S. V. and Sotirchos, S. V., "A Variable Diffusivity Shrinking-Core Model and its Application to the Direct Sulfation of Limestone," *The Canadian Journal of Chemical Engineering*. 71:734-745, 1993a.

Krishnan, S. V. and Sotirchos, S. V., "Sulfation of High Purity Limestones Under Simulated PFBC Conditions," *The Canadian Journal of Chemical Engineering*. 71:244-255, 1993b.

Krishnan, S. V. and Sotirchos, S. V., "Experimental and Theoretical Investigation of Factors Affecting the Direct Limestone-H<sub>2</sub>S Reaction," *Industrial Engineering Chemistry Research*. 33(6):1444-1453, 1994.

Lange's Handbook of Chemistry, 11th ed., McGraw-Hill Book Company; New York, p 4-88, 1973.

LeVan, M. D., "Fixed-Bed Adsorption of Gases: Effect of Velocity Variations on Transition Types," *AIChE Journal*. 34(6):996-1005, 1988.

Levenspiel, O., Chemical Reaction Engineering, 2nd ed., John Wiley and Sons, Inc., New York, 1972.

Lewis, W. H., Nitrogen Oxides Removal, Noyes Data Corporation; Park Ridge, New Jersey, 1975.

Lyon, R. K., "Thermal DeNO<sub>x</sub>: Controlling Nitrogen Oxides Emissions by a Noncatalytic Process," *Environmental Science and Technology*. 21 (3):231-236, 1987.

Lyon, R.K., New Technology for Controlling NO<sub>x</sub> from Jet Engine Test Cells, ESL-TR-89-16, HQ AFESC, Tyndall AFB, Florida, 1991.

Marsh, D. W. and Ulrichson, D. L., "Rate and Diffusional Study of the Reaction of Calcium Oxide with Sulfur Dioxide," *Chemical Engineering Science*. 40(3):423-433, 1985.

Mejias, J. A.; Marquez, A. M.; Fernandez Sanz, J.; Fernandez-Garcia, M.; Ricart, J. A.; Sousa, C.; and Illas, F., "On modelling the interaction of CO on the MgO(100) Surface," *Surface Science*. 327:59-73, 1995.

Meubus, P., "Catalytic Decomposition of Nitric Oxide in the Presence of Alkaline Earth Oxides," *J. Electrochem. Soc.: Electrochemical Science and Technology*. 124(1):49-58, 1977.

Neal, D. D.; Hoke, S. H.; and Spencer, W. P., NO<sub>x</sub> - Sources, Properties and Analytical Procedures, Technical Report 8907, U.S. Army Biomedical Research and Development Laboratory, Fort Detrick, Maryland, 1981.

Mutasher, E. I.; Khan, A. R.; and Bowen, J. H., "Communications: Reversible, Noncatalytic Reactions Between Gases and Solids in Fixed Beds," *Industrial Engineering Chemistry Research*. 28(10):1550-1553, 1989.

Nelson, B.W.; Nelson, S.G.; and Higgins, M.O., A New Catalyst for NO<sub>x</sub> Control, ESL-TR-89-11, HQ AFESC, Tyndall AFB, Florida, 1989.

Nelson, B.W.; Van Stone, D.A.; and Nelson, S.G., Development and Demonstration of a New Filter System to Control Emissions During Jet Engine Testing, CEL-TR-92-49, HQ AFCEA, Tyndall AFB, Florida, 1992.

Nelson, S.G.; Van Stone, D.A.; Little, R.C.; and Peterson, K.A., Laboratory Evaluation of a Reactive Baffle Approach to NO<sub>x</sub> Control, Final Report, Contract Number FO8635-90-C-0053, HQ AFCEA, Tyndall AFB, Florida, 1993.

Nelson, S.G., (Sanitech, Inc.), U.S. Patent 4,721,582 (Jan. 26, 1988).

Nelson, S.G.; Nelson, B.W.; and Higgins, M.O., Study of the Regenerability of a Unique New Sorbent that Removes SO<sub>2</sub>-NO<sub>x</sub> from Flue Gases, Phase II Final Report, EPA SBIR Contract 68-D80066, Sanitech, Inc., Twinsburg, Ohio, 1990.

Newton, G. H.; Chen, S. L.; and Kramlich, J. C., "Role of Porosity Loss in Limiting SO<sub>2</sub> Capture by Calcium Based Sorbents," *AIChE Journal*. 35(6):988-994, 1989.

NTIS Tech Notes, "Process Eliminates 99% of NO<sub>x</sub> from Exhaust in Lab Tests," DOE Technology Application, July 1987.

Organization for Economic Cooperation and Development (OECD), Control Technology for Nitrogen Oxide Emissions from Stationary Sources, Paris, France, 1983.

Pakrasi, A., "Kinetic Studies on the Removal of Hydrogen Chloride from Flue Gas by Hydrated Lime Powders in a Bench Scale Fixed Bed Reactor," Ph.D. Dissertation; University of Tennessee, Knoxville, Tennessee, 1992.

Perry, R. A. and Siebers, D. L., "Rapid Reduction of Nitrogen Oxides in Exhaust Gas Streams," *Nature*. 324 (18):657-658, 1986.

Petrik, M.A., Use of Metal Oxide Electrocatalysts to Control NO<sub>x</sub> Emissions from Fixed Sources, ESL-TR-89-29, HQ AFESC, Tyndall AFB, Florida, 1991.

Pigford, R. L. and Sliger, G., "Rate of Diffusion-Controlled Reaction Between a Gas and a Porous Solid Sphere," *Industrial Engineering Chemistry Process Design and Development*. 12(1):85-91, 1973.

Quarles, J. and Lewis, W.H. The New Clean Air Act: A Guide to the Clean Air Program as Amended in 1990, Morgan, Lewis and Bockius; Washington, D.C., 1990.

Ramachandran, P. A. and Smith, J. M., "A Single-Pore Model for Gas-Solid Noncatalytic Reactions," *AIChE Journal*. 23 (3):353-361, 1977.

Ruch, R.J.; Krauss, C.J.; Bacon, W.E., Nelson, S.G.; and Nelson, B.W., The Physical Nature and the Chemical Reactivity of a Heterogeneous MgO/Vermiculite Flue-Gas Sorbent, Project Report. Kent State University, Kent, Ohio, and Sanitech, Inc., Twinsburg, Ohio, 1990.

Ruthven, D. M., "A Simple Method of Calculating Mass Transfer Factors for Heterogeneous Catalytic Reactions," *Chemical Engineering Science*. 23:759-764, 1968.

Ruthven, D. M., "Adsorption Kinetics," *Adsorption: Science and Technology*. NATO Advanced Science Institutes Series. Series E: Applied Sciences. 158:87-114, 1989.

Sidgwick, N. V., The Chemical Elements and Their Compounds, Volume I. Oxford at the Clarendon Press; Oxford, England, pp 235-239, 1952.

Simons, G. A., "Parameters Limiting Sulfation by CaO," *AIChE Journal*. 34(1):167-170, 1988.

Snow, M. J. H.; Longwell, J. P.; and Sarofim, A. F., "Direct Sulfation of Calcium Carbonate," *Industrial Engineering Chemistry Research*. 27(2):268-273, 1988.

Sotirchos, S. V. and Yu, H. C., "Mathematical Modelling of Gas-Solid Reactions with Solid Product," *Chemical Engineering Science*. 40(11):2039-2052, 1985.

Sotirchos, S. V. and Zarkanitis, S., "Inaccessible Pore Volume Formation During Sulfation of Calcined Limestones," *AIChE Journal*. 38(10):1536-1550, 1992.

Spicer, C.W.; Holdren, M.W.; and Smith, D.L., Aircraft Emissions Characterization: F101 and F110 Engines, ESL-TR-89-13, HQ AFESC, Tyndall AFB, Florida, 1990.

Spicer, C. W.; Kenny, D. V.; Ward, G. F.; Billick, I.H.; and Leslie, N. P. "Evaluation of NO<sub>2</sub> Measurement Methods for Indoor Air Quality Applications," *Air and Waste*. 44:163-168, 1994.

Steciak, J.; Levendis, Y. A.; and Wise, D. L., "Effectiveness of Calcium Magnesium Acetate as Dual SO<sub>2</sub>-NO<sub>x</sub> Emission Control Agent," *AIChE Journal*. 41(3):712-722, 1995.

Steffenson, D. M. and Stedman, D. H., "Optimization of the Operating Parameters of Chemiluminescent Nitric Oxide Detectors," *Analytical Chemistry*. 46 (12):1704-1708, 1974.

Svensson, R.; Ljungstrom, E.; and Lindqvist, O., "Kinetics of the Reaction Between Nitrogen Dioxide and Water Vapour," *Atmospheric Environment*. 21(7):1529-1539, 1987.

Szekely, J.; Evans, J.W.; and Sohn, H.Y., Gas-Solid Reactions, Academic Press, New York, 1976, pp 257-258.

Tambe, S.; Gauri, K. L.; and Cobourn, W. G., "Kinetic Study of SO<sub>2</sub> Reaction with Dolomite," *Environmental Science and Technology*. 25(12):2071-2075, 1991.

Tanabe, K. and Fukuda, Y., "Basic Properties of Alkaline Earth Metal Oxides and Their Catalytic Activity in the Decomposition of Diacetone Alcohol," *Reaction Kinetics and Catalysis Letters*. 1 (1):21-24, 1974.

Tidona, R. J.; Nizami, A. A.; and Cernansky, N. P., "Reducing Interference Effects in the Chemiluminescent Measurement of Nitric Oxides from Combustion Systems," *Journal of the Air Pollution Control Association*. 38(6):806-811, 1988.

Wander, J.D. and Nelson, S.G., "NO<sub>x</sub> Control for Jet Engine Test Cells," 93-RA-83C-01, Paper presented at the 86th Annual Meeting and Exhibition of the Air and Waste Management Association, June 13-18, 1993, Denver, Colorado.

Wark, K. and Warner C.F., Air Pollution: Its Origin and Control, 2nd ed., HarperCollinsPublishers; New York, 1981, pp 371-423.

Wells, A. F., Structural Inorganic Chemistry, 2nd ed., Oxford at the Clarendon Press; Oxford, England, pp 362, 416-417, 1952.

Wen, C. Y. and Ishida, M., "Reaction Rate of Sulfur Dioxide with Particles Containing Calcium Oxide," *Environmental Science and Technology*. 7(8):703-708, 1973.

Wicke, B. G.; Grady, K. A.; and Ratcliffe, J. W., "Limitations on the Rapid Reduction of Nitrogen Oxides in Exhaust Gas Streams," *Nature*. 338:492-493, 1989.

Wickham, D. T. and Koel, B. E., "Steady-State Kinetics of the Catalytic Reduction of Nitrogen Dioxide by Carbon Monoxide on Platinum," *Journal of Catalysis*. 114:207-216, 1988.

Wolff, E. H. P.; Gerritsen, A. W.; and Van Den Bleek, C. M., "Multiple Reactor Testing of a Synthetic Sorbent for Regenerative Sulfur Capture in Fluidized Bed Combustion of Coal," *The Canadian Journal of Chemical Engineering*. 71:83-93, 1993.

Yagi, S. and Kunii, D., "Fluidized-solids reactors with continuous feed - III. Conversion in experimental fluidized-solid reactors," *Chemical Engineering Science*. 16(3):364 -391, 1961.

Yang, R. T. and Chen, J. M., "Kinetics of Desulfurization of Hot Fuel Gas with Calcium Oxide. Reaction between Carbonyl Sulfide and Calcium Oxide," *Environmental Science and Technology*. 13(5):549-553, 1979.


Zhang, X.; Walters, A. B.; and Vannice, M. A., "Catalytic Reduction of NO by CH<sub>4</sub> over Li-Promoted MgO," *Journal of Catalysis*. 146(2):568-578, 1994.

Zhidomirov, N. U., "Active Centres of Magnesium Oxide Surface and Calculations of Dissociative Chemisorption of Methane on Modified MgO," *Catalysis Today*. 13:517-522, 1992.

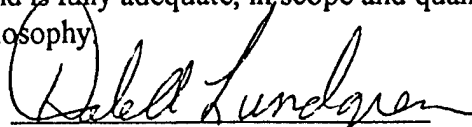
## BIOGRAPHICAL SKETCH

Major Larry Thomas Kimm was born in Mount Clemens, Michigan, on November 6, 1960. After graduation from Fraser High School , in Fraser, Michigan, in 1978, he attended the U.S. Air Force Academy at Colorado Springs, Colorado, until his graduation and commissioning as a second lieutenant in the U.S. Air Force in 1982. He received a Master of Science degree in biology (industrial hygiene) from Old Dominion University, Norfolk, Virginia, in 1988. He was competitively selected to continue his education under the USAF Biomedical Sciences Corps advanced education program, and came to the University of Florida and the Department of Environmental Engineering Sciences to begin his Ph.D. studies in August 1991. Serving as a bioenvironmental engineer in the U.S. Air Force, Major Kimm returns to his career after receiving his degree. He has been married to the former Lisa Anne Wilson since 1987, and is the father of two children, a daughter, Meredyth Grace, and a son, Wilson Carl.

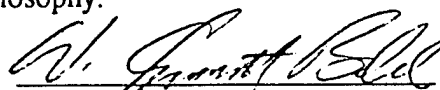
I certify that I have read this study and that in my opinion it conforms to acceptable standards of scholarly presentation and is fully adequate, in scope and quality, as a dissertation for the degree of Doctor of Philosophy.

  
Eric R. Allen, Chair  
Professor of Environmental  
Engineering Sciences

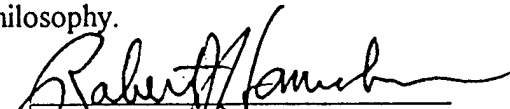
I certify that I have read this study and that in my opinion it conforms to acceptable standards of scholarly presentation and is fully adequate, in scope and quality, as a dissertation for the degree of Doctor of Philosophy.

  
Dale A. Lundgren  
Professor Emeritus of Environmental  
Engineering Sciences

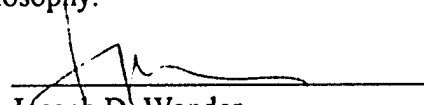
I certify that I have read this study and that in my opinion it conforms to acceptable standards of scholarly presentation and is fully adequate, in scope and quality, as a dissertation for the degree of Doctor of Philosophy.

  
W. Emmett Bolch, Jr.  
Professor of Environmental  
Engineering Sciences

I certify that I have read this study and that in my opinion it conforms to acceptable standards of scholarly presentation and is fully adequate, in scope and quality, as a dissertation for the degree of Doctor of Philosophy.

  
Robert J. Hargahan  
Professor of Chemistry

I certify that I have read this study and that in my opinion it conforms to acceptable standards of scholarly presentation and is fully adequate, in scope and quality, as a dissertation for the degree of Doctor of Philosophy.

  
Joseph D. Wander  
Adjunct Associate Professor of  
Environmental Engineering Sciences